

Investigation of Steel-Stringer Bridges: Superstructures and Substructures, Volume II



Final Report
October 2007

Sponsored by
the Iowa Highway Research Board (Project TR-522)
and the Iowa Department of Transportation (CTRE Project 04-184).



**IOWA STATE
UNIVERSITY**

About the Bridge Engineering Center

The mission of the Bridge Engineering Center is to conduct research on bridge technologies to help bridge designers/owners design, build, and maintain long-lasting bridges.

Disclaimer Notice

The contents of this report reflect the views of the authors, who are responsible for the facts and the accuracy of the information presented herein. The opinions, findings and conclusions expressed in this publication are those of the authors and not necessarily those of the sponsors.

The sponsors assume no liability for the contents or use of the information contained in this document. This report does not constitute a standard, specification, or regulation.

The sponsors do not endorse products or manufacturers. Trademarks or manufacturers' names appear in this report only because they are considered essential to the objective of the document.

Nondiscrimination Statement

Iowa State University does not discriminate on the basis of race, color, age, religion, national origin, sexual orientation, gender identity, sex, marital status, disability, or status as a U.S. veteran. Inquiries can be directed to the Director of Equal Opportunity and Diversity, (515) 294-7612.

Technical Report Documentation Page

1. Report No. IHRB Project TR-522	2. Government Accession No.	3. Recipient's Catalog No.	
4. Title and Subtitle Investigation of Steel-Stringer Bridges: Substructure and Superstructure, Volume II.		5. Report Date October 2007	
		6. Performing Organization Code	
7. Author(s) David White, Mohamed Mekkawy, Wayne Klaiber, Terry Wipf		8. Performing Organization Report No. CTRE Project 04-184	
9. Performing Organization Name and Address Center for Transportation Research and Education Iowa State University 2901 South Loop Drive, Suite 3100 Ames, IA 50010-8634		10. Work Unit No. (TRAIS)	
		11. Contract or Grant No.	
12. Sponsoring Organization Name and Address Iowa Department of Transportation 800 Lincoln Way Ames, IA 50010		13. Type of Report and Period Covered Final Report	
		14. Sponsoring Agency Code	
15. Supplementary Notes			
16. Abstract <p>Problems with unknown bridge foundations in Iowa are often associated with timber substructures. Timber piles are subject to biological and physical deterioration, which makes quantifying in-service pile capacity difficult. Currently there are no reliable means to estimate the residual carrying capacity of an in-service deteriorated pile; and thus, the overall safety of the bridge cannot be determined. The lack of reliable evaluation methods can lead to conservative and costly maintenance practices. This research study was undertaken to investigate procedures for assessing bridge substructures, and evaluating procedures for rehabilitating/strengthening/replacing inadequate substructure components.</p> <p>The report includes an extensive literature review, a field reconnaissance study of 49 bridges, a survey of substructure problems from the perspective of County Engineers, a laboratory study aiming to correlate nondestructive tests to residual pile strength and stiffness values, nondestructive and destructive load tests for 6 bridges with poor substructures, and finally a laboratory study evaluating selected repair methods.</p>			
17. Key Words: load tests— nondestructive evaluation— pile deterioration—pile repair—timber substructure—unknown bridge foundation		18. Distribution Statement No restrictions.	
19. Security Classification (of this report) Unclassified.	20. Security Classification (of this page) Unclassified.	21. No. of Pages 293	22. Price NA

INVESTIGATION OF STEEL-STRINGER BRIDGES: SUPERSTRUCTURES AND SUBSTRUCTURES, VOLUME II

**Final Report
October 2007**

Principal Investigator

F. Wayne Klaiber
Professor, Department of Civil, Construction, and Environmental Engineering
Iowa State University

Co-Principal Investigators

David J. White
Associate Professor, Department of Civil, Construction, and Environmental Engineering
Iowa State University

Terry J. Wipf
Professor, Department of Civil, Construction, and Environmental Engineering
Iowa State University

Research Assistants

Mohamed Mekkawy
Jeremy Koskie

Sponsored by
the Iowa Highway Research Board
(IHRB Project TR-522)

Preparation of this report was financed in part
through funds provided by the Iowa Department of Transportation
through its research management agreement with the
Center for Transportation Research and Education
CTRE Project 04-184.

Center for Transportation Research and Education

Iowa State University
2901 South Loop Drive, Suite 3100
Ames, IA 50010-8632
Phone: 515-294-8103
Fax: 515-294-0467
www.ctre.iastate.edu

TABLE OF CONTENTS

ACKNOWLEDGMENTS	XXI
EXECUTIVE SUMMARY	XXIII
1. INTRODUCTION	1
1.1. Research Objectives.....	1
1.2. Research Tasks	1
2. LITERATURE REVIEW	3
2.1. Introduction.....	3
2.2. Timber Piles	3
2.2.1. Biological Deterioration	4
2.2.2. Physical Deterioration.....	5
2.2.3. Mechanical Properties of Wood	6
2.3. Steel Piles.....	7
2.4. Concrete Piles	8
2.5. Assessing Integrity of Pile Elements	8
2.6. Visual Inspection	8
2.7. Nondestructive Testing	12
2.7.1. Hammer Sounding	12
2.7.2. Increment Borer	12
2.7.3. Stress Wave Timing.....	12
2.8. Determining Length of In-Service Piles	16
2.8.1. Surface Methods	16
2.8.2. Borehole Methods.....	20
2.9. Determination of Pile Strength	24
2.10. Pile Maintenance Practices	25
2.10.1. Preventative Maintenance.....	26
2.10.2. Remedial Maintenance	27
2.10.3. Major Maintenance	32
3. QUESTIONNAIRE RESULTS	34
4. FIELD RECONNAISSANCE	37
4.1. Biological Deterioration	37
4.2. Physical Deterioration.....	37
4.3. Other Causes of Pile Deterioration	37
4.4. Substructure Remediation Techniques	42
4.5. Summary	46

5. LABORATORY TESTING.....	47
5.1. Ultrasonic Stress Wave Technique	47
5.1.1. Background	47
5.1.2. Difficulties and Limitations	48
5.1.3. Description of Equipment	48
5.1.4. Image Processing	49
5.1.5. Test Procedure	51
5.1.6. Test Verification and Repeatability	52
5.1.7. Test Results	56
5.2. Axial Compression Tests	56
5.3. Correlation between Compression and Ultrasonic Stress Wave Tests	56
5.4. Summary	61
6. EXPERIMENTAL METHODS FOR FIELD INVESTIGATION.....	63
6.1. Introduction.....	63
6.2. Ultrasonic Stress Wave Test	63
6.3. Static Load Test	63
6.4. Pile Coring	70
7. BRIDGE NO. 7710 BOONE COUNTY.....	72
7.1. Bridge Description	72
7.2. Load Test Setup and Instrumentation	76
7.3. Test Results	77
7.3.1. North Abutment – West Edge	77
7.3.2. North Abutment – Centerline	77
7.3.3. North Abutment – East Edge	77
8. BRIDGE NO. 243470 MARSHALL COUNTY	82
8.1. Bridge Description	82
8.2. Load Test Setup and Instrumentation	87
8.3. Test Results	88
8.3.1. North Abutment – West Edge	88
8.3.2. North Abutment – Centerline	90
8.3.3. North Abutment – East Edge	90
8.3.4. South Abutment – West Edge	91
8.3.5. South Abutment – Centerline	97
8.3.6. South Abutment – East Edge	97
9. BRIDGE NO. 237350 MAHASKA COUNTY	102
9.1. Bridge Description	102
9.2. Load Test Setup and Instrumentation	107
9.3. Test Results	107
9.3.1. North Abutment – West Edge	107
9.3.2. North Abutment – Centerline	109

9.3.3. North Abutment – East Edge	109
9.3.4. South Abutment – West Edge	114
9.3.5. South Abutment – Centerline	114
9.3.6. South Abutment – East Edge	114
9.4. Foundation Design	118
9.5. Pile Integrity Testing	122
9.5.1. Instrumentation and Testing Procedure	122
9.5.2. Determination of Wave Speed	125
9.5.3. Estimation of Pile Length	126
10. BRIDGE NO. 094680 CARROLL COUNTY	129
10.1. Bridge Description	129
10.2. Load Test Setup and Instrumentation	133
10.3. Test Results	137
10.3.1. North Abutment – West Edge	137
10.3.2. North Abutment – Centerline	139
10.3.3. North Abutment – East Edge	139
10.3.4. South Abutment – West Edge	142
10.3.5. South Abutment – Centerline	142
10.3.6. South Abutment – East Edge	142
11. BRIDGE NO. 237380 MAHASKA COUNTY	146
11.1. Bridge Description	146
11.2. Load Test Setup and Instrumentation	150
11.3. Test Results	152
11.3.1. Northwest Abutment – North Edge	152
11.3.2. Northwest Abutment – Centerline	152
11.3.3. Northwest Abutment – South Edge	152
11.3.4. Southeast Abutment – North Edge	156
11.3.5. Southeast Abutment – Centerline	156
11.3.6. Southeast Abutment – South Edge	156
11.4. Foundation Design	160
12. BRIDGE NO. 029070 HUMBOLDT COUNTY	163
12.1. Bridge Description	163
12.2. Load Test Setup and Instrumentation	171
12.3. Nondestructive Test Results	177
12.3.1. West Abutment – North Edge	177
12.3.2. West Abutment – Centerline	177
12.3.3. West Abutment – South Edge	177
12.3.4. East Abutment – North Edge	181
12.3.5. East Abutment – Centerline	181
12.3.6. East Abutment – South Edge	181
12.4. Destructive Test Results	185
12.4.1. Test No. 1 – Pile No. 7 Jacked	185

12.4.2. Test No. 2 – Pile No. 7 Removed	188
12.4.3. Test No. 3 – Pile Nos. 3 and 7 Jacked	192
12.4.4. Test No. 4 – Pile No. 3 Removed and Pile No. 7 Jacked.....	197
12.4.5. Test No. 5 – Pile Nos. 3 and 7 Removed	200
12.4.6. Test No. 6 – Pile Nos. 3, 6 and 7 Removed	204
12.4.7. Test No. 7 – Pile Nos. 3 and 6 Removed and Pile No. 7 Repaired.....	208
12.5. Foundation Design	212
12.6. Key Findings from Field Testing	215
12.6.1. Ultrasonic Stress Wave Test	215
12.6.2. Increment Borer	215
12.6.3. Nondestructive Static Load Tests	215
12.6.4. Destructive Static Load Tests	216
13. PILE REPAIR STUDY.....	217
13.1. Introduction.....	217
13.2. Experimental Plan.....	217
13.3. Test Setup	217
13.4. Repair Methods.....	219
13.4.1. Control Sections.....	219
13.4.2. Repair Method A – Mechanical Splicing	219
13.4.3. Repair Method B – New Pile Section with FRP Wrap.....	221
13.4.4. Repair Method C – Epoxy Grout with FRP Wrap.....	223
13.5. Material Properties.....	226
13.6. Results.....	227
13.7. Summary and Conclusions	230
14. SUMMARY AND CONCLUSIONS	231
14.1. Relevant Research.....	231
14.2. Field Reconnaissance.....	231
14.3. Laboratory Testing.....	231
14.4. Field Testing	232
14.4.1. Ultrasonic Stress Wave Test.....	232
14.4.2. Increment Borer	232
14.4.3. Nondestructive Static Load Tests	232
14.4.4. Destructive Static Load Tests	233
14.5. Pile Repair Study	233
15. RECOMMENDATIONS AND FUTURE RESEARCH.....	235
REFERENCES	236
APPENDIX A.....	A-1

APPENDIX B	B-1
APPENDIX C	C-1

LIST OF FIGURES

Figure 2.1. Climate index for decay hazard. Higher numbers indicate greater decay hazard (USDA 1999)	4
Figure 2.2. Stages of timber pile deterioration by overloading (reproduced from Buslov and Scola 1991)	6
Figure 2.3. Three principal axes of wood with respect to the grain and growth rings (modified from USDA 1999).....	7
Figure 2.4. Damage to timber piles from biological sources (reproduced from U.S. Army Corps of Engineering et al. 2001)	9
Figure 2.5. Damage to timber piles from physical sources (reproduced from U.S. Army Corps of Engineering et al. 2001).....	10
Figure 2.6. Typical damage of concrete piles from physical sources (reproduced from U.S. Army Corps. Of Engineering et al. 2001)	11
Figure 2.7. Concept of stress wave timing for detecting internal decay (modified from Wang et al. 2004)	13
Figure 2.8. Dispersive wave propagation field test setup	15
Figure 2.9. Hammer impact and sensor location for inaccessible pile head (reproduced from Brooks and Burk 1994).....	19
Figure 2.10. Principle of parallel seismic test (reproduced from Davis 1995).....	21
Figure 2.11. Borehole radar system (reproduced from Wightman et al. 2003).....	22
Figure 2.12. Tomographic survey design (reproduced from Wightman et al. 2003)	23
Figure 2.13. Induction field method setup (reproduced from Olson et al. 1998)	24
Figure 2.14. Splicing timber piles using concrete jacket or timber fishplate (Wipf et al. 2003a, and U.S. Army Corps. of Engineers et al. 2001)	28
Figure 2.15. Diagram of pile posting using epoxy (modified from Ritter 1992)	28
Figure 2.16. Concrete encasement repairs to timber, steel or concrete piles (U.S. Army Corps. of Engineers et al. 2001)	29
Figure 2.17. Wrapping timber piles with polyvinyl chloride (U.S. Army Corps. Of Engineers et al. 2001)	30
Figure 2.18. Cross section of timber pile repaired with fiber reinforced polymer composite shells (Lopez-Anido et al. 2005).....	31
Figure 2.19. Fiber reinforced polymer composite repair system with (reproduced from Lopez-Anido et al. 2005)	32
Figure 2.20. Addition of supplemental timber or steel piles (reproduced from U.S. Army Corps. of Engineers et al. 2001)	33
Figure 2.21. Addition of supplemental concrete or steel piles (reproduced from U.S. Army Corps. of Engineers et al. 2001)	33
Figure 3.1. Iowa County Engineers rating of common steel pile problems	34
Figure 3.2. Iowa County Engineers rating of common timber pile problems	35
Figure 3.3. Iowa County Engineers rating of methods used to detect substructure and superstructure problems	35
Figure 3.4. Frequency of remediation and/or strengthening methods used in Iowa.....	36
Figure 4.1. Timber pile biological deterioration.....	38
Figure 4.2. Pile cracking near the pile top (Bridge No. 1045 Black Hawk County – April 2 2005).....	39
Figure 4.3. Reduction of pile cross section by abrasion from flowing debris and ice (Bridge No. 27-74-23 – February 15 2007)	39

Figure 4.4. Compression failure of pile section caused by overloading.....	40
Figure 4.5. Ultraviolet degradation of a timber pile (Bridge No. 23-73-50 Mahaska County – July 8 2005)	41
Figure 4.6. Misalignment of a timber pile (Bridge No. 22-00-44 Buchanan County – February 15 2005)	41
Figure 4.7. Deterioration of pile cap.....	42
Figure 4.8. Encasing the center piers with concrete for pile restoration (Bridge No. 149 Boone County – February 11 2005).....	43
Figure 4.9. Spalling and cracking of concrete casing (Bridge No. 149 Boone County – February 11 2005)	43
Figure 4.10. New steel pile driven adjacent to defective pile (Bridge on Indian Creek Road Black Hawk County – April 2 2005)	44
Figure 4.11. Bridge No. 31-72-50 Tama County – October 27 2005.....	44
Figure 4.12. A section from the concrete deck is removed for driving timber piles (Bridge No. 31-72-50 Tama County – September 8 2005).....	45
Figure 4.13. New timber abutment system constructed at the north side (Bridge No. 31-72-50 Tama County – September 8 2005)	45
Figure 4.14. Steel piles used to replace deteriorated timber abutment (Bridge in Boone County – June 1 2005).....	46
Figure 5.1. Significant internal pile deterioration that is difficult to detected using the stress wave technique (Bridge No. 31-72-50 Tama County – June 10 2005).....	48
Figure 5.2. James Instrument Velocity Meter.....	49
Figure 5.3. Construction of model grid of nodes with intervening voxels	50
Figure 5.4. Possible test arrangements with 4 to 8 test points (Divos and Szalai 2002)	51
Figure 5.5. Incremental testing to obtain multiple 2 dimensional images.....	51
Figure 5.6. Comparison of tomography and digital images generated for damaged piles	54
Figure 5.7. Normal distribution plots of the damaged pile sections evaluating accuracy and precision of the ultrasonic stress wave test procedure.....	55
Figure 5.8. Generated tomography images of a timber pile specimen (Pile 1 North Abutment Marshall County Bridge)	57
Figure 5.9. Pile compression test.....	59
Figure 5.10. Stress-strain data for timber pile sections	59
Figure 5.11. Correlation between E determined using ultrasonic stress wave tests and axial compression tests	60
Figure 5.12. Multiple regression models for predicting E.....	61
Figure 6.1. Tandem axle truck using to carry out static load tests	64
Figure 6.2. Schematic of tandem axle truck used to static loading	65
Figure 6.3. Applying three load increments above the bridge abutment.....	66
Figure 6.4. Schematic diagram of the axle footprint	67
Figure 6.5. Wheel loads measured using a portable axle/wheel scale.....	68
Figure 6.6. A BDI strain transducer.....	68
Figure 6.7. A BDI strain transducer with an extension (Bridge No. 02-90-70 Humboldt County – July 10 2006)	69
Figure 6.8. Timber piles and backwall instrumented with strain transducer (Bridge No. 23-73-50 Mahaska County – October 28 2005)	69
Figure 6.9. STS Units connected to strain transducers (Bridge No. 24-34-70 Marshall County – July 28 2005)	70
Figure 6.10. Increment borer used to obtain a pile core (Bridge No. 09-46-80 Carroll County –	

May 12 2006).....	70
Figure 6.11. Pile core showing level of creosote penetration.....	71
Figure 7.1. Bridge No. 7710 Boone County – looking south (June 24 2005)	72
Figure 7.2. Seven supporting timber piles at each abutment with a timber backwall and double c-channel cap (Bridge No. 7710 Boone County – June 1 2005)	73
Figure 7.3. Piles denoted by numbers 1 through 7 at the north abutment (Bridge No. 7710 Boone County – July 1 2005).....	73
Figure 7.4. Schematic diagram of the north abutment (Bridge No. 7710 – Boone County)	74
Figure 7.5. Schematic diagram of the bridge cross section (reproduced from the bridge construction plans).....	74
Figure 7.6. Deterioration at pile No. 1 (Bridge No. 7710 Boone County – July 1 2005).....	75
Figure 7.7. Soft section at pile No. 7 above the water level (Bridge No. 7710 Boone County – July 1 2005)	75
Figure 7.8. Sheet pile wall driven behind the south abutment to prevent backfill erosion (Bridge No. 7710 Boone County – June 1 2005).....	76
Figure 7.9. Locations of strain transducers at the north abutment (Bridge No. 7710 – Boone County)	76
Figure 7.10. Pile strains for north abutment – West edge (Bridge No. 7710 – Boone County)....	78
Figure 7.11. Pile strains at north abutment – Centerline (Bridge No. 7710 – Boone County).....	79
Figure 7.12. Pile strains at the north abutment – East edge (Bridge No. 7710 – Boone County)	80
Figure 7.13. Possible eccentric loading caused by misalignment of pile cap (Bridge No. 7710 – Boone County).....	81
Figure 8.1. North view of Marshall County Bridge No. 243470 (July 22 2005)	83
Figure 8.2. Plan view of the bridge abutment (Bridge No. 243470 – Marshall County)	83
Figure 8.3. North abutment (Bridge No. 243470 Marshall County – July 22 2005).....	84
Figure 8.4. South abutment (Bridge No. 243470 Marshall County – July 22 2005).....	84
Figure 8.5. Schematic of the bridge substructure (Bridge No. 243470 – Marshall County).....	85
Figure 8.6. Hammer sounding and probing revealed a hollow core at pile no. 2 at the north abutment (Bridge No. 243470 Marshall County – June 22 2005).....	86
Figure 8.7. Pile no. 4 at the north abutment undergoing biological deterioration (Bridge No. 243470 Marshall County – July 27 2005)	86
Figure 8.8. Rotting pile sections at the south abutment caused by high moisture content near the ground level (Bridge No. 243470 Marshall County – July 22 2005)	87
Figure 8.9. Construction of the new bridge foundation (Bridge No. 243470 Marshall County – August 19 2005).....	87
Figure 8.10. Strain transducers attached to exposed pile sections (Bridge No. 243470 – Marshall County)	88
Figure 8.11. Static load test at the west edge (Bridge No. 243470 – Marshall County)	89
Figure 8.12. Static load test at the centerline (Bridge No. 243470 – Marshall County)	90
Figure 8.13. Static load test at the east edge (Bridge No. 243470 – Marshall County)	91
Figure 8.14. Calculated load carried by pile nos. 1 and 6 at the north abutment (Bridge No. 243470 – Marshall County)	93
Figure 8.15. South abutment instrumented with strain transducers (Bridge No. 243470 Marshall County – July 27 2005).....	94
Figure 8.16. Strain transducers crossing over the tie back rod (Bridge No. 243470 Marshall County – July 27 2005).....	95
Figure 8.17. Static load test at the west edge (Bridge No. 243470 – Marshall County)	96
Figure 8.18. Pile cap partially resting on the timber backwall (Bridge No. 243470 – Marshall	

County – July 28 2005).....	97
Figure 8.19. Static load test at the centerline (Bridge No. 243470 – Marshall County)	98
Figure 8.20. Static load test at the east edge (Bridge No. 243470 – Marshall County)	99
Figure 8.21. Calculated load carried by south abutment piles (Bridge No. 243470 – Marshall County)	101
Figure 9.1. Bridge No. 237350 – Looking north (October 25 2005).....	102
Figure 9.2. North abutment (Bridge No. 237350 Mahaska County – October 25 2005)	103
Figure 9.3. Schematic diagram of the north abutment (Bridge No. 237350 – Mahaska County).....	103
Figure 9.4. Biological deterioration of pile No. 1 at the ground level (Bridge No. 237350 Mahaska County – October 25 2005)	104
Figure 9.5. Deterioration observed at pile No. 5 (Bridge No. 237350 Mahaska County – October 25 2005)	104
Figure 9.6. South abutment (Bridge No. 237350 Mahaska County – October 25 2005)	105
Figure 9.7. Schematic diagram of the south abutment (Bridge No. 237350 – Mahaska County).....	105
Figure 9.8. Brooming of pile No. 2 near the ground level (Bridge No. 237350 Mahaska County – October 25 2005)	106
Figure 9.9. Rotting observed at pile No. 5 (Bridge No. 237350 Mahaska County – October 25 2005)	106
Figure 9.10. Substructure instrumentation (Bridge No. 237350 Mahaska County – October 28 2005)	108
Figure 9.11. Soil excavated around piles to allow for strain transducer installation across deteriorated regions (Bridge No. 237350 Mahaska County – October 28 2005)	109
Figure 9.12. Static load test at the west edge (Bridge No. 237350 – Mahaska County)	110
Figure 9.13. Pile cap partially resting on the timber backwall (Bridge No. 237350 Mahaska County – October 28 2005)	111
Figure 9.14. Static load test at the centerline (Bridge No. 237350 – Mahaska County)	112
Figure 9.15. Static load test at the east edge (Bridge No. 237350 – Mahaska County)	113
Figure 9.16. Static load test at the west edge (Bridge No. 237350 – Mahaska County)	115
Figure 9.17. Static load test at the centerline (Bridge No. 237350 – Mahaska County)	116
Figure 9.18. Static load test at the east edge (Bridge No. 237350 – Mahaska County)	117
Figure 9.19. CPT conducted 66 ft north of the north abutment (Bridge No. 237350 – Mahaska County)	120
Figure 9.20. CPT conducted 65 ft south of the south abutment (Bridge No. 237350 – Mahaska County)	121
Figure 9.21. Equipment used in Pile Integrity Testing	123
Figure 9.22. Two accelerometers attached to pile no. 2 at the north abutment (Bridge No. 237350 Mahaska County – August 17 2006)	123
Figure 9.23. Notches created in the exposed piles to allow for axial impact (Bridge No. 237350 Mahaska County – August 17 2006)	124
Figure 9.24. Applying an axial impact to the notched pile (Bridge No. 237350 Mahaska County – August 17 2006).....	124
Figure 9.25. Determination of wave speed by matching the rising slope of two input pulses	125
Figure 9.26. Results of PIT on pile no. 2 at the north abutment (Bridge No. 237350 – Mahaska County)	127
Figure 9.27. Results of PIT on pile no. 2 at the south abutment (Bridge No. 237350 – Mahaska County)	128
Figure 10.1. Side view of the bridge looking northwest (Bridge No. 094680 Carroll County – May 16 2006).....	129

Figure 10.2. Concrete deck patched with asphalt (Bridge No. 094680 Carroll County – May 16 2006)	129
Figure 10.3. Soil erosion near the north abutment (Bridge No. 094680 Carroll County – April 15 2006)	130
Figure 10.4. Severe deterioration observed at the northeast wingwall piles (Bridge No. 094680 Carroll County – April 15 2006).....	131
Figure 10.5. North abutment (Bridge No. 094680 Carroll County – April 15 2006).....	131
Figure 10.6. A schematic diagram of the north abutment (Bridge No. 094680 – Carroll County).....	132
Figure 10.7. South abutment (Bridge No. 094680 Carroll County – April 15 2006).....	132
Figure 10.8. Schematic diagram of the south abutment (Bridge No. 094680 – Carroll County).....	133
Figure 10.9. Bridge No. 094680 Carroll County	134
Figure 10.10. Anchor block located outside the zone of maximum efficiency (Bridge No. 094680 – Carroll County)	135
Figure 10.11. Locations of the strain transducers (Bridge No. 094680 – Carroll County)	136
Figure 10.12. Strain transducers attached below the tie back road at the south abutment (Bridge No. 094680 – Carroll County)	137
Figure 10.13. Static load test at the west edge (Bridge No. 094680 – Carroll County)	138
Figure 10.14. Pile cap partially resting on the backwall (Bridge No. 094680 Carroll County – May 16 2006).....	139
Figure 10.15. Static load test at the centerline (Bridge No. 094680 – Carroll County)	140
Figure 10.16. Static load test at the east edge (Bridge No. 094680 – Carroll County)	141
Figure 10.17. Static load test at the west edge (Bridge No. 094680 – Carroll County)	143
Figure 10.18. Static load test at the centerline (Bridge No. 094680 – Carroll County)	144
Figure 10.19. Static load test at the east edge (Bridge No. 094680 – Carroll County)	145
Figure 11.1. Bridge No. 237380 – Mahaska County (April 16 2006).....	146
Figure 11.2. Schematic diagram of the northwest abutment (Bridge No. 237380 – Mahaska County)	147
Figure 11.3. Northwest abutment (Bridge No. 237380 Mahaska County – April 16 2006)	147
Figure 11.4. Deterioration of pile no. 1 (Bridge No. 237380 Mahaska County – April 16 2006).....	148
Figure 11.5. Biological deterioration at the northwest abutment (Bridge No. 237380 Mahaska County – April 16 2006).....	148
Figure 11.6. Southeast abutment at a higher elevation than the water level (Bridge No. 237380 Mahaska County – April 16 2006)	149
Figure 11.7. Schematic diagram of the southeast abutment (Bridge No. 237380 – Mahaska County)	149
Figure 11.8. Location of strain transducers (Bridge No. 237380 – Mahaska County).....	151
Figure 11.9. Static load test at the north edge (Bridge No. 237380 – Mahaska County).....	153
Figure 11.10. Static load test at the centerline (Bridge No. 237380 – Mahaska County)	154
Figure 11.11. Static load test at the south edge (Bridge No. 237380 – Mahaska County).....	155
Figure 11.12. Static load test at the north edge (Bridge No. 237380 – Mahaska County).....	157
Figure 11.13. Static load test at the centerline (Bridge No. 237380 – Mahaska County)	158
Figure 11.14. Static load test at the south edge (Bridge No. 237380 – Mahaska County).....	159
Figure 11.15. Partial bearing of the pile cap on the southeast abutment backwall (Bridge No. 237380 Mahaska County – May 27 2006).....	160
Figure 11.16. CPT carried out 100 ft north of the north abutment (Bridge No. 237380 – Mahaska County)	161
Figure 11.17. CPT carried out near the south abutment (Bridge No. 237380 – Mahaska County).....	161
Figure 12.1. Bridge No. 029070 Humboldt County – Looking east (April 4 2006)	163

Figure 12.2. Center pier added in the 1970s (Bridge No. 029070 Humboldt County – April 4 2006)	163
Figure 12.3. Center pier supported by 2 timber piles on each side of the bridge (Bridge No. 029070 Humboldt County – April 4 2006).....	164
Figure 12.4. Cutting the timber piles supporting the bridge pier (Bridge No. 029070 Humboldt County – July 10 2006).....	164
Figure 12.5. Lowering the steel girder (Bridge No. 029070 Humboldt County – July 10 2006)	165
Figure 12.6. Plan view of bridge abutment (Bridge No. 029070 – Humboldt County)	166
Figure 12.7. East abutment (Bridge No. 029070 Humboldt County – April 4 2006)	166
Figure 12.8. Schematic diagram of the east abutment (Bridge No. 029070 – Humboldt County)	167
Figure 12.9. Advanced section loss at pile No. 6 at the east abutment (Bridge No. 029070 Humboldt County – July 12 2006).....	167
Figure 12.10. West abutment (Bridge No. 029070 Humboldt County – April 4 2006)	168
Figure 12.11. Schematic diagram of the west abutment (Bridge No. 029070 – Humboldt County)	168
Figure 12.12. Removing the bridge super structure – looking west (Bridge No. 029070 Humboldt County – July 28 2006).....	170
Figure 12.13. New box culvert – view looking north (Bridge No. 029070 Humboldt County – October 5 2006)	170
Figure 12.14. Stress-strain curves for pile Nos. 3 and 6 at the west abutment (Bridge No. 029070 – Humboldt County)	171
Figure 12.15. Axle footprints (Bridge No. 029070 – Humboldt County)	172
Figure 12.16. Strain transducers attached to the exposed timber piles (Bridge No. 029070 – Humboldt County)	174
Figure 12.17. Destructive static load test (Bridge No. 029070 Humboldt County – July 12 2006)	174
Figure 12.18. Pile nos. 3 and 7 removed at the east abutment (Bridge No. 029070 Humboldt County – July 12 2006).....	175
Figure 12.19. Mechanical jack and load cell used to restore and record the load carried by pile no. 7 (Bridge No. 029070 Humboldt County – July 12 2006)	175
Figure 12.20. A section of Pile no. 6 removed near the ground level (Bridge No. 029070 Humboldt County – July 12 2006).....	176
Figure 12.21. Installing a new timber section to repair pile no. 7 (Bridge No. 029070 Humboldt County – July 12 2006).....	176
Figure 12.22. Metal screws used to connect the new section to the existing timber pile (Bridge No. 029070 Humboldt County – July 12 2006).....	177
Figure 12.23. Static load test at the north edge of the west abutment (Bridge No. 029070 – Humboldt County)	178
Figure 12.24. Static load test at the centerline of the west abutment (Bridge No. 029070 – Humboldt County)	179
Figure 12.25. Static load test at the south edge of the west abutment (Bridge No. 029070 – Humboldt County)	180
Figure 12.26. Static load test at the north edge of the east abutment (Bridge No. 029070 – Humboldt County)	182
Figure 12.27. Static load test at the centerline of the east abutment (Bridge No. 029070 – Humboldt County)	183
Figure 12.28. Static load test at the south edge of the east abutment (Bridge No. 029070 – Humboldt County)	184
Figure 12.29. Static load test at the centerline with pile No. 7 jacked (Bridge No. 029070 – Humboldt County)	186

Figure 12.30. Static load test at the south edge with pile No. 7 jacked (Bridge No. 029070 – Humboldt County)	187
Figure 12.31. Static load test at the north edge with pile No. 7 removed (Bridge No. 029070 – Humboldt County)	189
Figure 12.32. Static load test at the centerline with pile No. 7 removed (Bridge No. 029070 – Humboldt County)	190
Figure 12.33. Static load test at the south edge with pile No. 7 removed (Bridge No. 029070 – Humboldt County)	191
Figure 12.34. Pile Nos. 3 and 7 jacked (Bridge No. 029070 Humboldt County – July 12 2006)	192
Figure 12.35. Static load test at the north edge with pile Nos. 7 and 3 jacked (Bridge No. 029070 – Humboldt County)	194
Figure 12.36. Static load test at the centerline pile Nos. 7 and 3 jacked (Bridge No. 029070 – Humboldt County)	195
Figure 12.37. Static load test at the south edge pile Nos. 7 and 3 jacked (Bridge No. 029070 – Humboldt County)	196
Figure 12.38. Static load test at the north edge with pile no. 3 removed and pile no. 7 jacked (Bridge No. 029070 – Humboldt County)	198
Figure 12.39. Static load test at the centerline pile No. 3 removed and pile No. 7 jacked (Bridge No. 029070 – Humboldt County)	199
Figure 12.40. Static load test at the north edge with pile Nos. 3 and 7 removed (Bridge No. 029070 – Humboldt County)	201
Figure 12.41. Static load test at the centerline with pile Nos. 3 and 7 removed (Bridge No. 029070 – Humboldt County)	202
Figure 12.42. Static load test at the south edge with pile Nos. 3 and 7 removed (Bridge No. 029070 – Humboldt County)	203
Figure 12.43. Static load test at the north edge with pile Nos. 3, 6 and 7 removed (Bridge No. 029070 – Humboldt County)	205
Figure 12.44. Static load test at the centerline with pile Nos. 3, 6 and 7 removed (Bridge No. 029070 – Humboldt County)	206
Figure 12.45. Static load test at the south edge with pile Nos. 3, 6 and 7 removed (Bridge No. 029070 – Humboldt County)	207
Figure 12.46. Static load test at the north edge with pile nos. 3 and 6 removed and pile no. 7 repaired (Bridge No. 029070 – Humboldt County)	209
Figure 12.47. Static load test at the centerline with pile Nos. 3 and 6 removed and pile No. 7 repaired (Bridge No. 029070 – Humboldt County)	210
Figure 12.48. Static load test at the south edge with pile nos. 3 and 6 removed and pile no. 7 repaired (Bridge No. 029070 – Humboldt County)	211
Figure 12.49. CPT test conducted near the east abutment (Bridge No. 029070 Humboldt County)	213
Figure 12.50. CPT test conducted near the west abutment (Bridge No. 029070 – Humboldt County)	213
Figure 13.1. Angular supports and loading plate used during a trial bending test	217
Figure 13.2. Bending test setup	218
Figure 13.3. Pile sides flattened for conducting bending tests	218
Figure 13.4. Reduced cross sectional area of control timber pile section	219
Figure 13.5. Repair method A.....	220
Figure 13.6. Pile section repaired using a mechanical splicing techniques.....	220
Figure 13.7. Repair method B.....	221
Figure 13.8. Applying the bonding epoxy using a paint roller	222

Figure 13.9. Wrapping the FRP sheet around the timber pile	222
Figure 13.10. Two piles repaired using repair method B	223
Figure 13.11. Schematic diagram of repair method C	224
Figure 13.12. Forming the FRP shell.....	224
Figure 13.13. FRP shell detached from PVC pipe after curing for three days	225
Figure 13.14. Expandable wood filler epoxy applied to fill the void between the pile and the FRP shell	225
Figure 13.15. Axial and bending load tests	228
Figure 13.16. Summary of axial compression test results	229
Figure 13.17. Summary of bending test results	229
Figure B1. Pile no. 1 - Generated two-dimensional tomography images.....	2
Figure B2. Pile no. 2 - Generated two-dimensional tomography images.....	3
Figure B3. Pile no. 3 - Generated two-dimensional tomography images.....	4
Figure B4. Pile no. 4 - Generated two-dimensional tomography images.....	5
Figure B5. Pile no. 6 - Generated two-dimensional tomography images.....	6
Figure B6. Pile no. 7 - Generated two-dimensional tomography images.....	7
Figure B7. Pile no. 9 - Generated two-dimensional tomography images (Pile no. 2 South Abutment Marshall County Bridge)	8
Figure B8. Pile no. 10 - Generated two-dimensional tomography images (Pile 3 no. South Abutment Marshall County Bridge)	9
Figure B9. Pile no. 11 - Generated two-dimensional tomography images (Pile no. 5 South Abutment Marshall County Bridge)	10
Figure B10. Pile no. 12 – Generated two-dimensional tomography images	11
Figure C1. Pile integrity test results at pile no. 2 at the north abutment (distance between A1 and A2 = 5 ft).....	2
Figure C2. Pile integrity test results at pile no. 3 at the north abutment (distance between A1 and A2 = 3 ft).....	3
Figure C3. Pile integrity test results at pile no. 3 at the north abutment (distance between A1 and A2 = 2 ft).....	4
Figure C4. Pile integrity test results at pile no. 3 at the north abutment (distance between A1 and A2 = 5 ft).....	5
Figure C5. Pile integrity test results at pile no. 5 at the south abutment (distance between A1 and A2 = 2 ft).....	6
Figure C6. Pile integrity test results at pile no. 5 at the south abutment (distance between A1 and A2 = 5 ft).....	7
Figure C7. Pile integrity test results at pile no. 3 at the south abutment (distance between A1 and A2 = 2 ft).....	8
Figure C8. Pile integrity test results at pile no. 3 at the south abutment (distance between A1 and A2 = 4.5 ft).....	9
Figure C9. Pile integrity test results at pile no. 3 at the south abutment (distance between A1 and A2 = 2.5 ft).....	10
Figure C10. Pile integrity test results at pile no. 2 at the south abutment (distance between A1 and A2 = 2 ft).....	11

LIST OF TABLES

Table 2.1. Strength properties of Southern Yellow Pine wood Species (USDA 1999)	7
Table 2.2. Capability of each level of inspection for detecting damage (modified from U.S. Army Corps of Engineering et al. 2001)	9
Table 2.3. Stress wave transmission time for various species of nondegraded wood (modified from Wang et al. 2004)	13
Table 2.4. Pile condition criteria for Southern Yellow Pine (Aggour 1991).....	14
Table 2.5. Stress wave transmission time adjustment factors for Douglas-fir (Ross et al. 1999)	14
Table 2.6. Strength properties of various species of timber (from USDA 1999 and ASTM D2555-98)	25
Table 2.7. Stress wave transmission times and compressive properties for eastern white pine timber (Ross et al. 2001)	25
Table 5.1. Summary of destructive and nondestructive test results.....	58
Table 6.1. Summary of truck dimensions and wheel loads	65
Table 8.1. Properties of pile sections obtained from Bridge No. 243470 – Marshall County.....	89
Table 8.2. Summary of loads carried by piles 1 and 6 at the north abutment (Bridge No. 243470 – Marshall County)	92
Table 8.3. Summary of loads carried by south abutment piles (Bridge No. 243470 – Marshall County)	100
Table 9.1. Summary of measured piles densities (Bridge No. 237350 – Mahaska County)	107
Table 9.2. Summary of pile length computations (Bridge No. 237350 – Mahaska County)	121
Table 9.3. Summary of Pile Integrity Tests ((Bridge No. 237350 – Mahaska County)	126
Table 10.1. Summary of measured piles densities (Bridge No. 094680 – Carroll County)	135
Table 11.1. Summary of piles densities (Bridge No. 237380 – Mahaska County)	150
Table 11.2. Summary of pile length computations (Bridge No. 237380 – Mahaska County)	162
Table 12.1. Summary of pile densities (Bridge No. 029070 – Humboldt County)	169
Table 12.2. Summary of pile length computations (Bridge No. 029070 – Humboldt County)...	214
Table 13.1. Properties of FRP material.....	226
Table 13.2. Properties of bonding epoxy material.....	226
Table 13.3. Compressive stress at failure measured for the repair methods	230
Table 13.4. Ultimate load and deflection at failure measured for the repair methods.....	230

ACKNOWLEDGMENTS

This research project was sponsored by the Iowa Department of Transportation under contract TR-522. The authors would like to thank the Technical Advisory Committee and the County Engineers for their participation in the questionnaire, assistance in identifying bridges with poor timber superstructure and substructures for investigation, and providing timber specimens needed for laboratory testing. The authors would like to thank Douglas Wood, and undergraduate research assistants for their help with the bridge instrumentation, data collection, and laboratory testing. Special thanks to Humboldt County Engineers for their help in identifying the bridge, providing bridge plans, and assistance in conducting the destructive static load tests.

Finally the authors would like to thank Pete Milligan with Fyfe Co. LLC for providing Fiber Reinforced Polymer material and epoxy grout needed for the pile repair study and Mark Rawlings with GRL Engineers, Inc. for conducting and analyzing pile integrity test results at one bridge site.

EXECUTIVE SUMMARY

There are a number of structurally deficient or functionally obsolete bridges located within the state of Iowa. With the majority of these bridges located on rural county roads where there is limited funding available to replace the bridges, diagnostic load testing can be utilized to determine the actual load carrying capacity of the bridge. One particular type or family of bridges that has been determined to be desirable for load testing consists of single span bridges with non-composite, cast-in-place concrete decks, steel stringers, and timber substructure. This family of bridges is desirable for load testing because the codified ratings are often overly conservative due to the non-composite section properties and assumed simply supported boundary conditions. Further, timber abutments are subjected to physical and biological deterioration, which is difficult to detect and quantify. This deterioration influences the load carrying capacity of timber substructure and thus affects the overall performance of the bridge system.

Six bridges with poor performing superstructure and substructure from the aforementioned family of bridges were selected to be load tested. The six bridges were located on rural roads in five different counties in Iowa: Boone, Carroll, Humboldt, Mahaska, and Marshall. Volume I of this report presents diagnostic load tests for the six bridges. The results of the diagnostic load tests were used to calibrate analytical models of the bridges for rating purposes. All of the bridges were independently rated by three rating agencies using a codified approach. Those ratings were then compared to ratings calculated using a bridge model calibrated to the actual response of the bridge due to the load test. Volume II of this report focuses on evaluating the timber substructure for this family of bridges. This volume discusses procedures for detecting pile internal decay using nondestructive ultrasonic stress wave techniques, correlating nondestructive ultrasonic stress wave techniques to axial compression tests to estimate deteriorated pile residual strength, and evaluate load distribution through poor performing timber substructures by instrumenting and load testing the abutments of the selected six bridges. Also, this volume evaluates pile repair methods in restoring axial and bending capacities.

Problems with unknown bridge foundations in Iowa are often associated with timber substructures. Timber piles are subject to deterioration, which, at initial stages, can be difficult to detect. Further, information regarding soil profile and pile length is often unavailable. There are currently no reliable means to estimate the residual carrying capacity of an in-service deteriorated pile; and thus, the overall safety of the bridge cannot be determined. The lack of a reliable evaluation method can result in conservative and costly maintenance practices such as replacing the entire substructure system. This study was undertaken to investigate procedures for assessing the substructure conditions of bridges and to evaluate selected rehabilitation/strengthening/replacement techniques for timber pile substructure components or entire substructures. This research study included (1) an extensive literature review to locate previous pertinent substructure work, (2) a questionnaire submitted to all County Engineers to assist in the identification inadequate substructure systems, (3) a field reconnaissance of 49 bridges identifying common substructure problems, (4) laboratory testing to correlate nondestructive ultrasonic stress wave methods to destructive axial compression tests, (5) the results of instrumenting and load testing 6 bridges with poor substructure conditions, and (6) evaluating selected pile repair methods in restoring axial and bending pile capacities.

1. INTRODUCTION

This project is Phase II of the recently completed project, “Alternative Solutions to Meet the Service of Low Volume Bridges in Iowa” (TR-452). In Phase I, the overall objective was to develop a state of the practice in the area of the bridge maintenance/rehabilitation/strengthening. Information was obtained from extensive literature reviews and from two questionnaires – a national questionnaire and a questionnaire sent only to Iowa County Engineers (ICEs). The questionnaire to ICEs was to obtain information on unique solutions to various bridge problems specifically associated with low volume road (LVR) bridges. Based on the evaluation of the information obtained from Phase I, and input from several ICEs, problems with substructure and posted steel stringer bridges were identified. Discussed in this volume are field problems and proposed solutions associated with substructure systems. For a detailed discussion on the findings of the superstructure component, refer to Volume I.

The current rating system of bridges in Iowa relies mostly on information correlated from the superstructure performance. The ratings do not incorporate the condition of the bridge substructure. The substructure condition, however, can be a governing factor especially in cases of bridges with unknown foundations or bridges supported on timber piling. In most cases, there are no design or as-built bridge plans, and no documentation of the type, depth, geometry, or materials incorporated in the foundation of these bridges. Timber piles exhibit deterioration with time due to biological and physical factors. If not detected and mitigated, pile deterioration can considerably reduce the pile capacity. Also, the effect of a deteriorated pile on the load distribution throughout the substructure system is not fully understood. In order to incorporate the substructure condition in the rating system, it is necessary to develop reliable yet simple means of evaluation. Nondestructive evaluation is a promising technology, which can help detect internal pile damage, determine pile length below ground level, and estimate residual pile capacity. By integrating nondestructive techniques as part of the bridge foundation inspection routine, the substructure condition can be accounted for during the overall bridge rating. Nondestructive techniques can also be used to identify localized deteriorated zones, thus leading to selection of effective rehabilitation/strengthening methods. Successfully assessing the integrity of existing substructures and rehabilitating/strengthening inadequate substructures components will extend the life of bridges that have adequate superstructure components.

1.1. Research Objectives

The main objectives of this study were as follows:

- Development of procedures for assessing the substructures of bridges
- Development of various procedures for rehabilitating/strengthening/replacing inadequate substructure components or entire substructure.

1.2. Research Tasks

To attain the objectives of this study the following task items were identified and completed:

- An extensive literature review was completed to study previous pertinent substructure work (testing, rehabilitating/strengthening and replacement).
- Based on the findings of the literature review, and the experience of the research team in the experimental assessment of other types of structures, nondestructive procedures were proposed for detecting pile internal damage, determining pile length below ground level, and estimating residual capacity of deteriorated timber pile elements.
- Several Iowa bridges with timber substructure systems were inspected to document current substructure problems.
- A questionnaire was submitted to Iowa County Engineers to assist in the identification of inadequate substructures.
- Based on the findings of a field reconnaissance, assistance of the project advisory committee, and the questionnaire responses, six bridges with poor substructure conditions were identified and selected for detailed field testing.
- Several techniques for the rehabilitation/strengthening of deteriorated timber piles were evaluated in a succinct laboratory study. The axial and bending capacities before and after pile repair were measured.
- Techniques to replace one or more of the deficient substructure elements or at some bridge sites replace the entire substructure were developed. The most promising of these techniques is recommended for the implementation and evaluation in future projects.

2. LITERATURE REVIEW

2.1. Introduction

According to the National Bridge Inventory, there are approximately 580,000 highway bridges in the USA. The type and/or depth of the foundations in about 104,000 of these bridges are unknown. In most cases, there are no design or as-built bridge plans, and no documentation of the type, depth, geometry, or materials incorporated in the foundations (Olson et al. 1998). These unknown bridge foundations pose a significant problem to State Department of Transportations due mostly to their scour vulnerability.

In Iowa, problems of low volume bridge foundations are often associated with timber substructures. Timber piles are subjected to deterioration, which, at initial stages, can be difficult to detect. Furthermore, information regarding soil profile and pile length at a given bridge site is often unavailable. There are currently no reliable means to estimate the residual capacity of an in-service deteriorated pile; and thus, the overall safety of the bridge cannot be determined with confidence. Although the majority of inadequate substructures have timber piling, there are numerous cases in which the steel substructures are inadequate (problems with corrosion, misalignment, damage due to impact, etc.). If procedures can be developed to assess the integrity of existing substructures and rehabilitate/strengthen inadequate substructures components, it will be possible to extend the life of those bridges and have increased confidence in predicting performance.

2.2. Timber Piles

Timber piles are one of the most common foundation elements used in bridge construction due to relatively low cost of raw wood compared to steel and concrete, simple installation techniques, and availability and ease of handling relative to other materials (Chen and Kim 1997 and U.S. Army Corps of Engineers et al. 2001). According to an estimate by Holt et al. (1994), there are as many as 240,000 bridges in the United States supported by timber piles. However a limitation of timber piles is their susceptibility to damage and degradation. Timber bridges by their very nature and use are exposed to deteriorating factors. Even though wood pile deterioration can be mitigated to some extent with the use of preservative treatments, deterioration still remains a concern for long term performance (Lopez-Anido et al. 2004).

According to Toutanji (2004), timber deterioration, in most cases, is continuous; degrading actions from one or more agents change the timber properties making it susceptible to degradation from other agents. The causes of timber pile deterioration can be categorized into biological deterioration and physical deterioration. Biological deterioration includes (1) fungi, (2) bacteria, and (3) insect attack. Physical deterioration includes (1) abrasion, (2) overloading, and (3) fire. Other less frequent problems include pile misalignment and ultra violet degradation. Wang et al. (2000) reported that 7,000 to 8,000 tons of mechanically or biologically deteriorated timber piles are currently removed from U.S. Naval facilities annually at a cost of at least \$20 million per year.

2.2.1. Biological Deterioration

2.2.1.1. Fungi

Fungi have the unique capability to break down and utilize wood cell wall material as food (Johnson 2004). Fungi generally attack above the water level where sufficient oxygen allows them to survive and decay the wood. For this reason, foundation piles buried below the water table or ground level are not subjected to decay by typical wood-decay fungi. Fungi decay also depends heavily on temperature and moisture conditions. Shown in Figure 2.1 is the climate index for decay hazard. Iowa has a climate index ranging from 35 to 70. Higher numbers indicate a higher decay hazard (USDA 1999). For fungi to be active and degrade wood, the moisture content of wood has to be 30% or higher (Lopez-Anido et al. 2004). The fungus in an area of decaying wood is generally invisible but present as a growing network of microscopic threads randomly penetrated throughout the wood (Johnson 2004).

There are two major decay fungi recognized: brown-rot, often termed “dry rot” and white-rot. Brown-rot fungi extensively remove cellulose causing the wood to have a brown color, which contributes to cracking across the grain, shrinking, collapse, and crushing into powder (USDA 1999). A danger with brown-rot fungi decay is that wood can lose up to 70% of its modulus of rupture and modulus of elasticity (E) and yet appear visually sound (Lopez-Anido et al. 2004). White-rot fungi removes both lignin and cellulose leaving the wood with a “whiter” than normal color, it does not cause cracks across the grain, and until severely degraded; it retains its outward dimensions and does not shrink or collapse. Soft rot is a third kind of decay with less importance. It is favored by wet conditions and causes softening of the wood. However, its effect is relatively shallow and therefore it is most likely to damage thin pieces of wood (USDA 1999 and U.S. Army Corps of Engineers et al. 2001).

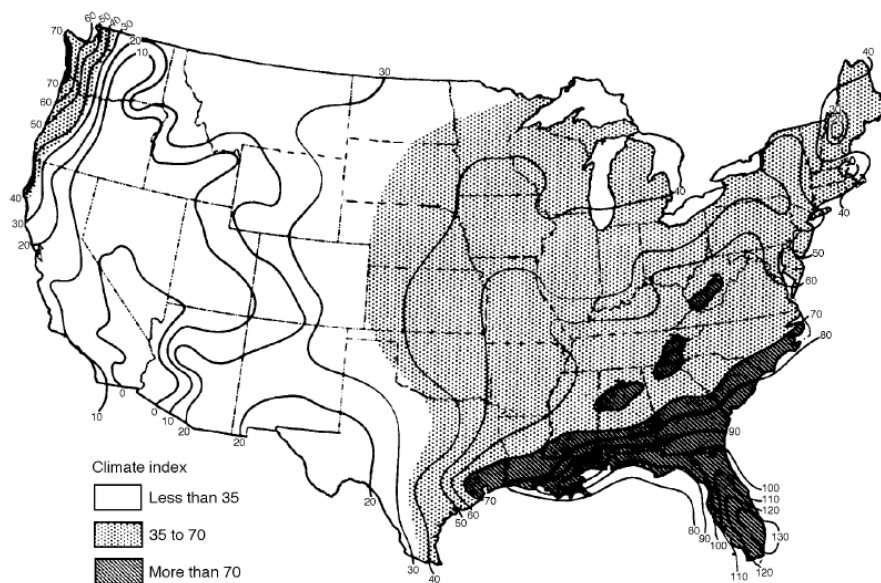


Figure 2.1. Climate index for decay hazard.
Higher numbers indicate greater decay hazard (USDA 1999)

In addition to moduli, decay affects toughness of wood or the ability to withstand impacts which is followed by strength reduction. According to the USDA (1999), by the time 1% of weight loss has occurred in wood by fungal attack, losses in toughness range from 6 to 50%. By the time 10% weight loss has occurred, strength losses are expected to exceed 50%. At this stage, decay is only detectable microscopically; therefore, it may be reasonably assumed that the strength of wood with visual evidence of decay has been greatly reduced. Aggour (1991) reported that the crushing strength of specimens collected from deteriorated piles above the ground level had been reduced by 60%. Furthermore, he also reported that for red pine piles in-service for 85 years, the modulus of rupture, E, and the specific gravity were 32, 27 and 12% lower, respectively, than the published values by ASTM D2555-98 [Standard Test Methods for Establishing Clear Wood Strength Values].

2.2.1.2. Bacteria

Wood that has been wet for a considerable length of time will probably contain bacteria. Bacterial deterioration proceeds slowly compared to fungal decay, and has little effect on wood properties, except over long periods. Bacteria however, can cause softening and make wood excessively absorptive to moisture and preservatives during treatment (Aggour 1991). Bacteria may also destroy preservatives such as creosotes making the wood more susceptible to degradation from less chemically tolerated organisms (USDA 1999).

2.2.1.3. Insects

Out of 26 insect orders, termites, beetles, bees, wasps, and ants are the primary causes of most insect-related deterioration. Insect attack is generally apparent from tunnels or cavities in the wood, which often contain wood powder. In addition to removing portions of the wood structure, insects may also carry decay fungi that further deteriorate wood (USDA 1999).

2.2.2. *Physical Deterioration*

2.2.2.1. Abrasion

According to Manuel (1984), abrasion of timber piles can occur by impact from floating debris and ice in streams. The velocity of water moving past the pile and the quantity, shape, size, and hardness of particles being transported have been linked to the rate of abrasion (U.S. Army Corps of Engineers et al. 2001).

2.2.2.2. Overloading

Overloading of piles can result from continuous heavy loads, infrequent severe loads, loss of the pile structural capacity, or more frequently, complete loss of adjacent supports. Failure of one pile requires the adjacent piles to carry additional load. Overloading can be caused by vertical and/or horizontal loads. Continuous overloading results in several modes of compression failure including splitting of the top portion and misalignment or “mushrooming” at a hollow portion after breakage (USDA 1999). Stages of timber pile deterioration, caused by overloading, are illustrated in Figure 2.2. These stages include development of initial entry holes, active

deterioration of the inner core with significant increase in the size of the hollow space, compression failure of the shell, and finally separation of the hanging top portion of the pile from the pile cap (Buslov and Scola 1991).

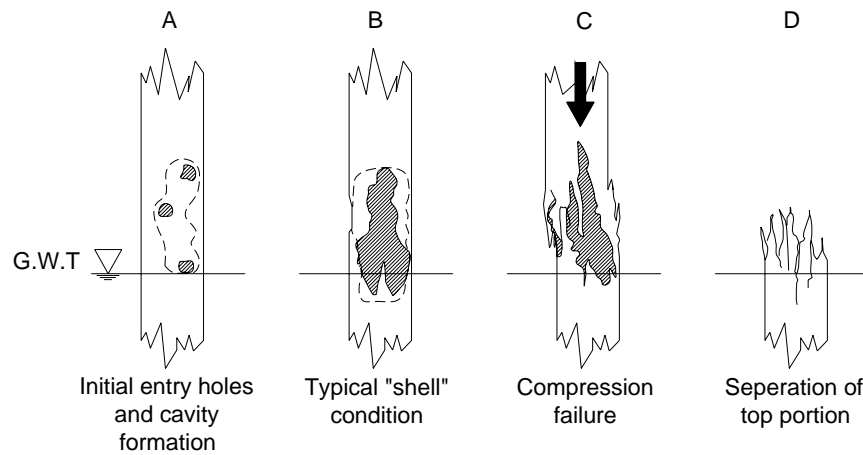


Figure 2.2. Stages of timber pile deterioration by overloading (reproduced from Buslov and Scola 1991)

2.2.2.3. Fire

Wood will burn when exposed to heat and air. Thermal degradation of wood occurs in stages. The degradation process and the exact products of thermal degradation depend upon the rate of heating as well as the temperature. A timber pile has a generally uniform strength throughout its cross section. Thus, the unburned section of the timber pile retains its strength, and its load carrying capacity is reduced in proportion to the loss of cross section. When exposed to high temperatures, wood will decompose providing an insulating layer of char that retards further degradation. Therefore, the amount of charring of a cross section controls the fire endurance of a timber pile (USDA 1999).

2.2.2.4. Other Physical Agents

Other noteworthy physical agents that damage timber piles are connection failure, which exposes untreated wood allowing entry for fungi or insects, ultraviolet (UV) degradation, chemical degradation, and foundation settlement (Manuel 1984).

2.2.3. Mechanical Properties of Wood

Wood may be described as an orthotropic material; that is, it has unique and independent mechanical properties in the directions of three perpendicular axes; longitudinal, radial, and tangential (USDA 1999). The longitudinal axis is parallel to the fiber (grain), the radial axis is normal to the growth rings, and the tangential axis is perpendicular to the grain but tangent to the growth rings (See Figure 2.3).

The wood species typically used to manufacture timber piles in Iowa are shortleaf, longleaf, loblolly or slash. Wood produced from all four species is marketed as Southern Yellow Pine.

Mechanical properties of Southern Yellow Pine are presented in Table 2.1. The reported values were determined by testing small clear specimens in the green and air dried condition.

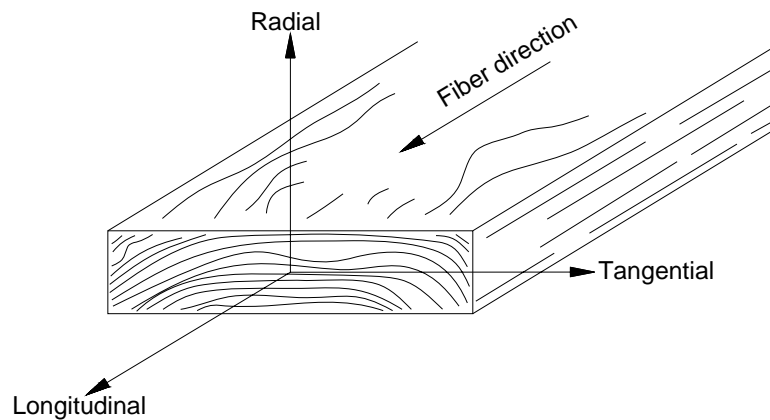


Figure 2.3. Three principal axes of wood with respect to the grain and growth rings (modified from USDA 1999)

Table 2.1. Strength properties of Southern Yellow Pine wood Species (USDA 1999)

Property	Species			
	Shortleaf	Longleaf	Loblolly	Slash
Specific Gravity	0.47	0.54	0.49	0.54
E^a x10⁶ (lb/in²)	1.39	1.59	1.4	1.53
Poisson's Ratio^b	NA	0.332	0.328	0.392
Compression parallel to the grain (lb/in²)	3,350	4,324	3,510	3,820
Compression perpendicular to the grain (lb/in²)	350	480	390	530

a. E was measured using static bending on a span depth ratio of 14/1.

b. Reported values were determined by applying stress parallel to the longitudinal axis and measuring lateral deformation in the radial direction.

2.3. Steel Piles

Steel is used extensively in construction and repair of bridge substructures due to its availability, ease of fabrication, physical and mechanical properties, and designers' experience with it. Most steels are susceptible to corrosion when freely exposed to air and water. According to McCormac (1994), corrosion causes rust, scale, and holes in H-piles which reduce the pile carrying capacity. Overloading is another concern in steel piles which can be evidenced as deformation or compression of a bearing or battered H-pile (U.S. Army Corps of Engineers et al. 2001). Another undesirable property of steel is that its strength may be reduced if subjected to a large number of stress reversals, which obviously would cause a reduction in pile strength. Fire also reduces the steel strength, which makes it susceptible to buckling, abrasion, and under certain conditions brittle fracture (McCormac 1994).

2.4. Concrete Piles

Reinforced concrete is used in bridge substructures due to its durability, strength, and bulk properties. There are many factors that contribute to concrete deterioration. Corrosion of reinforcing steel is considered a major cause of concrete deterioration. Typically, the alkalinity of cement paste protects the steel from corrosion. However, with improper mix designs the alkali film around the reinforcing steel is reduced. With sufficient moisture and oxygen the steel corrodes, and the rust significantly increases in volume. This causes loss of steel-concrete bond, reduction of reinforcement cross section, and cracking and spalling of concrete (Mindess et al. 2003). Alkali aggregate reaction is another cause of deterioration in concrete piles. Poor quality aggregate reacts with alkali cement expanding the aggregate and cracking the concrete (U.S. Army Corps of Engineering et al. 2001). Frost action also contributes to damaging concrete piles. Freezing of water in the cement pores causes difference in ion concentrations, which withdraws water from capillary voids. This causes the cement paste to crack and accelerates pile deterioration. Additional factors such as abrasion wear, overloading, and shrinkage contribute to concrete pile deterioration (Mindess et al. 2003).

2.5. Assessing Integrity of Pile Elements

According to the U.S. Corps of Engineering (2001) there are three levels of inspection. Level I is general visual inspection that involves no cleaning of any structural elements. The purpose of this general inspection is to confirm as-built plans, provide an input for an inspection strategy, and detect any obvious major deterioration, corrosion, or extensive biological decay. Level II inspection is a close-up visual inspection that detects surface damages that may be hidden by surface deterioration, and obtains a limited amount of deterioration measurements. This level of inspection may require surface cleaning. Level III inspection is a highly detailed inspection that normally requires the use of nondestructive testing techniques and partially destructive testing, such as core sampling of timber and concrete structures. The capabilities of each level of inspection are presented in Table 2.2.

2.6. Visual Inspection

Inspection of timber piles is ordinarily done visually (Johnson 2004). Both biological and physical damage can be identified. Hammer soundings will often indicate hidden areas of deterioration. Probing with a moderately pointed tool is also useful in detecting decay (U.S. Army Corps of Engineering et al. 2001 and Manuel 1984). Illustrated in Figure 2.4 and Figure 2.5 are typical biological and physical damages that can be identified during visual inspection.

Visual inspection of concrete piles is performed to evaluate surface conditions such as cracks, pop-outs, and spalls. Unsound concrete just below the surface is usually detected by its hollow sound when tapped with a hammer. Furthermore, rust stains, widths of cracks, and abrasion wear are also detected (Manuel 1984). Figure 2.6 shows typical damage of concrete piles from physical sources that can be observed during visual inspections.

Visual inspection of steel piles generally involves checking for rust and corrosion, especially at

the ground line or splash zone in water crossings. Furthermore, length, size, and location of cracks are carefully noted for future inspections (Manuel 1984).

Table 2.2. Capability of each level of inspection for detecting damage (modified from U.S. Army Corps of Engineering et al. 2001)

Level	Purpose	Detectable Defects		
		Steel	Concrete	Wood
I	General visual to confirm as-built conditions and detect severe damage	Extensive corrosion	Major spalling and cracking	Major losses of wood
		Severe mechanical damage	Severe reinforcement corrosion	Broken piles
				Severe abrasion
			Broken piles	
II	Detect surface defects	Moderate mechanical damage	Surface cracking and crumbling	External pile diameter reduction
			Rust staining	Splintered piling
		Major pitting	Exposed rebar	Loss of bolts or fasteners
III	Detect hidden and imminent damage	Reduced thickness of material	Location of rebar	Internal damage
			Beginning corrosion of rebar	Decrease in material strength
			Internal voids	

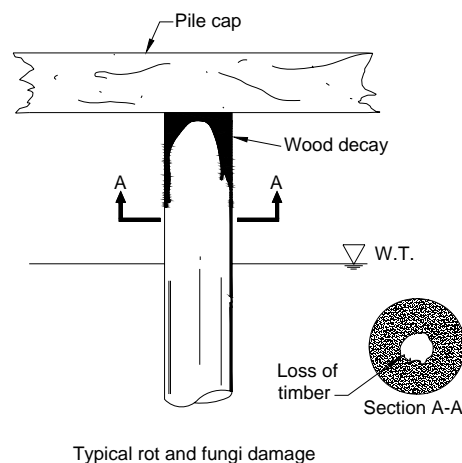


Figure 2.4. Damage to timber piles from biological sources (reproduced from U.S. Army Corps of Engineering et al. 2001)

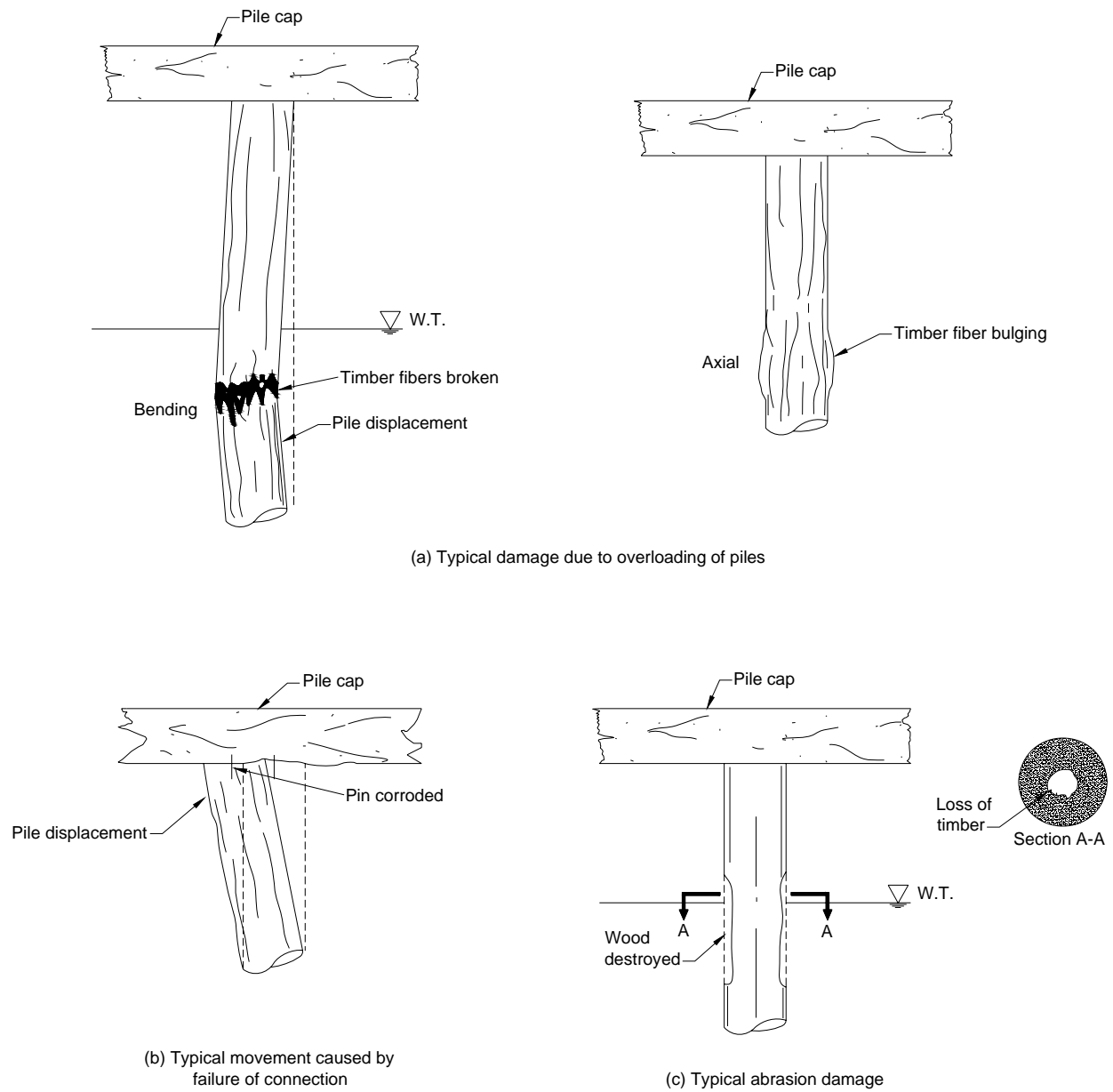


Figure 2.5. Damage to timber piles from physical sources (reproduced from U.S. Army Corps of Engineering et al. 2001)

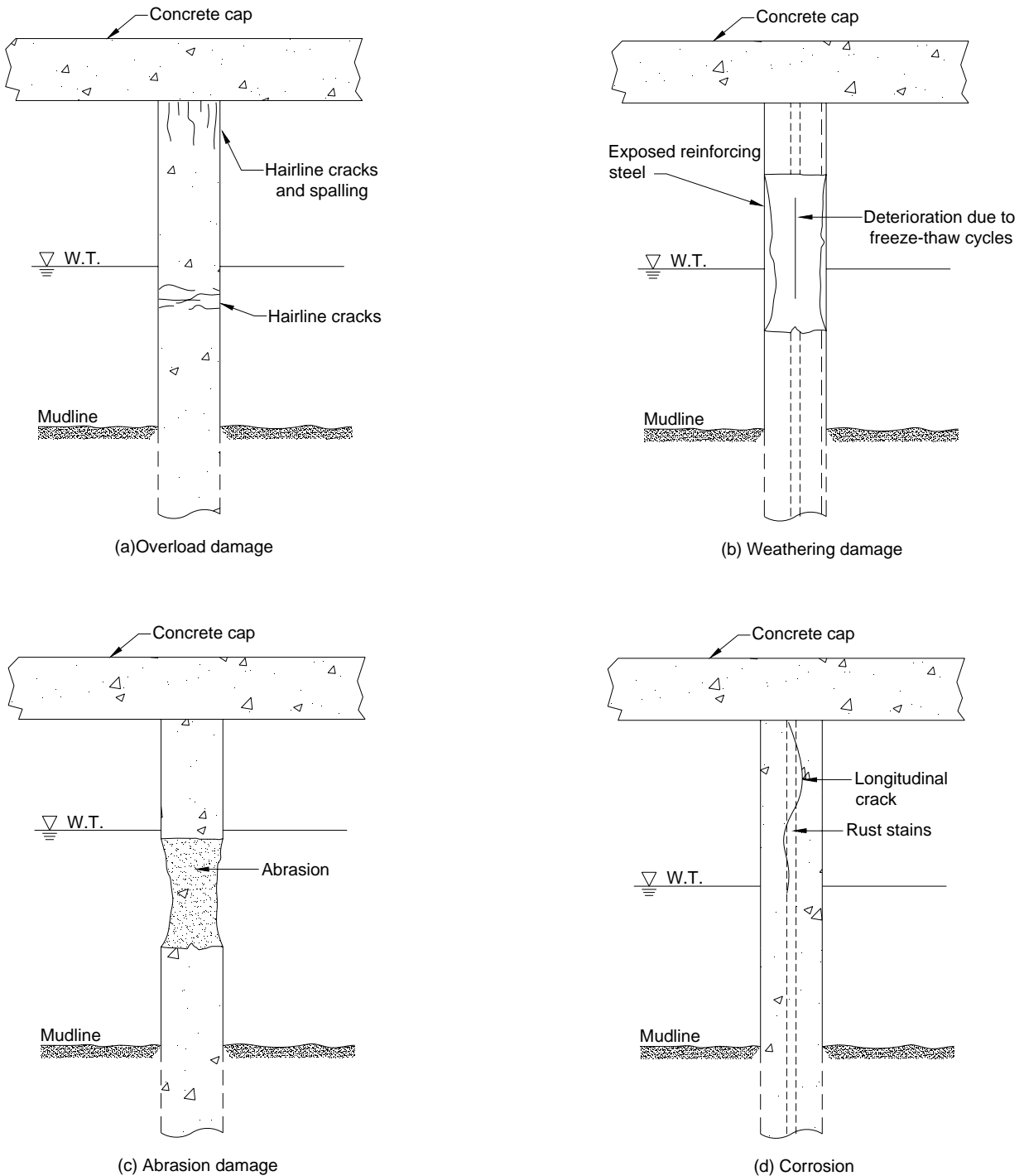


Figure 2.6. Typical damage of concrete piles from physical sources (reproduced from U.S. Army Corps. Of Engineering et al. 2001)

Visual inspection may sometimes be misleading because the extent and effect of decay or loss in cross sectional area can extend internally. For example, a timber pile may be completely decayed internally, whereas its external appearance is adequate (Aggour 1991). Therefore, more advanced techniques are needed for better assessment.

2.7. Nondestructive Testing

Several nondestructive testing techniques (NDT) have been suggested by previous researchers as a means of detecting biological or mechanical damage in piles. NDT for timber is considered the most complex due to timber's biodegradability, inelastic behavior, fibrous composition, porosity, and nonhomogeneity (Seavey and Larson 2002).

2.7.1. Hammer Sounding

Hammer sounding is considered the simplest nondestructive technique. This method has been used for centuries and is still used today. The procedure includes hitting the timber pile with a hammer and determining the quality of sound. A dull or hollow sound indicates deterioration and the need of further advanced investigation techniques whereas a ringing sound indicates that the wood is undamaged (Seavey and Larson 2002). The hammer sounding technique is limited; however, since the assessment of hammer sounding depends on judgment, the deterioration has to be near the pile surface to be detected, and testing can only be done above the water or ground level (Aggour 1991).

2.7.2. Increment Borer

Another rapid technique for evaluating the soundness of wood is probing. An awl or a fine-bladed knife is used to probe the surface of the wood to detect shell rot or other decay near the surface. The depth of penetration of the probe into the wood is an indication of its soundness. An increment borer can also be used as a diagnostic tool to detect decay near the pile core by extracting a small like dowel specimen from the timber pile (Seavey and Larson 2002).

2.7.3. Stress Wave Timing

Stress waves are generated from an impact on the surface of the material under investigation. The stress waves propagate at the speed of sound through the material and reflect from external surfaces, internal flaws, and boundaries between adjacent materials (Emerson et al. 1999). By measuring the wave transmission time through a pile in the radial direction, the internal condition of the pile can be evaluated fairly accurately. This measured time, when converted to a transmission time on a per length basis or wave propagation speed, can be used as a predictor of the internal condition of the pile (Wang et al. 2004). The concept of stress wave timing for detecting internal decay in piles is presented in Figure 2.7.

A stress wave is induced by striking the pile with an impact device that is instrumented with an accelerometer emitting a start signal to a timer. As the stress wave propagates through the pile, a second accelerometer held in contact at the opposite side of the pile sends a stop signal to the timer. The elapsed time of the stress wave propagation between the accelerometers is displayed on the timer (Ross et al. 1999). Stress wave propagation times for various species of nondegraded wood in the radial direction are presented in Table 2.3.

Stress wave velocities can be determined from the stress wave propagation time and used to evaluate the pile element. According to Aggour (1991), the condition of the pile can be

estimated according to the wave velocity. For example, Table 2.4 which relates the wave velocity to the pile condition, was developed for yellow southern pine piles. A velocity of 3,000 ft/sec perpendicular to the grain indicates that the pile is in a poor condition. When no velocity reading is obtained, the pile probably has a large internal decay area.

There are three arrangements possible when using the stress wave timing equipment: a direct transmission arrangement in which the transducers are facing each others across the section of the material tested, a semi direct transmission in which the two transducers are facing each other but at different elevations, and finally an indirect transmission with both transducers at the same surface (Aggour 1991).

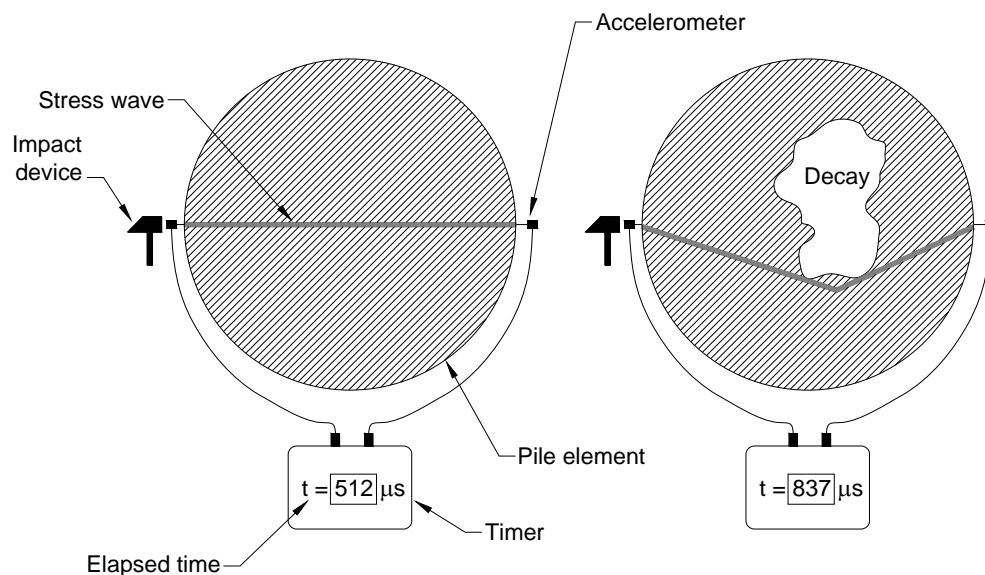


Figure 2.7. Concept of stress wave timing for detecting internal decay (modified from Wang et al. 2004)

Table 2.3. Stress wave transmission time for various species of nondegraded wood (modified from Wang et al. 2004)

Species	Radial stress wave transmission time	
	$\mu s/ft$	$ft/\mu s \times 10^{-3}$
Douglas-fir	230-337	4.4-2.9
Fir	261-335	3.8-3.0
Larch	228-298	4.4-3.4
Pine	266-286	3.8-3.5
Spruce	281-327	3.6-3.1

Table 2.4. Pile condition criteria for Southern Yellow Pine (Aggour 1991)

Wave velocity*, V_N ft/sec	Pile condition
5500 and higher	Excellent (new)
4500-5500	Very good (new)
4000-4500	Good
3500-4000	Average
3000-3500	Questionable
Less than 3000	Poor

*Wave velocity measured perpendicular to the grain

In addition to pile defects, the moisture content of the pile can affect the stress wave travel time. It is reported by Ross et al. (1999) that at moisture contents less than approximately 30%, the wave propagation time decreases with decreasing moisture content. Adjustment factors are therefore used to correct the propagation time (See Table 2.5) and are sensitive to temperature as well. At moisture contents greater than 30%, little or no change in the propagation time occurs; therefore no adjustment factors are needed.

The sensitivity of the stress wave timing technique is limited. A single stress wave measurement can only detect internal decay that is above 20% of the total cross section of the pile. Therefore, it is recommended to conduct multiple measurements in different orientations at the same cross section to increase the test reliability (Wang et al. 2004).

Table 2.5. Stress wave transmission time adjustment factors for Douglas-fir (Ross et al. 1999)

Moisture content (%)	Adjustment factors			
	0°F (-18°C)	38°F (3°C)	80°F (27°C)	120°F (49°C)
1.8	0.94	0.95	0.97	0.98
3.9	0.95	0.96	0.98	0.99
7.2	0.93	0.98	1.00	1.01
12.8	0.97	0.99	1.00	1.01
16.5	0.99	1.01	1.03	1.05
23.7	1.05	1.07	1.09	1.14
27.2	1.07	1.10	1.12	1.17

2.7.1.2. Dispersive Wave Propagation

Chen and Kim (1997) stated that dispersive wave propagation is a technique which considers how wave motion in solid materials is affected by the mechanical properties and geometry as may be caused by deterioration or change in cross sectional area. A disturbance, or wave, in a solid material with bounded surfaces continuously changes its shape and elongates as time passes and thus a single speed cannot be determined. This phenomenon is known as dispersion. The dispersive wave propagation method is reportedly an excellent nondestructive technique to determine the degree of hollowness in piles. In short, this technique generates surface and

transverse wave groups traveling along the length of the pile due to a transverse strike to the side of the pile. The dispersive surface waves and transverse waves generated contain most of the energy put into the signal and are the easiest to record and study (Stegman and Holt 2000).

Dispersive waves in materials, which have linear stress-strain diagrams, can be represented mathematically as the algebraic sum of numerous separate frequencies, each traveling at its own velocity (Stegman and Holt 2000). As they travel through a solid, the frequencies reflect and refract from internal boundaries (e.g. pile tip or significant fractures or breaks). Thus, analyzing a dispersive wave to determine the distance to the pile tip, or to determine the location of a significant fracture or break, becomes the problem of determining the individual wave speeds of individual frequencies and determining the time needed for each to travel to, and reflect from, one of those boundaries (Stegman and Holt 2000).

Dispersive wave propagation tests are conducted by temporarily attaching accelerometers at selected locations on the pile's exposed surface and applying a strike impulse at various potential positions. A schematic for such a field test setup is illustrated in Figure 2.8

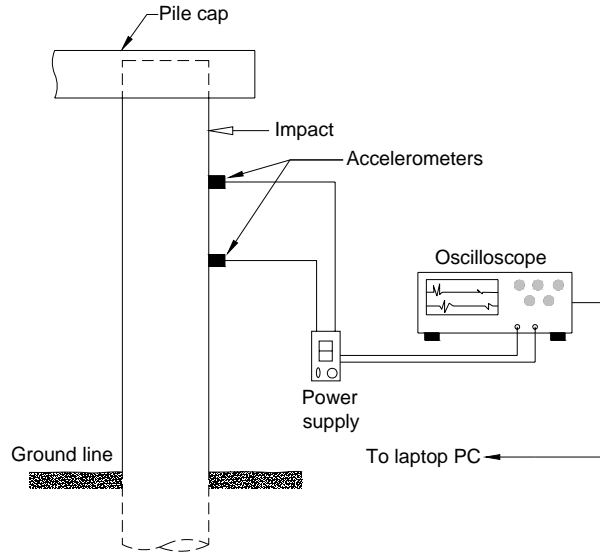


Figure 2.8. Dispersive wave propagation field test setup

According to Chen and Kim (1997), the wave propagation analysis can be done using the short kernel method (SKM). Holt et al. (1994) stated that a single value of the SKM at a particular frequency can be calculated using Equation 1.1. The SKM is calculated at selected intervals resulting in a plot with positive and negative peaks. The first significant positive peaks in the SKM plot are used to calculate a phase velocity using Equation 2.1.

$$SKM(j,k) = \sum_{i=1}^{N_2-N_1} f(\tau_i) \cdot g[(\tau_i + j \cdot \Delta t), k] \cdot \Delta t \quad (2.1)$$

Where $SKM(j,k)$ is j^{th} term of the cross-correlation currently being performed at the k^{th}

frequency, f is the time record from one accelerometer, g is the fragment of kernel used to perform the cross correlation, N_2 is the number of data points in f , and N_1 is the number of data points in g .

$$V_p = \frac{G_L}{N_{pts} \cdot \Delta t} \quad (2.2)$$

Where V_p is the phase velocity, G_L is the length separating the accelerometers, N_{pts} is the number of data points between the first two significant peaks in the SKM plot, and Δt is the time step at which the time records were stored originally.

Based on their findings, Chen and Kim (1997) proposed the following equation to determine the degree of hollowness in a pile.

$$H = A \cdot V_p^2 + B \cdot V_p + D \quad (2.3)$$

Where H is percentage of hollowness, V_p is SKM wave speed, and A , B , and D are real scalars determined by a curve fitting procedure.

Chen and Kim (1997) also reported that the wave variation between the first and the return pass maybe able to disclose the structural integrity in the region between the accelerometers and the pile tip. It was found that a speed reduction in the return pass is analogous to a severely damaged pile, and can range from 28 to 35%.

2.8. Determining Length of In-Service Piles

An essential part of pile inspection is to determine its overall length after years of service. This determines whether a pile is still able to support a structure safely (Holt et al. 1994).

Determining the length of timber piles is of particular importance because most timber piles in use today were installed years ago and there are no as-built records of their installation. There are several nondestructive techniques which can be used to determine the pile length. Some of those techniques are discussed below.

2.8.1. Surface Methods

Nondestructive surface methods are applied to an accessible surface of the foundation element. Therefore, the pile is used directly as the medium for transmitting the acoustic energy.

2.8.1.1. Bending Wave Method

Several types of stress waves are generated whenever a solid with bounded geometry is struck. The waves include compression, shear, surface, and bending waves. The bending wave method uses flexural (bending) waves to determine the unknown depth of the piles. Bending waves are highly dispersive and decrease with increasing wavelength with most of the velocity decrease occurring at wavelengths longer than the pile diameter (Olson et al. 1998).

This method involves striking the side of the pile which is useful in cases where the pile head is inaccessible. The bending wave method is limited to timber piles, concrete piles, and drilled shafts that extend above the water or ground level. Bending wave tests for driven H-piles is expected to show higher attenuation of wave energy as compared to timber and concrete piles (Wightman et al. 2003).

Striking a pile transversely to its longitudinal axis creates two separate sets of bending waves. One set travels upward toward the pile head where it is reflected and sent downward along the pile. The second wave set travels towards the pile toe (Holt et al. 1994). The wave propagations are monitored by two horizontal accelerometers mounted on the same side of the pile from the impact (Refer to Figure 2.8). As the waves pass the accelerometer locations, wave speeds and travel time are recorded, and from these records the travel distance can be calculated (Olson et al. 1998).

Since bending waves are highly dispersive, the SKM processing signal technique discussed previously is used to determine the pile length. The mathematical basis of determining the pile length is given by Equation 2.4.

$$OL = T_b + \frac{V_p \cdot N_{pts} \cdot \Delta t}{2} \quad (2.4)$$

Where OL is the pile overall length, T_b is the distance from the head to the particular transducer being used for computation, V_p is the phase velocity from Equation 2.2, N_{pts} is the number of data points between the first two significant peaks in the SKM plot, and, Δt is the time step at which the accelerometer records were stored.

Previous studies have determined that pile length predictions can be achieved with an accuracy of $\pm 10\%$ (Anthony and Pandey 1996). Holt et al. (1994) used the bending wave method to estimate the pile length for 16 timber piles. The difference between the computed and the measured pile lengths ranged from -10.8% to +6.7%. The negative percentage implies that the lengths calculated were too short and the positive percentage implies that the computed lengths were too long.

Factors affecting the overall length calculations include soil confinement, pile condition, and the effect of tapered piles on wave speeds (Holt et al. 1994). This method provides a quick and economical means to estimate the pile length. However, this method cannot be used for H-piles because of higher attenuation of wave energy. In addition, this method requires complex interpretations, stiff soil layers can result in short pile length prediction, and reflection from the top of the grade may be present in the recorded data resulting in false interpretations (Wightman et al. 2003 and Rausche 2004).

2.8.1.2. PS/CPT

PS/CPT is a recently developed system which combines testing of the soil near the foundation using the functions of a Cone Penetration Test (CPT), and evaluation of the unknown bridge foundation using the functions of Parallel Seismic testing (PS) system. Parallel seismic testing is

normally performed with a transducer in a cased borehole drilled next to the foundation. This method is described in more details by Sack et al. 2004.

The standard CPT system can be modified to add the capability for PS testing. A special seismic piezocone incorporating a transducer (geophone or accelerometer) into the body of the cone, which is used to record the wave energy from the PS test impacts at a series of depths throughout the insertion of the cone probe (Sack et al. 2004).

Impacting the exposed pile vertically or horizontally generates compression or bending waves, which travel down the pile which are transmitted into the surrounding soil and received by the transducer in the cone probe. The new system benefits from the accuracy of the PS test in measuring depths of inaccessible piles and does not require casing or pre-drilling (Sack et al. 2004).

Site conditions must be suitable for CPT. Sites with shallow rock or boulders are not suited for this type of testing. Furthermore, sites with homogeneous soil profiles especially near the pile tip improve the accuracy of this method (Sack et al. 2004).

2.8.1.3. Pile Integrity Method

This method is based on impacting the pile head and measuring the time for the reflected stress wave to reach an accelerometer. The pile integrity method can estimate the length of the pile within approximately 15% of the actual length (Wightman et al. 2003). This method uses a compression wave rather than the flexural waves used in the bending wave method. There are two methods for interpreting the measured data: (1) the Sonic Echo method which uses the time domain method, and (2) the Impulse Response method which uses the frequency domain method (Wightman et al. 2003 and Brooks and Burk 1994). The impulse response method is also referred to as the Transient Response Method. When the pile head is inaccessible, an arrangement similar to the one shown in Figure 2.9 is possible. A large nail is inserted into the pile and struck with a hammer to generate stress waves in the pile. This nondestructive testing technique has been standardized by ASTM D5882-95 [Standard Test Method for Low Strain Integrity Testing of Piles].

Sonic echo data can be used to determine the length of the pile based on the time difference between the first arrival and the first reflection or between two consecutive reflections according to the following equation (Wightman et al. 2003).

$$L = V \times \frac{\Delta t}{2} \quad (2.5)$$

Where L is pile length, and V is velocity of compression wave

The compression wave speed is also a function of the pile material properties. Massoudi and Teferra (2004) and Townsend et al. (1996) reported the following relationship.

$$V = \sqrt{\frac{E}{\rho}} \quad (2.6)$$

Where E is modulus of elasticity, and ρ is mass density

For best results, it is important to know the velocity in the pile element. Velocity in concrete piles varies based on aggregate type and age of structure, while velocity in timber piles varies depending on the moisture content (Brooks and Burk 1994). It is estimated that a “wet” velocity is approximately 90% of the “dry” velocity. A source placed at a measured distance from a sensor along the side of the pile can be used to approximate the velocity (Wightman et al. 2003).

The Impulse Response data is also used to determine the pile length using Equation 2.7.

$$L = \frac{V}{(2 \times \Delta f)} \quad (2.7)$$

Where Δf = distance between two peaks or between zero frequency and the first peak on the velocity verses frequency plot.

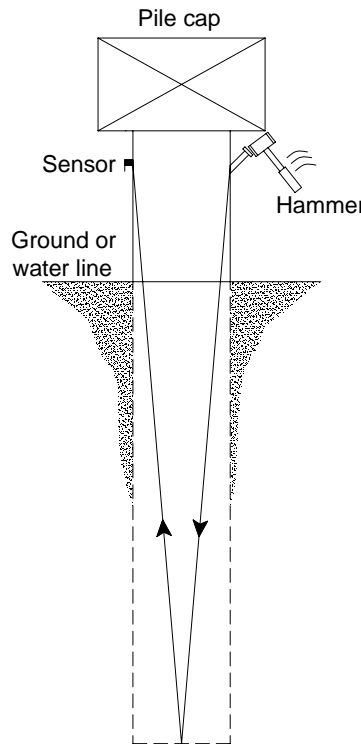


Figure 2.9. Hammer impact and sensor location for inaccessible pile head (reproduced from Brooks and Burk 1994)

The quality of the pile integrity method depends on the operator’s experience as well as pile surface preparation and sensor attachments (Anthony and Pandey 1996). Furthermore, piles in stiff soils will have no identifiable bottom echo due to excessive dampening (Olson et al. 1998). Excessive dampening is even more substantial in H-piles due to their higher surface areas. A

bottom reflection is also not possible if the pile is socketed in bedrock of similar stiffness (Massoudi and Teferra 2004). In cases where the superstructure is connected to the substructure, pile toe reflections may be “masked” by superstructure reflections and damping of the stress wave complicating the data interpretation (Wightman et al. 2003 and Townsend et al. 1996).

2.8.2. Borehole Methods

These nondestructive testing methods require an accessible borehole close to the foundation in question.

2.8.2.1. Parallel Seismic Test

The parallel seismic testing (PS) method is a nondestructive borehole method which uses parallel seismic theory to determine the depth of concrete, timber, and steel piles (Townsend 1996). This method can be used when pile heads are not accessible or when the piles are too long and slender (Wightman et al. 2003). This method requires drilling of a 2 to 4 inch borehole close to the pile (Preferably within 5-7 ft). The borehole must extend beyond the estimated depth of the pile for 5-15 ft. If the borehole is shorter than the pile length, the test will only indicate a minimum length (Sack et al. 2004). The borehole is normally lined with plastic tube to retain water as an acoustic couplant. If a hydrophone is used as the receiving probe, the borehole must be filled with water. The borehole must be dry if a geophone, which is the preferred method, is used. The void between the soil and the borehole casing ideally must be cement grouted for best results with geophones (Townsend et al. 1996).

The receiving probe is placed inside the borehole at the top and the structure is struck as close to the head of the foundation as possible with the trigger hammer. The signals from the hammer and the receiver are recorded on a data acquisition system (Davis 1995). The probe is then lowered in uniform increments and the time required for each impact wave to reach the hydrophone is determined graphically for successive hydrometer depths (Townsend et al. 1996 and Olson et al. 1998). The principle of the parallel seismic test is illustrated in Figure 2.10a.

The speed of wave propagation in most granular or fine grained soils is typically 2 to 12 times slower than the speed of wave travel in concrete and timber and 3 to 16 times slower than the speed of wave travel in steel. This difference in the speed of wave propagation is required for the test to be successful. Note that some types of shale, granite, and sandstone have wave propagation speeds similar to that of concrete, timber, and steel (Davis 1995). Since the effect of the soil between the pile and the borehole is constant, the time for the signal to be received increases with depth (Figure 2.10b). When the hydrophone passes the pile tip, the time for the signal to be received will increase at a higher rate due to the effect of the lower velocity of the intervening soil. The lines linking the signal arrival points on the graph will show a distinct deflection at the pile tip. Therefore, the depth where a change in slope occurs is taken as the pile depth (Olson et al. 1998).

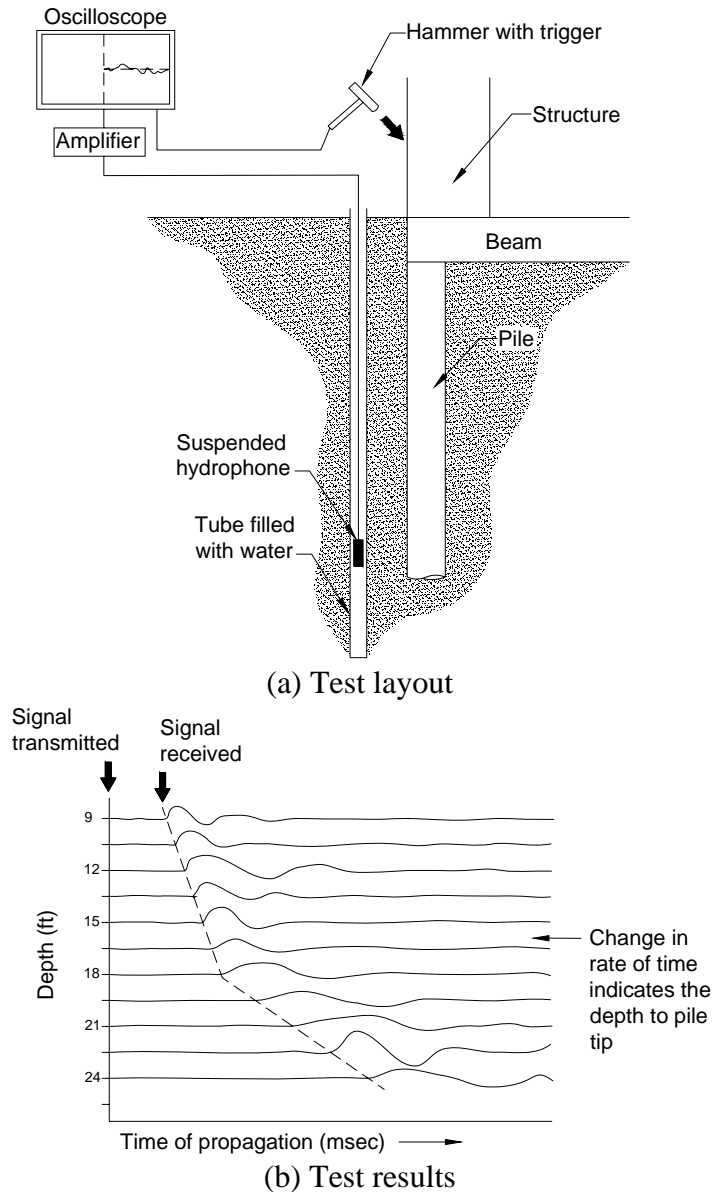


Figure 2.10. Principle of parallel seismic test (reproduced from Davis 1995)

Rausche (2004) reported that the PS method is more accurate and more versatile than other nondestructive surface techniques for determining the unknown pile length since results are not dependant on an assumed wave speed. The accuracy of the method depends on the variability of the velocity in the surrounding soil (Wightman et al. 2003). Typical accuracies of the PS test are 5%. However, when the inflection point is difficult to see, the accuracies are closer to 10% (Sack et al. 2004)

Again, this method is not effective for embedded pile lengths greater than 30 ft since the impact wave may be dampened out prior to reaching the hydrophone (Townsend et al. 1996). Moreover, mechanical splices complicate the interpretation and limit the success of the test. As the borehole moves away from the pile, interpretation of the data becomes more difficult and the

uncertainty of depth determination increases. Therefore, this method is limited to bridge sites where the borehole can be drilled close to the foundation piles (Wightman et al. 2003).

2.8.2.2. Borehole Radar

This method uses a ground penetrating radar (GPR) antenna lowered to a borehole with a PVC casing to obtain reflection echoes from the pile for determination of both depth and geometry. An antenna transmits radar waves into the soil, and a receiver records reflections from interfaces with different dielectric constant (Wightman et al. 2003). An illustration of the borehole radar system is shown in Figure 2.11

For an unknown pile length, the radar wave will be reflected from the pile until the pile toe is reached. There will be no reflections beneath the pile toe except from those produced by geologic conditions (Wightman et al. 2003).

This method will not work with a steel casing. In addition, the depth of penetration is significantly affected by electrical conductivity of the surrounding rocks and soils. Drilling the borehole as close to the pile as possible will improve the efficiency of this method in conductive materials (Wightman et al. 2003).

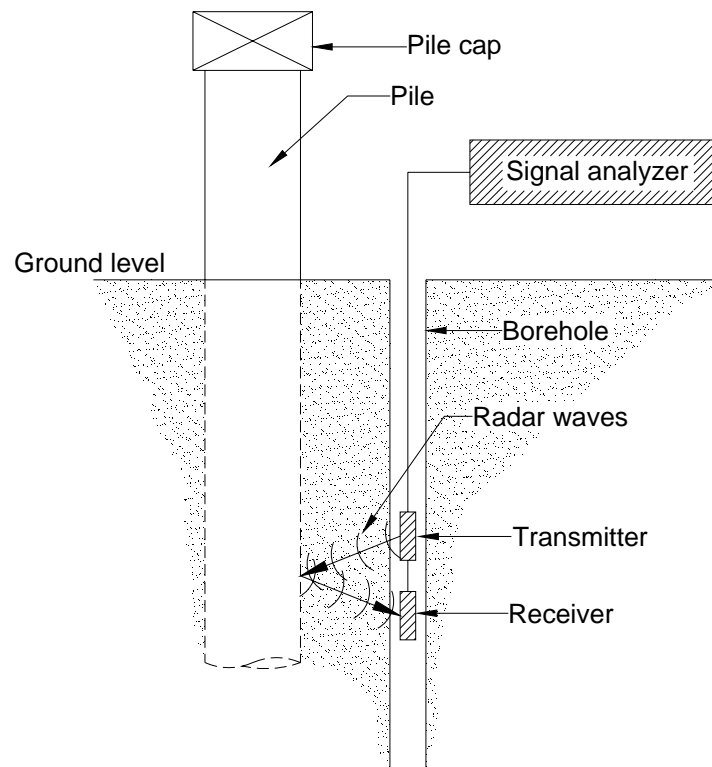


Figure 2.11. Borehole radar system (reproduced from Wightman et al. 2003)

2.8.2.3. Cross-borehole Seismic Tomography

This nondestructive method provides a two-dimensional or a three-dimensional tomography which can be used for high resolution imaging of the foundation between boreholes (Wightman et al. 2003). Cross-hole velocity tomography surveys are conducted by pairing a seismic source in one borehole and a string of receivers in an adjacent borehole. The source is systematically moved from bottom to top in constant intervals. This procedure is repeated until all possible source-receiver combinations are incorporated (see Figure 2.12). Piles within the surveyed area are indicated in the tomograms as relatively higher seismic velocity zones than the surrounding soils (Wightman et al. 2003).

According to Wightman et al. (2003) this method is data intensive and specialized three-dimensional analyses software is needed for true 3-dimensional imaging.

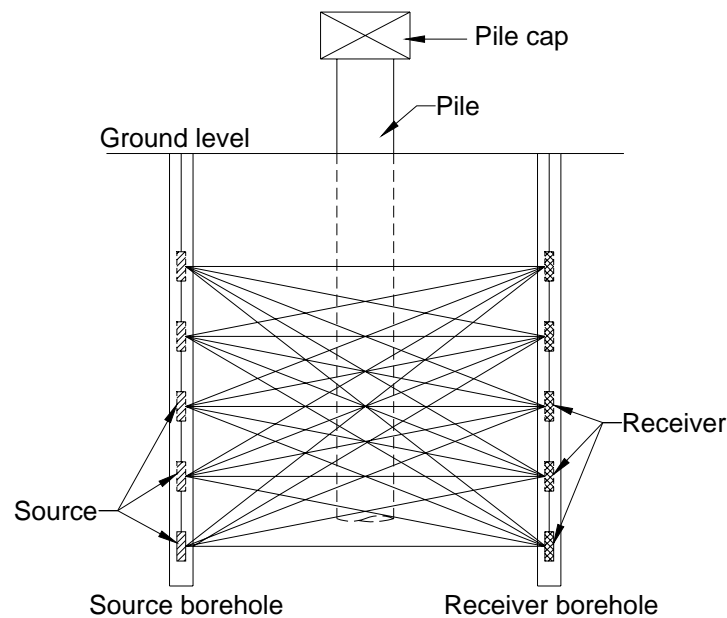


Figure 2.12. Tomographic survey design (reproduced from Wightman et al. 2003)

2.8.2.4. Induction Field

The induction field method is used for the determination of unknown depth of steel and continuously reinforced concrete piles. An AC current is induced into a steel pile or the rebar in a reinforced concrete pile from which the current couples into the subsurface and finally to a return electrode. The return electrode can be another pile, or it can be a piece of rebar driven into the ground. A magnetic field is generated alongside the pile, which is detected using a search coil (detector) in a borehole drilled close to the pile (Olson et al. 1998). The borehole must have a PVC casing. No signal is received if a steel casing is used. As the depth of the search coil increase, the induced voltage decreases linearly down the length of the pile. By plotting the magnitude of the induced voltage versus the depth of the search coil, an indication of the pile length is provided (Wightman et al. 2003). A schematic of the induction field method setup is presented in Figure 2.13.

The basic limitation of this method is that the pile element must contain electrically conductive materials along its entire length. Therefore, this method can not be applied to timber piles. Furthermore, data interpretation can be complicated by the existence of conductive materials in the surrounding soil including water (Olson et al. 1998).

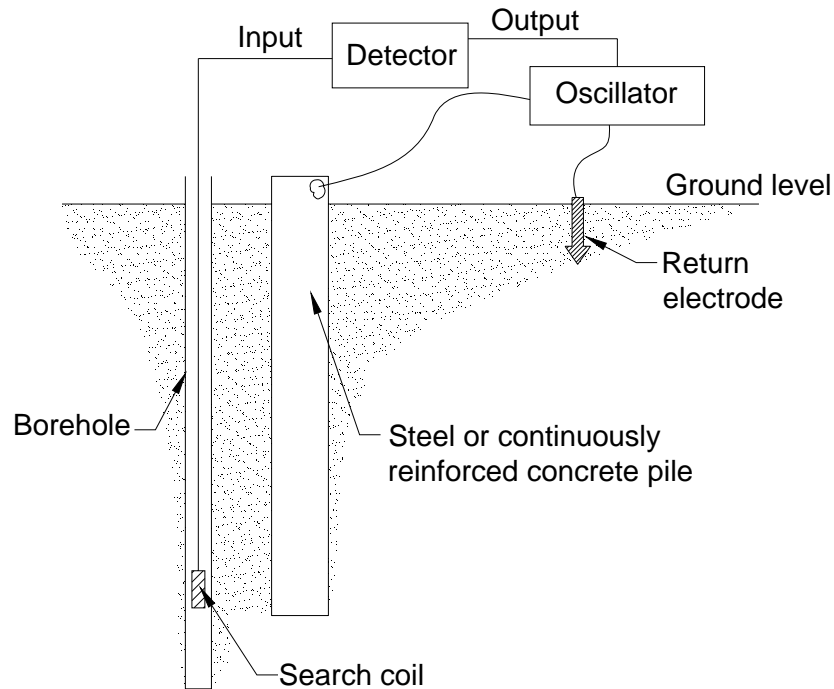


Figure 2.13. Induction field method setup (reproduced from Olson et al. 1998)

2.9. Determination of Pile Strength

The most important factors in determining the strength of a timber pile are the wood species and the amount of deterioration. Typical strength values for nondegraded wood are published by ASTM D2555-98 [Standard Test Method for Establishing Clear Wood Strength Values] and by the USDA (1999). Table 2.6 summarizes some of the reported compressive strength values.

The stress wave transmission time through timber is influenced by the degree of internal decay, moisture content, and temperature as discussed previously. Therefore, stress wave transmission can be used as an indication of the residual strength of timber piles. Ross et al. (2001) designed a pilot study to examine the relationship between stress wave transmission time and residual compressive strength of timber. It was reported that there is a linear relationship between stress wave transmission time and compressive strength. Therefore, specimens with long transmission time have low load carrying capacity. Table 2.7, which was prepared for eastern white pine specimens, presents the relation between stress wave transmission times and compressive strength. These results agree with the visual assessment of the specimens.

Wang et al. (2004) reported that a 30% increase in stress wave transmission time implies that the strength has been reduced by 50%. A 50% increase in time indicates severely decayed wood.

Table 2.6. Strength properties of various species of timber (from USDA 1999 and ASTM D2555-98)

Common species name	Property					
	Specific gravity		Compression parallel to grain (lb/in ²)		Compression perpendicular to grain (lb/in ²)	
	ASTM	USDA	ASTM	USDA	ASTM	USDA
Pine:						
Eastern white	0.35	0.34	2,440	2,440	218	220
Jack	0.40	0.40	2,950	2,950	296	300
Lodgepole	0.39	0.38	2,610	2,610	252	250
Ponderosa	0.39	0.38	2,450	2,450	282	280
Red	0.42	0.41	2,730	2,730	259	260
Sugar	0.34	0.34	2,459	2,460	214	210
Western white	0.35	0.35	2,434	2,430	192	190
Douglas-fir:						
Coast	0.45	0.45	3,784	3,780	382	380
Interior West	0.46	0.46	3,872	3,870	418	420
Interior North	0.45	0.45	3,469	3,470	256	360
Interior South	0.43	0.43	3,113	3,110	337	340

Table 2.7. Stress wave transmission times and compressive properties for eastern white pine timber (Ross et al. 2001)

Specimen no.	Stress wave transmission time ^a (ft/μs x 10 ⁻³)	Compressive stress (lb/in ²)	Visual assessment of specimen condition
1	4.6	562	Sound
2	4.7	533	Sound
3	4.8	543	Sound
4	4.0	465	Sound
5	1.9	170	Center severely deteriorated
6	0.8	-	Severely deteriorated ^b
7	0.5	-	Severely deteriorated ^b
8	0.3	-	Severely deteriorated ^b

a. Transmission time measured parallel to the grain

b. Specimen fell apart during preparation of static testing

2.10. Pile Maintenance Practices

Ritter (1992) divided pile maintenance activities into three categories. The first category is preventative maintenance, in which the repair involves keeping the structure in a “good state”. At this stage, deterioration has not started, but the conditions or potential are present. The second category is early remedial maintenance. At this stage, deterioration is present; however, the

capacity or performance of the structure is not affected. More severe damage is imminent unless corrective action is taken. The last category is major maintenance, which involves immediate corrective measures to restore the structure to its original condition.

2.10.1. Preventative Maintenance

The simplest preventative maintenance for timber piles is moisture control. Moisture control can be used as an effective technique to extend the service life of many timber piles. When exposure to moisture is reduced, timber piles will dry to moisture contents below that required for fungus and insect growth (Ritter 1992 and Seavy and Larson 2002).

In-place treatment is another common preventative maintenance technique applied to timber piles. Surface treatments and fumigants are two types of in-place treatment that are frequently used.

2.10.1.1. Surface Treatments

According to Ritter (1992), surface treatments are applied to newly exposed, untreated wood to prevent decay or supplement the initial treatment. Surface treatment is most effective when applied before decay starts. It is commonly used for treating checks, splits, delaminations, or mechanical damage. Creosote heated to 150 to 200 °F is the most common preservative used for surface treatments. The effectiveness of surface treatments depends on the thoroughness of application, wood species, size, and moisture content at the time of application. Wet wood absorbs less preservative than dry wood. It is recommended that surface treatments be systematically reapplied at 3 to 5 years intervals to ensure adequate protection. One limitation of the surface treatment is the shallow penetration which limits their effectiveness against internal decay.

2.10.1.2. Fumigants

Fumigants are preservative chemicals in liquid or solid form that are placed in prebored holes to terminate internal decay. The fumigants volatilize into toxic gases that move through the wood eliminating decay and insects. Fumigants are able to diffuse for 8 ft or more from the point of application. To be more effective, the fumigant must be applied to sound wood. When applied to very porous wood, some of the fumigant can be lost to the atmosphere by diffusion. Some fumigants can remain effective for 10 to 15 years but will eventually diffuse out of wood allowing fungi to recolonize. Therefore, treatments must be made at regular intervals (Ritter 1992).

2.10.1.3. Repair Small to Medium Cracks

Small to medium cracks and splits caused by weathering or shrinkage create pathways for decay fungi to enter the untreated wood at the core of the timber pile (Emerson 2004 and U.S. Army Corps. of Engineers et al. 2001). Therefore, cracks and splits must be repaired regularly.

Epoxy grout can be injected under pressure for filling checks and splits. The epoxy seals the

affected area preventing water and other debris from entering. It can also restore the bond between separated sections, increase shear capacity, and reduce further splitting. Low viscosity epoxy is injected to fill the void, which is then sealed using a sealing epoxy (U.S. Army Corps of Engineers et al. 2001 and Ritter 1992).

2.10.2. Remedial Maintenance

Once wood decay has begun, it tends to grow exponentially. Often the damage caused by decay is localized around the wet-dry area near the water level, which can cause strength reduction. Restoring strength of the pile elements by repairing the damaged portion can be achieved by many techniques (Purvis 1994).

2.10.2.1. Posting/Splicing

This method is used for repairing timber piles that are deteriorated at or above the ground level. The method involves cutting out the deteriorated section and replacing it with a new timber treated section. No more than half the piles in a bent should be repaired using this method.

A Timber strut is installed to support the hydraulic equipment needed to lift the pile cap. The old section is cut below the damaged, rotted, or insect infested area. The new pile section is then placed at the same location as the original pile (Avent 1989). Splicing can be done using concrete jackets as shown in Figure 2.14a. There should be a minimum cover of 6 inches around the pile. Using concrete jackets as a splicing method greatly enlarge the pile diameter which could cause flow restrictions on the waterway (Wipf et al. 2003a).

Timber fishplates can also be used as a splicing technique as shown in Figure 2.14b. If timber fishplates are used, they must be treated and bolted to the pile using galvanized bolts. All ends and cuts must be treated (Wipf et al. 2003a and U.S. Army Corps of Engineers et al. 2001). There is difficulty in providing full load transfer using mechanical connectors in wood. Furthermore, the flexural stiffness of the pile is usually greatly reduced, and the mechanical connections are subject to corrosion (Avent 1989).

Another technique was developed for pile splicing using epoxy as a bonding agent. The procedure consists of cutting out the deteriorated section and replacing it with a new treated pile section. The butt ends of the old and new pile sections are epoxy grouted to produce a permanent bond. The new section is positioned with a 1/8 to 1/4 inch gap and wedged tightly against the existing pile cutoffs. Holes are drilled at a steep downward angle above the joints for steel pins and spaced 90 degrees apart. Steel pins are driven through the holes, and the joints are filled and sealed with epoxy gel (Figure 2.15) (Ritter et al. 1992). This method has proven to be economical and effectively restores the original ultimate compressive strength and axial stiffness of deteriorated piles. The ultimate flexural strength however may be reduced by 50 to 75% (Avent 1989 and Purvis 1994). This method works best when a few piles need repair. In addition, the cause of damage must be determined and remedied before using this method.

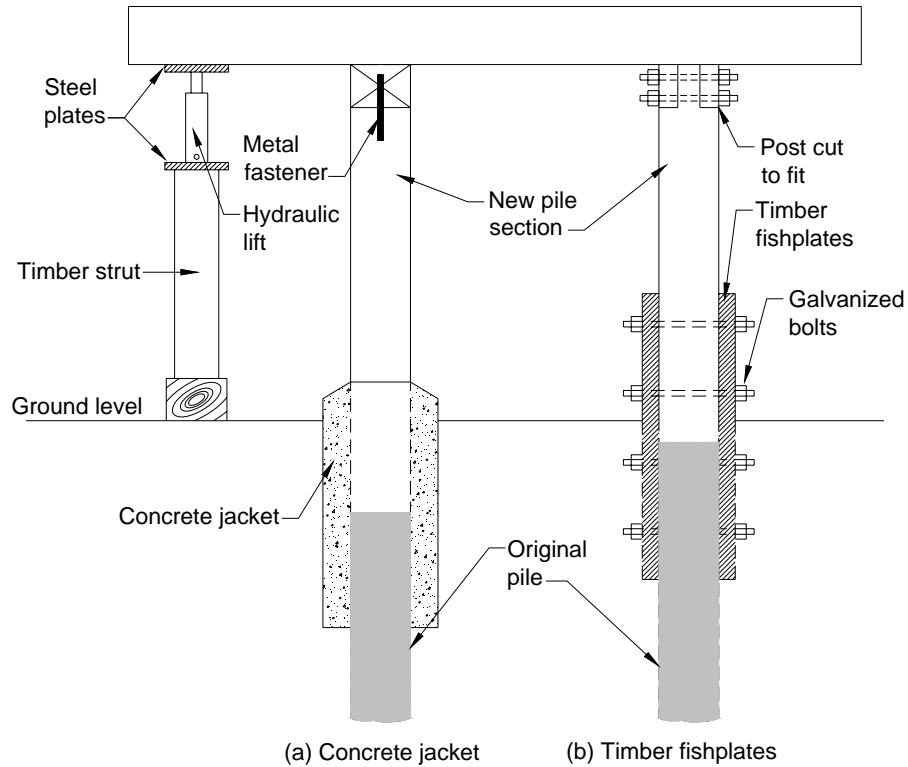


Figure 2.14. Splicing timber piles using concrete jacket or timber fishplate (Wipf et al. 2003a, and U.S. Army Corps. of Engineers et al. 2001)

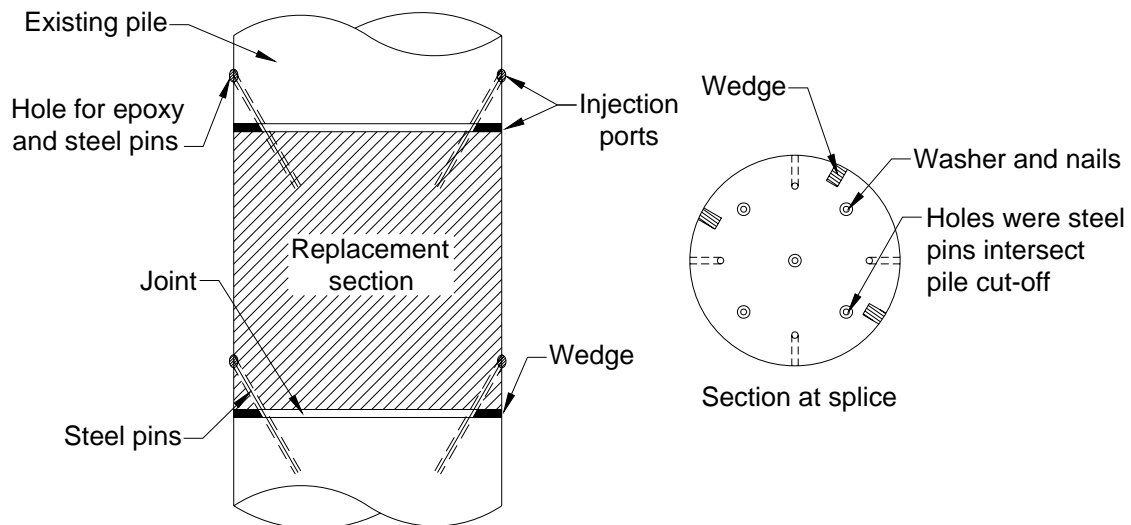


Figure 2.15. Diagram of pile posting using epoxy (modified from Ritter 1992)

2.10.2.2. Concrete Jacketing

According to NCHRP Report No. 222, this method may be used for repairing timber, steel, or concrete piles. Concrete jacketing can be used when approximately 10 to 50% of the cross sectional area of the pile has been lost by deterioration (Purvis 1994 and Wipf et al. 2003a).

A jacket form is wrapped around the length of the damaged area. The forms could be either flexible forms or split fiberboard forms. For the flexible form, the zipper should be closed, and the form is secured to the pile top and bottom, while for split fiberboard form, straps are installed and secured every 1 ft (Wipf et al. 2003a). A reinforcing cage is installed around the pile using spacers to keep the reinforcement in place (Figure 2.16). The forming jacket is then placed around the pile and sealed from the bottom against the pile surface. Concrete is then pumped into the form through the top. The top surface of the pile jacket should be sloped to allow runoff (U.S. Army Corps of Engineers et al. 2001 and University of Virginia Civil Engineering Department et al. 1980).

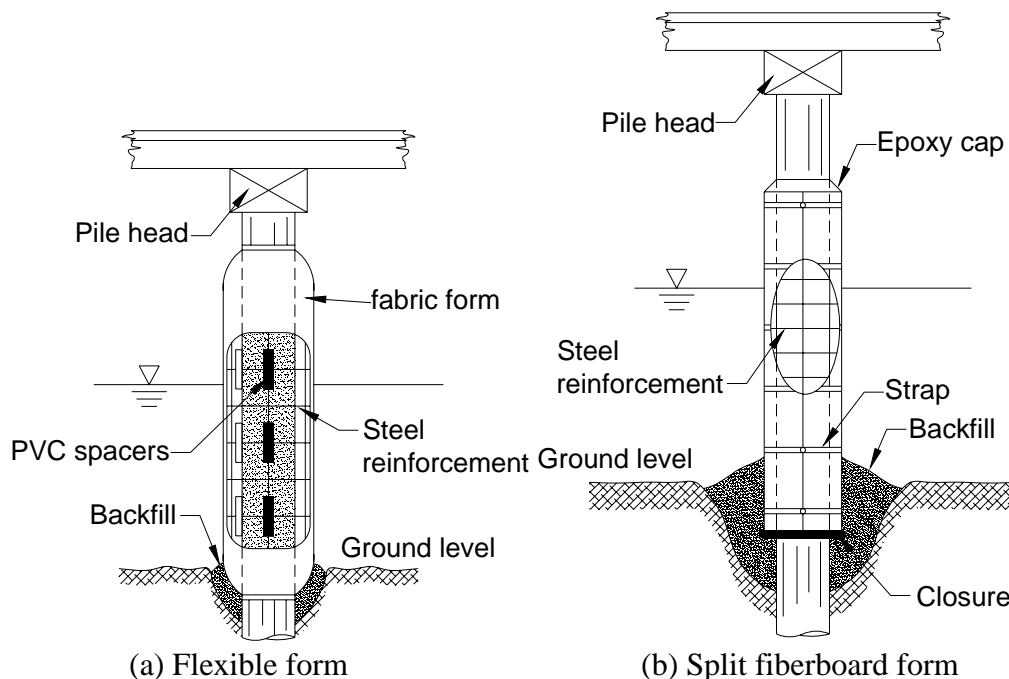


Figure 2.16. Concrete encasement repairs to timber, steel or concrete piles (U.S. Army Corps. of Engineers et al. 2001)

2.10.2.3. Polyvinyl Chloride (PVC) Wrap

This repair method comprises of a flexible plastic wrap tightly drawn and attached to the timber pile. This method is useful for pile regions subjected to wet-dry cycles since they are the regions most vulnerable for biological deterioration (Webber and Yao 2001). The PVC wrap prevents the exchange of water behind the pile wrap and the surrounding environment essentially making the environment toxic to wood parasites. PVC wraps can extend the life of infested piles by 35

years (U.S. Army Corps. of Engineers et al. 2001).

The PVC wrap consists of an upper unit which extends above the water level by at least 1 ft, and a lower unit which overlaps the upper unit and extends below the ground level. The PVC wrap is tightened using wood poles and fastened using aluminum alloy bands around the top and bottom and aluminum nails along the vertical joints (Figure 2.17). This method is cheaper than concrete jacketing. In addition, the PVC wraps provide protection against abrasion (U.S. Army Corps. of Engineers et al. 2001).

This method is used when deterioration is discovered and further damage needs to be prevented; however, this method can only be used with wood piles that have adequate structural capacity, since the method does not provide structural restoration (Lopez-Anido et al. 2005).

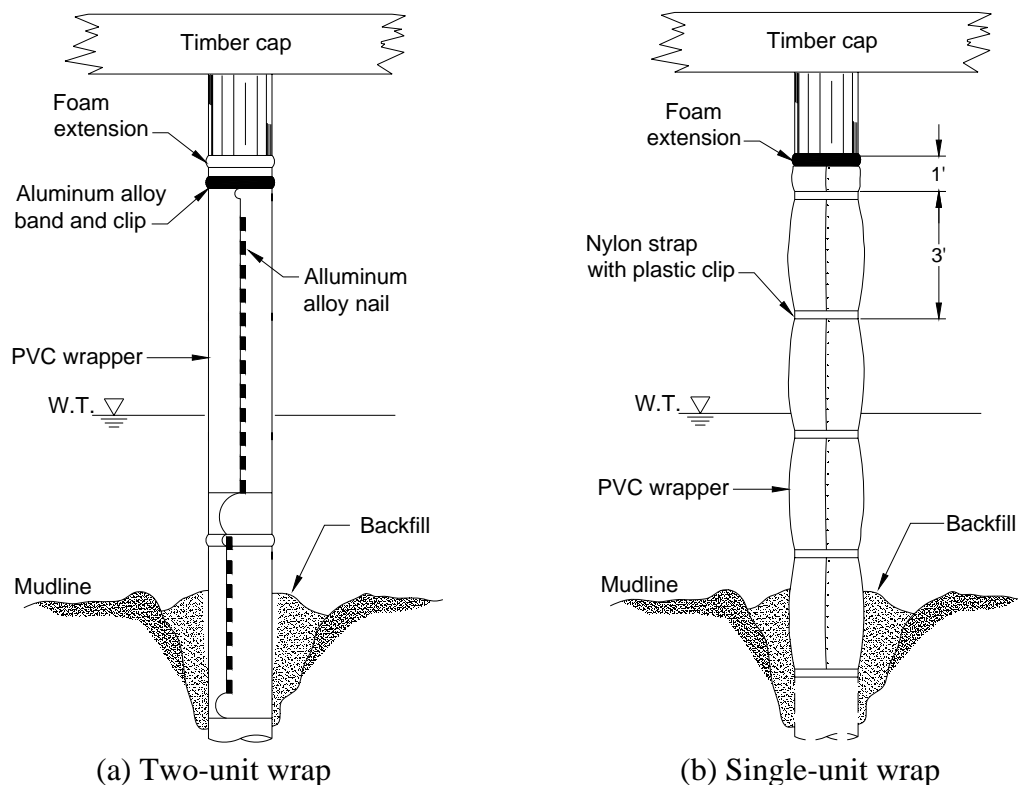


Figure 2.17. Wrapping timber piles with polyvinyl chloride (U.S. Army Corps. Of Engineers et al. 2001)

2.10.2.4. Fiber Reinforced Polymer (FRP)

This method is used when pile deterioration has occurred, or when increase in strength (retrofitting) of intact piles is desired. In either case, deterioration cannot be so extensive as to require replacement. This system provides shear transfer capability between the timber pile and the FRP composite shells, which strengthen the damaged portion. The FRP composite shells also act as a barrier between wood and wood parasites (Lopez-Anido et al. 2004). The fiber reinforced polymer has both axial fibers, which contributes to both the axial stiffness and

strength of the shell, and hoop fibers, which provide adequate integrity to the flexible shell allowing the shear strength and mechanical fastener support to be developed (Lopez-Anido et al. 2005)

The damaged portion of the pile is encased in a FRP shield made of bonded thin and flexible FRP composite prefabricated cylindrical shells. The cylindrical shells have a slit which enables them to be opened and placed around the deteriorated timber pile. It is advantageous to encase the pile with a series of overlapping FRP shells. A minimum of two shells are recommended; nonetheless, more shells can be used depending on the structural restoration required. The slits in each shell are staggered to avoid lines of weakness through the entire shield as shown in Figure 2.18 (Lopez-Anido et al. 2005).

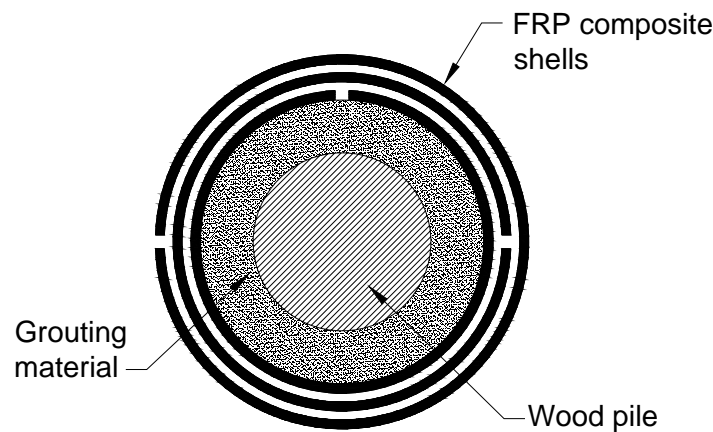


Figure 2.18. Cross section of timber pile repaired with fiber reinforced polymer composite shells (Lopez-Anido et al. 2005)

As shown in Figure 2.19, there are two types of load transfer mechanisms between the timber pile and the FRP composite shield. The first is a cement-based structural grout, and the second is steel shear connectors with an expanding polyurethane chemical grout.

According to a study by Lopez-Anido et al. (2003), two pre-damaged timber piles with 60% reduction in cross section were rehabilitated using the two load transfer mechanisms. The pile repaired using FRP with cement-based structural grout had a bending capacity which exceeded an intact reference wood pile. In addition, this load transfer mechanism resulted in three times the normalized peak load capacity of the intact reference wood pile. Only two thirds and 90% of the bending capacity and the normalized peak load capacity, respectively, were restored for the pile repaired using the FRP and shear connectors mechanism. Furthermore, transfer of stresses from the FRP shield to the wood pile is better accomplished using cement-based grout than with steel shear connectors.

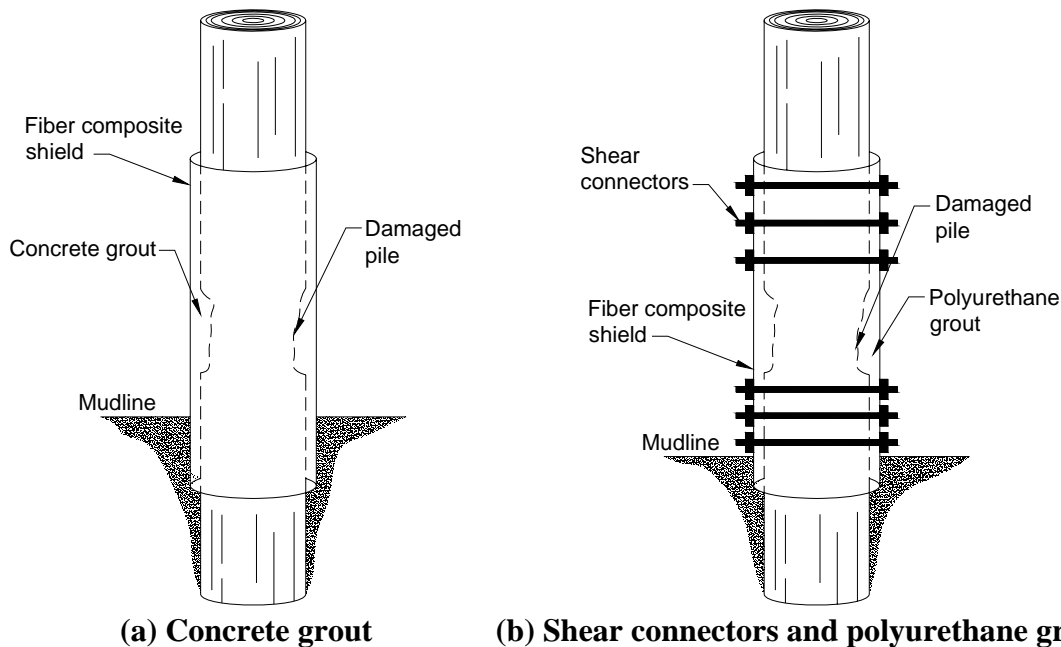


Figure 2.19. Fiber reinforced polymer composite repair system with (reproduced from Lopez-Anido et al. 2005)

2.10.3. Major Maintenance

Major maintenance corrective measures are conducted when deterioration has progressed to the point where major structural components have experienced moderate to severe strength loss and repair or replacement is mandatory to maintain the load carrying capacity (Ritter 1992).

2.10.3.1. Addition of Supplemental Piles

There are two methods involving replacement of severely deteriorated timber piles. The first method involves the addition of supplemental steel or timber piles under a timber deck, while the second method involves adding supplemental steel or concrete piles under a concrete deck.

Steel and timber piles can be supplemented by cutting the timber deck adjacent to the damaged pile. The new pile is driven and cut to fit under the pile cap. The pile is pulled laterally into place as shown in Figure 2.20. Shims are then placed as needed between the pile and pile cap. For timber piles, the pile is fixed to the pile cap using a 7/8 inch diameter drift pin, while for steel piles, the pile is secured to the pile cap using a 1 1/4 inch expansion bolts (U.S. Army Corps. of Engineers et al. 2001).

Using a similar procedure, concrete and steel piles are driven through a concrete deck. The piles are cut below the top of the concrete deck, and a capital is formed under the deck, on top of the new pile. The capital is then cast with the new section of the concrete deck as shown in Figure 2.21 (U.S. Army Corps. of Engineers et al. 2001). Both methods are limited mainly due to cost.

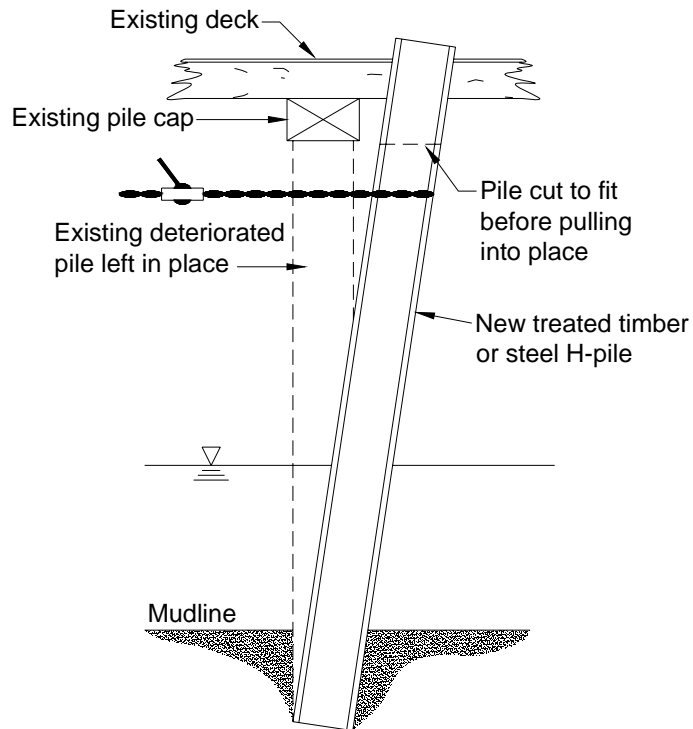


Figure 2.20. Addition of supplemental timber or steel piles (reproduced from U.S. Army Corps. of Engineers et al. 2001)

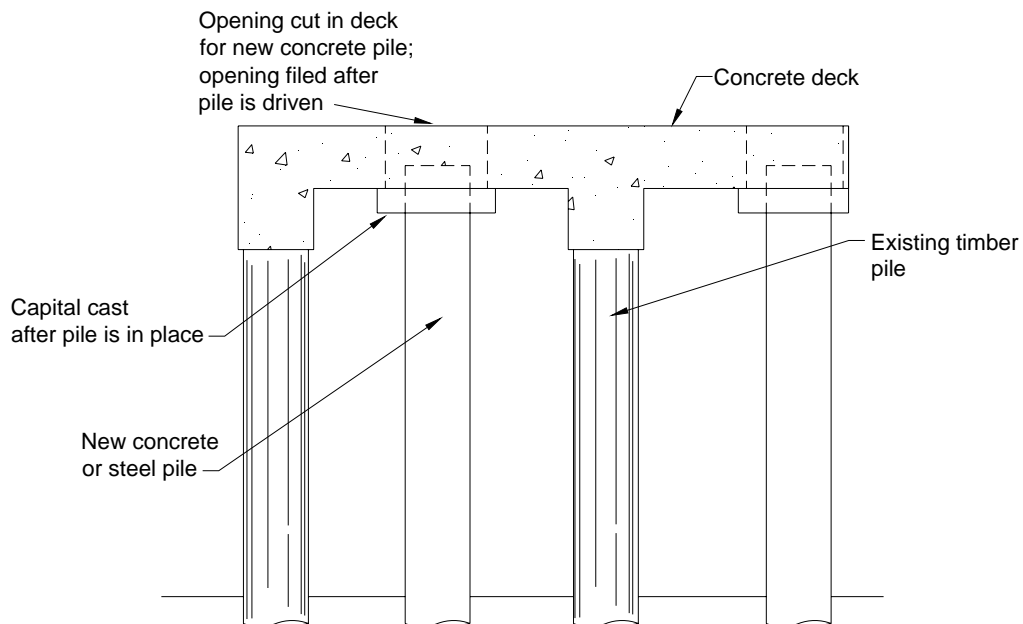


Figure 2.21. Addition of supplemental concrete or steel piles (reproduced from U.S. Army Corps. of Engineers et al. 2001)

3. QUESTIONNAIRE RESULTS

A questionnaire was sent to Iowa County Engineers (ICEs) to obtain information on common substructure problems and the typical remediation techniques they employed (See Appendix A). The return rate of the questionnaire was 60%. The majority of the results from the questionnaire are summarized in Figures 3.1 to 3.4 below. Figure 3.1 presents the frequency of the problems which affect the performance of steel piles. According to the ICEs, corrosion is the primary factor for deterioration of steel piles. Other factors that may contribute to deterioration of steel piles include misalignment and impact from floating debris. The major factors identified by the ICEs, which cause deterioration of timber piles, are scour, mechanical deterioration, biological deterioration and misalignment. There is an agreement however that biological deterioration of timber piles is the main factor (See Figure 3.2). As demonstrated in Figure 3.3, most counties rely on visual inspection in assessing superstructure and substructure components. Nondestructive evaluation techniques are almost never used as part of the bridge inspection. The questionnaire results also indicated that driving steel piles adjacent to defective piles is the most frequent maintenance practice implemented. Fewer counties use timber piles and concrete casings to strengthen deteriorated piles (See Figure 3.4). One other maintenance practice reported is the use of sheet piles to alleviate scour around abutments.

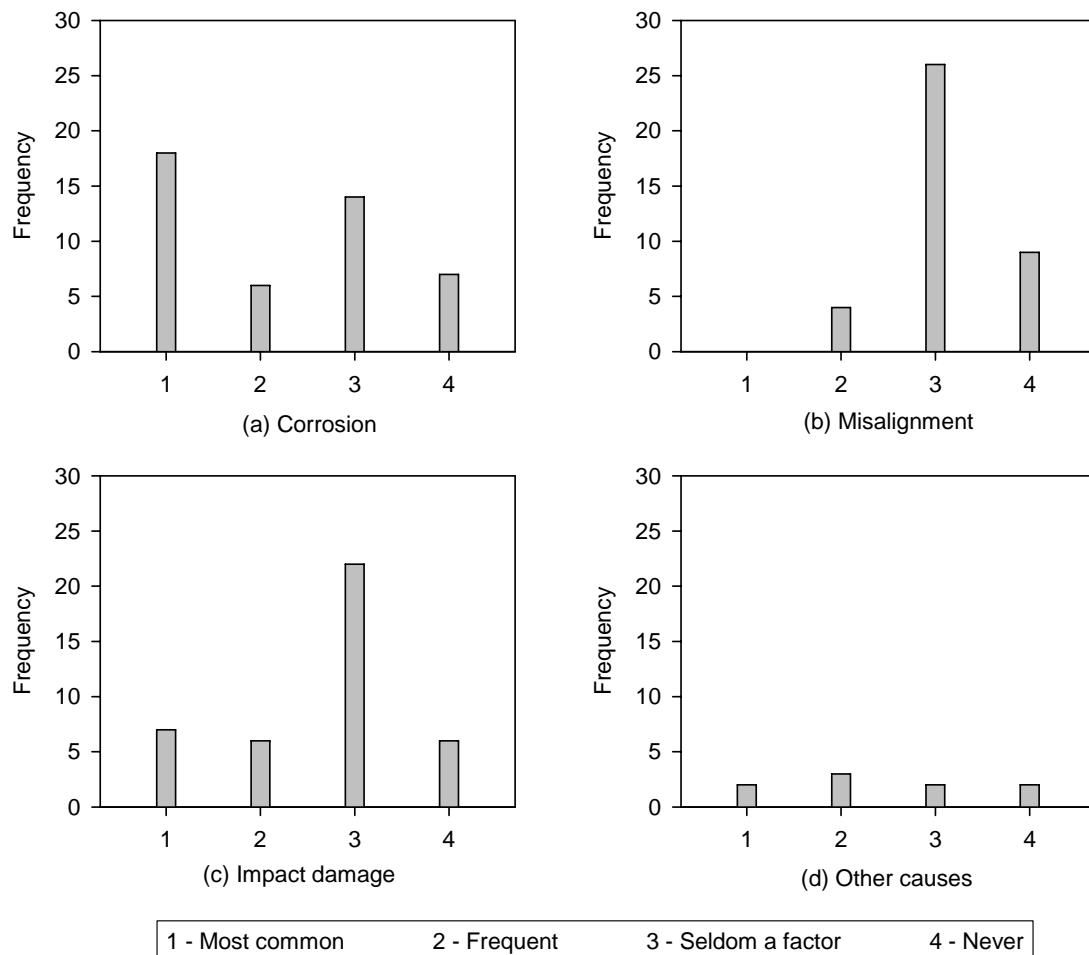


Figure 3.1. Iowa County Engineers rating of common steel pile problems

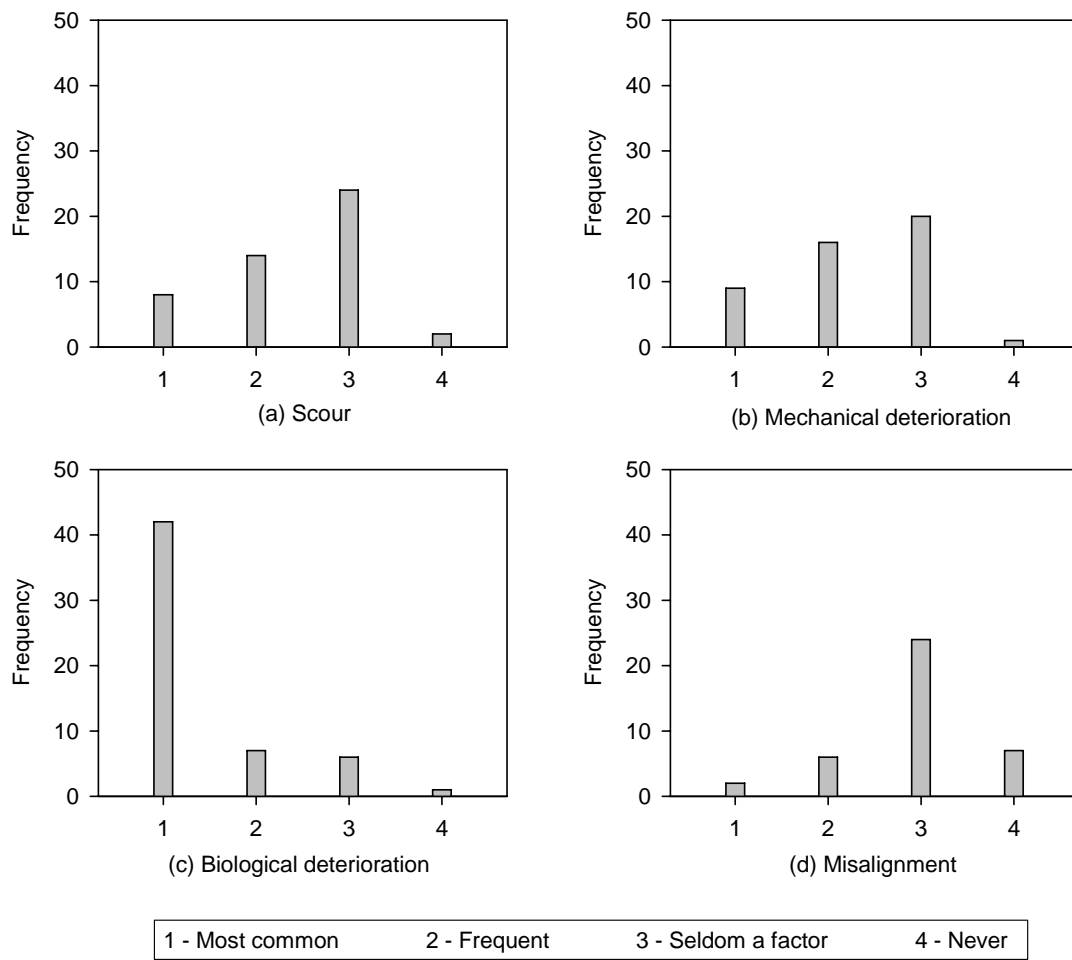


Figure 3.2. Iowa County Engineers rating of common timber pile problems

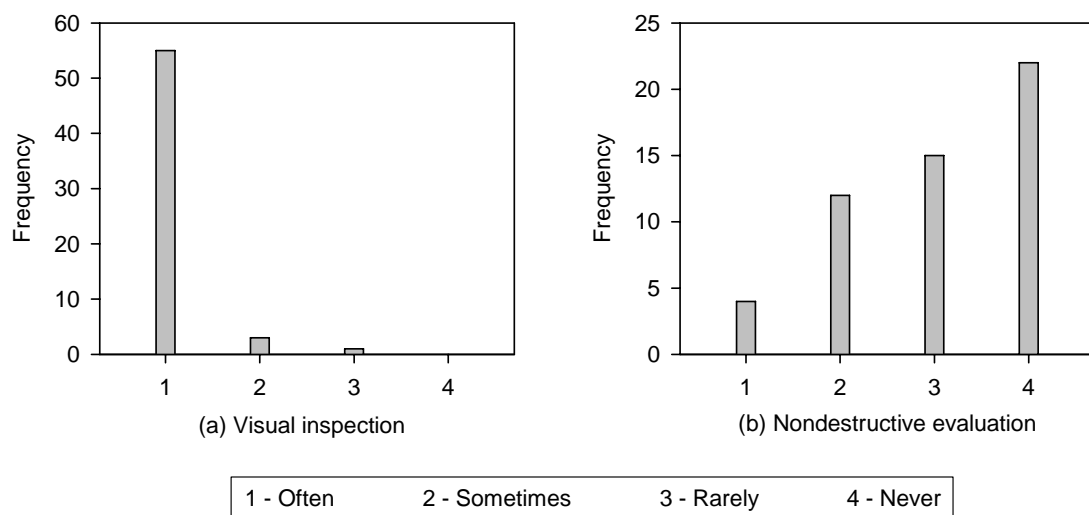


Figure 3.3. Iowa County Engineers rating of methods used to detect substructure and superstructure problems

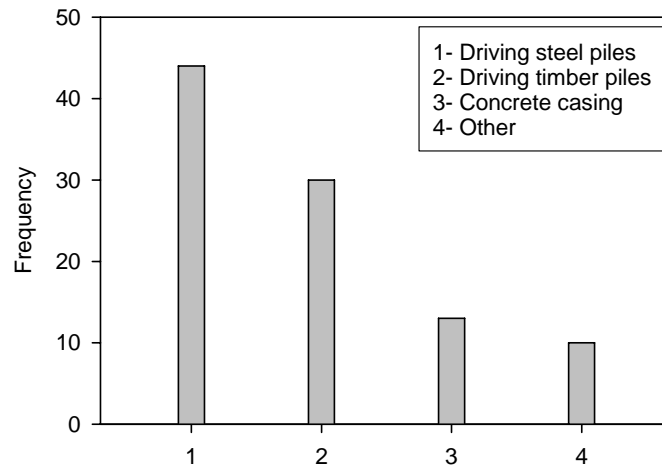


Figure 3.4. Frequency of remediation and/or strengthening methods used in Iowa

4. FIELD RECONNAISSANCE

There are many causes of substructure problems reported in previous related studies, and it was therefore determined that a field reconnaissance to identify the causes of substructure problems of low volume bridges in Iowa was necessary. Forty nine low volume bridges with problematic substructure in 10 counties were inspected. Even though this study only investigated steel stringer superstructures, the field reconnaissance for the substructure component included other superstructure types including timber deck and truss bridges. All inspected bridges had a timber substructure. The two most common problems observed were biological and physical deterioration. Other less occurring problems include UV degradation, misalignment of piles and pile cap deterioration.

4.1. Biological Deterioration

Biological deterioration of timber piles caused by bacteria and fungi attack was frequently observed. In all cases, deterioration originated near the ground or water level due to optimum moisture and oxygen conditions needed for biological activity. At initial stages, deterioration can be difficult to detect by conventional methods such as hammer sounding. If allowed to progress, fungi and bacteria attack can result in significant reduction in the pile cross section decreasing its load carrying capacity (Figure 4.1a). In extreme cases, biological deterioration can result in complete failure of the pile section (Figure 4.1b).

4.2. Physical Deterioration

Physical deterioration, which can exist in many forms such as severe cracks and splits, reduction of pile cross section by abrasion, broken piles, and brooming of the pile was also apparent at many sites. Cracks and splits near the pile top can occur while driving the pile, and can result in exposing the untreated pile core to insects and bacteria. An example of commonly observed pile cracks is shown in Figure 4.2. Flowing debris and ice are other factors that contribute to pile physical deterioration, and can result in reduction of pile cross section by abrasion as shown in Figure 4.3. Overloading the piles was observed at 20% of the inspected substructures. Overloading, which is mostly caused by failure of adjacent pile(s), can result in compression failure of the pile and separation of the top portion of the pile as shown in Figure 4.4a. Compression failure can also be in the form of bulging of wood fibers or “mushrooming” at a hollow pile section (See Figure 4.4b and c).

4.3. Other Causes of Pile Deterioration

From the field reconnaissance, other causes of pile deterioration that were less frequent and less threatening to the pile integrity were observed. These causes include UV degradation, misalignment of the pile and pile cap deterioration. UV rays break down the lignin, the natural glue which holds wood fibers together, at the surface causing fraying of wood and leaving it with a gray color (USDA 1999). Figure 4.5 shows a timber pile with advanced UV degradation; as a result, the wood at the surface can be peeled off.

Misalignment of timber piles is another factor contributing to poor substructure performance. Misalignment can result from failure of the connection between the pile cap and the pile due to corrosion. This results in movement of the pile away from the abutment. Further, misalignment can also occur during pile driving, which causes non-uniform bearing between the pile cap and the pile and in turn poor load transfer (See Figure 4.6).

Another observed form of substructure degradation was deterioration of pile caps. A corroded steel cap is presented in Figure 4.7a, while a biologically deteriorated timber cap is shown in Figure 4.7b. Deteriorated pile caps can result in poor load-bearing characteristics and overloading of adjacent piles.



(a) Reduction of pile cross section (Bridge No. 13-42-06 Buchanan County – February 16 2005)



(b) Complete deterioration of pile section (Bridge No. 27-42-00 Buchanan County – February 16 2005)

Figure 4.1. Timber pile biological deterioration



Figure 4.2. Pile cracking near the pile top (Bridge No. 1045 Black Hawk County – April 2 2005)



Figure 4.3. Reduction of pile cross section by abrasion from flowing debris and ice (Bridge No. 27-74-23 – February 15 2007)



(a) Separation of pile section (Bridge No. 23-70-00 Mahaska County – July 8 2005)



(b) Bulging of timber fibers (Bridge No. 35-87-00 Buchanan County – February 15 2005)



(c) “Mushrooming” of fibers at a hollow section (Bridge No. 23-70-00 Mahaska County – July 8 2005)

Figure 4.4. Compression failure of pile section caused by overloading



Figure 4.5. Ultraviolet degradation of a timber pile (Bridge No. 23-73-50 Mahaska County – July 8 2005)



Figure 4.6. Misalignment of a timber pile (Bridge No. 22-00-44 Buchanan County – February 15 2005)



(a) Corroded steel
(Bridge No. 1045 Black Hawk County
– April 2 2005)



(b) Biologically degraded timber cap
(Bridge No. 15-00-62 Buchanan County
– February 15 2005)

Figure 4.7. Deterioration of pile cap

4.4. Substructure Remediation Techniques

During the field reconnaissance, several substructure remediation techniques were observed. These techniques included (1) concrete casing; (2) addition of a timber or steel pile adjacent to the defective pile; and (3) constructing a new substructure system (i.e. replacing all existing piles).

As mentioned in the pile maintenance section, concrete casing, which can be used to restore timber, concrete or steel piles, is typically used when the pile cross sectional area is reduced by 10 to 50%. At one bridge, the center piers were encased with concrete as shown in Figure 4.8. Inspection at this site showed that longitudinal cracks and concrete spalling were present in all concrete casings, which may have resulted from corrosion of reinforcement and freeze-thaw degradation (See Figure 4.9). Another maintenance practice observed is the addition of a new pile adjacent to a defective pile. In the case of progressive deterioration at one pile, a new pile (timber or steel) is driven next to the faulty pile as shown in Figure 4.10. The final maintenance practice observed is the complete replacement of the existing abutment system, which mainly occurred when advanced deterioration is widespread in more than one pile threatening the integrity of the bridge.

In one bridge in Tama County, IA, complete replacement of an existing timber abutment with a new timber abutment system was documented. Replacement was conducted because of severe deterioration at both the north and south abutments. Several deterioration problems were identified at the north abutment such as brooming of the pile section due to overloading, soft section near the ground level with high moisture content, and hollow pile section caused by biological decay (See Figure 4.11). To drive new piles, a section of the concrete deck was removed and about 20 ft of the gravel road near the backwall was excavated (Figure 4.12). Four temporary timber piles (two on each side) were driven adjacent to the sides of the bridge and steel beams were placed on top of them under the existing girder to support the bridge as the

deteriorated piles were cut short. The new timber piles were driven next to the existing ones and a new timber pile cap was placed under the girders and connected to the new piles. The supporting beams were removed and the old and temporary piles were left in place (Figure 4.13). Leaving the deteriorated piles in place diverts the biological decay away from the new piles, however, it is still recommended to treat the causes of biological decay if the new piles are timber. As an alternative, steel piles can be used for maintenance as shown in Figure 4.14.



Figure 4.8. Encasing the center piers with concrete for pile restoration (Bridge No. 149 Boone County – February 11 2005)



Figure 4.9. Spalling and cracking of concrete casing (Bridge No. 149 Boone County – February 11 2005)



Figure 4.10. New steel pile driven adjacent to defective pile (Bridge on Indian Creek Road Black Hawk County – April 2 2005)



(a) Overview of the north abutment before replacement



(b) Brooming of pile at the east end of the north abutment



(c) Soft pile section with high moisture near the ground level



(d) hollow pile section near the ground level

Figure 4.11. Bridge No. 31-72-50 Tama County – October 27 2005



Figure 4.12. A section from the concrete deck is removed for driving timber piles (Bridge No. 31-72-50 Tama County – September 8 2005)



Figure 4.13. New timber abutment system constructed at the north side (Bridge No. 31-72-50 Tama County – September 8 2005)



Figure 4.14. Steel piles used to replace deteriorated timber abutment (Bridge in Boone County – June 1 2005)

4.5. Summary

- A field reconnaissance was carried out which 49 low volume bridges with problematic timber substructures were inspected.
- Most biological deterioration was observed near the water or ground level, where conditions are favorable for bacteria, fungi, and insect growth. Biological deterioration can considerably reduce the pile carrying capacity.
- Abrasion and overloading compression failure of timber piles are forms of physical deterioration, which were observed during the field study.
- Other causes of timber pile deterioration included UV degradation, misalignment, and pile cap deterioration.
- Rehabilitation methods observed during the field reconnaissance were (1) concrete casing, (2) driving a timber or steel pile adjacent to the defective pile, and (3) constructing a new substructure system.
- Longitudinal cracks and concrete spalling are common distresses associated with concrete casing.
- A new timber or steel pile is driven next to the faulty pile when deterioration is excessive and is localized in one pile.
- Complete replacement of the existing substructure takes place when advanced deterioration is widespread in more than one pile threatening the integrity of the bridge.

5. LABORATORY TESTING

The objective of the laboratory study was to develop a simple procedure to evaluate deterioration in timber piles. The significance of developing a simple evaluation method is that if applied to field applications, the in-service conditions of timber piles could be determined. The laboratory study consisted of destructive axial compression tests and nondestructive ultrasonic stress wave tests. The stress wave tests were used to generate tomography images of the internal pile condition. The ultrasonic stress wave test was conducted both perpendicular and parallel to the grain. Correlations were developed between the stress wave test measurements and the axial compression test measurements.

5.1. Ultrasonic Stress Wave Technique

5.1.1. Background

Ultrasonic stress waves, which typically have a frequency higher than 20 kHz, are generated by exciting a piezo-electric crystal with a high voltage pulse. The high frequency waves are transmitted to the tested material, which is in contact with the transducer containing the crystal. The wave can be fully transmitted or reflected from external surfaces, internal flaws, and boundaries between adjacent materials (Emerson et al. 1999). When a wave reaches a receiving transducer, it produces an output voltage. There are three basic types of stress waves created in a solid medium when an ultrasonic pulse is sent through a test object: compression wave (P-wave), shear wave (S-wave), and surface wave (R-wave) (Toutanji 2000). The speeds of the wave types are as follows (Leiphart 1997):

$$V_p = \sqrt{\frac{E(1-\mu)}{\rho(1-\mu)(1-2\mu)}} \quad (5.1)$$

$$V_s = \sqrt{\frac{E}{2\rho(1-\mu)}} \quad (5.2)$$

$$V_r = \left(\frac{0.87 + 1.12\mu}{1 + \mu} \right) C_s \quad (5.3)$$

Where V_p = the speed of the P-wave, V_s = the speed of the S-wave, V_r = the speed of the R-wave, E = the elastic modulus, ρ = the mass density, and μ = Poisson's ratio. It can be seen that the speed of the propagating wave is directly dependent on the material properties of the material in which the wave is traveling.

5.1.2. Difficulties and Limitations

A single stress wave measurement can only detect internal decay that is above 20% of the total cross section of the timber pile (Emerson et al. 1999). Therefore, multiple tests are often conducted to increase the test reliability. In the field, however, it is not always feasible to access the complete circumference of the pile due to the presence of the backwall behind the timber pile. Another limitation is coupling of the sensors with the timber surface. Most piles exhibit splits and cracks, which result in poor acoustic coupling between the transducer and the timber surface leading to unstable reading (Emerson et al. 1999). Furthermore, in severe internal pile deterioration, and due to high stress wave attenuation in void spaces, a stress wave travel time measurement may not be obtained.

An example of a deteriorated pile is shown in Figure 5.1. The rapid attenuation of the wave in the hollow region hindered the detection of the intact area near the pile core and prevented the wave from reaching the receiving transducer.



Figure 5.1. Significant internal pile deterioration that is difficult to detected using the stress wave technique (Bridge No. 31-72-50 Tama County – June 10 2005)

5.1.3. Description of Equipment

A James Instrument Velocity Meter (James V-Meter) manufactured by James Instruments, Inc. was used in this study; device components are shown in Figure 5.2. The instrument utilizes an ultrasonic pulse generator to impart a stress wave into the specimen. As the transmitting transducer imparts a wave into the member, the timer unit begins timing passage of the wave and as it reaches the receiving transducer, the timer stops. The transducers are p-type transducers (i.e. detect P-waves only) with a resonant frequency of 54 kHz. A key consideration when using this equipment is coupling. To obtain reliable results, the surface of the specimen must be free of debris, mud, or dirt. A coupling agent, provided by the manufacturer, is often used to facilitate measurements (Wang et al. 2004).

Even with the use of an ample coupling agent, it was difficult to obtain a stable reading between the flat transducer surface and the round timber surface. Therefore, the authors decided to retrofit the velocity meter with two brass cones as shown in Figure 5.2. By providing 2 fixed contact points at the pile surface, the cones improved the acoustic coupling of the transducers and the timber surface. The coupling agent was used at the interface between the transducers and the cones to prevent wave attenuation. To calibrate the device for the retrofitted cones, at the beginning of each test the brass cones, which were attached to the transducers, were brought in contact with each other. The instrument then takes an “offset” reading, which is then subtracted from all future readings.

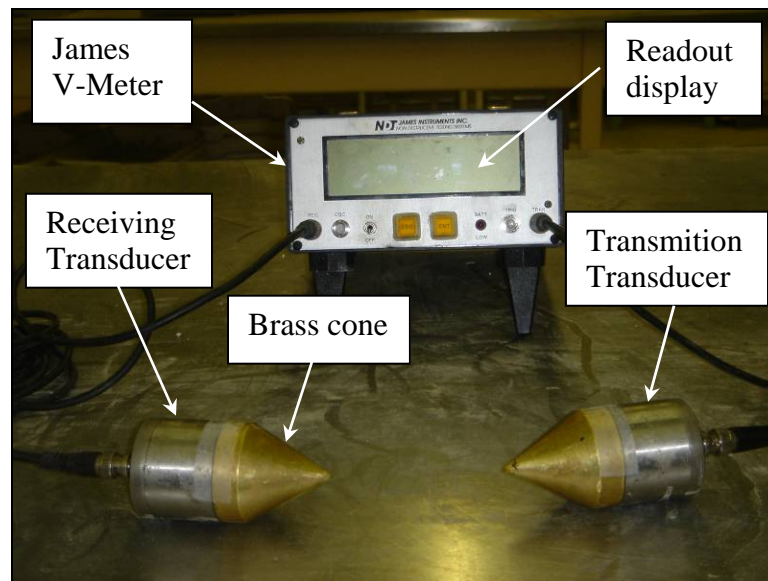


Figure 5.2. James Instrument Velocity Meter

5.1.4. Image Processing

The acoustical imaging software used in this laboratory study is 3DTOM: Three-Dimensional Geophysical Tomography developed by Jackson and Tweeton (1996) at the United States Bureau of Mines. The program uses an ASCII text input file, which includes source-receiver coordinates, and travel times, to produce a velocity tomogram. The tomogram is created by using a simultaneous iterative reconstruction technique (SIRT). As shown in Figure 5.3, a model is constructed as a grid of nodes with intervening voxels. SIRT includes three cyclic procedures that are repeated until pre-selected criteria are met. These procedures are (1) forward computation of model travel time, (2) calculation of residual travel times, and (3) application of velocity corrections. Forward computed of model travel time is compared to a calculated travel time of a particular ray to the measured travel time of that ray using Equation 5.4 (Jackson and Tweeton 1996).

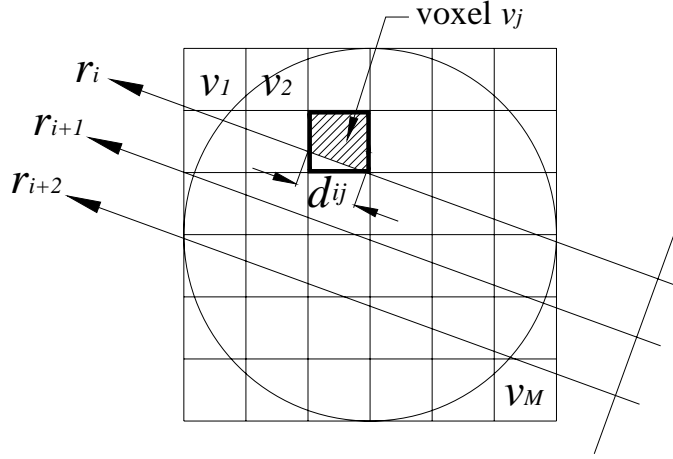


Figure 5.3. Construction of model grid of nodes with intervening voxels

$$t_i = \sum_{j=1}^M p_j d_{ij} \quad (5.4)$$

Where M = number of voxels in the image reconstruction grid, t_i = measured travel time for ray i , d_{ij} is the distance traveled by ray i through voxel j , and p_j = the average slowness (inverse velocity) of the ray in voxel j . The variable d_{ij} = nonzero for the voxels at which ray i passes. The residual of each ray (difference between the left hand side and right hand side of Equation 5.4) is used to calculate incremental correction factors for all voxels sampled by a particular ray. Since the imaging process uses a simultaneous reconstruction method, the correction factors of all individual rays are calculated and accumulated first before being applied to the voxels (Jackson and Tweeton 1996). The correction factor for ray i in voxel j is calculated as follows:

$$\Delta p_{ij} = \frac{\Delta t_i d_{ij}}{N_p \sum_{k=1}^M (d_{ik})^2} \quad (5.5)$$

Where Δp_{ij} = the slowness correction of ray i in voxel j , Δt_i = the travel time residual for ray i , d_{ij} is the path length for ray i in voxel j , N_p = the number of rays in voxel j , M = the number of voxels in the grid, and d_{ik} = the path length of ray i in each of the M voxels in the grid. The incremental slowness corrections are summed to obtain a net correction factor for voxel j as shown in the equation below:

$$\Delta p_j = \sum_{i=1}^N \Delta p_{ij} \quad (5.6)$$

Where Δp_j = the slowness correction of voxel j , N = number of rays, and Δp_{ij} = the slowness correction of ray i in voxel j . For example, if there are three rays that pass through voxel number 4, Equation 5.6 would become:

$$\Delta p_4 = \sum_{i=1}^3 \Delta p_{i4} = \Delta p_{14} + \Delta p_{24} + \Delta p_{34}$$

Correction factors for each grid node are then obtained by averaging the corrections calculated for each voxel attached to the node.

5.1.5. Test Procedure

Multiple measurements were performed at each cross section to obtain a tomographic image. The number of measurements adopted in this laboratory study for each 2-dimensional cross section was 20 (8 test points). The arrangements of the transducers are shown in Figure 5.4. According to Divos and Szalai (2002), this arrangement will allow for a 1% detectable defect. Other possible arrangements with higher percentage of detectable defect are also shown in Figure 5.4. Multiple images of the internal condition of the pile were generated by repeating the test every 4 inches along the length of the pile (See Figure 5.5). The purpose of generating multiple 2-dimensional images is an attempt to separate strong and weak areas inside the pile. It is believed that weak zones will govern the overall behavior and strength of the timber pile specimen.

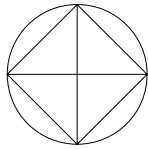
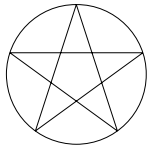
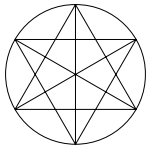
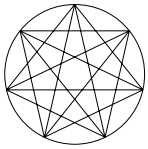
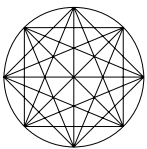
Setup					
Number of test points	4	5	6	7	8
Number of measurements	6	5	9	4	20
Number of reference velocities	2	1	2	2	3
Minimum detectable defect	8%	6%	3%	4%	1%

Figure 5.4. Possible test arrangements with 4 to 8 test points (Divos and Szalai 2002)

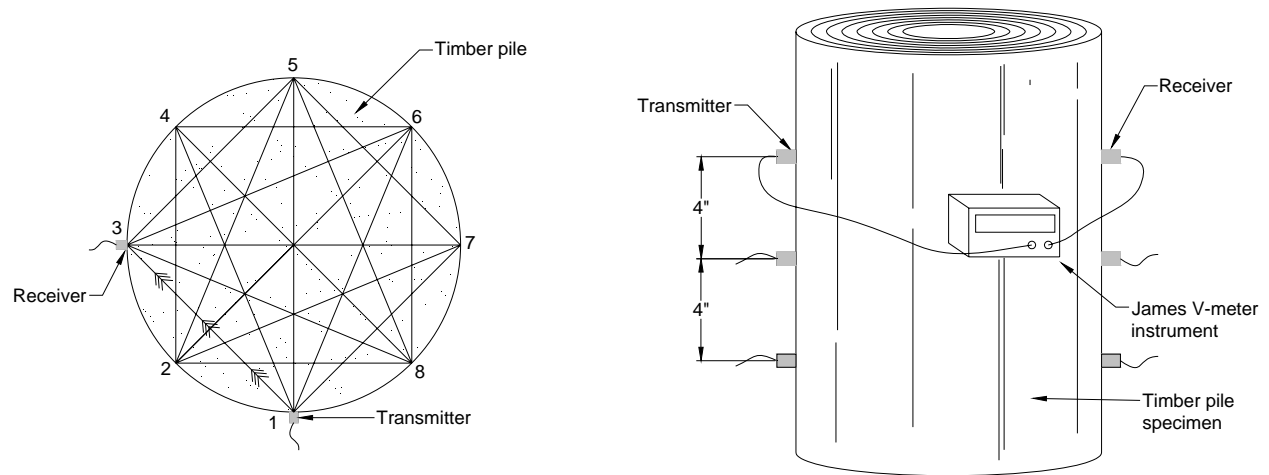
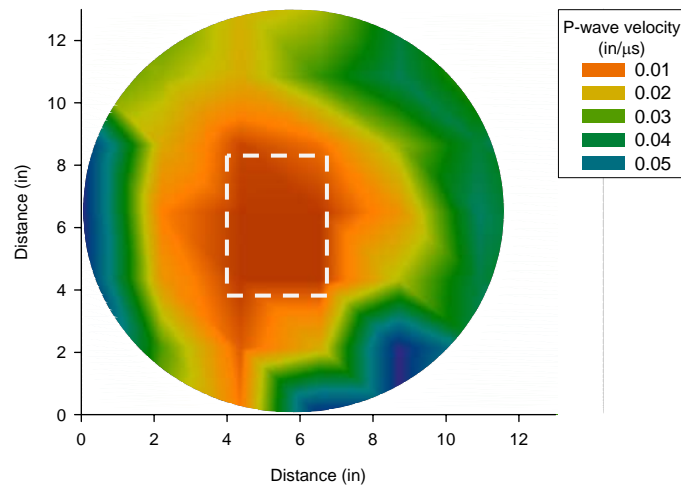
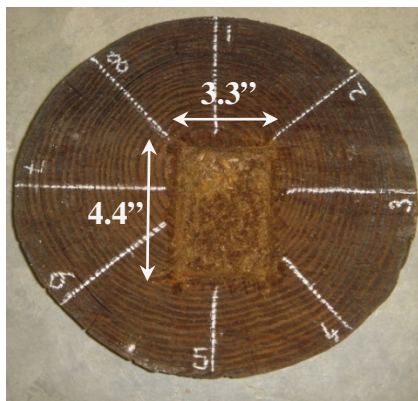


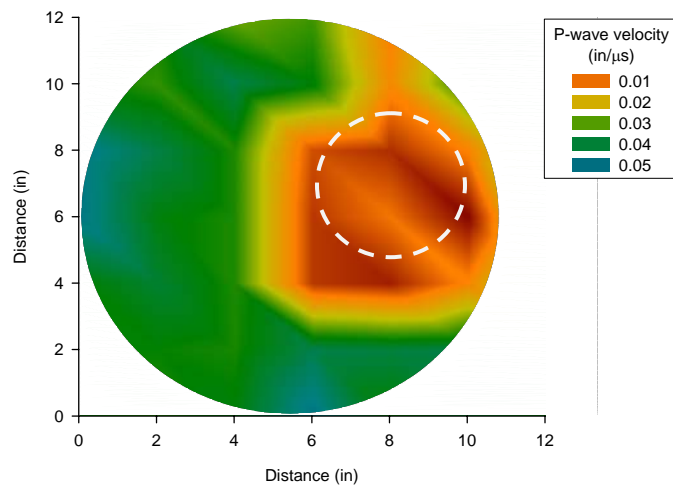
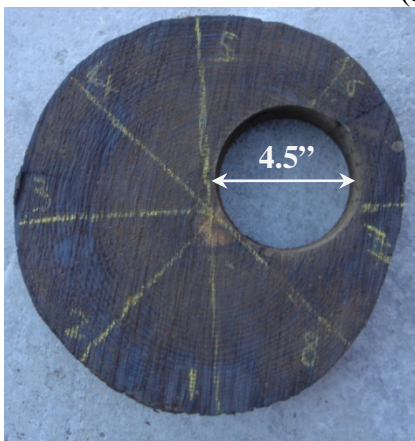
Figure 5.5. Incremental testing to obtain multiple 2 dimensional images

5.1.6. Test Verification and Repeatability

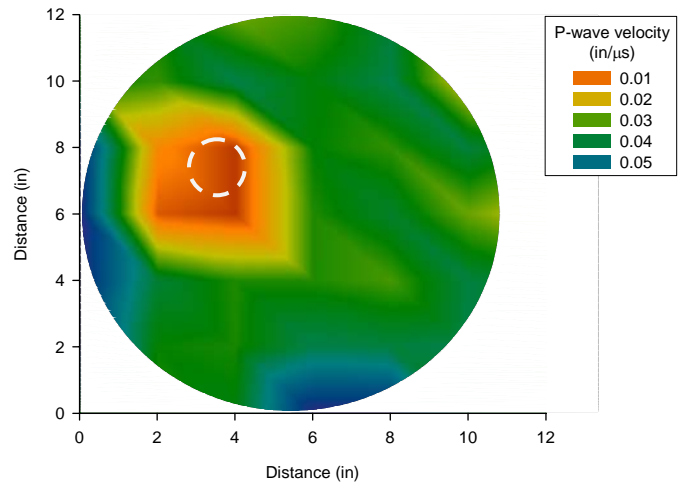
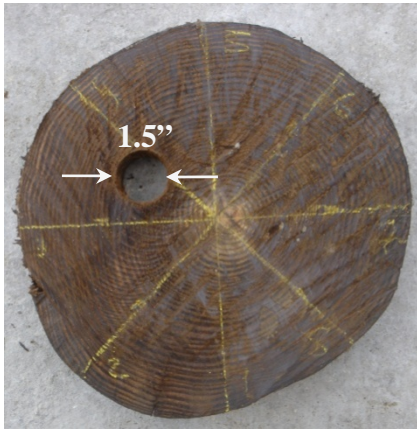
To verify that the selected imaging reconstruction technique and test procedure produce reliable results, tomographic images generated at the surface of several piles were compared to digital images. Four pile sections were damaged by creating a cavity near the pile core as shown in Figure 5.6 to simulate biological deterioration, which would not necessarily be visible from the outside of an in-service pile. A radial cut was made in one pile section to simulate pile cracking, which typically develops due to wet-dry cycles or during pile driving (See Figure 5.6e). The height and diameter of these pile sections were about 5 inches and 11.5 inches, respectively. Another pile section used in this study was obtained from a bridge abutment replaced in August 2005. The pile had considerable outer damage as depicted in Figure 5.6f. The pile height and diameter were approximately 22 inches and 12 inches, respectively. The results, demonstrated by the tomography images shown below, indicate that the selected test procedure and image reconstruction technique were successful in capturing the approximate shape and location of the internal damage. Results also show that the velocities in the hollow areas are lower than the velocities in the intact parts of the pile sections. Velocities in hollow areas were generally less than 0.02 inches/ μ s.



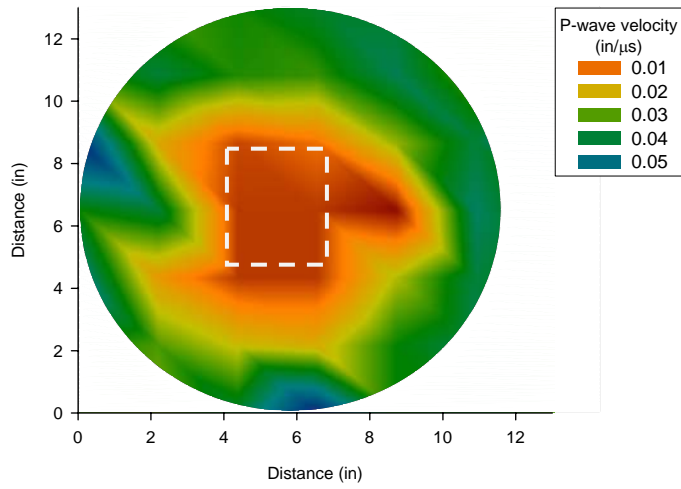
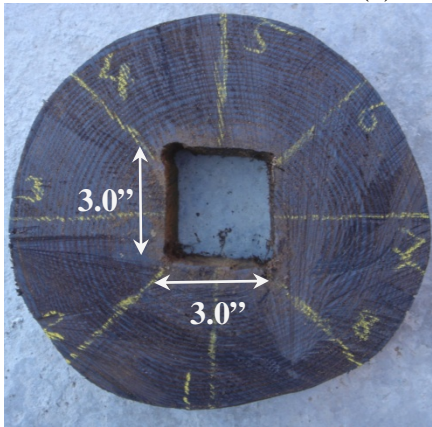
(a) Square cavity; 3.3"x4.4"



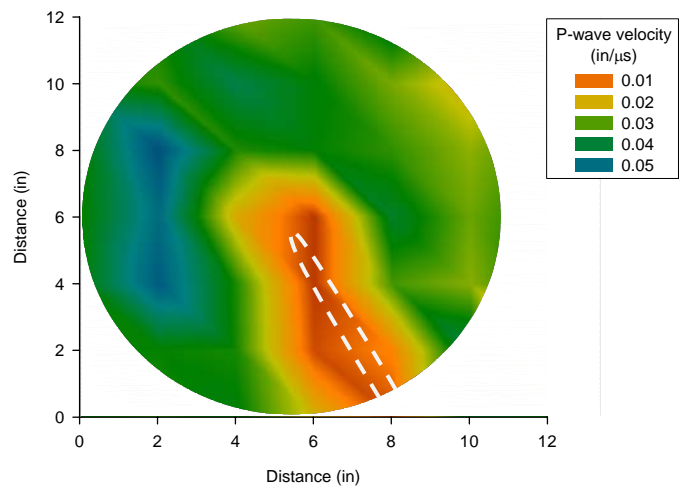
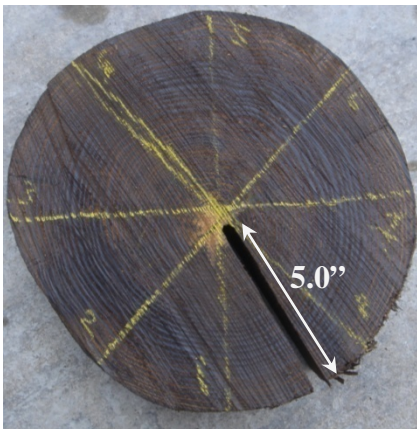
(b) Circular cavity; diameter = 4.5"



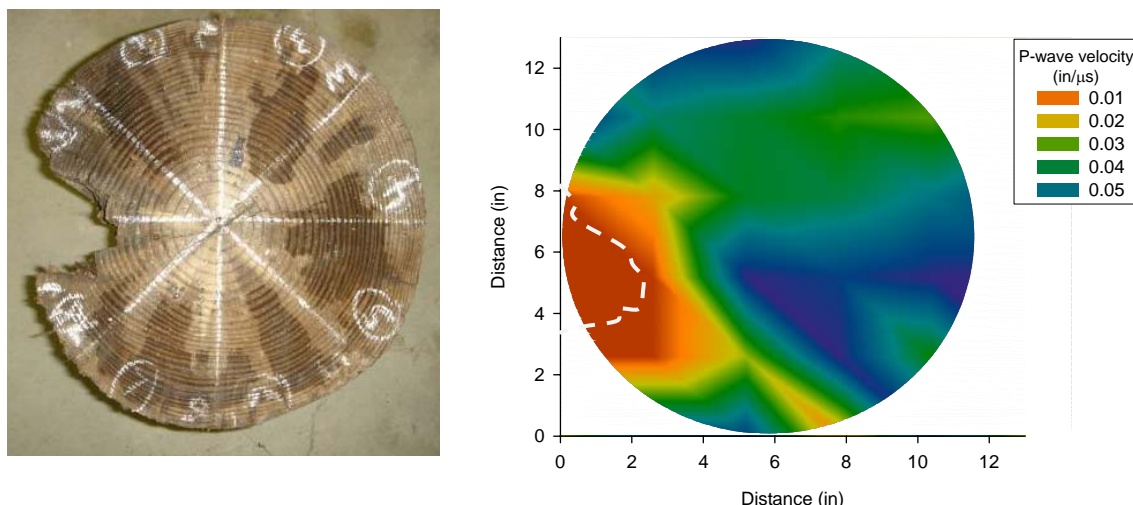
(c) Circular cavity; diameter = 1.5"



(d) Squared cavity; 3"x3"



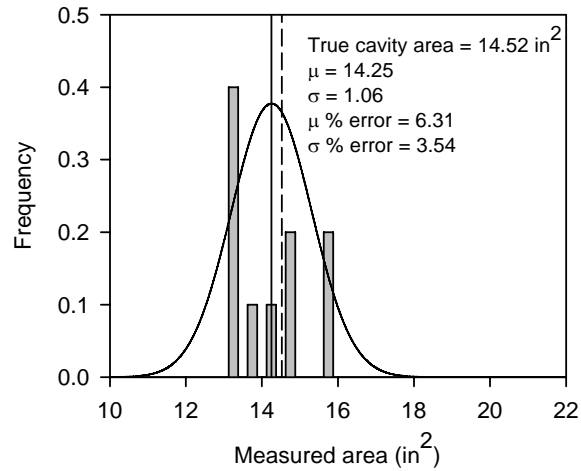
(e) Radial crack



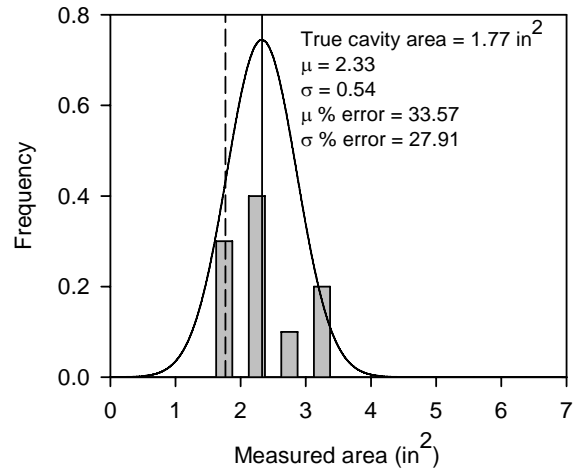
(f) Irregular outer cavity

Figure 5.6. Comparison of tomography and digital images generated for damaged piles

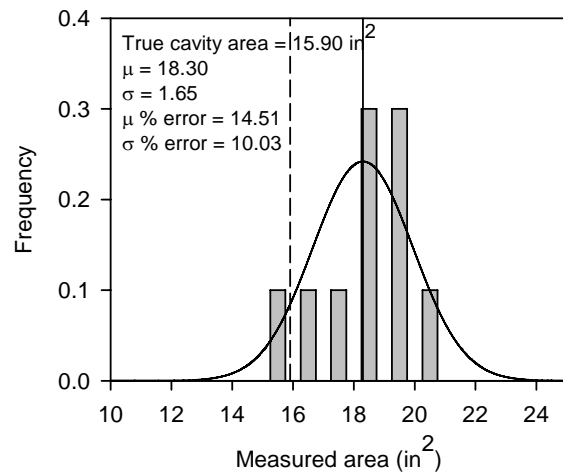
The accuracy and repeatability of the test procedure was evaluated by repeating the ultrasonic stress wave test 10 times for each pile section. At each test, the locations of the 8 test points, where the transmitting and receiving transducers were positioned, were shifted and a tomography image was generated (i.e. for each pile, 10 tomograms were created). From each image, the region enclosed by velocities less than 0.02 inches/ μ s was measured to estimate the hollow area of the pile, which was then compared to the true area. The difference between the true cavity area and mean measured area for each pile section gave an indication of the accuracy of the test procedure, while the difference between the measured areas gave an indication of the test procedure repeatability (precision). Normal distribution plots of the measured areas for the 6 pile sections are presented in Figure 5.7. The dashed lines depicted in the figure represent the true cavity areas. Apart from the results shown in Figure 5.7a, where the damage comprised of a square cavity with an area of 14.52 in² and the measured area was 14.25 in², the results demonstrate that the test procedure and/or the image reconstruction process have a “biased” tendency to over predict the cavity area. The range of over prediction, as evidenced by the mean of the percent error, ranged from 6 to 34% of the true cavity area. The results also show that the pile sections have different standard deviation of the percent error values. Due to this difference, it was concluded that the orientation of transducers influence the precision of the test procedure. This can be explained by the anisotropy of acoustic propagating velocities in wood (i.e. the elastic properties and the associated acoustical properties are very different in the radial, tangential, and longitudinal directions). The results also show that the size and shape of the internal defect can influence the precision of the test procedure. Small defects, relative to the pile diameter, such as the 1.5 inch circular cavity or the radial crack have higher mean and standard deviation percent error. This may be attributed to the number of measurements, which can only identify defects with limited precision. Increasing the number of measurements may decrease the influence of the internal defect size and shape on the test procedure precision.



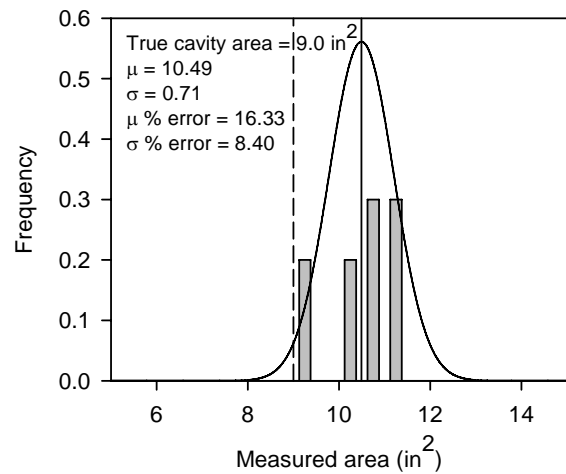
(a) Squared cavity; 3.3"x4.4"



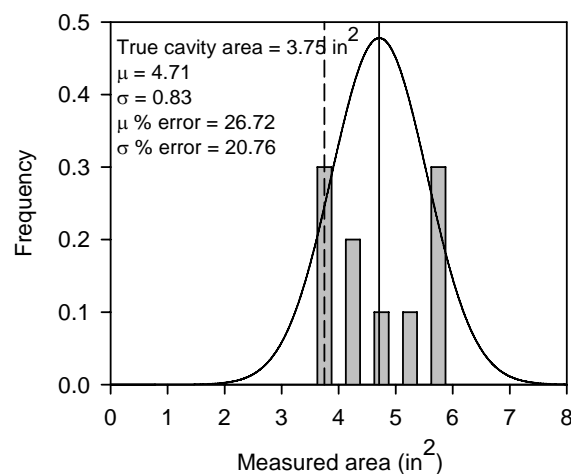
(b) Circular cavity; diameter = 4.5"



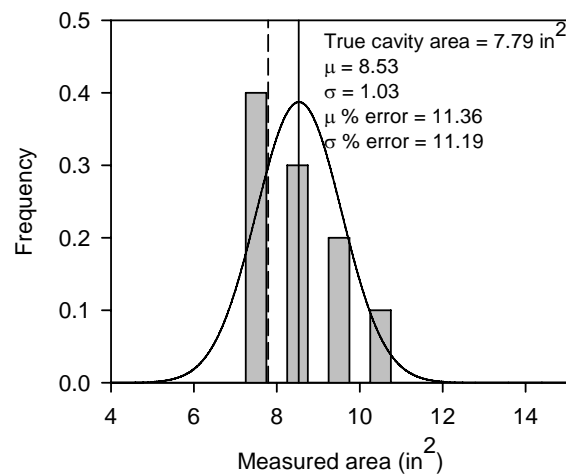
(c) Circular cavity; diameter = 1.5"



(d) Squared cavity; 3"x3"



(e) Radial crack



(f) Irregular outer cavity

Figure 5.7. Normal distribution plots of the damaged pile sections evaluating accuracy and precision of the ultrasonic stress wave test procedure

5.1.7. Test Results

The ultrasonic stress wave test was performed on 12 timber pile specimens for multiple cross sections for a given pile. Multiple measurements, using the transducers arrangement outlined earlier, were performed at each cross section to obtain a tomographic image every 4 inches revealing the pile internal condition. Out of the 12 specimens, 9 were previously in-service and 3 were new. An example of the output generated for each pile specimen is presented in Figure 5.8. This figure was generated for a pile obtained from the north abutment of a bridge in Marshall County, Iowa. Additional images of other timber specimens tested are presented in Appendix B.

For each timber pile, the generated tomographic image at each cross section was used to determine an average velocity for that particular cross section. The average velocities at the pre-selected elevations were then compared and a minimum and an average velocity were calculated for the entire specimen. The density and travel time parallel to the grain were also measured. By knowing the pile length, the velocity parallel to the grain was calculated. Equation 5.1 was used to calculate a dynamic modulus of elasticity (MOE_d). A Poisson's ratio of 0.49 was selected, which is a typical value for Southern Yellow Pine timber species (Refer to Table 2.1). A summary of pile properties, measured velocities, and calculated MOE_d is presented in Table 5.1. It was noted that the ultrasonic wave speed parallel to the grain was about 2-5 times higher than the wave speed perpendicular to the grain. Results from pertinent literature showed that wave speed parallel to the grain was 3 to 7 times higher than the wave speed perpendicular to the grain (Ross et al. 2001).

5.2. Axial Compression Tests

Upon completion of the nondestructive evaluation, each pile section was tested in compression to determine its modulus (E). The compression machine recorded both the applied load and pile displacement (See Figure 5.9). A stress-strain curve was produced for every pile section as shown in Figure 5.10. The stress-strain curves show that piles Nos. 1, 2, and 3, which were new piles, displayed a clear linear elastic region and a distinct yielding point beyond which the pile section failed. The yielding points for the other pile sections, which were in-service prior to testing and endured varying degrees of deterioration, were less distinct. These pile sections also showed higher displacement prior to failure. Overall, all pile sections demonstrated ductile behavior for the range of applied loads. E for the tested sections were calculated at 0.1 and 0.2% strain for new and in-service pile sections, respectively. E values obtained are summarized in Table 5.1.

5.3. Correlation between Compression and Ultrasonic Stress Wave Tests

Linear regression models were developed, shown in Figure 5.11, correlating E determined from axial compression tests and MOE_d predicted from the average velocity perpendicular to the grain, the minimum velocity perpendicular to the grain, and the average velocity parallel to the grain. The results show a relatively good correlation ($R^2 = 0.71$) between the MOE_d determined from radial velocities perpendicular to the grain and E. There is no significant difference between the models derived from the average and minimum velocities perpendicular to the grain. The model developed using the average velocity parallel to the grain showed the lowest

correlation ($R^2 = 0.50$). Multiple regression models were developed to evaluate whether combining velocity measurements parallel and perpendicular to the grain would improve the regression model predictability. In the first model, Figure 5.12a, the MOE_d determined from average and minimum velocities perpendicular to the grain were combined and used to predict E. In Figure 5.12b, the average MOE_d perpendicular to the grain and MOE_d parallel to the grain were used to estimate E. Figure 5.12c shows the third multiple regression model, which used the minimum MOE_d perpendicular to the grain and the MOE_d parallel to the grain to predict E. Finally, MOE_d determined from all three velocities were combined to estimate E. According to t-values calculated from multiple regression statistical analysis, combining the MOE_d does not considerably improve the regression model predictability compared to the linear regression models utilizing velocity measurements perpendicular to the grain.

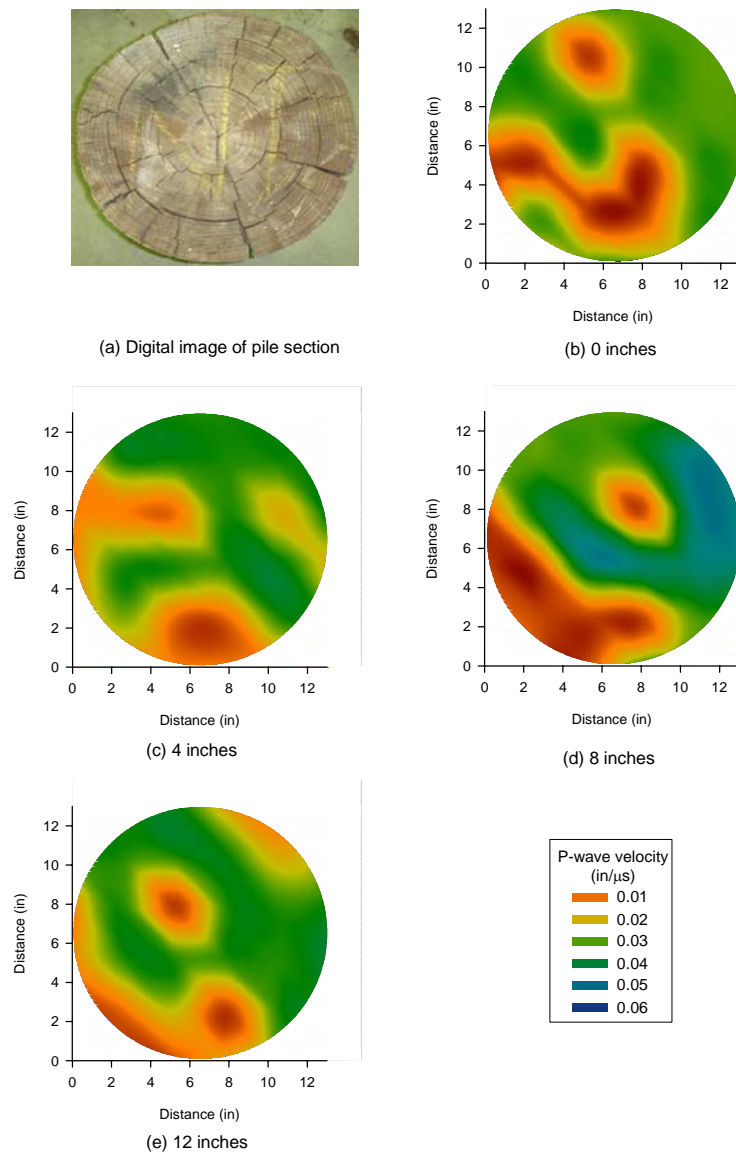


Figure 5.8. Generated tomography images of a timber pile specimen (Pile 1 North Abutment Marshall County Bridge)

Table 5.1. Summary of destructive and nondestructive test results

Specimen no.	Weight (lb)	Diameter (in)	Density (lb/ft³)	Average V_{radial} $\times 10^4$ (in/sec)	Minimum $m V_{\text{radial}}$ $\times 10^4$ (in/sec)	Average $V_{\text{long.}}$ $\times 10^4$ (in/sec)	MOE_d $\times 10^6$ from Avg. V_{radial} (lb/in²)	MOE_d $\times 10^6$ from Min. V_{radial} (lb/in²)	MOE_d $\times 10^6$ from $V_{\text{long.}}$ (lb/in²)	E $\times 10^5$ from axial compression (lb/in²)
1	29.42	7.75	45.33	3.87	3.23	17.0	1.05	0.73	20.3	8.5
2	20.56	8.0	44.18	3.75	3.21	14.0	0.72	0.53	10.1	7.3
3	16.9	9.17	29.02	3.54	3.16	18.7	0.42	0.34	11.8	4.2
4	43.85	11.3	42.93	3.08	2.48	9.10	0.47	0.31	4.08	2.3
5	68.4	12.0	46.86	1.86	1.57	12.8	0.19	0.13	8.83	1.4
6	41.9	11.3	40.56	2.02	1.56	11.6	0.19	0.11	6.31	0.8
7	67.7	11.1	53.26	3.27	2.78	12.2	0.66	0.48	9.16	2.5
8	63.45	12.6	49.54	2.71	2.04	11.1	0.42	0.24	7.10	1.8
9	61.81	12.0	41.97	3.04	2.82	13.2	0.45	0.39	8.43	2.8
10	81.5	12.0	51.88	2.89	2.65	15.0	0.50	0.42	13.5	2.3
11	81.75	13.0	44.81	2.83	2.30	12.2	0.42	0.27	7.74	2.2
12	35.25	11.5	38.15	3.58	2.88	12.0	0.57	0.37	6.41	3.4

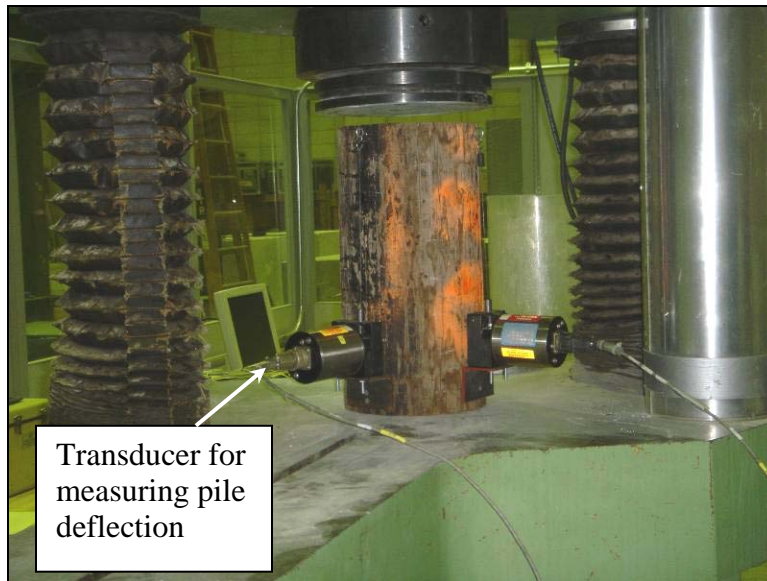


Figure 5.9. Pile compression test

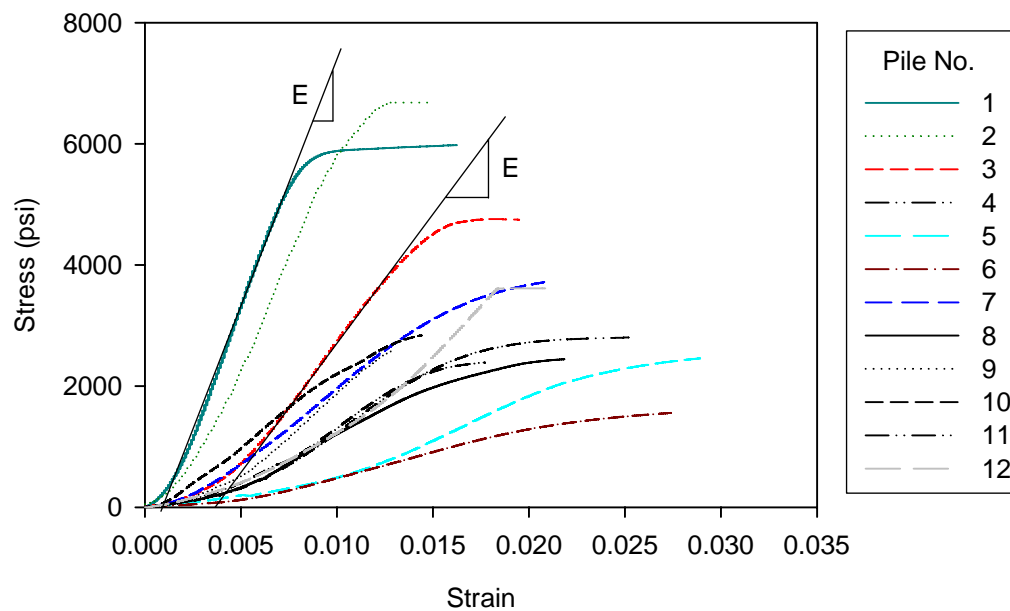
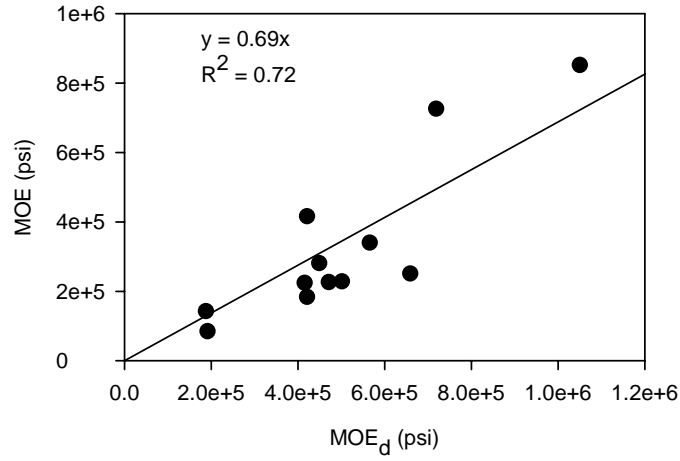
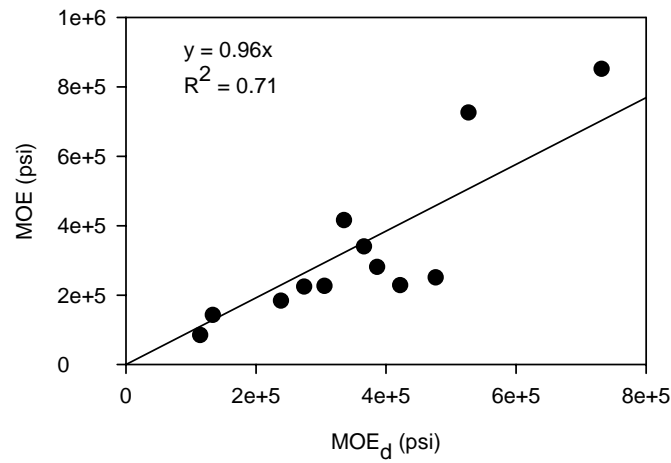


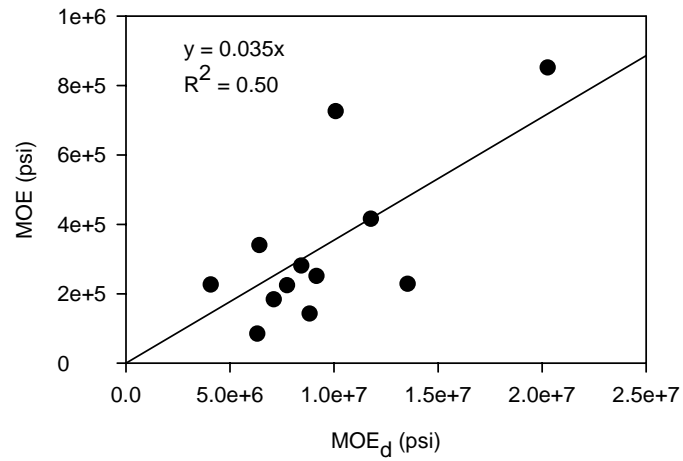
Figure 5.10. Stress-strain data for timber pile sections



(a) Average velocity perpendicular to the grain



(b) Minimum velocity perpendicular to the grain



(c) Average velocity parallel to the grain

Figure 5.11. Correlation between E determined using ultrasonic stress wave tests and axial compression tests

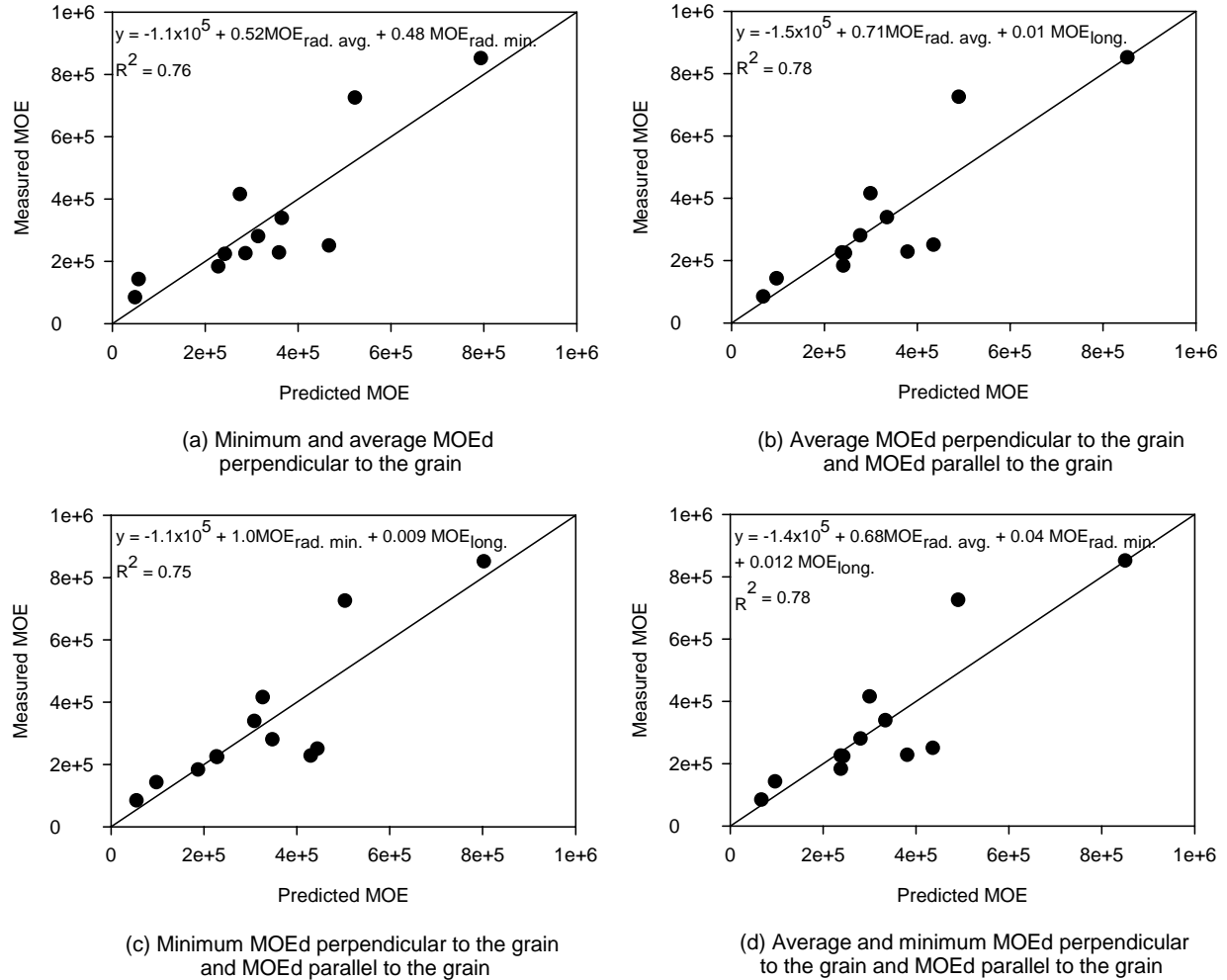


Figure 5.12. Multiple regression models for predicting E

5.4. Summary

- This laboratory investigation evaluated the potential of using nondestructive techniques to determine the internal condition of timber piles, and establish a correlation between destructive and nondestructive test method, which can assist in estimating the residual capacity of in-service piles.
- The nondestructive method used in this laboratory study was the ultrasonic stress wave technique. This method is directly correlated to the material properties, which is used to reveal the pile internal condition.
- The image reconstruction method used to generate 2-dimensional tomography images from multiple ultrasonic stress wave measurements is the Simultaneous Iterative Reconstruction Technique.
- The test procedure and the imaging reconstruction technique were able to display the internal pile condition.
- The test method, however, has a tendency of over predicting the size of the internal defect. The prediction error increases as the size of the internal defect decreases.

Increasing the number of test measurements can improve the accuracy of the test method.

- MOE_d parallel and perpendicular to the grain were calculated for 12 timber pile sections using the nondestructive stress wave test. Following the nondestructive tests, axial compression tests were performed on 12 timber pile specimens to calculate their E.
- Linear regression models show a relatively good correlation between the MOE_d and the E ($R^2 = 0.7$). Multiple regression models combining 2 or more MOE_d parallel and perpendicular to the grain did not considerably improve the model predictability.
- It is concluded that ultrasonic stress wave technique is a promising for use tool in evaluating timber substructure sections.
- Future research is needed to evaluate; (1) different transducers orientations, (2) other image reconstruction techniques, (3) the possibility of producing 3-dimensional images of the internal pile condition (i.e. transducers positioned at different elevations) and (4) alternative ultrasonic stress wave devices.

6. EXPERIMENTAL METHODS FOR FIELD INVESTIGATION

6.1. Introduction

To understand the behavior of deteriorating timber piles and their effect on load distribution through the substructure system, six bridges (discussed in Chapters 7 – 12) with timber substructures were identified and selected for field testing. The selected substructures had varying degrees of pile deterioration. At each bridge, nondestructive ultrasonic stress wave tests and static load tests were performed. Static load tests were conducted by positioning a loaded dump truck at predetermined locations on the bridge deck and measuring the strain in the multiple piles simultaneously. Furthermore, pile cores were collected using an increment borer to measure the density in deteriorated sections. Results of the ultrasonic stress wave and the static load test measurements were compared and analyzed to better understand how vehicle loads are distributed through the pile elements, and ultimately, how deteriorated pile sections in the bridge system contribute to bridge performance problems. Maintenance and repair alternatives were also investigated and discussed separately in Chapter 13.

6.2. Ultrasonic Stress Wave Test

Similar to the laboratory stress wave testing procedures, the stress wave test was conducted in the field for each pile. However, due to the presence of the backwall behind the piles, a 5 point grid was used (lower than the 8 point grid used in the laboratory tests). The test was conducted at 6 inch increments to obtain a 2-dimensional tomography image. According to Divos and Szalai (2002) conducting a 5 point grid (i.e. 5 measurements) results in a minimum detectable defect of 6% of the total cross sectional area. Internal pile deteriorations smaller than 6% would have required a higher number of test points (Refer to Figure 5.4). Since all the tested piles were in-service, the results could not be visually verified with a cross section. When significant cracks and splits were present at the pile surface, the test produced unstable travel time readings.

6.3. Static Load Test

Substructure static load tests were conducted at each bridge using a fully loaded tandem axle truck, which was positioned at predetermined locations along the bridge deck (See Figure 6.1). Figure 6.2 shows the dimensions of the truck, whereas Table 6.1 summarizes the truck loadings used on each bridge.

Three incremental point loads were applied by positioning the truck at predetermined locations on the bridge deck. The back wheel of the rear axle was positioned on the centerline of the abutment to apply the first loading increment. For the second loading increment, the truck was repositioned on the bridge deck so the front wheel of the rear axle was over the centerline of the piles. The third load was applied by positioning the wheels of the front axle over the centerline of the abutment (See Figure 6.3). The incremental loads were applied in three lanes along the bridge deck (e.g. west edge, centerline, east edge). A schematic of the axle footprint is shown in Figure 6.4. The load from each wheel was measured using portable axle/wheel weighing scales as shown in Figure 6.5.

To measure the strain, piles at each abutment were instrumented with strain transducers manufactured by Bridge Diagnostics, Inc. (BDI). Each strain transducer is 4.4 in x 1.2 in x 0.4 in with an appropriate length of lead wire attached to it (See Figure 6.6). Each transducer also has a unique number through which it can be identified by the data acquisition system. Once identified, the acquisition system calibrates and zeros the transducer using a pre-stored calibration factor. Each strain transducer can be attached to an extension to increase the 3-inch gage length as shown in Figure 6.7. This was used to enable averaging strains over a larger length to determine the behavior of a localized deteriorated zone along the exposed pile. The gage length can be extended in 3 inch increments only because of the pre-drilled holes in the extensions. Typically the strain transducers were attached to the piles using brass woodscrews that were about 2 inches long. Due to the non-homogeneity of wood, the exposed portion of each pile was instrumented with more than one strain transducer to capture pile behavior at both strong and weak sections. The arrangements of the strain transducers were generally based on weak and strong regions along the pile identified by the ultrasonic stress wave test and pile coring. In addition to instrumenting pile elements, strain transducer swere also attached to the timber backwall to measure strains induced by axial and/or lateral loads (See Figure 6.8).

The BDI strain transducers were connected to BDI STS units (See Figure 6.9), which transfer the data to the data acquisition system. One STS unit is capable of storing 50,000 data points during a single test and can be connected to four strain transducers (Wipf et al. 2003b).



Figure 6.1. Tandem axle truck using to carry out static load tests

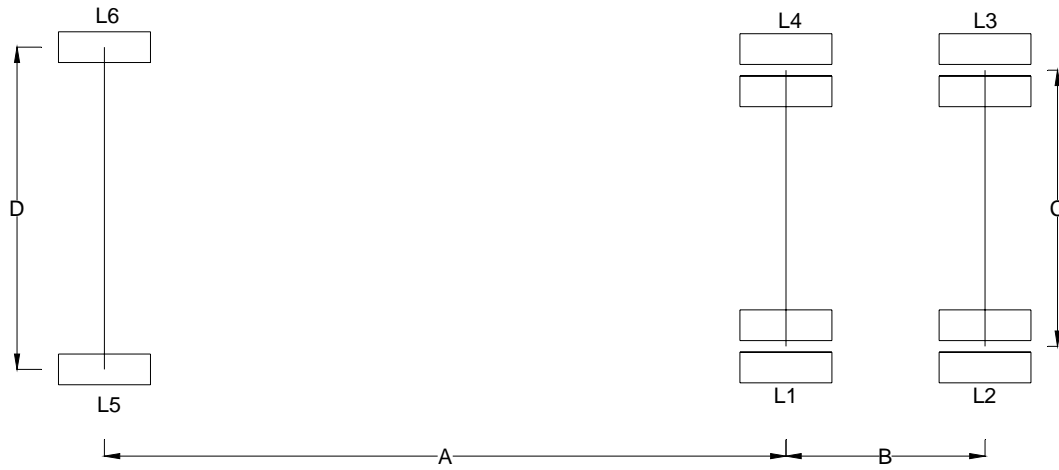
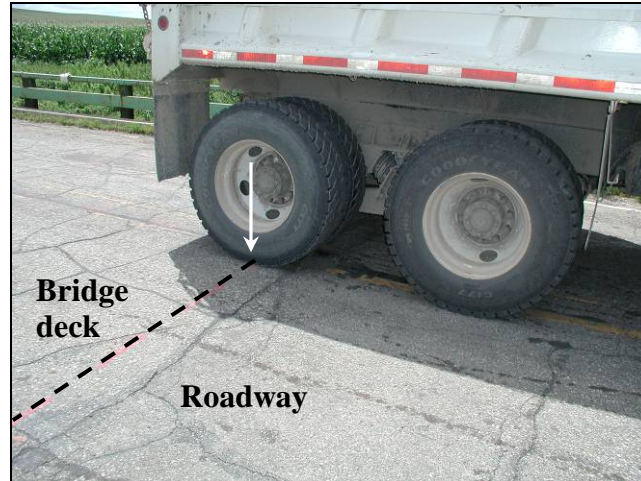


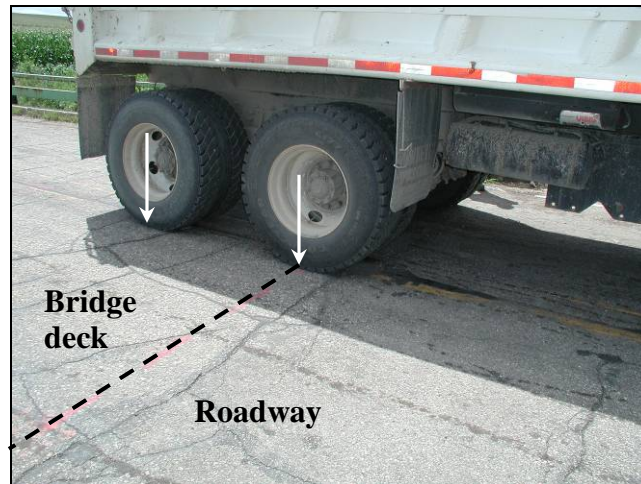
Figure 6.2. Schematic of tandem axle truck used to static loading

Table 6.1. Summary of truck dimensions and wheel loads

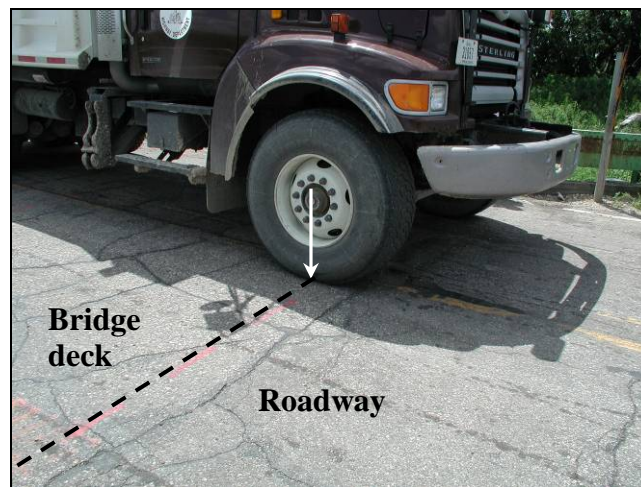
Bridge no.	County	A (ft)	B (ft)	C (ft)	D (ft)	L1 (lb)	L2 (lb)	L3 (lb)	L4 (lb)	L5 (lb)	L6 (lb)
7710	Boone	14.8	4.3	6	7	8,415	8,500	9,050	8,415	-	-
243470	Marshall	16.7	4.6	6	7	9,300	8,800	8,750	9,250	7,550	8,100
237350	Mahaska	15.4	4.2	6	7	9,350	9,150	9,400	9,550	8,850	8,950
094680	Carroll	16.5	4.4	6	7	10,200	10,550	8,800	8,900	7,900	7,900
237380	Mahaska	15.4	4.3	6	7	9,300	9,300	9,000	9,600	8,500	8,800
029070	Humboldt	14.2	4.5	6	7	8,450	8,500	9,850	10,400	7,050	8,000



(a) Rear wheel of the tandem axle



(b) Front wheel of the tandem axle



(c) Front wheel of the front axle

Figure 6.3. Applying three load increments above the bridge abutment

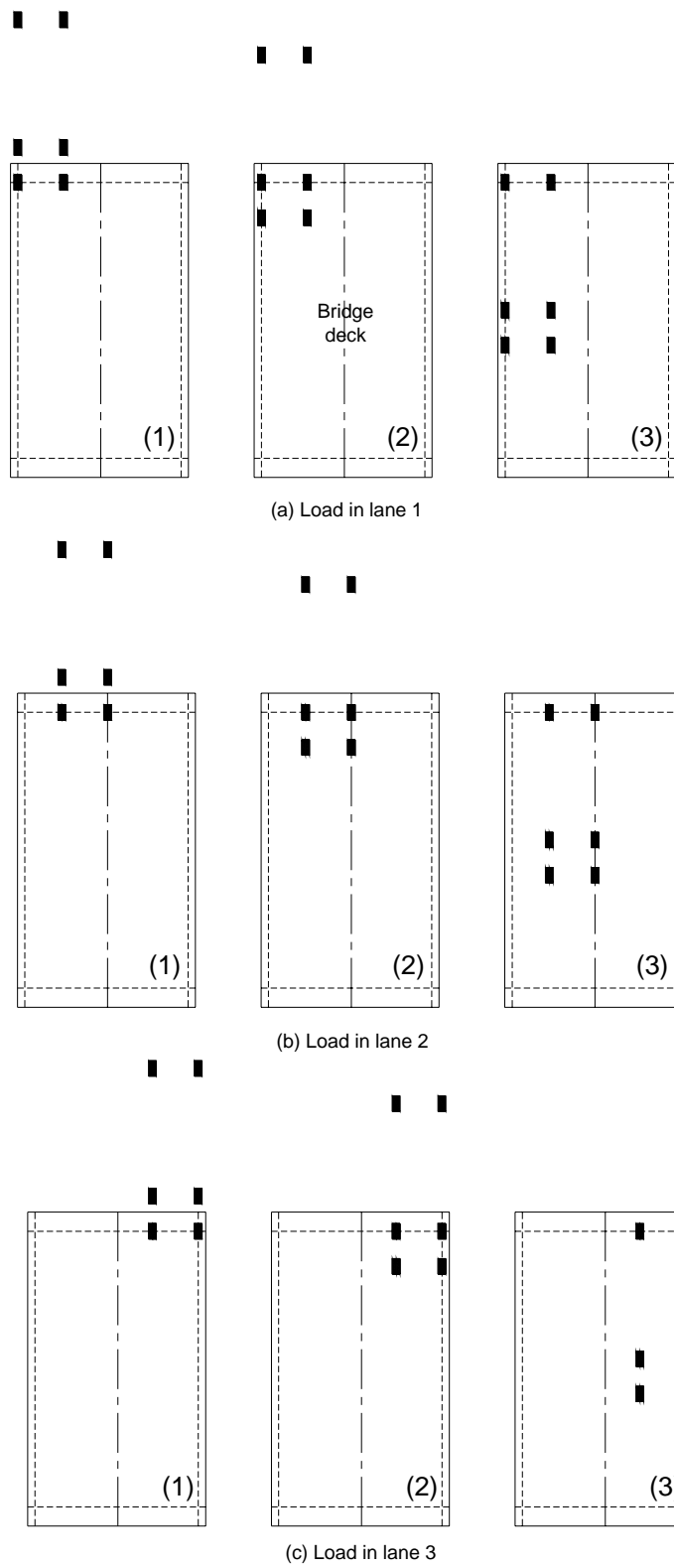


Figure 6.4. Schematic diagram of the axle footprint



Figure 6.5. Wheel loads measured using a portable axle/wheel scale



Figure 6.6. A BDI strain transducer



Figure 6.7. A BDI strain transducer with an extension (Bridge No. 02-90-70 Humboldt County – July 10 2006)

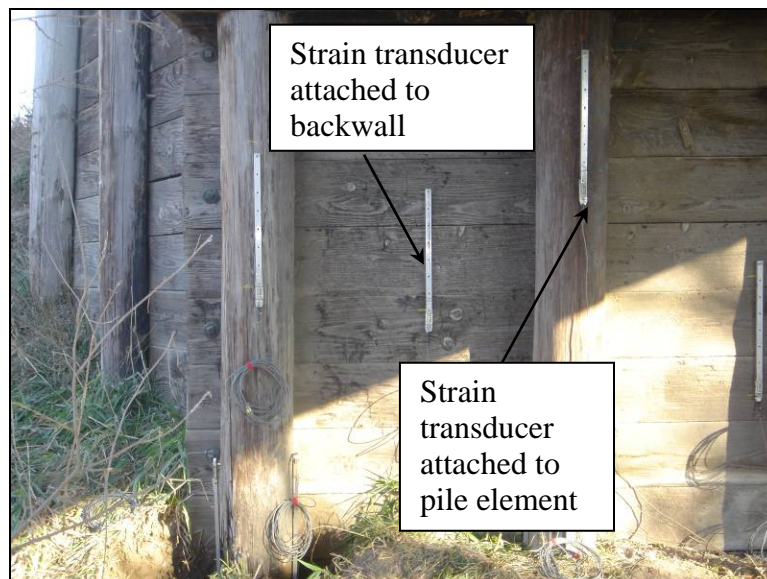


Figure 6.8. Timber piles and backwall instrumented with strain transducer (Bridge No. 23-73-50 Mahaska County – October 28 2005)

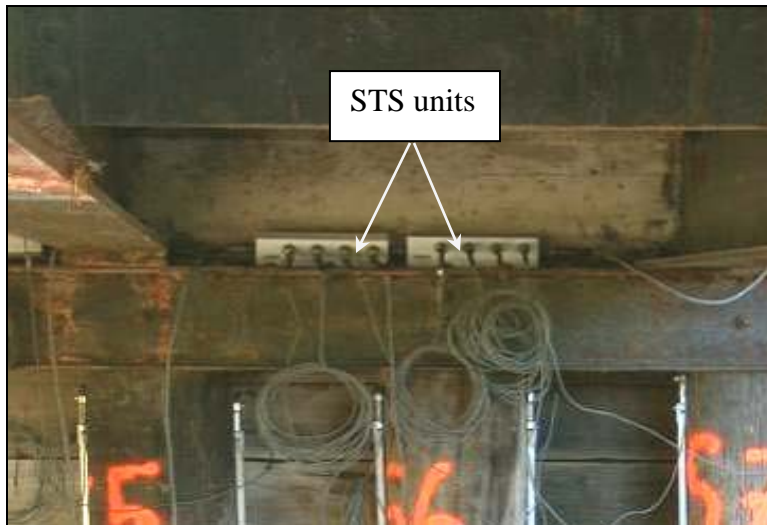


Figure 6.9. STS Units connected to strain transducers (Bridge No. 24-34-70 Marshall County – July 28 2005)

6.4. Pile Coring

An increment borer was used to obtain a pile core from each pile (See Figure 6.10). The increment borer, which has a diameter of 0.203 inches, was used to determine if the pile was hollow near its core, and to obtain a specimen for determining the wood density. For some piles, more than one core was obtained to determine the density profile along the pile. The extracted cores were also used to visually assess the level of creosote penetration in the piles. It was noted that the creosote diffusion in most piles was not high enough to reach the pile core. A core obtained from a pile in Bridge no. 094680 Carroll County is shown in Figure 6.11. The total length of the core was about 4.9 inches. The creosote penetrated a distance of about 3.3 inches into the pile. The typical penetration distance for creosote in the piles supporting the six bridges investigated ranged from 2 to 4 inches.

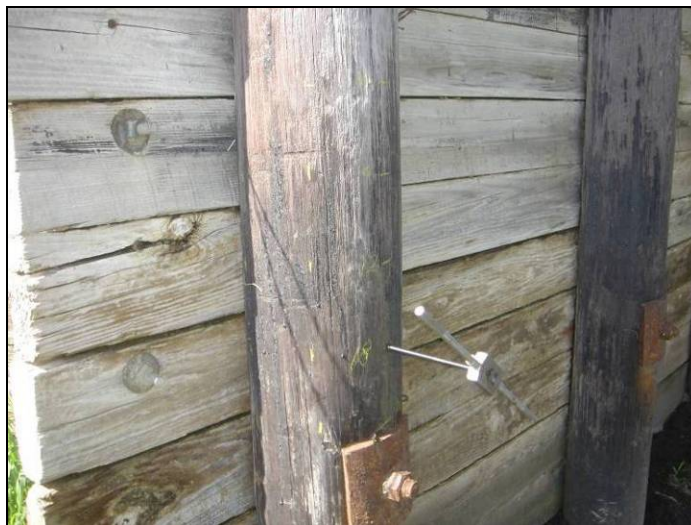


Figure 6.10. Increment borer used to obtain a pile core (Bridge No. 09-46-80 Carroll County – May 12 2006)

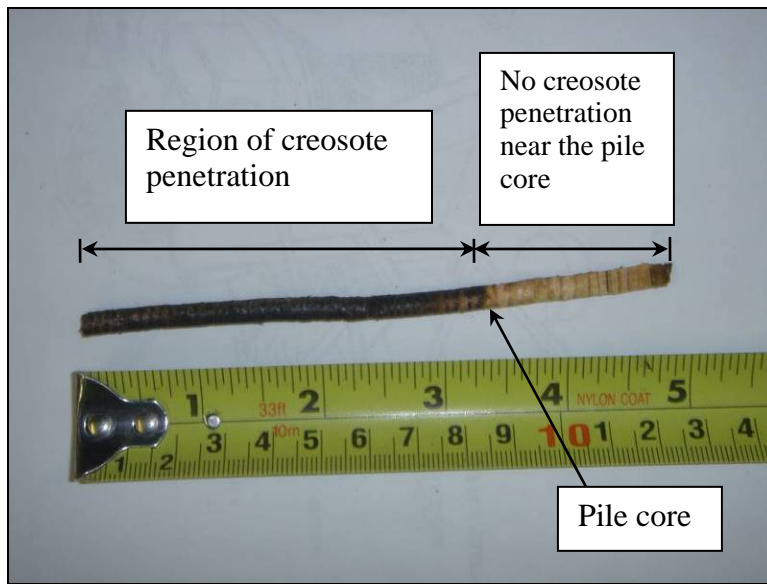


Figure 6.11. Pile core showing level of creosote penetration

7. BRIDGE NO. 7710 BOONE COUNTY

7.1. Bridge Description

This bridge is located in Boone County, Iowa and is about 1 mile west of Highway U.S. 169, on G Avenue crossing Little Beaver Creek (See Figure 7.1). This bridge, which was constructed in 1900, has a 0° skew, a span of 36 ft, a concrete deck, and 6 steel girders.

Each abutment is comprised of seven timber piles about 7 inches in diameter, a timber backwall, and a double c-channel cap (See Figure 7.2). The average exposed length of the piles above the water table was about 50 inches. The pile length below ground level is unknown since no bridge plans were available. The piles at the north abutment were denoted as no. 1 located at the northwest edge of the bridge, through no. 7 as shown in Figure 7.3. The dimensions of the north abutment are shown in Figure 7.4. A schematic diagram of the abutment, shown in Figure 7.5, indicates that the bridge does not have a conventional stub-abutment detail; the girder ends are integrally connected to a concrete diaphragm, which rests directly on top of the pile cap. This integral connection complicates the substructure analysis due to the difficulty in quantitatively, isolating, and understanding its effect on load distribution through the substructure components. Inspection of the north abutment revealed decay at pile no. 1 about 32 inches above the water level (See Figure 7.6). Also, a soft pile section right above the water table was observed at pile no. 7 as shown in Figure 7.7. The soft section may be a result of high levels of moisture due to the variation of the water table, which in turn triggers biological activity. Excessive scour occurred near the south abutment undermining the timber backwall. This led to exposure and erosion of the backfill material creating a void behind the backwall. In 1993, as shown in Figure 7.8, a sheet pile wall was driven behind the south abutment to prevent further erosion; the erosion-induced void was filled with concrete.



Figure 7.1. Bridge No. 7710 Boone County – looking south (June 24 2005)



Figure 7.2. Seven supporting timber piles at each abutment with a timber backwall and double c-channel cap (Bridge No. 7710 Boone County – June 1 2005)



Figure 7.3. Piles denoted by numbers 1 through 7 at the north abutment (Bridge No. 7710 Boone County – July 1 2005)

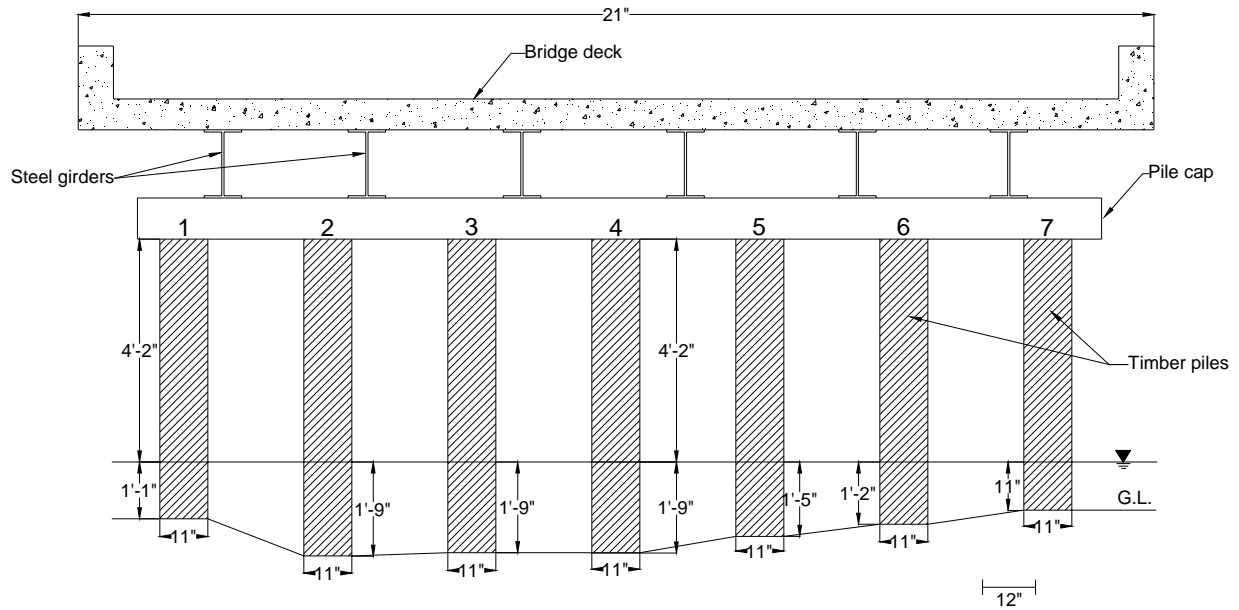


Figure 7.4. Schematic diagram of the north abutment (Bridge No. 7710 – Boone County)

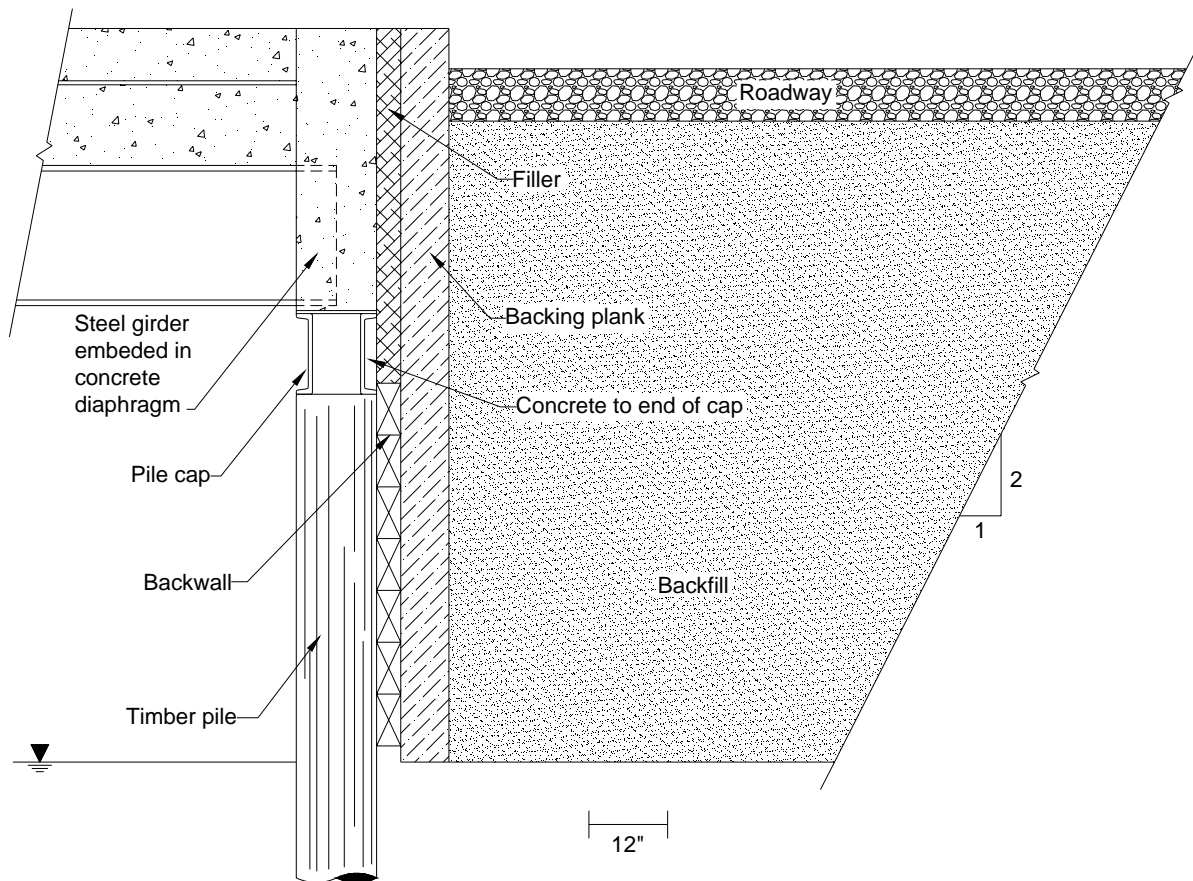


Figure 7.5. Schematic diagram of the bridge cross section (reproduced from the bridge construction plans)



Figure 7.6. Deterioration at pile No. 1 (Bridge No. 7710 Boone County – July 1 2005)



Figure 7.7. Soft section at pile No. 7 above the water level (Bridge No. 7710 Boone County – July 1 2005)



Figure 7.8. Sheet pile wall driven behind the south abutment to prevent backfill erosion (Bridge No. 7710 Boone County – June 1 2005)

7.2. Load Test Setup and Instrumentation

At this bridge, strain measurements from each pile were collected at the first two loading stages only (i.e. loads applied from the tandem axle only). Each pile was instrumented with four strain transducers along the exposed part of the pile. Some of the strain transducers extended below the water level to capture the strain in soft sections that are usually encountered near the water level. The gage lengths ranged from 12 to 24 inches as shown in Figure 7.9. Each strain transducer is denoted by two numbers. The first number refers the strain transducer number, while the second refers the pile numbers.

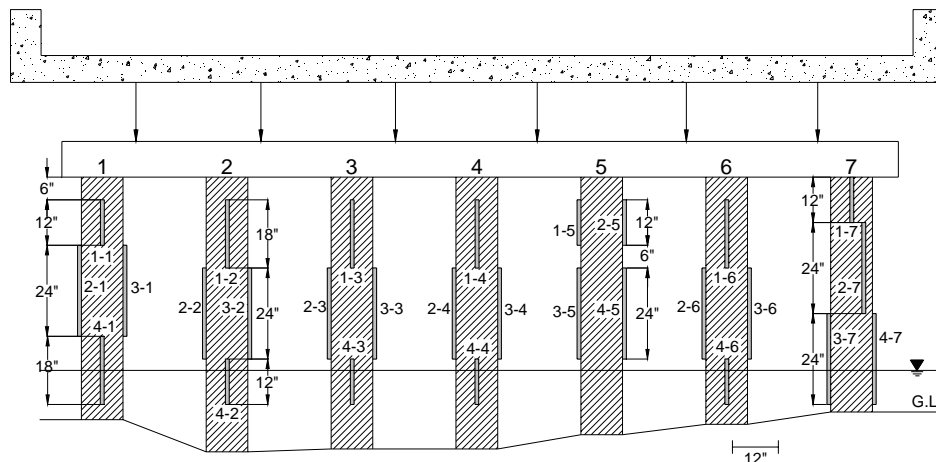


Figure 7.9. Locations of strain transducers at the north abutment (Bridge No. 7710 – Boone County)

7.3. Test Results

7.3.1. North Abutment – West Edge

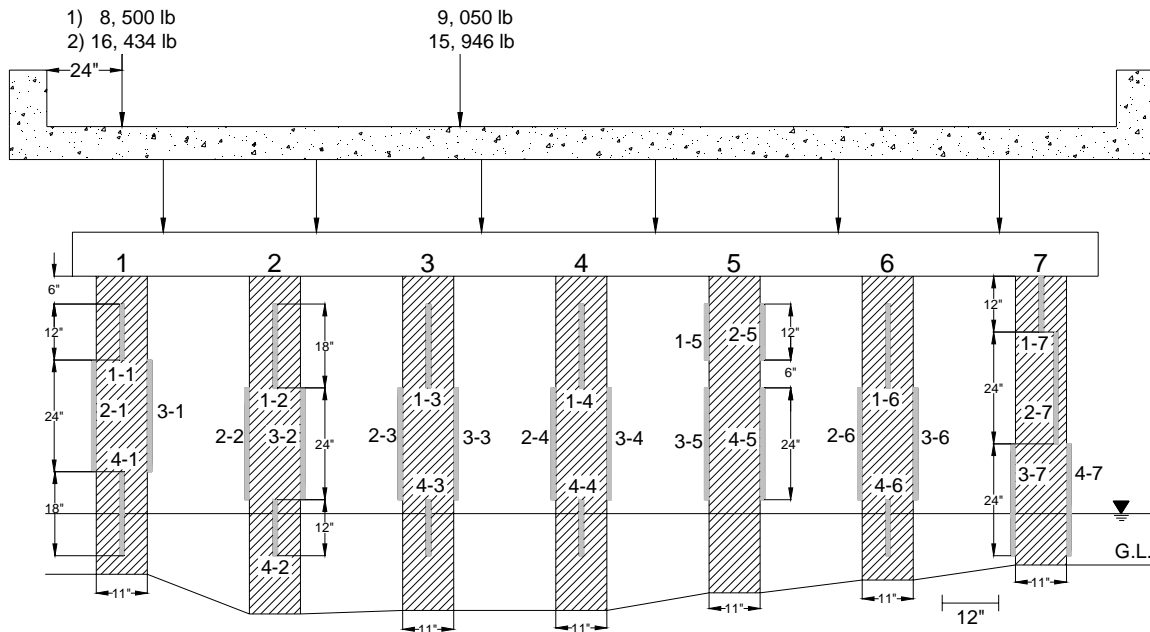
The north abutment was loaded at the west edge of the bridge. Summarized in Figure 7.10 are the strains measured in each pile and the locations of the applied loads. Load configurations 1 and 2 correspond to positioning the rear wheel then the front wheel of the tandem axle over the centerline of the piles, respectively (Refer to Figure 6.4 for loading pattern). The highest strains measured, which occurred in pile no. 1, were about -40 and -78 microstrains at both load configurations. Without knowing the pile modulus, it is not possible to determine whether the high strains are a result of higher load or higher pile compression caused by internal decay. The field data revealed that strain values decreased with increasing distance from the applied load so that there was essentially no strain in pile no. 7. The difference in strain values between piles is an indication of the flexible behavior of the pile cap. The strain transducer 1-3 on pile no. 3 showed positive strains (top 18 inches). This may be caused by pile bending due to eccentric axial load and/or mobilization of lateral earth pressure. Below this region, however, strain measurements for pile no. 3 were negative. At each pile and for a specific load configuration, the strains varied both longitudinally and transversally along the exposed portion of the pile. This finding, which is attributed to the anisotropic behavior of timber and to localized degraded regions along the pile, further increased the difficulty in characterizing the pile's condition.

7.3.2. North Abutment – Centerline

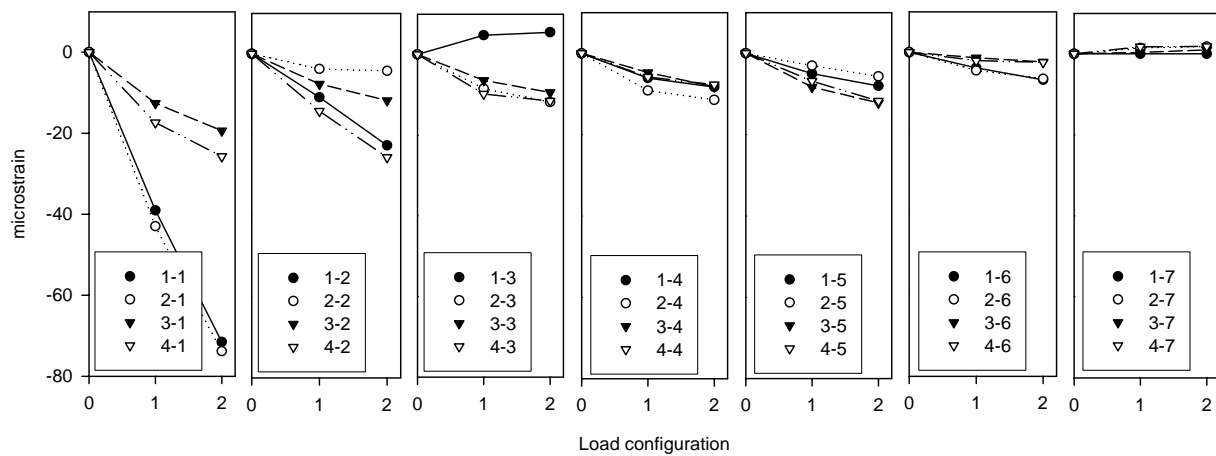
The second loading location was at the centerline of the bridge. Pile strains and the locations of the applied static loads for this load case is shown in Figure 7.11. For the first and second loading configurations, strain transducers 1-1 and 2-1, which were attached to pile no. 1, measured the highest strain. Since high strains were measured at pile no. 1 during loading both the west end and centerline lanes, it is surmised that pile no. 1 was compressing more than adjacent piles due to its degraded condition (Refer to Figure 7.6) assuming reduced stiffness. Also, pile nos. 2, 5, and 6 measured high strains. Similar to the previous test, strain transducer 1-3 measured positive strains in the upper portion of the pile.

7.3.3. North Abutment – East Edge

In the third test conducted, load was applied at the east edge of the bridge. The strains and the locations of the applied loads are shown in Figure 7.12. The highest strains were measured in pile no. 6. One interpretation of the high strains is the transfer of axial load from the adjacent pile no. 7 due to the soft pile section observed at the water level (Refer to Figure 7.7). The strain transducer attached to pile no. 7 (denoted by 1-7) measured positive strain values. As shown in Figure 7.13, the pile cap is not aligned over the centerline of pile no. 7 and is partially resting on the backwall. This may have produced eccentric axial loads, which may lead to pile bending and hence positive strains in the upper portion of the pile. The same observation was noted when the abutment was previously loaded at the centerline of the bridge. All strains measured in pile no. 1 were positive. This indicates that pile no. 1 was subjected to tension due to a net uplift force on the west edge of the pile cap.

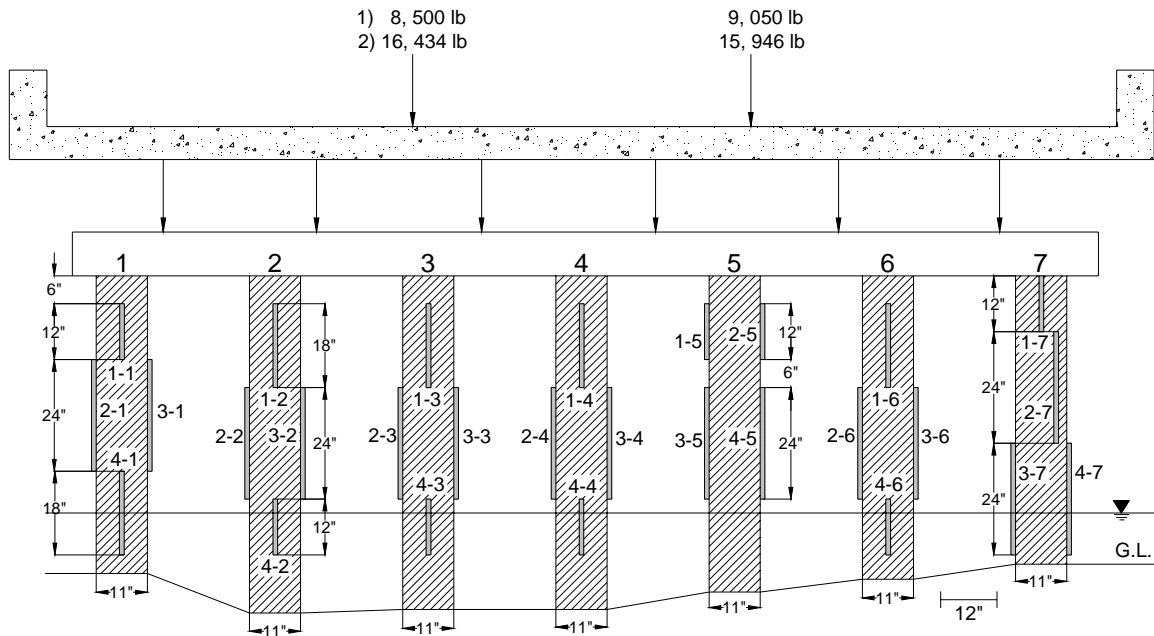


(a) Location of strain transducers and axial loads

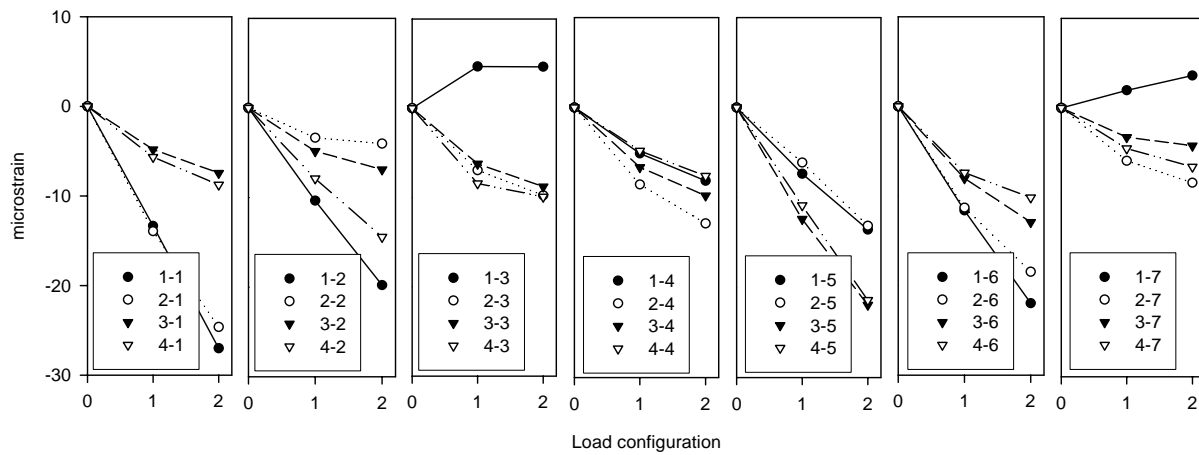


(b) Pile strains

Figure 7.10. Pile strains for north abutment – West edge (Bridge No. 7710 – Boone County)

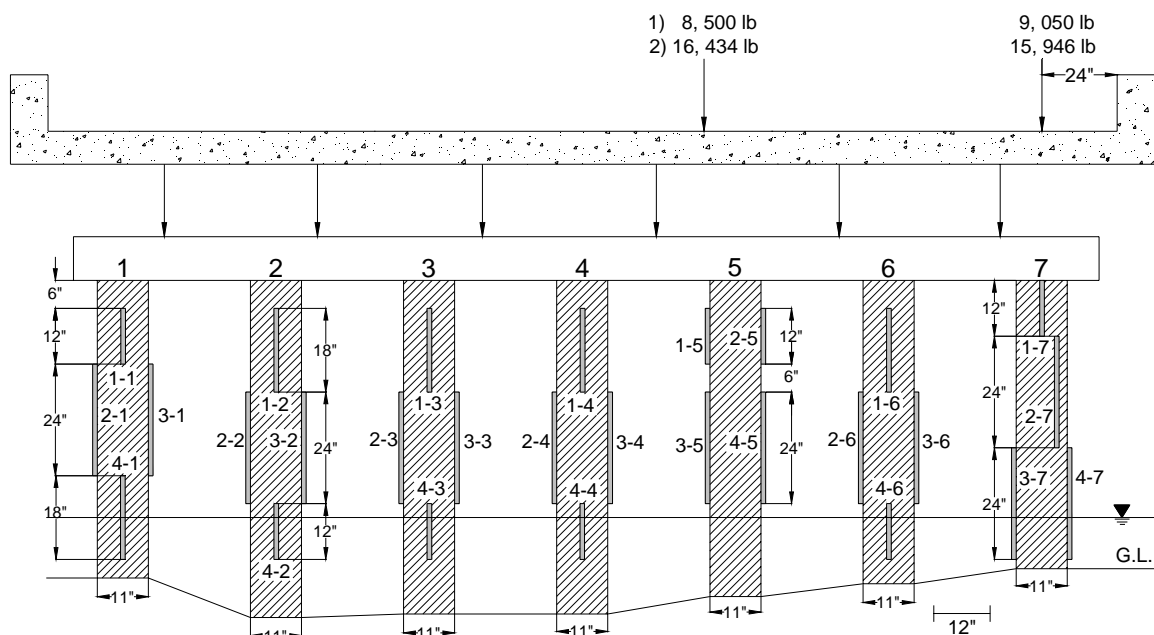


(a) Location of strain transducers and axial loads

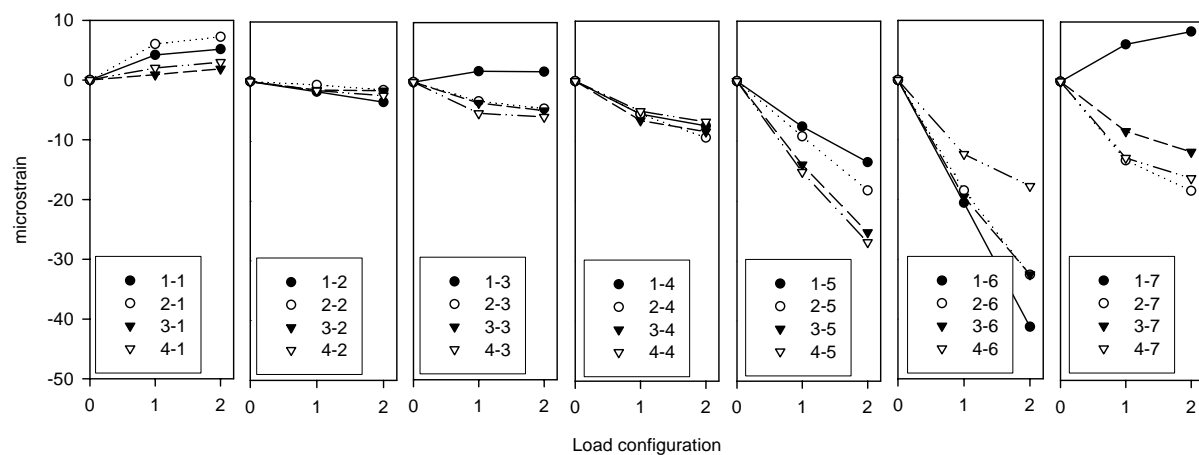


(b) Pile strains

Figure 7.11. Pile strains at north abutment – Centerline (Bridge No. 7710 – Boone County)



(a) Location of strain transducers and axial loads



(b) Pile strains

Figure 7.12. Pile strains at the north abutment – East edge (Bridge No. 7710 – Boone County)



**Figure 7.13. Possible eccentric loading caused by misalignment of pile cap (Bridge No. 7710
– Boone County)**

8. BRIDGE NO. 243470 MARSHALL COUNTY

8.1. Bridge Description

This bridge is located in Marshall County, Iowa crossing Summit Road over a creek. The bridge, was constructed in 1941 and consists of a single span structure with six steel girders, concrete deck and a 5 inch asphalt overlay (See Figure 8.1). The bridge had 0° skew and was 40 ft long and 24 ft wide with an estimated daily traffic of 940.

According to the bridge plans, each abutment was supported on six piles, which were 30 ft long, and 6 wingwall piles, which were 25 ft long. Each pile had a tie back rod at a depth of 56 inches from the pile head. The tie back rods extended a distance of 16 ft behind the backwall and are connected to a 1 ft thick dead man (See Figure 8.2). Field inspections revealed that additional piles were driven at a later date. One pile was driven between pile nos. 1 and 3 at the north abutment and another pile was driven between pile nos. 5 and 7 at the south abutment. The date these additional piles were driven is unknown. Both abutments were thus supported on seven timber piles with a timber backwall and a double c-channel cap (See Figure 8.3 and Figure 8.4). The average exposed pile length at the north and south abutments were about 1.1 ft and 4.6 ft, respectively. The estimated embedded pile length was about 29 ft and 25 ft for the north and south abutments, respectively. A schematic diagram of both abutments illustrating pile diameters, exposed pile lengths, and pile spacing is shown in Figure 8.5.

According to maintenance records, the substructure was inspected in spring of 1998. Pile no. 2 (added at a later date) and pile no. 4 at the north abutment were identified as having about 50% section loss. Prior to 1998, substructure rating varied between good and satisfactory. The bridge was inspected again by a consultant in December 2003. The bridge substructure was given a poor condition rating with seven piles undergoing decay. These piles, however, were not identified in the inspection report.

Visual inspection revealed that both abutments showed signs deterioration. At the north abutment, hammer sounding and probing indicated that pile no. 2 had a hollow core. Considerable pile cracking was also noted (See Figure 8.6). Also, advanced biological deterioration was observed at pile no. 4; the intact pile diameter was about 3 inches as shown in Figure 8.7. The intact pile was surrounded by timber powder, which was reddish brown in color, possibly caused by brown-rot fungi. At the south abutment, high moisture content was observed at the ground level resulting in a rotted section in piles nos. 1 and 4 (See Figure 8.8).

Two weeks after load testing the bridge, and due to the poor conditions of the superstructure and substructure, the bridge was demolished and replaced with a new bridge. Figure 8.9 shows the location of the old south abutment and the construction of the new bridge foundation. The exposed part of some timber piles from both abutments were obtained and were tested in the laboratory to measure their strength properties.



Figure 8.1. North view of Marshall County Bridge No. 243470 (July 22 2005)

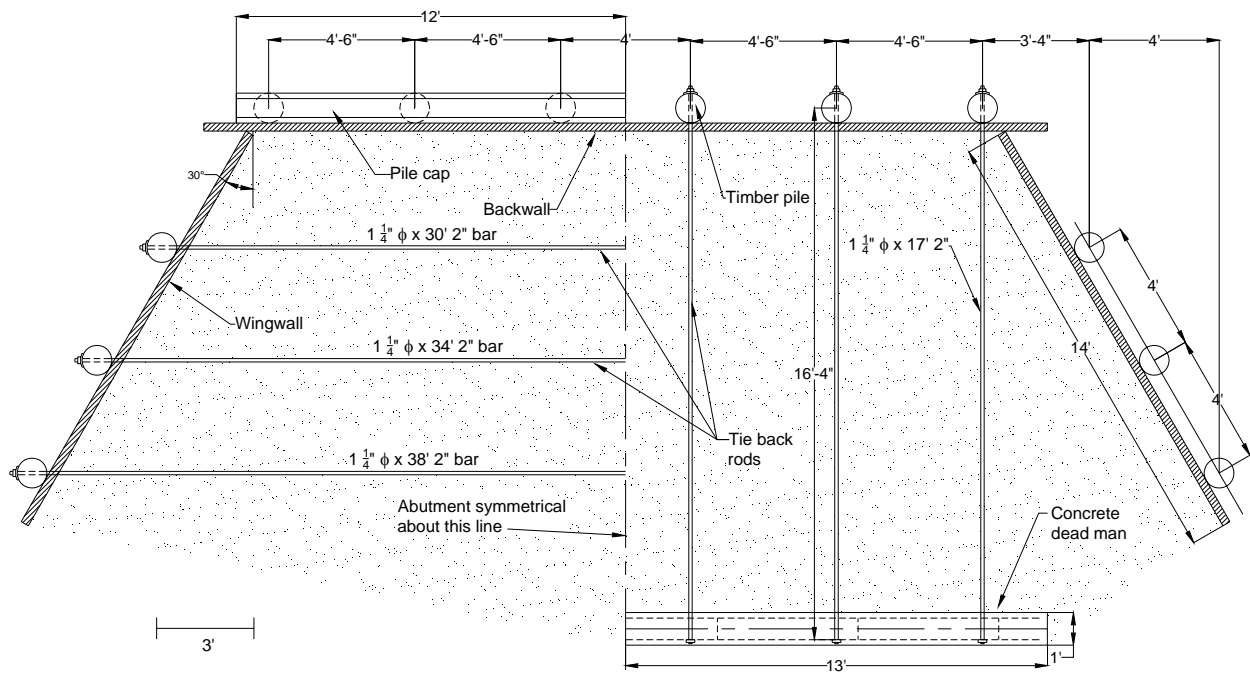


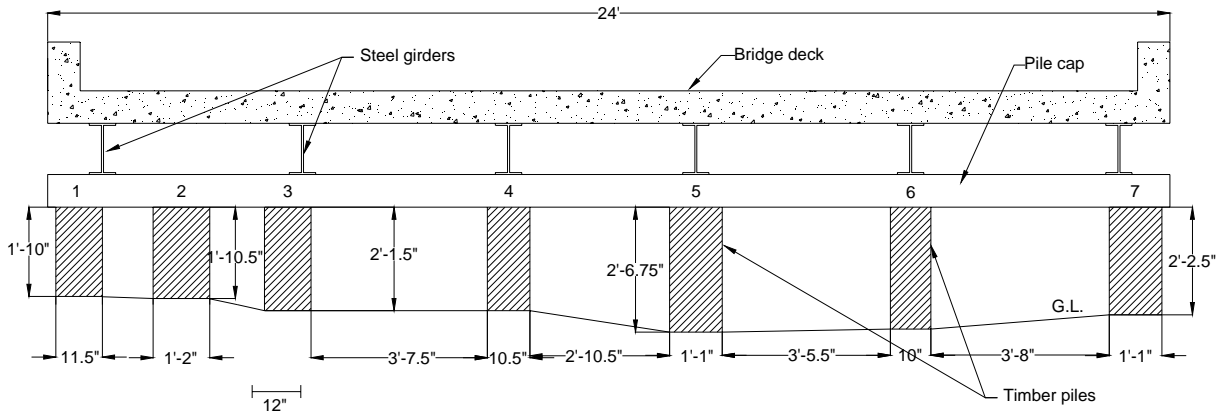
Figure 8.2. Plan view of the bridge abutment (Bridge No. 243470 – Marshall County)



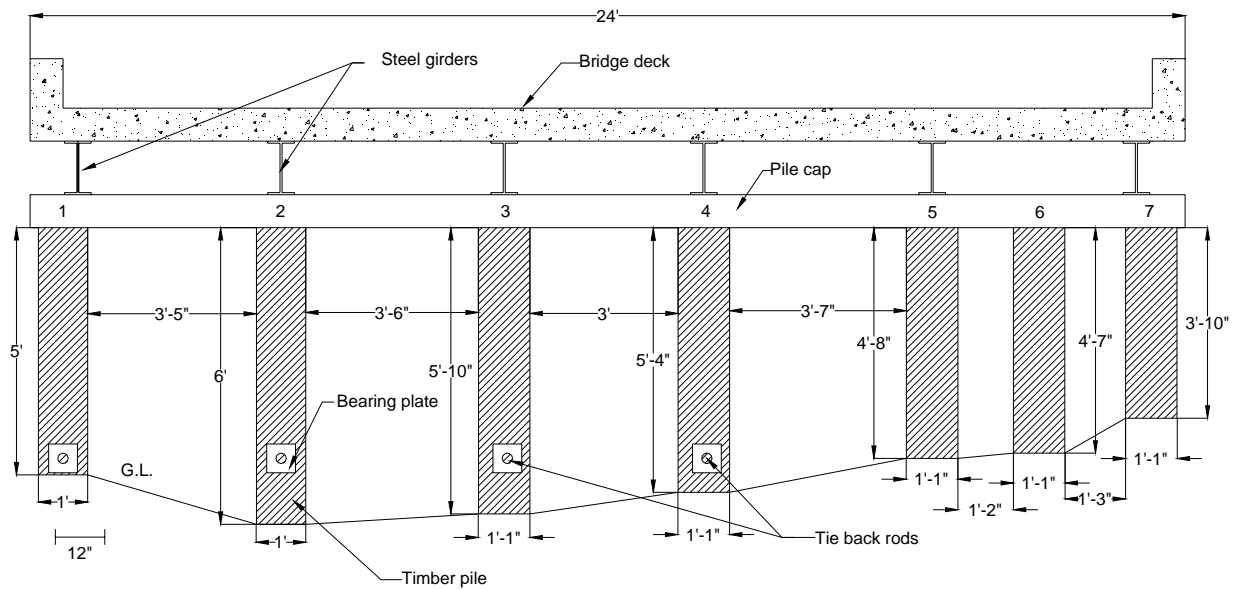
Figure 8.3. North abutment (Bridge No. 243470 Marshall County – July 22 2005)



Figure 8.4. South abutment (Bridge No. 243470 Marshall County – July 22 2005)



(a) North abutment



(b) South abutment

Figure 8.5. Schematic of the bridge substructure (Bridge No. 243470 – Marshall County)



Figure 8.6. Hammer sounding and probing revealed a hollow core at pile no. 2 at the north abutment (Bridge No. 243470 Marshall County – June 22 2005)

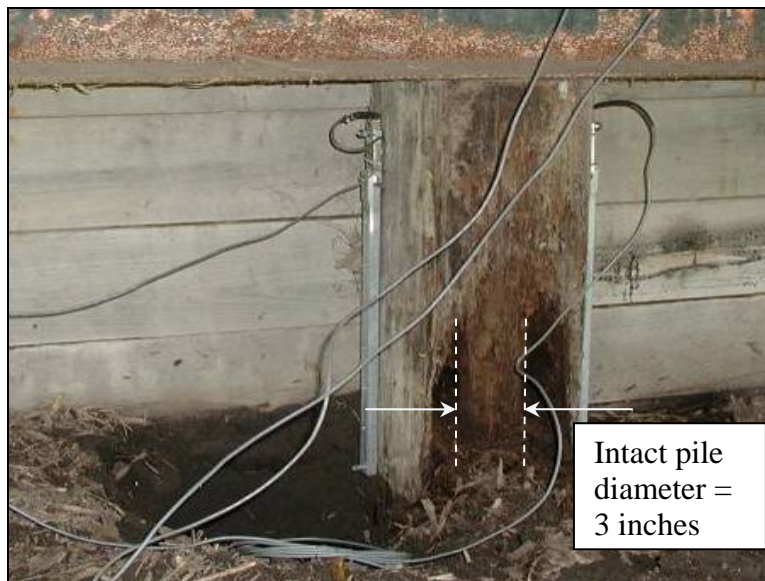


Figure 8.7. Pile no. 4 at the north abutment undergoing biological deterioration (Bridge No. 243470 Marshall County – July 27 2005)



(a) Pile no. 1



(b) Pile no. 4

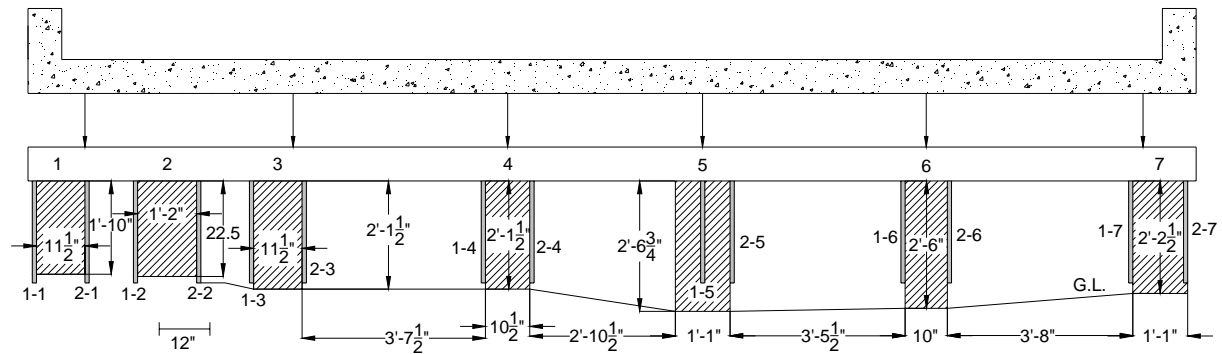
Figure 8.8. Rotting pile sections at the south abutment caused by high moisture content near the ground level (Bridge No. 243470 Marshall County – July 22 2005)



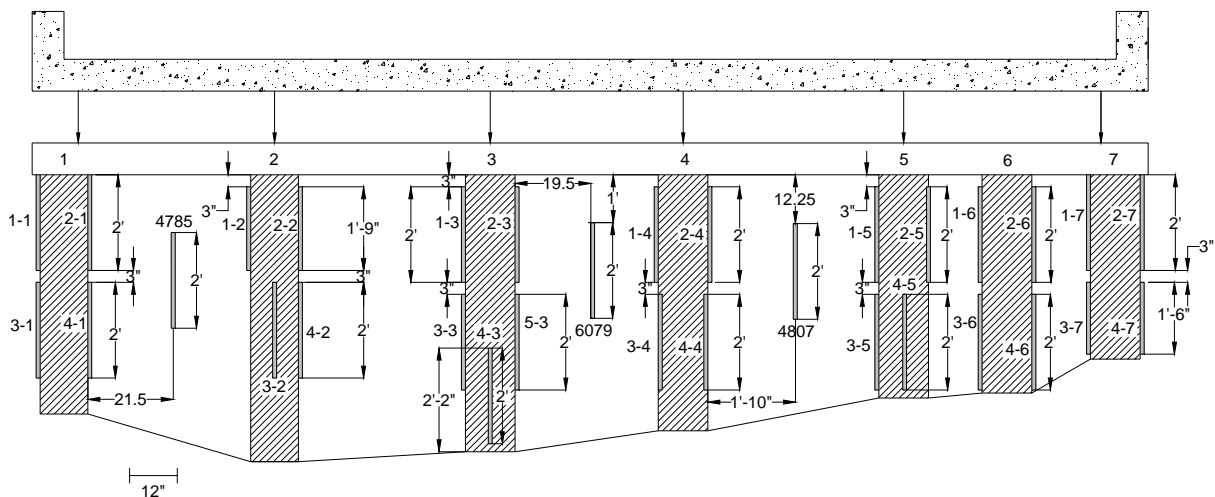
Figure 8.9. Construction of the new bridge foundation (Bridge No. 243470 Marshall County – August 19 2005)

8.2. Load Test Setup and Instrumentation

A static load test was carried out at the north and south abutments. At the north abutment, each pile was instrumented with two strain transducers with a gage length of 24 inches (See Figure 8.10a). At the south abutment, the exposed part of each pile was instrumented with four strain transducers; the gage lengths varied from 18 to 24 inches. To study the influence of the tie back rods on pile strain behavior, at pile no. 3, a fifth strain transducer was installed crossing the tie back rod. Strains measured with this transducer were compared to other strain values measured along the pile. Furthermore, three strain transducers were attached to the timber backwall to measure strains induced by axial and/or lateral loads (See Figure 8.10b)



(a) North abutment



(b) South abutment

Figure 8.10. Strain transducers attached to exposed pile sections (Bridge No. 243470 – Marshall County)

8.3. Test Results

The exposed part of several pile sections were obtained after the bridge was removed to measure their properties. E, which was later used in combination with field strain measurements to determine the load carried by each pile, was determined using an axial compression tests. Then for each pile, the length, diameter, and density were recorded. Table 8.1 summarizes the measured properties.

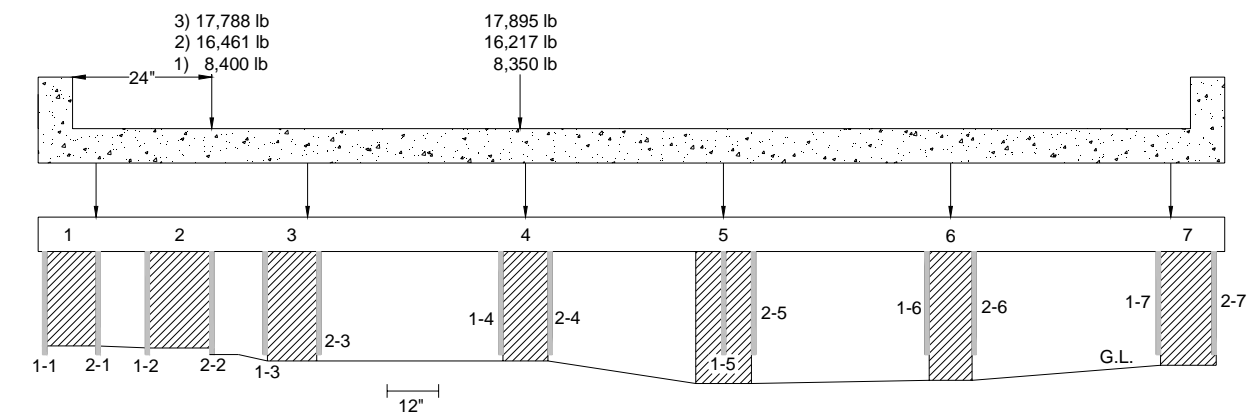
8.3.1. North Abutment – West Edge

The first static load test conducted was at the west edge of the north abutment. The pile strains and the location of the applied loads are shown in Figure 8.11. The results indicate that the highest strain values for all three load configurations were measured in pile no. 1. At load configuration 3, the strain measured in pile no. 1 was about -39 microstrains.

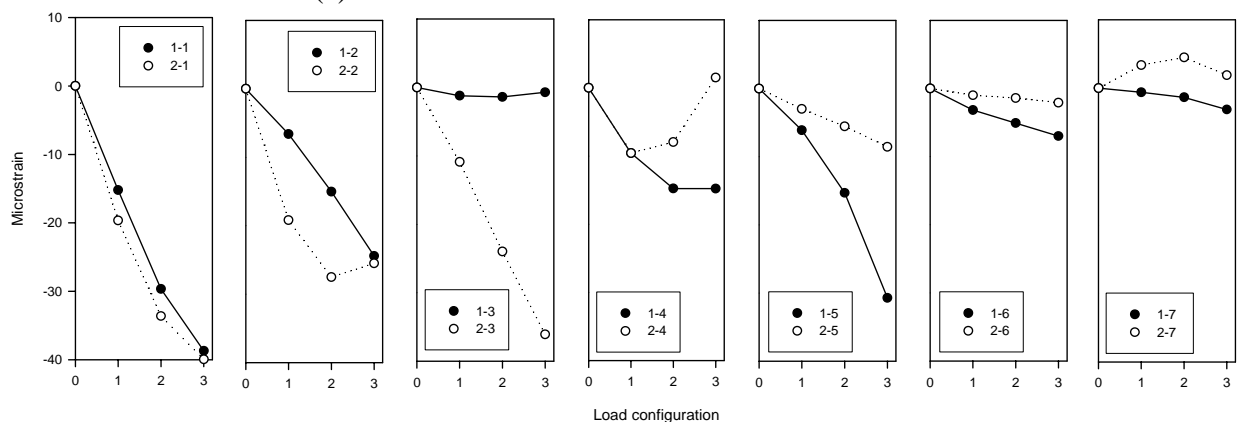
The strain transducers attached to the deteriorated pile Nos. 2 and 4 showed increasing strain to a certain strain level after which the strain values decreased with increasing load. The overall strain of adjacent pile nos. 1, 3 and 5 increased. Pile no. 7 showed positive strain values.

Table 8.1. Properties of pile sections obtained from Bridge No. 243470 – Marshall County

Abutment	Pile no.	Length (in)	Diameter (in)	Density (lb/ft ³)	E x 10 ⁵ (lb/in ²)
North	1	20.5	12.6	49.5	1.8
	6	22.3	12.0	46.9	1.5
South	2	24.0	12.0	51.9	2.8
	3	22.5	12.0	42.0	2.8
	5	23.8	13.3	44.8	2.3
	7	23.5	12.0	55.1	2.8



(a) Location of strain transducers and axial loads



(b) Pile strains

Figure 8.11. Static load test at the west edge (Bridge No. 243470 – Marshall County)

8.3.2. North Abutment – Centerline

The second load test was carried out by aligning the truck wheel on the centerline of the bridge deck. Location of the applied loads and the pile strains are shown in Figure 8.12. Similar to the previous load test, pile nos. 1, 3 and 5 had the highest strains. Also, the deteriorated pile nos. 2 and 4 demonstrated behavior similar to the previous test where the strains increased initially to a maximum value after which they decreased. The maximum strain value recorded for pile no. 2 was about -27 microstrains. Strain transducer 1-4 increased to a value of -12 microstrains at load configuration 1 and then decreased with increasing load. Strain transducer 2-4 reached a maximum strain value of -14 microstrains at load configuration 2 and remained constant with increasing load. The results from the west edge and the centerline load tests illustrate that strain transducer 1-3 experienced essentially no strain.

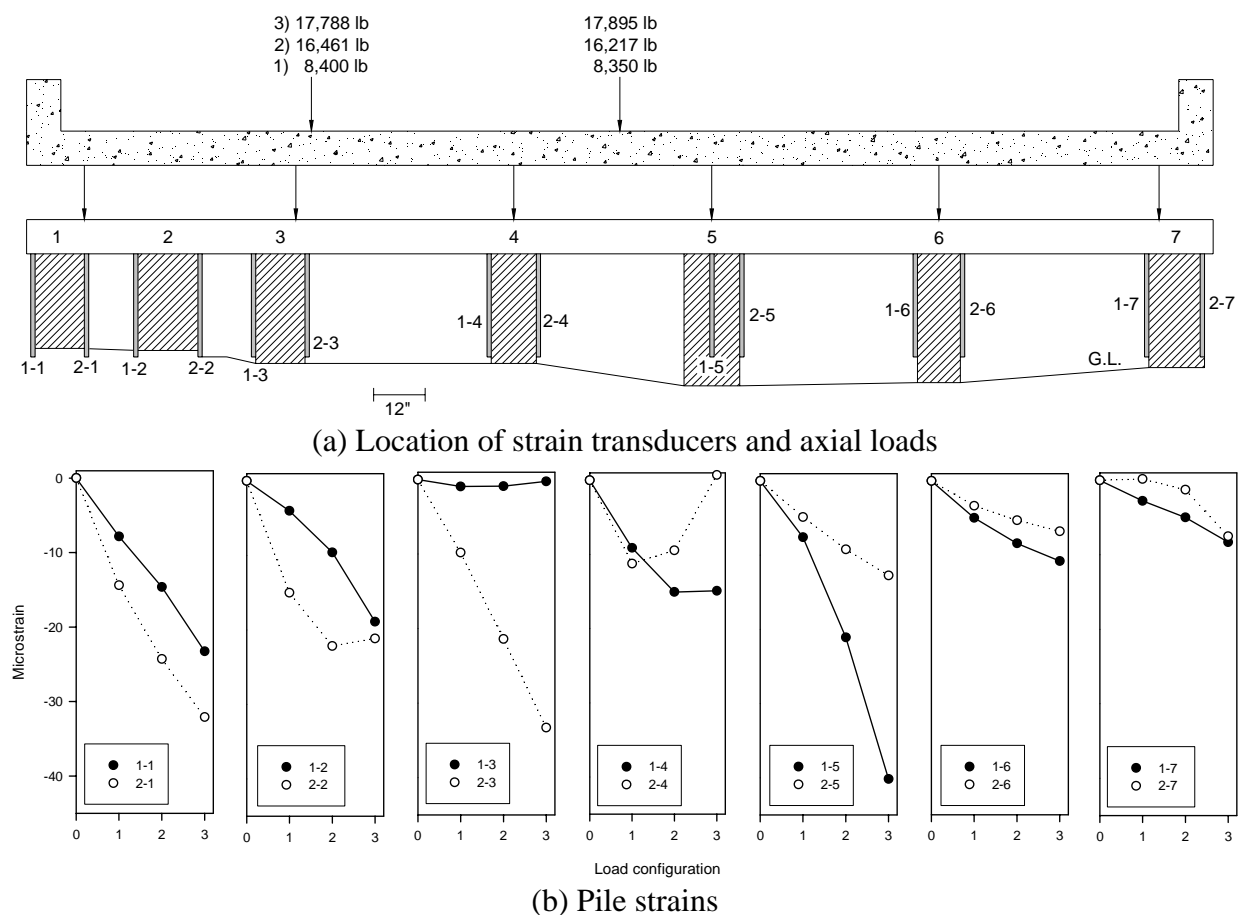


Figure 8.12. Static load test at the centerline (Bridge No. 243470 – Marshall County)

8.3.3. North Abutment – East Edge

The third load test was conducted with the loading at the east edge of the bridge. The locations of the loads and the piles strains are shown in Figure 8.13. Pile nos. 5, 6 and 7 had the highest strains, which decreased with distance from the applied loads. This demonstrated that the pile cap was acting flexible, which resulted in a non-uniform load distribution through the

substructure. The strain transducers attached to pile no. 4 reached a maximum value of -12 microstrains after which it decreased with increasing load. The strain transducer denoted by 1-1 measured positive strains.

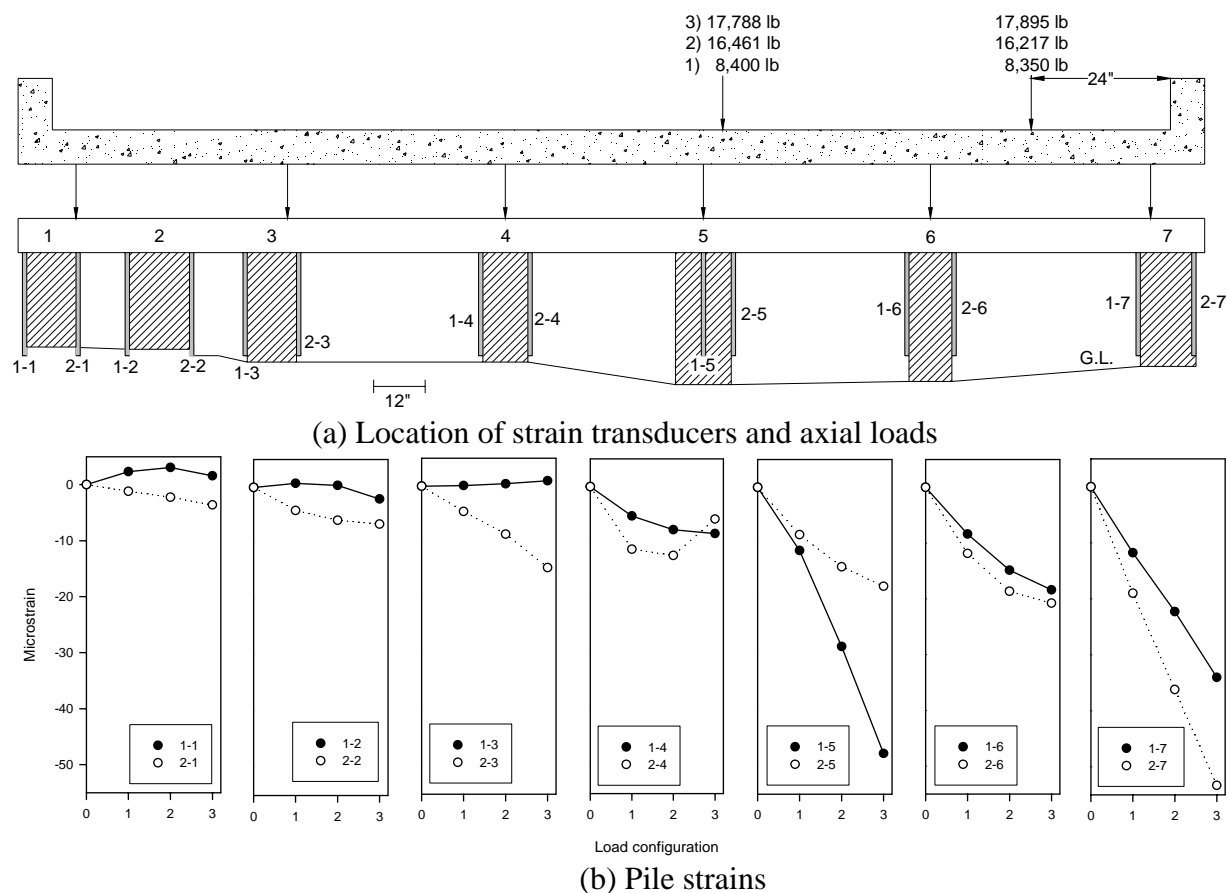


Figure 8.13. Static load test at the east edge (Bridge No. 243470 – Marshall County)

Using E determined by conducting axial compression tests, the loads carried by pile nos. 1 and 6 were determined. Table 8.2 summarizes the calculated loads carried by each pile. The results show that the percent load carried by pile no. 1 during the west edge test was about 13% for load configurations 1 and 2 and about 14% for load configuration 3. The load carried by pile no. 6, however, was about 0.4, 0.5 and 1.1% for load configurations 1, 2, and 3, respectively. It was noted that for load configuration 3, where the highest axial load was applied, the percent load carried by the piles increased compared to previous load configurations. This can be explained by load transfer from adjacent deteriorated piles as their maximum load carrying capacity was reached. The loads carried by the piles during the centerline and east edge tests are also shown in Table 8.2. Figure 8.14 is a graphical representation of the loads carried by pile nos. 1 and 6.

8.3.4. South Abutment – West Edge

The exposed portion of the timber piles at the south abutment were instrumented as shown in

Figure 8.15. Additional strain transducers, with a 24 inch gage length, were attached to the timber backwall. At pile no. 3, a fifth strain transducer, with a 24 inch gage length, was attached so that it crossed the tie back rod to study the influence of lateral restraint on strains induced by axial and horizontal loads (See Figure 8.16). The first load test on the south abutment was conducted at the west edge. Figure 8.17a shows the location of the applied axial load, while Figure 8.17b and c show the piles and backwall strains, respectively. Pile nos. 5, 6, and 7 had the maximum strains. The strains decreased with increasing distance from the applied loads. At pile no. 1, the strain transducer denoted by 1-1 measured positive strains, while the opposing strain transducer 2-1 measured negative strains. This may be due to pile bending in the upper portion of the pile about the weak axis (bending plane perpendicular to the backwall) causing tension on the outer side of the pile and compression on the inner side. Strain transducers 3-1 and 4-1, which were attached near the ground level, measured essentially zero strain. At pile no. 3, strain transducer 4-3, which was crossing the tie back rod, experience essentially zero strain. The lateral constraint caused by the tie back rod may have alleviated the axial compression and/or bending at this location.

Similar to the pile strains, the backwall strains were higher directly under the live load and decreased with increasing distance from the load location. Figure 8.18 shows the pile cap partially resting on the top of the timber backwall; therefore, the measured negative strains may be a result of axial compression of the backwall.

Table 8.2. Summary of loads carried by piles 1 and 6 at the north abutment (Bridge No. 243470 – Marshall County)

Pile no.	Load configuration 1		Load configuration 2		Load configuration 3	
	Calculated load (lb)	% load carried by pile	Calculated load (lb)	% load carried by pile	Calculated load (lb)	% load carried by pile
West edge						
1	2,200	13.0	4,250	13	4,959	14.0
6	73	0.4	163	0.49	378	1.1
Centerline						
1	1,400	8.4	2453	7.5	3,490	9.8
6	199	1.2	379	1.2	957	2.7
East edge						
1	148	0.9	265	0.8	459	1.3
6	1,863	11.1	3,544	10.8	5,287	14.8

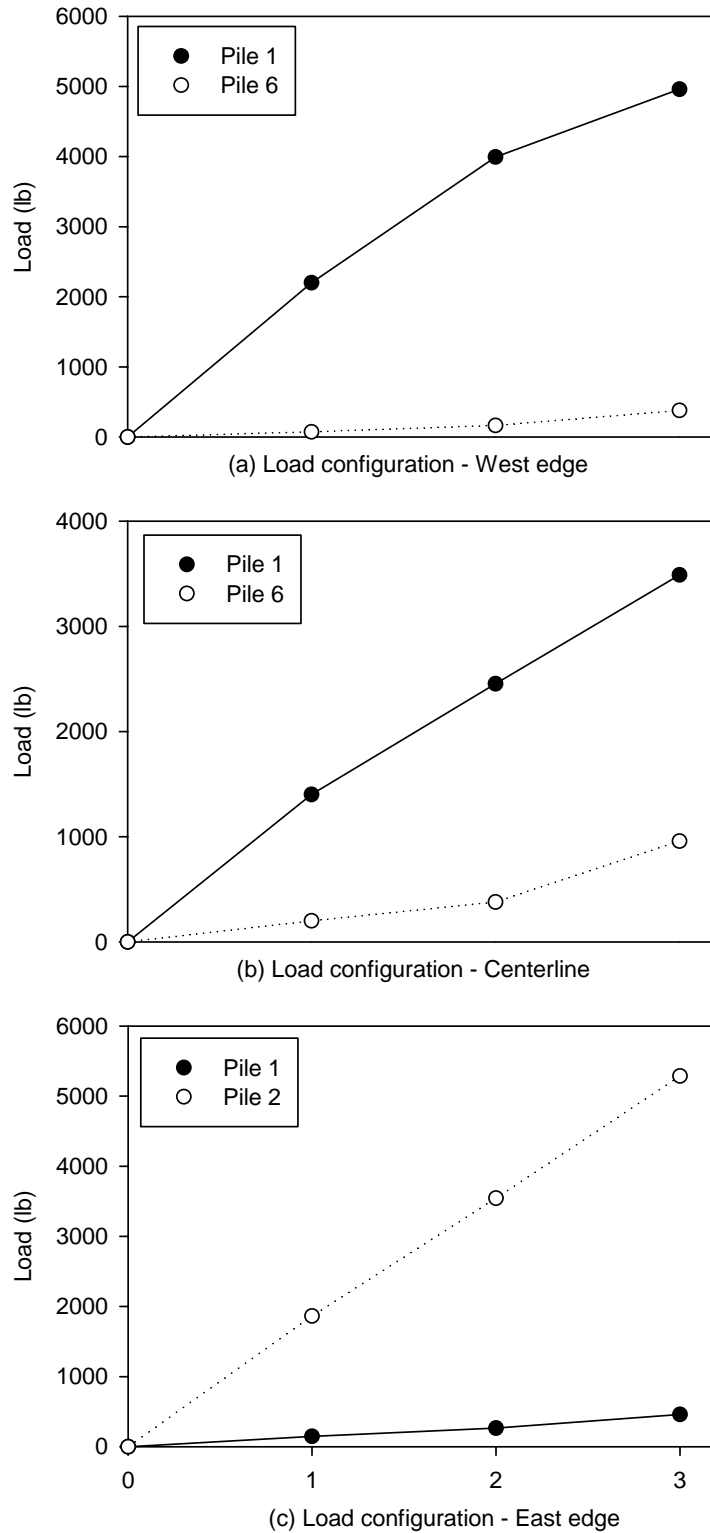
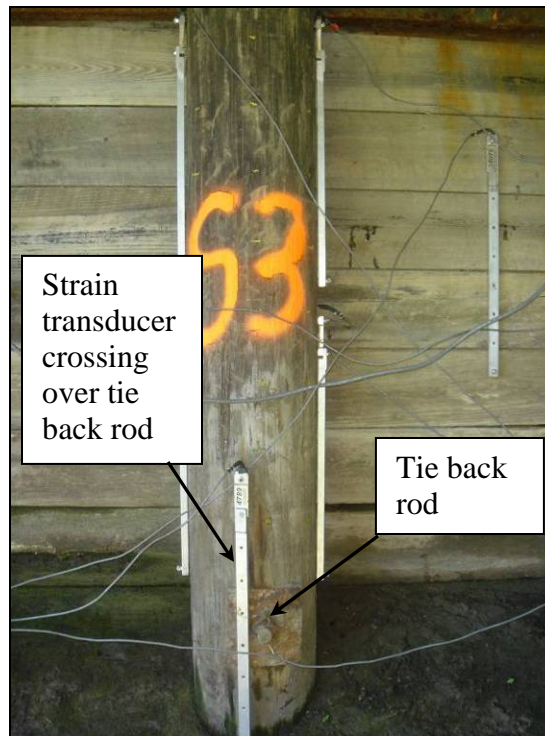


Figure 8.14. Calculated load carried by pile nos. 1 and 6 at the north abutment (Bridge No. 243470 – Marshall County)



**Figure 8.15. South abutment instrumented with strain transducers (Bridge No. 243470
Marshall County – July 27 2005)**



(a) Pile no. 3 at the south abutment



(b) Pile no. 5 at the south abutment

Figure 8.16. Strain transducers crossing over the tie back rod (Bridge No. 243470 Marshall County – July 27 2005)



Figure 8.18. Pile cap partially resting on the timber backwall (Bridge No. 243470 – Marshall County – July 28 2005)

8.3.5. South Abutment – Centerline

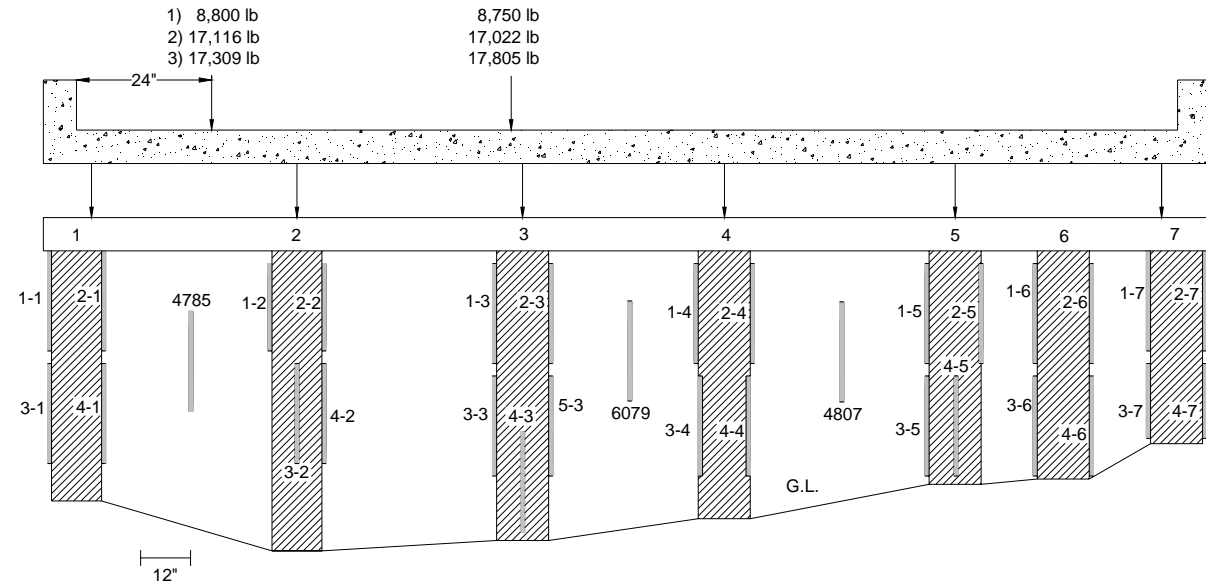
The second load test at the south abutment was completed with the loads at the centerline of the bridge deck. The locations of the applied loads, recorded pile strains, and backwall strains are shown in Figure 8.19. The strains were greatest in pile nos. 4 through 6, and decreased with increasing distance from the applied load. Similar to the previous test, the strain transducer bridging over the tie back rod (transducer 4-3) measured low strains compared to the other strain transducers attached to pile no. 3.

The backwall strains, which were more uniformly distributed compared to the previous test (See Figure 8.19c), were negative during the third load configuration due to the partial bearing of the pile cap on the backwall.

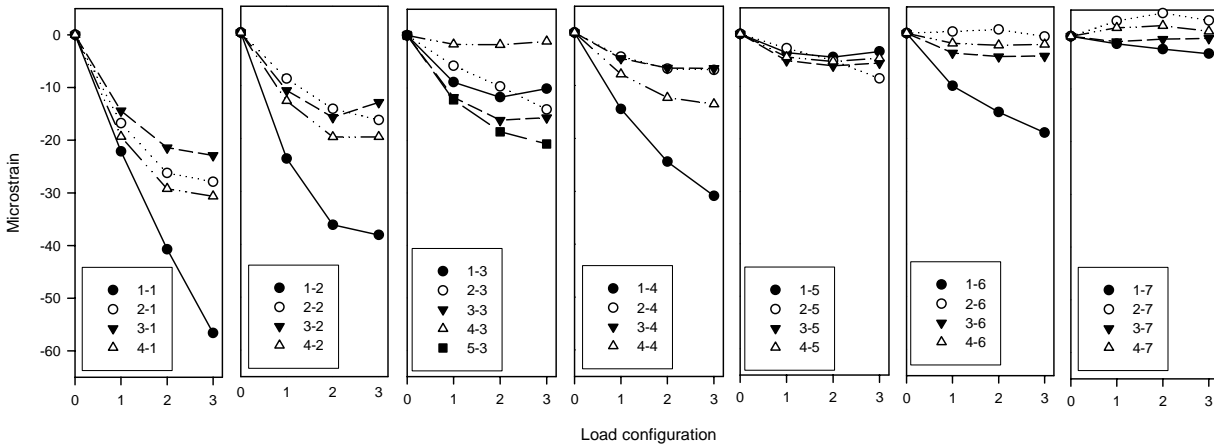
8.3.6. South Abutment – East Edge

The third test was carried out with the loads positioned at the east edge. The location of the applied axial loads, pile strains, and backwall strains are shown in Figure 8.20. The highest measured strains were directly under the applied load (i.e. pile nos. 1, 2, and 3), and decreased with increasing distance from the location of the applied load. The strain transducer attached over the tie back rod at pile no. 3 indicated negligible strain values. At pile no. 7, strain transducers 2-7 and 4-7, which were connected to the outer side of the pile, recorded positive strain values. The opposing strain transducers 1-7 and 3-7 recorded negative strains.

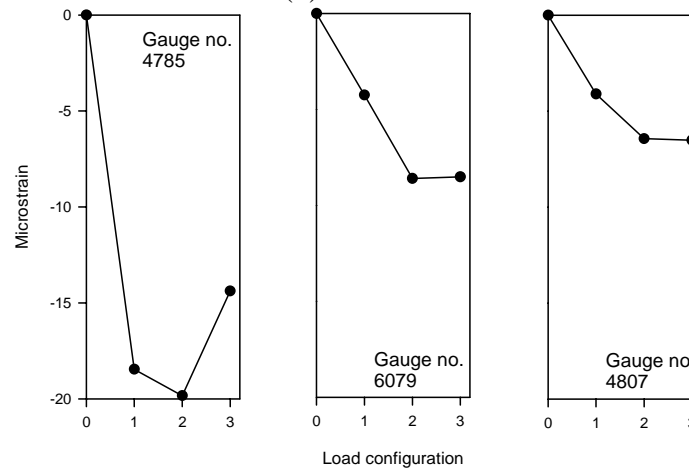
The strains measured in the backwall showed a non-uniform distribution. Strains were higher at the east side of the bridge directly under the live load and decreased with increasing distance from the load location.



(a) Location of strain transducers and axial loads



(b) Pile strains



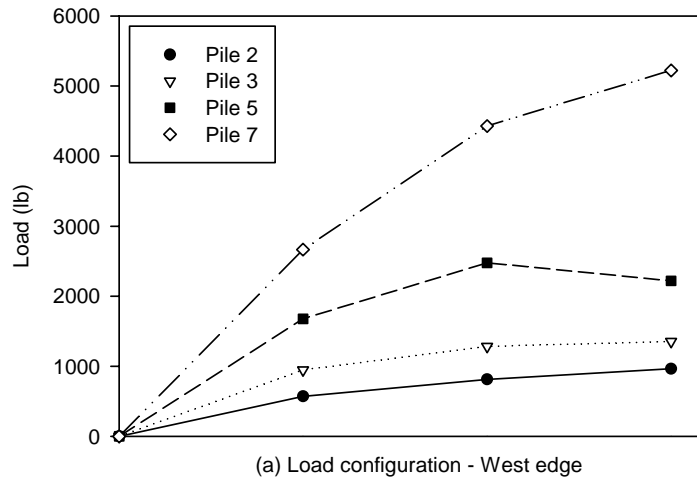
(c) Backwall strains

Figure 8.20. Static load test at the east edge (Bridge No. 243470 – Marshall County)

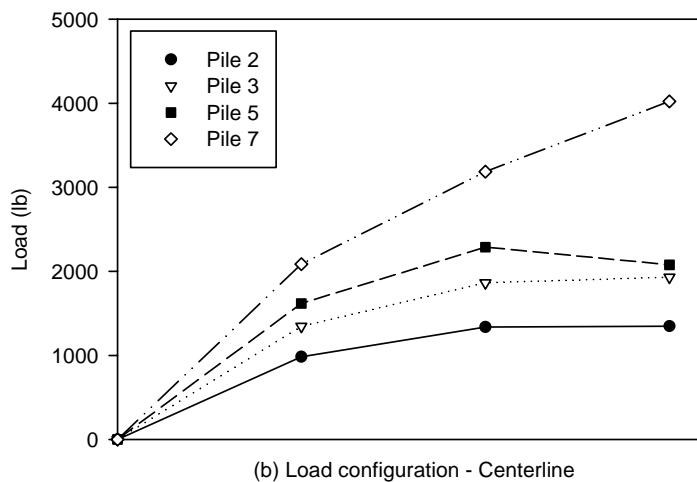
The loads carried by pile nos. 2, 3, 5, and 7 in the south abutment were calculated using their measured E and strain values. Table 8.3 summarizes the calculated loads and the percentage relative to the total applied load. When the load was at the west edge, the percent load resisted by pile No. 7 varied from 13 to 15%, which is comparable to the load carried by pile no. 1 in the north abutment. When the load was at the opposite side of the bridge, the percent load carried by pile 7 ranged from 1 to 1.4%. Loading the bridge at the centerline appears to distribute the load more evenly between piles. Pile no. 2 carried about 10% of the load when the load was positioned directly over it. This is also comparable to pile no. 6 in the north abutment where the carried load ranged from 11 to 15%. The load carried by all four piles was about 30% of the total load. Loads carried by the south abutment piles are presented in Figure 8.21.

Table 8.3. Summary of loads carried by south abutment piles (Bridge No. 243470 – Marshall County)

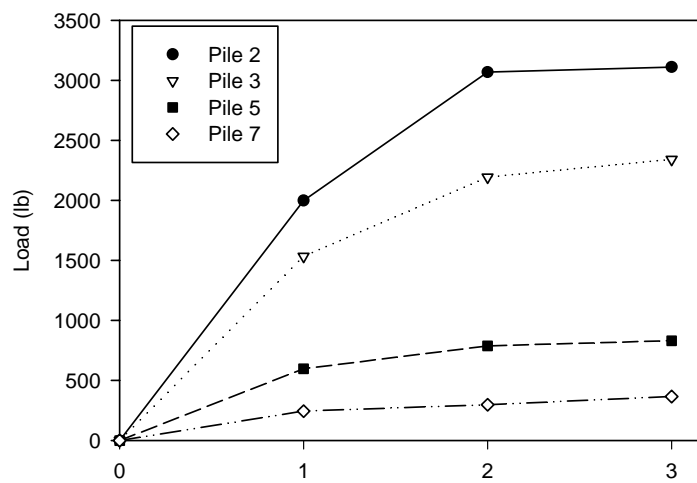
Pile No.	Load configuration 1		Load configuration 2		Load configuration 3	
	Calculated load (lb)	% load carried by pile	Calculated load (lb)	% load carried by pile	Calculated load (lb)	% load carried by pile
West edge						
2	571	3	813	2	963	3
3	946	5	1283	4	1353	4
5	1677	10	2476	7	2219	6
7	2664	15	4429	13	5223	15
Centerline						
2	982	6	1337	4	1347	4
3	1346	8	1863	6	1929	6
5	1617	9	2288	7	2077	6
7	2085	12	3186	9	4021	12
East edge						
2	1999	11	3068	9	3110	9
3	1534	9	2193	6	2341	7
5	596	3	788	2	831	2
7	243	1	297	1	366	1



(a) Load configuration - West edge



(b) Load configuration - Centerline



(c) Load configuration - East edge

Figure 8.21. Calculated load carried by south abutment piles (Bridge No. 243470 – Marshall County)

9. BRIDGE NO. 237350 MAHASKA COUNTY

9.1. Bridge Description

This bridge is located in Mahaska County on Rutledge Avenue near Oskaloosa, Iowa. The bridge, which is a single span, is about 33.3 ft long and 17.5 ft wide (See Figure 9.1). The superstructure, which has a 0° skew, has a concrete deck, which is supported on five steel girders. No plans were available for this bridge.



Figure 9.1. Bridge No. 237350 – Looking north (October 25 2005)

Each abutment is supported on five timber piles in front of a timber backwall with two timber piles at each wingwall. The pile cap is comprised of two double c-channel steel sections. The average exposed pile length and pile spacing at the north abutment are 98 inches and 46 inches, respectively (See Figure 9.2). A schematic of the north abutment illustrating the exposed pile lengths, location of girders, pile spacing, and tie back rod elevations is shown in Figure 9.3. The tie back rods are located at a depth of about 94 inches from the pile heads. Since no plans are available for this bridge, the pile lengths and the length of the tie back rods are unknown. Pile no. 1 at the northwest corner of the bridge showed signs of biological deterioration near the ground level as shown in Figure 9.4. Pile no. 5 at the northeast corner of the bridge showed signs of UV degradation as evidenced by the broken wood fibers on the pile surface; this pile also had a soft section near the water level (See Figure 9.5).

The south abutment, shown in Figure 9.6, has an average exposed pile length of about 94 inches and an average pile spacing of 49 inches. The tie back rods are about 6.5 ft from the pile heads. Figure 9.7 is a schematic diagram of the south abutment illustrating the exposed pile lengths and spacing. Visual observation revealed brooming in pile no. 2 near the ground level as shown in Figure 9.8. For pile no. 5, rotting near the ground level was observed (See Figure 9.9).



Figure 9.2. North abutment (Bridge No. 237350 Mahaska County – October 25 2005)

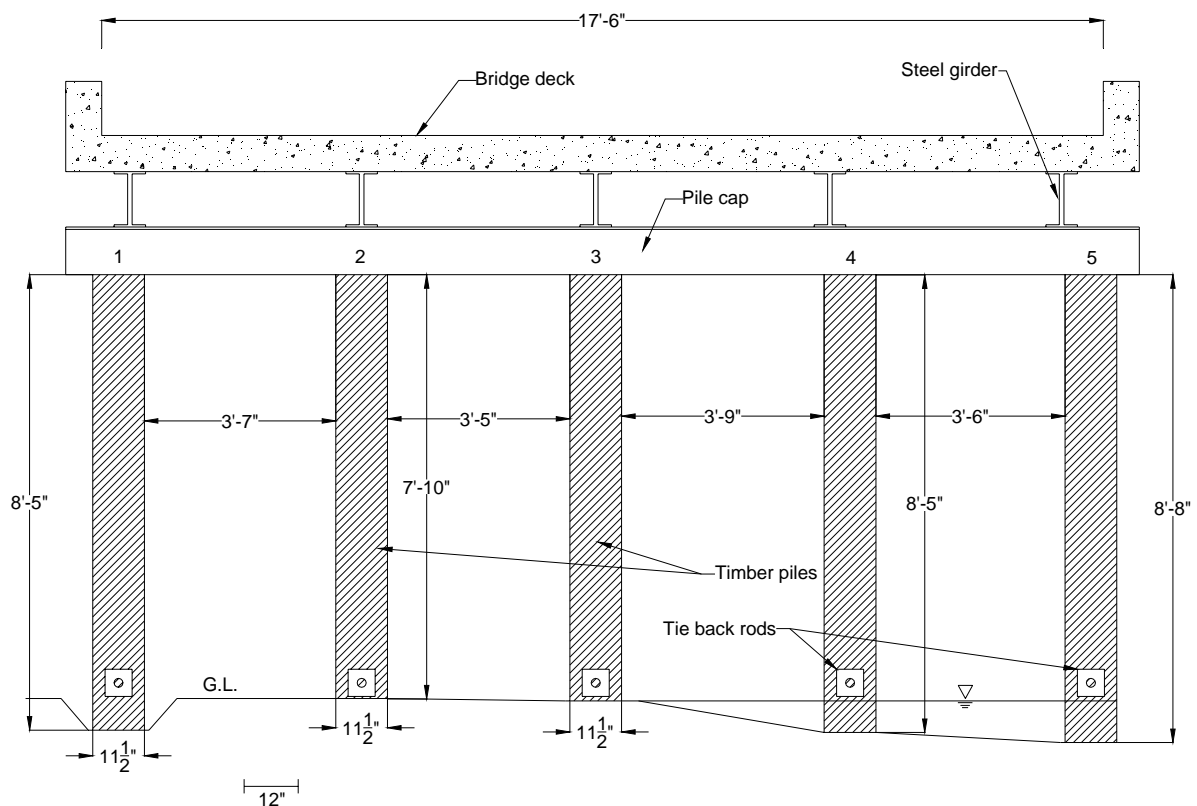


Figure 9.3. Schematic diagram of the north abutment (Bridge No. 237350 – Mahaska County)



Figure 9.4. Biological deterioration of pile No. 1 at the ground level (Bridge No. 237350 Mahaska County – October 25 2005)



(a) UV degradation



(b) Soft section near the water level

Figure 9.5. Deterioration observed at pile No. 5 (Bridge No. 237350 Mahaska County – October 25 2005)



Figure 9.6. South abutment (Bridge No. 237350 Mahaska County – October 25 2005)

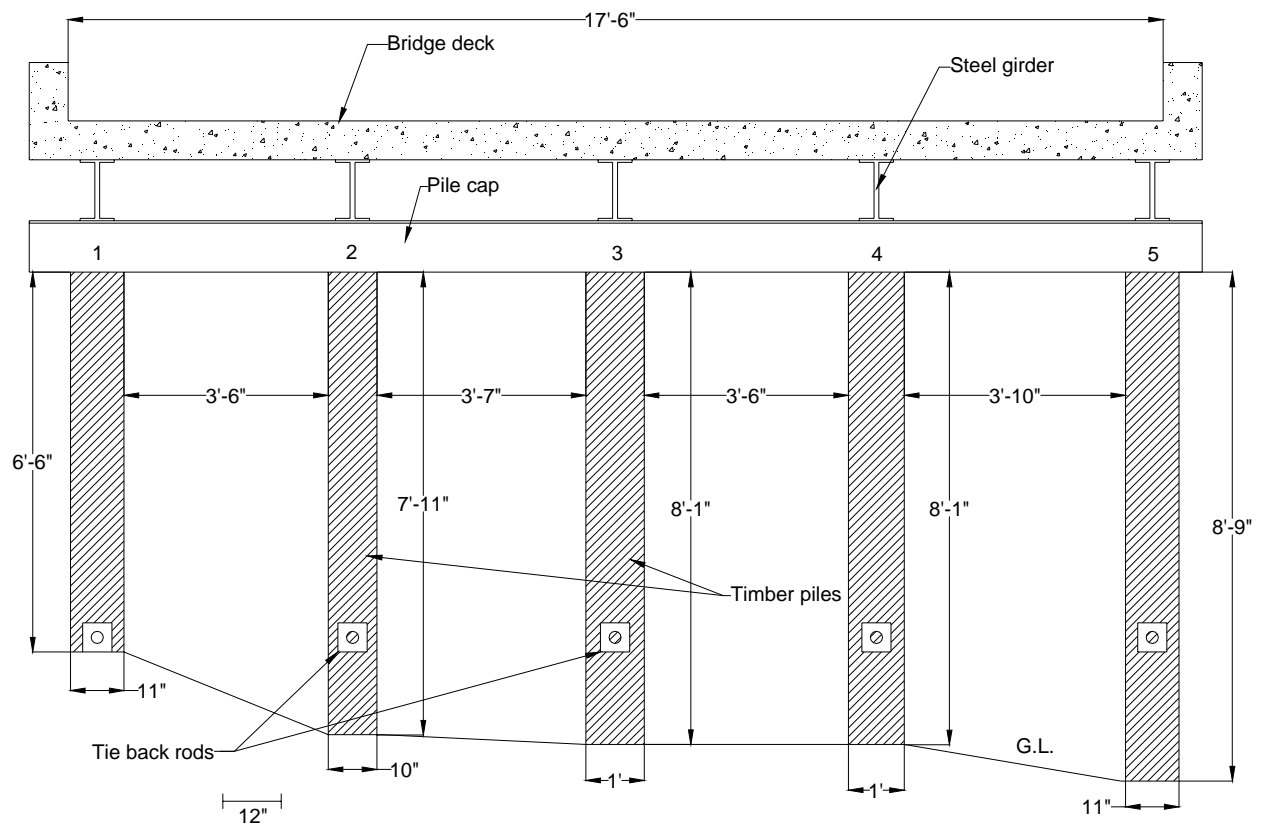


Figure 9.7. Schematic diagram of the south abutment (Bridge No. 237350 – Mahaska County)



Figure 9.8. Brooming of pile No. 2 near the ground level (Bridge No. 237350 Mahaska County – October 25 2005)



Figure 9.9. Rotting observed at pile No. 5 (Bridge No. 237350 Mahaska County – October 25 2005)

An increment borer was used to obtain a core sample from each pile. A summary of the measured densities are shown in Table 9.1. The core obtained from pile no. 1 at the north abutment was in the deteriorated region near the ground level, had a density of 38.5 lb/ft^3 . As can be seen in Table 9.1, wood densities ranged from 38.5 lb/ft^3 to 68.9 lb/ft^3 illustrating the non-uniformity of wood material.

Table 9.1. Summary of measured piles densities (Bridge No. 237350 – Mahaska County)

Abutment	Pile	Elevation (in)*	Core length (in)	Density (pcf)
North	1	12	4.9	38.5
	2	48	4.8	40.3
	3	49	5.0	56.0
	4	52	5.1	68.9
	5	48	4.6	46.0
South	1	48	3.9	57.7
	2	18	4.0	41.6
	3	26	4.2	43.8
	4	36	4.8	43.1
	5	18	4.6	46.1

*Elevations are relative to ground level

9.2. Load Test Setup and Instrumentation

A static load test was performed at the north and south abutments where three loading increments were applied. Each pile was instrumented with three strain transducers with a gage length equal to 24 inches. Each timber backwall was also instrumented with three strain transducers with 24 inches gage lengths (See Figure 9.10). The soil was excavated around pile nos. 1 and 5 at the north and south abutments, respectively, to allow for installation of the strain transducer across the biologically deteriorated region (See Figure 9.11).

9.3. Test Results

9.3.1. North Abutment – West Edge

The first load test was performed with the load at the west edge of the bridge. The load was offset about 2 ft from the curb. Figure 9.12 shows the location and magnitude of the loads, pile strains, and backwall strains. The highest strain measured was in pile no. 1 and was about -29 microstrains during load configuration 3. The measured strain decreased with increasing distance from the location of the applied loads. Strain transducer 2-1, which was attached to a biologically deteriorated section, indicated a higher strain measurement when compared to other strain measurements in pile no. 1.

The backwall strains were highest near the applied load, and decreased with increasing distance from the location of the loads. For load configurations 2 and 3, the recorded strain decreased due to reduction in axial load. Negative strains were recorded at load configuration 3 because of the partial bearing of the pile cap on the backwall (See Figure 9.13).



(a) North abutment

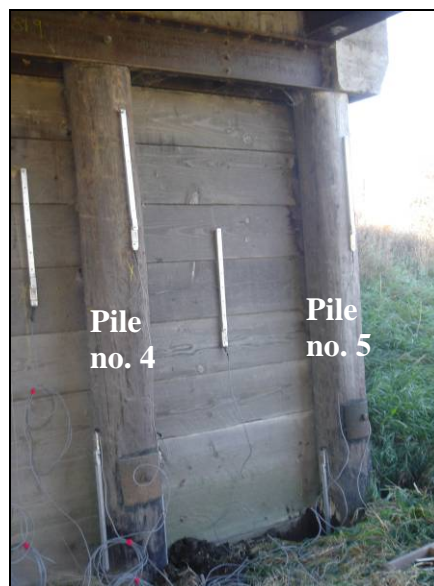


(b) South abutment

Figure 9.10. Substructure instrumentation (Bridge No. 237350 Mahaska County – October 28 2005)



(a) Pile no. 1 at the north abutment



(b) Pile nos. 4 and 5 at the south abutment

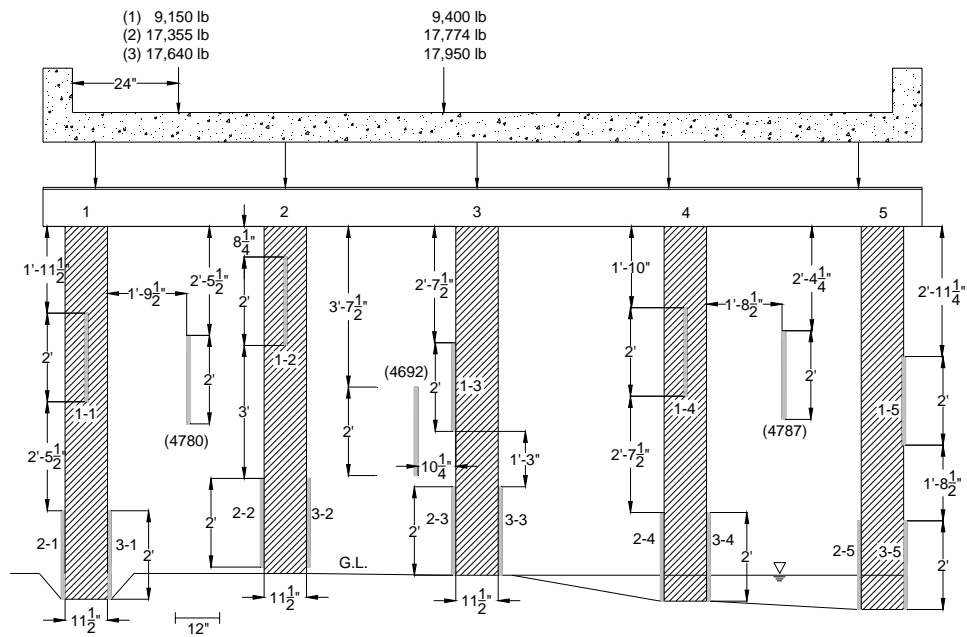
Figure 9.11. Soil excavated around piles to allow for strain transducer installation across deteriorated regions (Bridge No. 237350 Mahaska County – October 28 2005)

9.3.2. North Abutment – Centerline

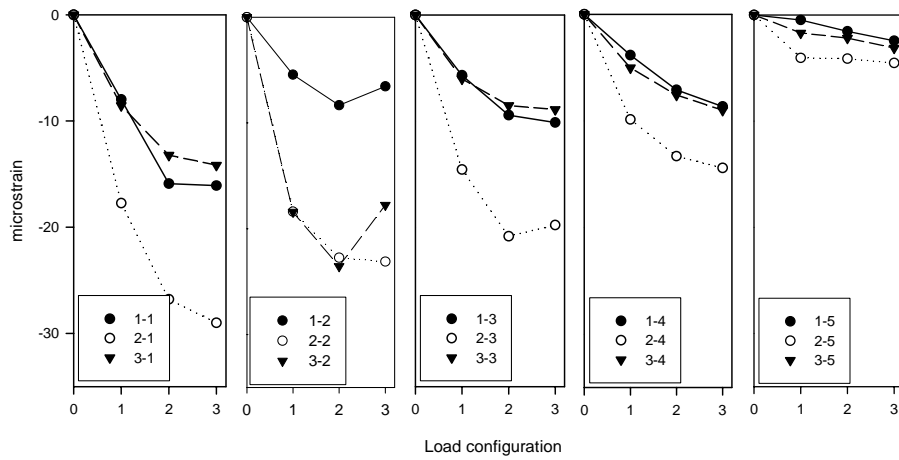
The second load test was performed with the load in the centerline lane. The location and magnitude of the applied axial loads, pile strains, and backwall strains are shown in Figure 9.14. The recorded strains were highest in pile nos. 2, 3, and 4 and decreased with increasing distance from the location of the applied load. The highest strain occurred in pile no. 4 and was about -20 microstrains in load configuration 3. Strain transducer 2-1 continued to show higher strain compared to other strains measured in pile no. 1. Similarly, the backwall strains were highest directly under the applied load (i.e. between pile nos. 2 and 3). In load configuration 1, the highest strain measured was about -21 microstrains between pile nos. 2 and 3.

9.3.3. North Abutment – East Edge

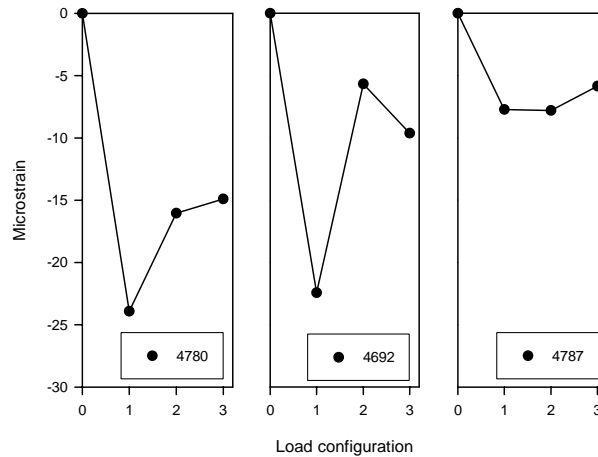
The third load test was performed with the load at the east edge of the bridge. The load was offset about 2 ft from the curb. The location and magnitude of the applied axial loads, piles strains, and backwall strains are shown in Figure 9.15. The highest strain was measured in pile no. 5 and was about -21 microstrains in load configuration 3. The measured strain decreased with increasing distance from the location of the applied loads. The backwall strains were highest near the applied load (i.e. between pile nos. 4 and 5), and decreased with increasing distance from the location of the axial loads. In load configuration 1, the highest strain measured was about -23 microstrains.



(a) Location of strain transducers and axial loads



(b) Pile strains

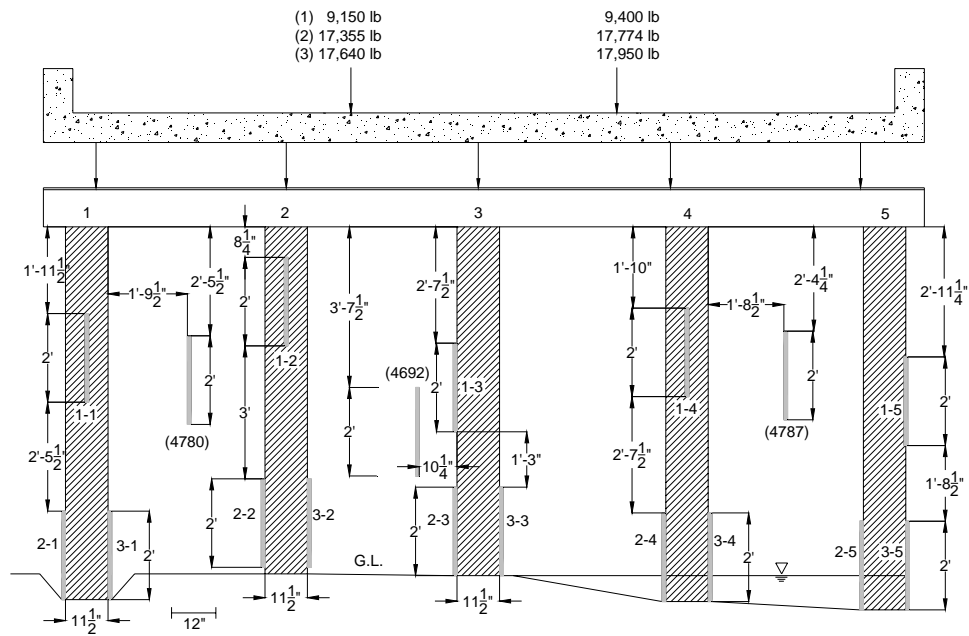


(c) Backwall strains

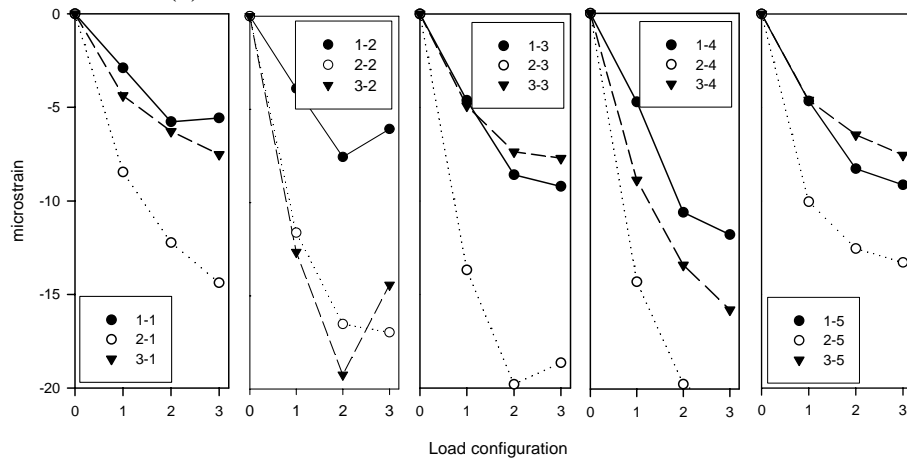
Figure 9.12. Static load test at the west edge (Bridge No. 237350 – Mahaska County)



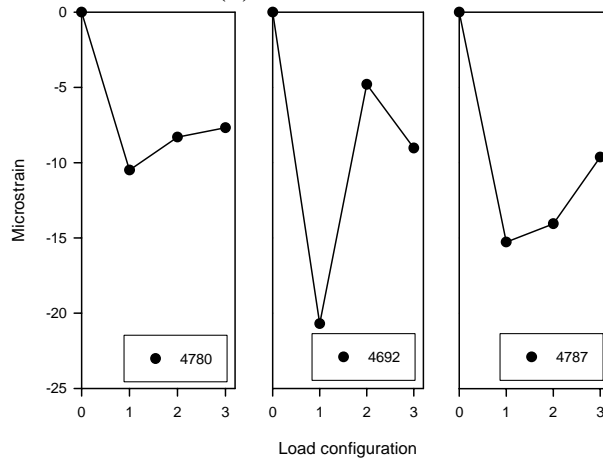
Figure 9.13. Pile cap partially resting on the timber backwall (Bridge No. 237350 Mahaska County – October 28 2005)



(a) Location of strain transducers and axial loads

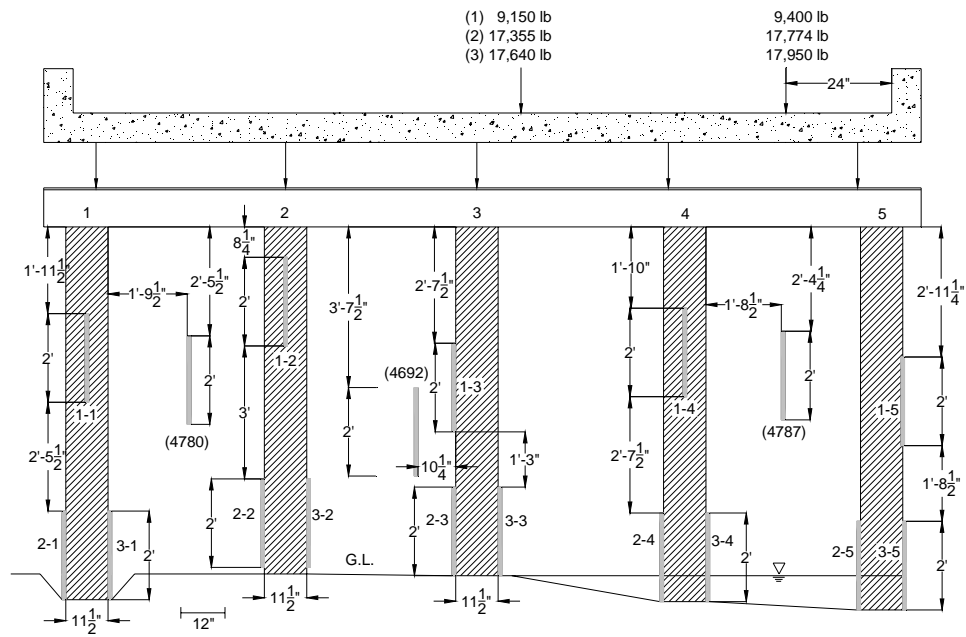


(b) Pile strains

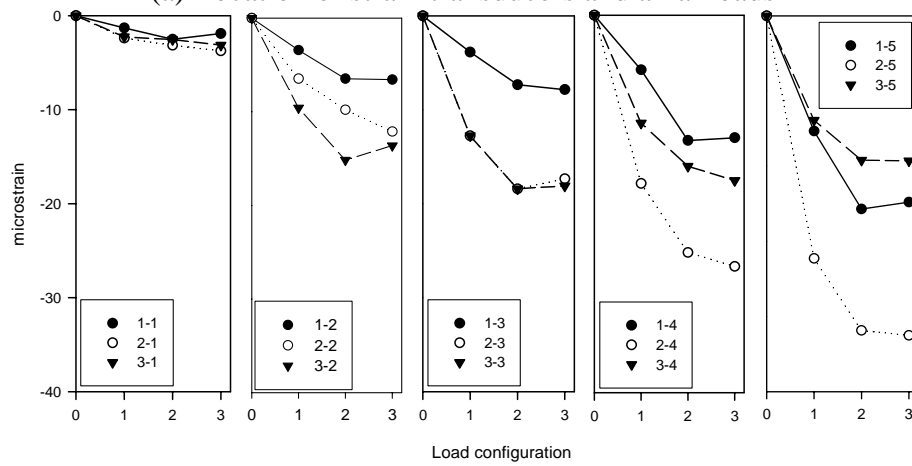


(c) Backwall strains

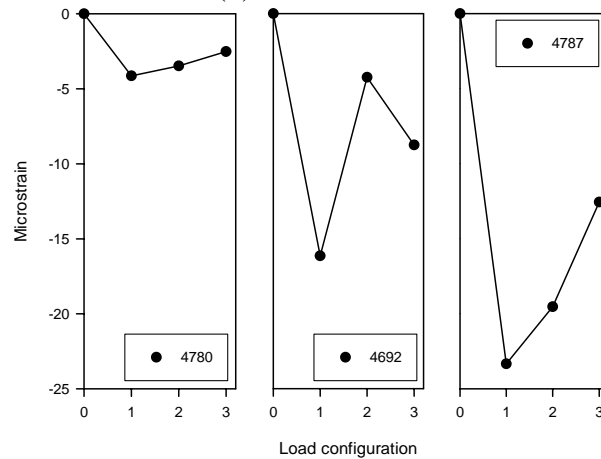
Figure 9.14. Static load test at the centerline (Bridge No. 237350 – Mahaska County)



(a) Location of strain transducers and axial loads



(b) Pile strains



(c) Backwall strains

Figure 9.15. Static load test at the east edge (Bridge No. 237350 – Mahaska County)

9.3.4. South Abutment – West Edge

At the south abutment, the first static load test was performed with the load at the west edge of the bridge. The load was offset about 2 ft from the curb. The location and magnitude of the applied axial loads, piles strains, and backwall strains are presented in Figure 9.16. The highest strain was measured in pile no. 5 and was about -34 microstrains at load configuration 3. The measured strain decreased with increasing distance from the location of the applied loads. Strain transducers 3-2 and 2-5, which were attached to soft sections near the ground level, displayed higher strains compared to other strain measurements in pile nos. 2 and 5.

The highest backwall strain was between pile nos. 3 and 4 directly under the applied load and was about -20 microstrains. Backwall strains decreased with increasing distance from the location of the axial loads. In load configurations 2 and 3, the backwall showed positive strain values.

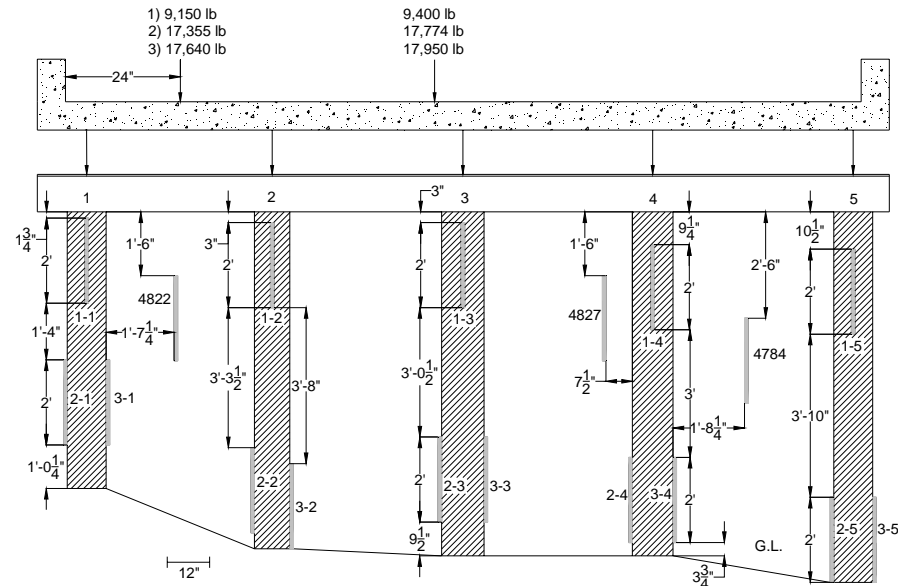
9.3.5. South Abutment – Centerline

The second load test was performed with the load at the centerline of the bridge deck. The location and magnitude of the applied axial loads, pile strains, and backwall strains are presented in Figure 9.17. The results indicate a more uniform strain distribution, compared to the west edge test, through the substructure components. The highest strain was measured in pile no. 2 and was about -29 microstrains in the third load configuration. Strain transducers 3-2 and 2-5 indicated higher strains since they were attached to softer pile sections. Backwall strains continued to show negative values in load configuration 1, and positive values in load configurations 2 and 3.

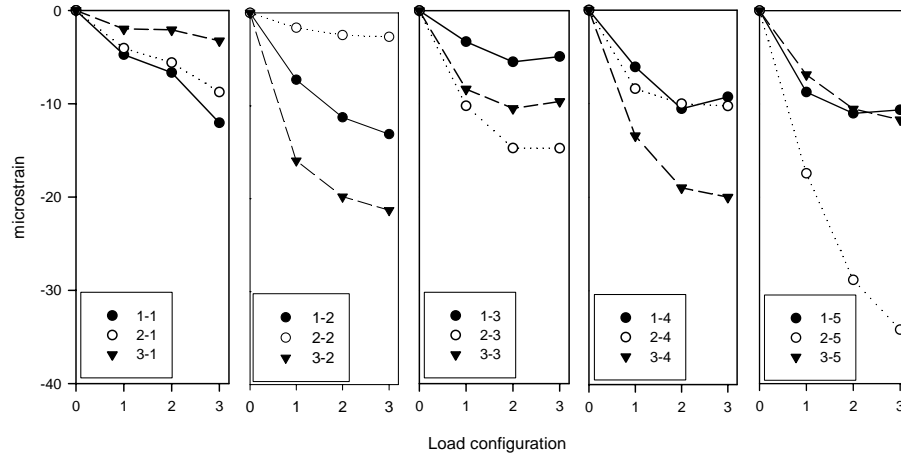
9.3.6. South Abutment – East Edge

The third load test was performed with the load at the east edge of the bridge. The load was offset about 2 ft from the curb. The location and magnitude of the applied axial loads, piles strains, and backwall strains are presented in Figure 9.18. The highest strain was measured in pile no. 1 and was about -42 microstrains in load configuration 3. The measured strain decreased with increasing distance from the location of the applied loads. The strain transducers attached to the deteriorated pile section (i.e. strain transducers 3-2 and 2-5) recorded higher strains compared to other strains measured in pile nos. 2 and 5.

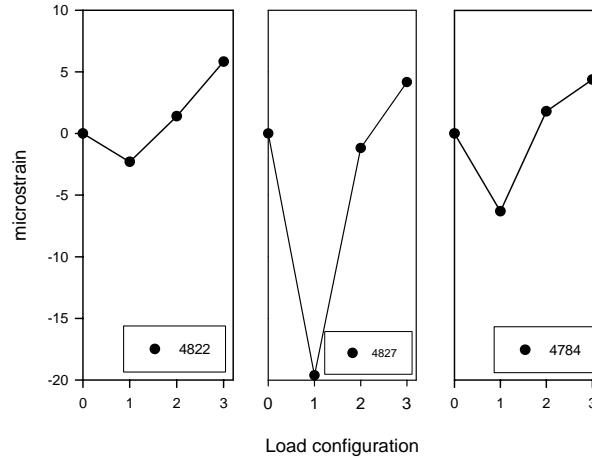
The backwall strain was highest under the applied load (i.e. between pile nos. 1 and 2) and was about -14.4 microstrains in the first load configuration. The strains decreased with increasing distance from the location of the axial loads. In load configurations 2 and 3, the strain transducer between pile nos. 1 and 2 (transducer no. 4822) recorded high positive values, which may be a result of bending in the timber backwall.



(a) Location of strain transducers and axial loads

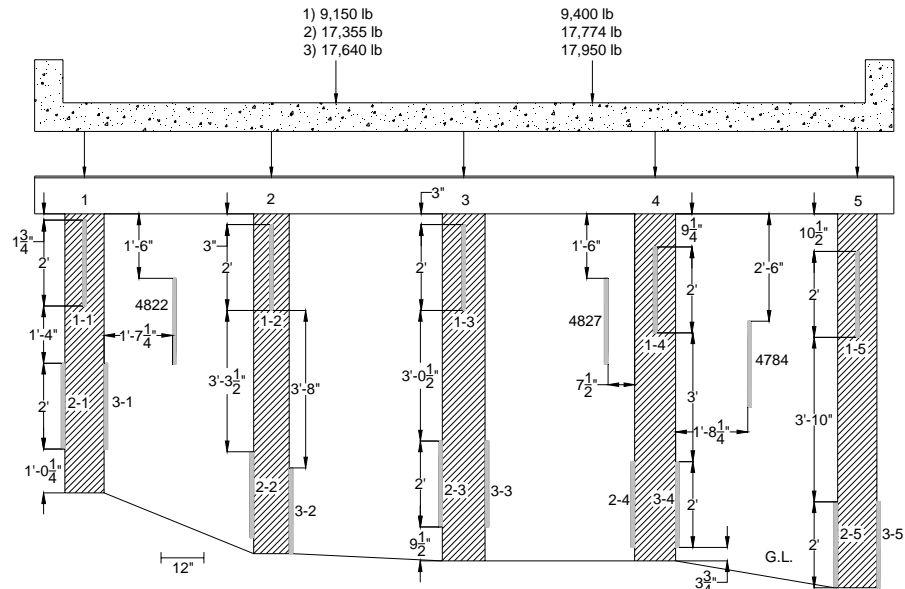


(b) Pile strains

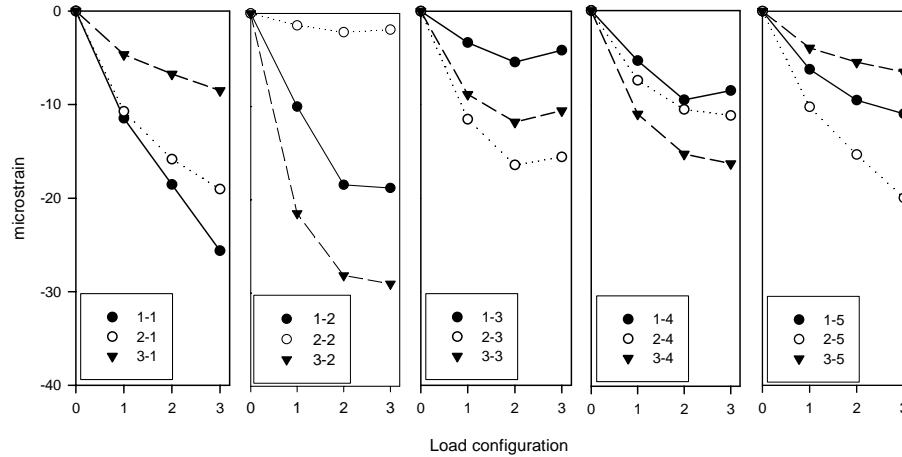


(c) Backwall strains

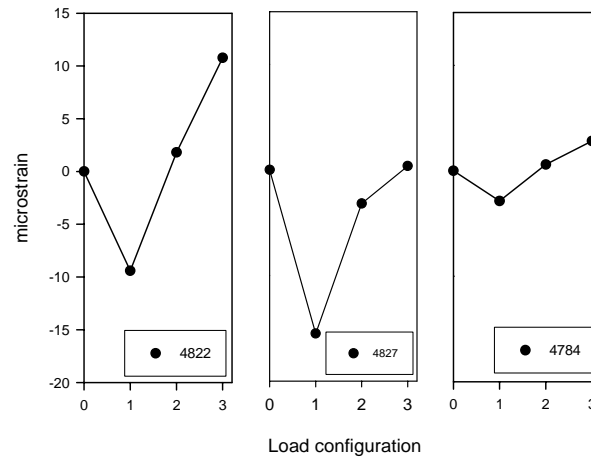
Figure 9.16. Static load test at the west edge (Bridge No. 237350 – Mahaska County)



(a) Location of strain transducers and axial loads

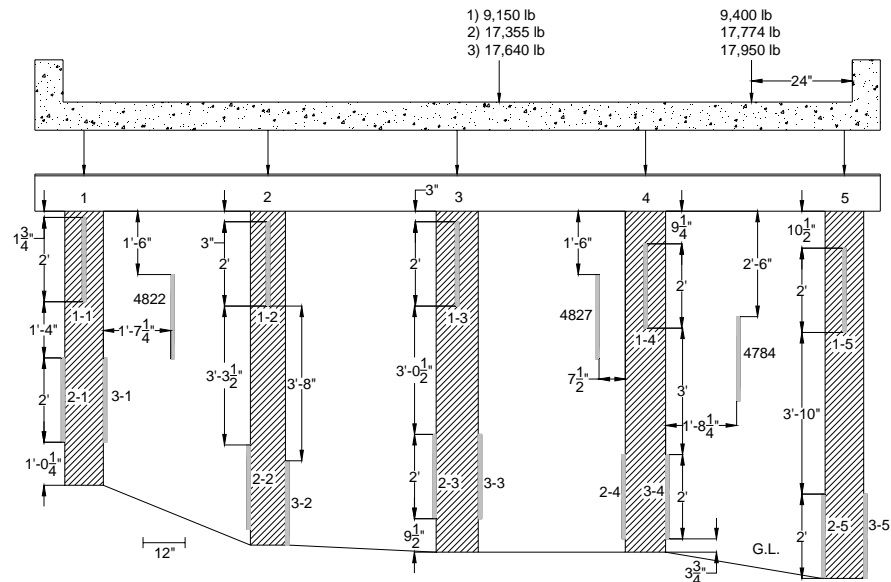


(b) Pile strains

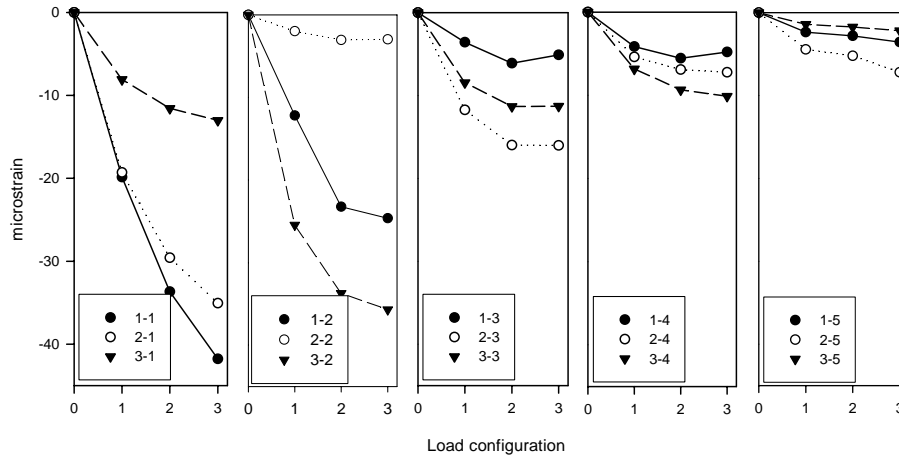


(c) Backwall strains

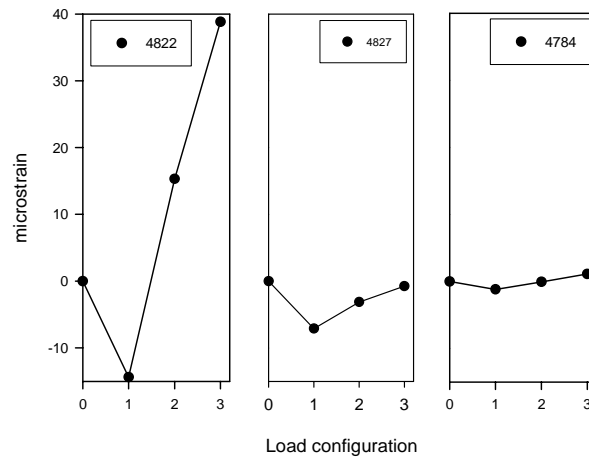
Figure 9.17. Static load test at the centerline (Bridge No. 237350 – Mahaska County)



(a) Location of strain transducers and axial loads



(b) Pile strains



(c) Backwall strains

Figure 9.18. Static load test at the east edge (Bridge No. 237350 – Mahaska County)

9.4. Foundation Design

The foundation design for many existing low volume bridges was apparently based on engineering judgment and past experience. For many sites, no design documentation is available. On many occasions considerable deterioration in more than one pile was observed, yet the bridge is still open to traffic and appeared to be functioning adequately. To evaluate existing conditions, three bridge sites, where in situ soil testing was available, were investigated. The foundations were designed according to the Cone Penetration Test (CPT) Nottingham and Schmertmann (1975) method which is summarized in Hannigan et al. (1997) and by the design method outlined by Klaiber et al. (2004). A summary of the selected design methods are outlined below.

The Nottingham and Schmertmann method is an empirical procedure that uses CPT data to compute pile toe and shaft resistance. The ultimate shaft resistance, Q_s , in cohesionless soils is determined from the equation below.

$$Q_s = K \left[\frac{1}{2} \left(\frac{1}{\bar{f}_s} A_s \right)_{0 \text{ to } 8b} + \left(\bar{f}_s A_s \right)_{8b \text{ to } D} \right] \quad (9.1)$$

Where K is ratio of unit pile shaft resistance to unit cone sleeve friction, \bar{f}_s is average unit sleeve friction over the depth interval indicated by the subscript, A_s is pile-soil surface area over \bar{f}_s depth interval, b is pile width or diameter, and D is embedded pile length. For cohesive soils, Q_s can be calculated using Equation 9.2.

$$Q_s = \alpha' \bar{f}_s A_s \quad (9.2)$$

Where α' is the ratio of pile shaft resistance to cone sleeve friction. The estimation of pile toe resistance (Q_p) is computed by averaging the cone tip resistance from eight pile diameters above the pile toe (q_{c1}) and the cone tip resistance from $0.7b$ to $4b$ (q_{c2}). The ultimate pile capacity (Q_u) is the summation of Q_p and Q_s . A factor of safety of 3.0 is commonly used to determine the allowable pile capacity (Q_a).

A substructure design methodology was developed by Klaiber et al. (2004). Total dead load abutment reactions for steel girder bridges were determined from the figures developed in this reference for a 24 ft roadway width. Total live load abutment reaction was determined based on a HS20-44 truck load, which was found to be the governing load for bridge spans between 20 and 90 ft. The maximum live load occurs when the back axle is placed directly over the centerline of the piles with the front and middle axles on the bridge. Live load impact is not included in the substructure design (Refer to Iowa DOT BDM Section 6.5)

The axial pile load is a function of the abutment reaction (dead load + live load), total number of piles and the pile spacing. A nominal axial pile factor was developed to account for various superstructure systems, pile layouts, and non-uniform distribution of abutment loads. This factor, which is multiplied by the abutment reaction, was developed by modeling the pile cap as a continuous beam with the assumption of simple supports at each pile. For a steel girder bridge, this factor is 1.4. The total pile axial load is calculated as follows:

$$\text{Pile axial load} = \frac{\text{Abutment reaction} \times 1.4}{\text{No. of piles}} \quad (7.1)$$

According to Section 6.2.6.3 in the Iowa DOT BDM, the maximum axial pile load must not exceed 20 tons for piles between 20 to 30 ft long, and 25 tons for piles between 35 and 55 ft long. This limitation is essential because of indeterminate bending stresses in integral abutment bridges.

CPT soundings were carried out near the north and south abutment. The tests utilized a 20 ton capacity truck-mounted rig, which hydraulically advanced a cone. The electronic cone had a 60° tip angle, tip area of 1.55 in², net area ratio of 0.8, and a friction sleeve area of 23.25 in², and was advanced at a rate of 1 inch per second. The results of the 2 CPT tests are shown in Figure 9.19 and Figure 9.20. The test, which was conducted to a depth of about 30 ft, demonstrated that the underlying soil was a fairly uniform cohesive soil varying from clay to silty clay. At approximately 26 ft, a layer of silty sand to sandy silt was encountered. The water level was about 11 ft and 20 ft below grade at the north and south abutments, respectively.

Since the pile length is unknown, several iterations were carried out to determine the appropriate pile length for a group of 5 piles, which would resist the ultimate pile load. An average f_s value of 0.7 tsf was calculated. Due to the uniformity of the soil profile, the same f_s value was selected for depths greater than 30 ft. The two design methods demonstrated that the required pile length below ground level should be about 45 ft when the factor of safety is 3.0 (See Table 9.2). The calculated pile lengths are based on the assumption that the soil properties are uniform below 30 ft. If stiffer soils are encountered below 30 ft, the pile length may be decreased. As may be seen in this table, both methods resulted in equal pile length.

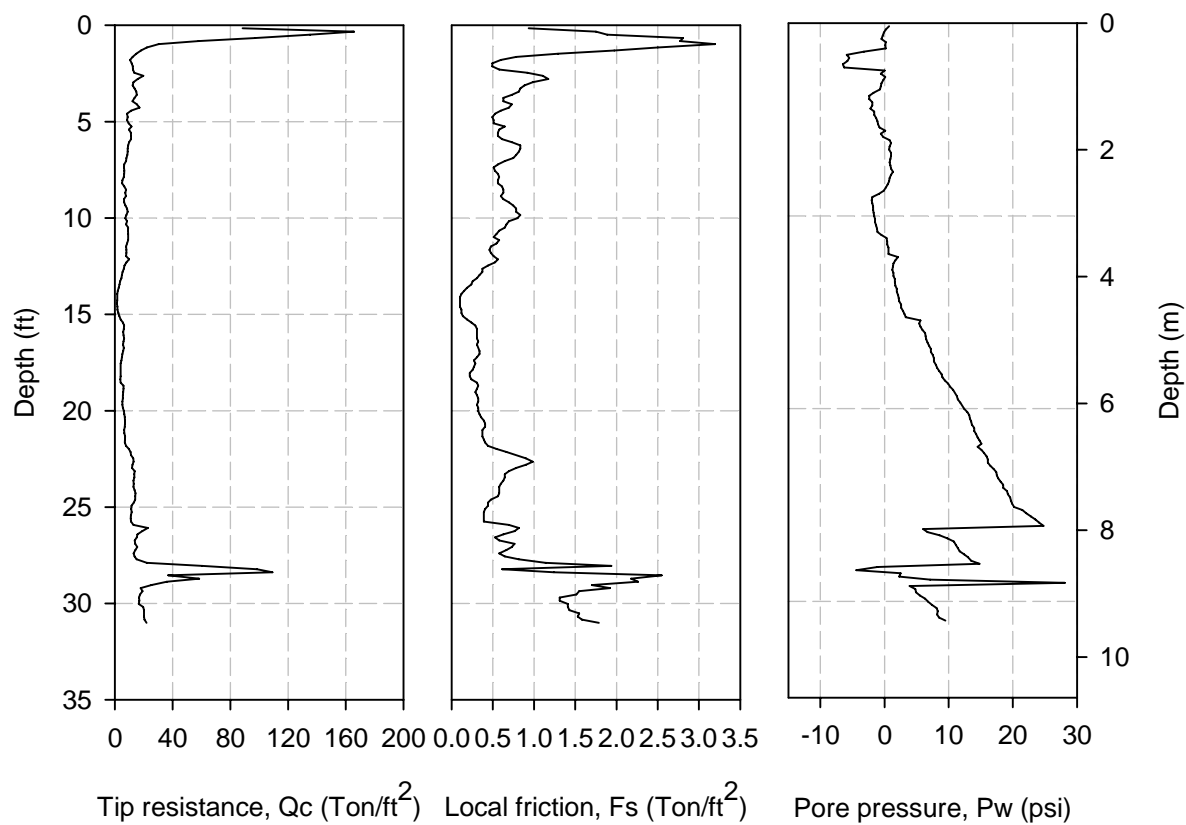


Figure 9.19. CPT conducted 66 ft north of the north abutment (Bridge No. 237350 – Mahaska County)

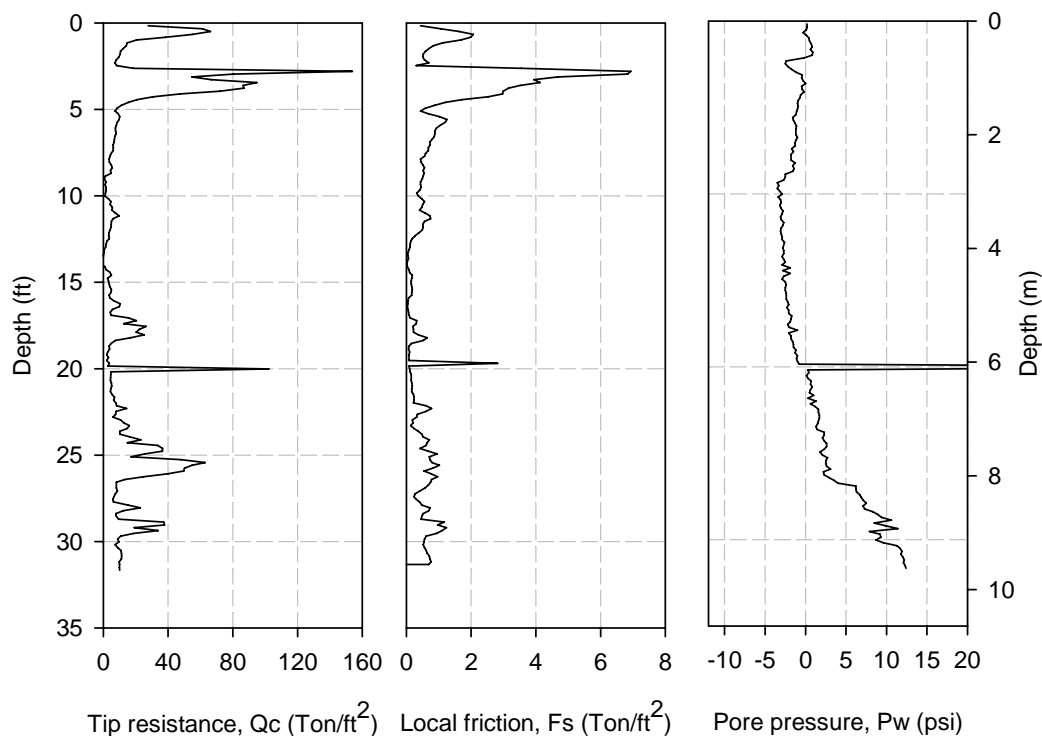


Figure 9.20. CPT conducted 65 ft south of the south abutment (Bridge No. 237350 – Mahaska County)

Table 9.2. Summary of pile length computations (Bridge No. 237350 – Mahaska County)

General bridge input	Superstructure system	Steel girders		
	Span length (ft)	33.3		
	Roadway width (ft)	24		
	Backwall height (ft)	10.4		
	Number of piles	5		
	Dead load (kip)	112.6		
	Live load (kip)	103.2		
	Allowable load per pile (tons)	21		
Foundation material	q_{c2} (tsf)	3		
	q_{c1} (tsf)	5		
	Q_p (tons)	3		
	f_s (tsf)	0.7		
	α'	0.63		
	A_s (ft ²)	141.3		
	Q_s (tons)	62		
	Q_u (tons)	65		
	F.S.	3.0	2.0	1.0
	Q_a (tons)	22 > 21 o.k.		
	Assumed pile length (CPT method) (ft)	45	30	15
	Computed pile length (Klaiber et al. 2004) (ft)	45	30	15

9.5. Pile Integrity Testing

Low strain pile integrity testing was conducted on the substructure of this bridge. Five timber piles, two at the north abutment and three at the south abutment, were tested to evaluate the Pile Integrity Testing Method (PIT) in assessing the structural integrity and determining the length of these piles.

9.5.1. Instrumentation and Testing Procedure

The equipment used for the PIT included a PIT collector, two accelerometers, and two hammers with Nylon or Lexan tips, roughly 2 lb and 7 lb (See Figure 9.21). Due to the complexity of the structure, 2 accelerometers were attached to the pile during testing. Using two accelerometers helped in (1) determination of the wave speed in timber piles and (2) distinguishing upward traveling wave signals from downward traveling signals to help interpret data collected under complex conditions. The two accelerometers are denoted by A1 and A2 as shown in Figure 9.22. A downwards travelling stress wave is always recorded by A1 first, then by A2, while an upward travelling stress wave is first recorded by A2 then by A1. The distance between the accelerometers varied from 2 ft to 5 ft. Typically, the larger the distance between the accelerometers, the more accurate the wave speed determination. Due to field conditions and exposed pile lengths, the largest distance possible between the accelerometers was 5 ft.

Two methods of impact were used to create a compressive stress wave. The first impact method was on the surface of the bridge deck using the 7 lb hammer. The stress waves induced by the impact pass through the deck and pile cap into the supporting piles. However, reflection from interfaces between the superstructure and substructure components created multiple stress waves travelling down the pile, which complicated the analysis. The second impact method was carried out by creating a notch in the exposed part of the piles (See Figure 9.23), which was then axially impacted using the 2 lb hammer (See Figure 9.24). One limitation of this impact method is that the impact is not always at 90 degrees to the notched surface, which creates a point contact between the hammer and the pile instead of a desirable plane contact. Another limitation is that this impact method is quasi-destructive; however, and as discussed in the literature review chapter, when the pile head is inaccessible, another possibility is to use a large nail driven into the pile side at a 45 degree angle and impact it with a hammer to generate compression waves.



Figure 9.21. Equipment used in Pile Integrity Testing

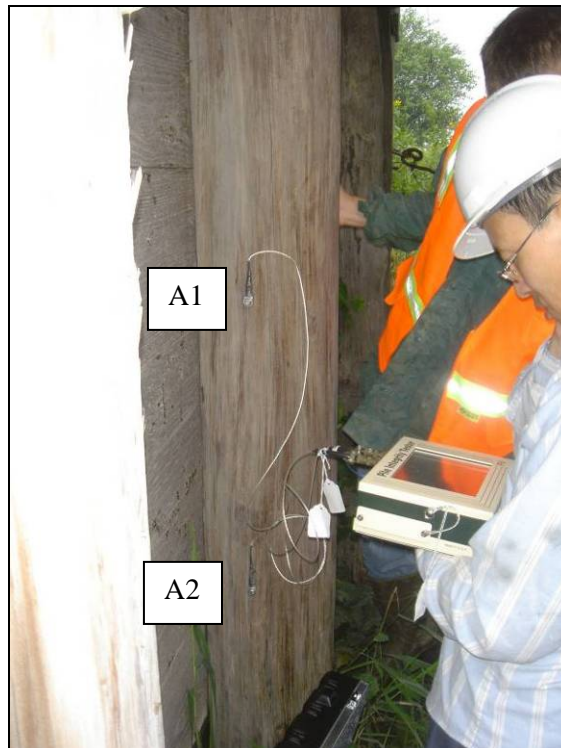


Figure 9.22. Two accelerometers attached to pile no. 2 at the north abutment (Bridge No. 237350 Mahaska County – August 17 2006)



Figure 9.23. Notches created in the exposed piles to allow for axial impact (Bridge No. 237350 Mahaska County – August 17 2006)



Figure 9.24. Applying an axial impact to the notched pile (Bridge No. 237350 Mahaska County – August 17 2006)

9.5.2. Determination of Wave Speed

With two accelerometers attached to the pile, it is possible to calculate the wave speed by comparing the input pulses of accelerometers A1 and A2. Presented in Figure 9.25 are the results obtained by performing PIT on pile no. 3 of the north abutment. Figure 9.25a shows the A1 and A2 curves with an assumed velocity of 12,000 ft/s. In this test, the distance between A1 and A2 was 5 ft; therefore, the second curve (A2) was shifted forward by 2.5 ft, which is half the distance between A1 and A2, with the velocity equal to 12,000 ft/s (See Figure 9.25b). It was observed that the rising slopes of both curves did not match well. By repeating the same process using wave speeds equal to 13,000 ft/s (Figure 9.25c) and 14,000 ft/s (Figure 9.25d), it was concluded that a wave speed of 13,000 ft/s is the best match for the timber piles tested.

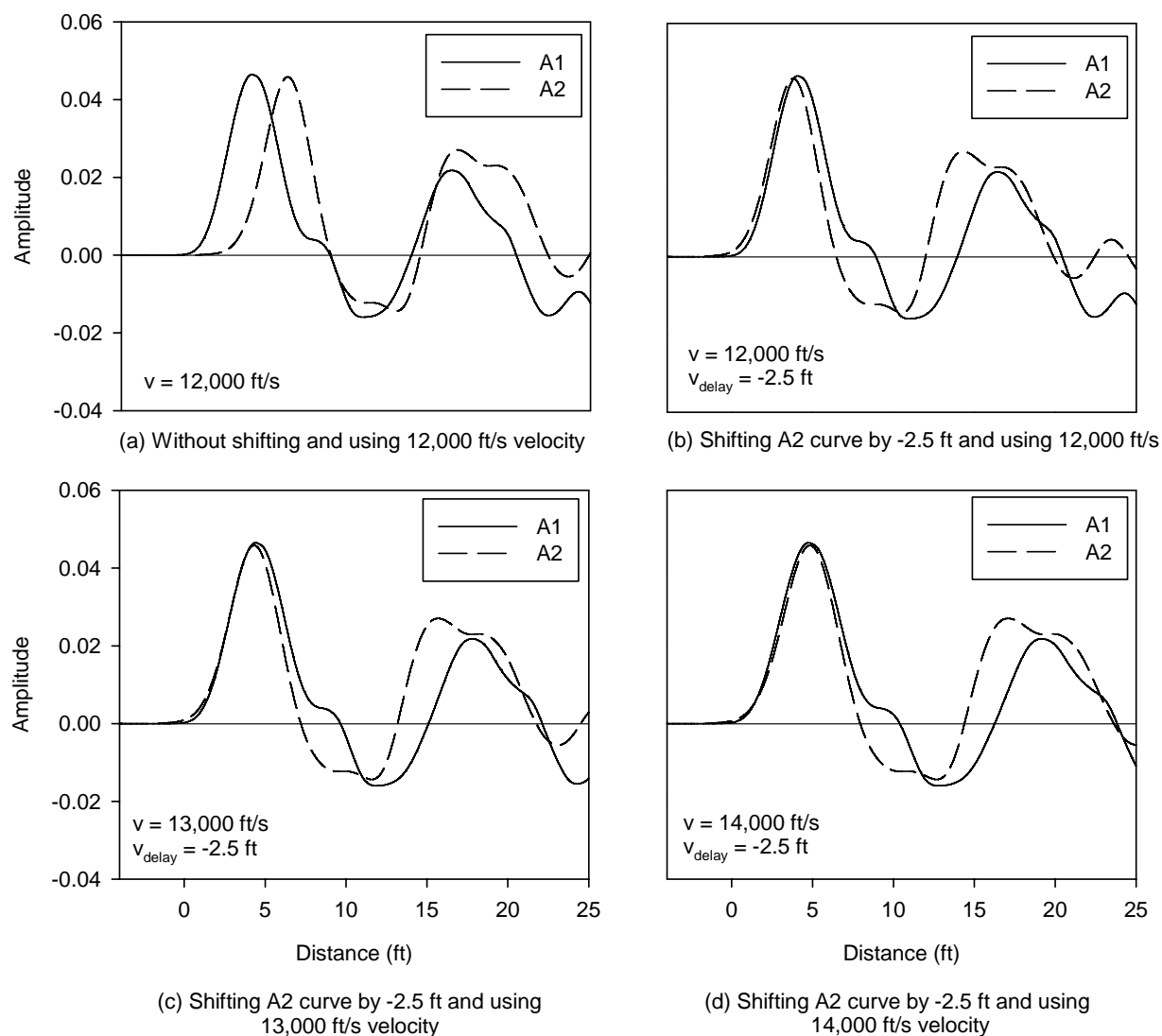


Figure 9.25. Determination of wave speed by matching the rising slope of two input pulses

9.5.3. Estimation of Pile Length

Since the pile head is connected to the pile cap and the superstructure, the reflections recorded are from above and below the transducer locations. To differentiate between upward and downward reflections, the order in which a pulse detail appear is noted. If a pulse detail appears first on A1 (solid curve) and then later on A2 (dashed curve), this pulse is considered a downward reflection from above the transducer. If a pulse detail appears first on A2 followed by A1, this pulse is considered an upward reflection from below the transducer as a result of impedance variation cause by a defect or pile toe. Test results for pile no. 2 at the north abutment are presented in Figure 9.26. An upward reflection was observed at about 16 ft below accelerometer A1, which was about 5 ft below the piles head. Therefore the total pile length was an estimated 21 ft. However, not all tests yielded a clear upward reflection. Figure 9.27 illustrates the test results for pile no. 2 at the south abutment. The biological deterioration at the ground level, which is 8 ft from the pile head, resulted in a wide input pulse and prevented “seeing” beyond this point. Also, multiple reflections from the superstructure complicated the analysis. Table 9.3 summarizes the results of the PITs performed on the piles in this bridge. It was calculated that the lengths of pile nos. 2 and 3 at the north abutment are 21 ft and 20 ft, respectively. The lengths of other piles at the south abutment could not be determined due to the deteriorated section at the ground level. For the complete PIT results, refer to Appendix C.

Table 9.3. Summary of Pile Integrity Tests ((Bridge No. 237350 – Mahaska County)

Abutment	Pile No.	Distance between A1 and A2 (ft)	Comments
North	2	2	Possible pile toe or defect at 21 ft (16 ft below A1 + 4.7 ft)
	2	5	
	3	3	Possible pile toe or defect at 20 ft (15 ft below A1 + 4.7 ft)
	3	2	
	3	5	
South	2	2	The defect at about 8 ft from the pile head makes the input pulse wide and prevents from seeing beyond this point
	2	4.5	
	3	2.5	The defect at about 7 ft from the pile head makes the input pulse wide and prevents from seeing beyond this point
	3	4.5	
	5	2	The defect at about 7 ft from the pile head makes the input pulse wide and prevents from seeing beyond this point
	5	5	

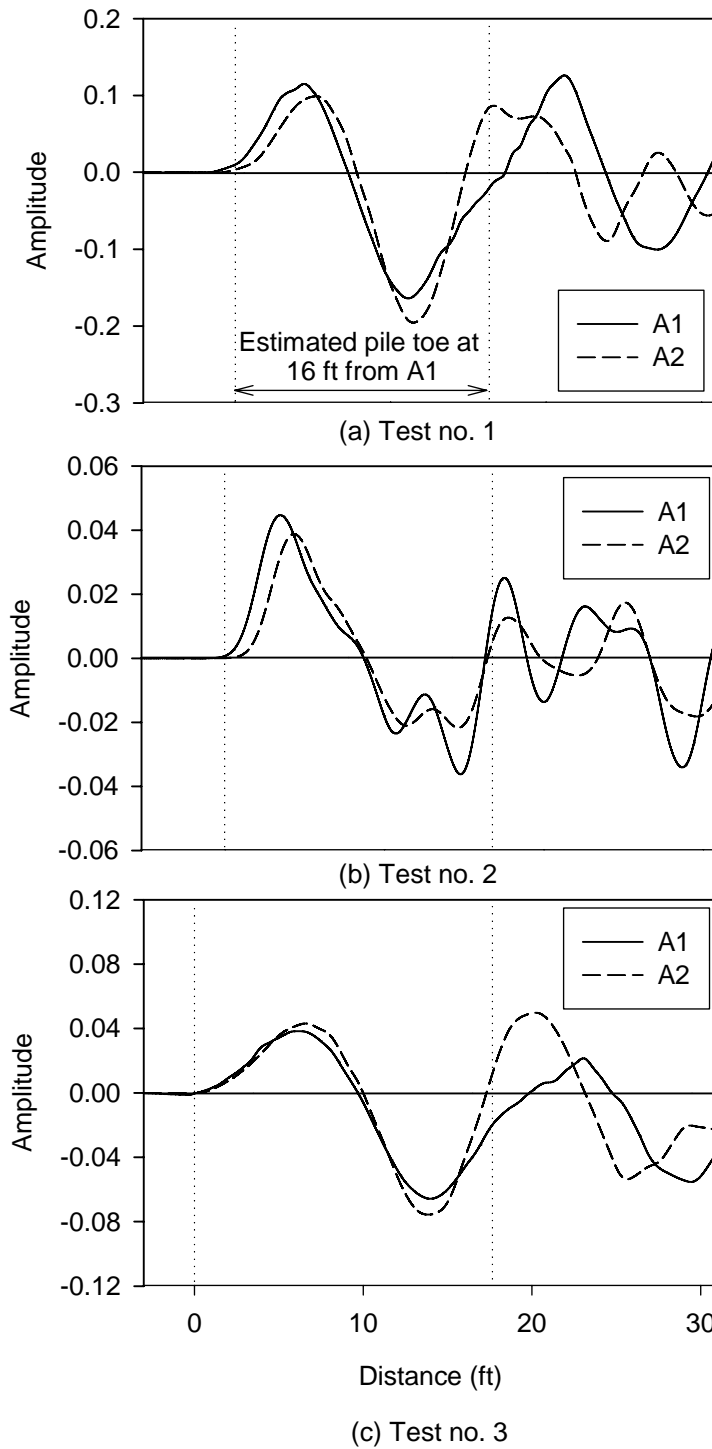
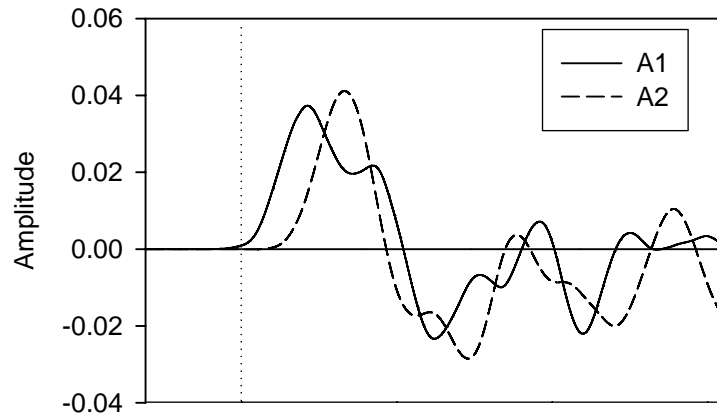
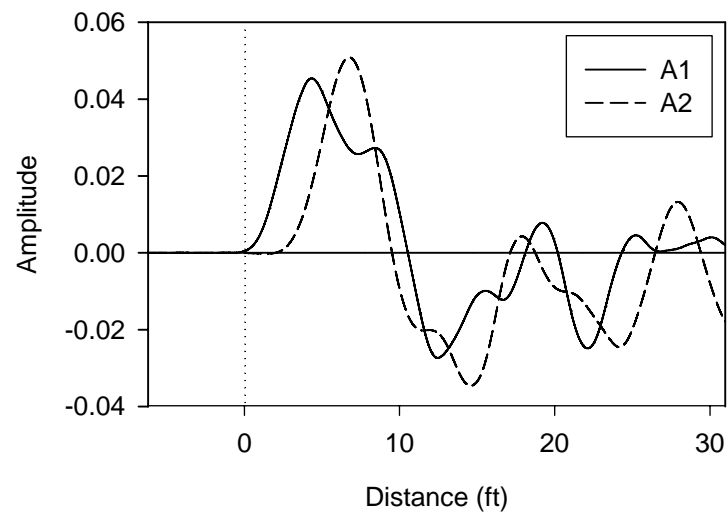


Figure 9.26. Results of PIT on pile no. 2 at the north abutment (Bridge No. 237350 – Mahaska County)



(a) Test no. 1



(b) Test no. 2

Figure 9.27. Results of PIT on pile no. 2 at the south abutment (Bridge No. 237350 – Mahaska County)

10. BRIDGE NO. 094680 CARROLL COUNTY

10.1. Bridge Description

The fourth bridge tested was in Carroll County, Iowa. The bridge, which was 33.5 ft long, 22 ft wide, and has a 0° skew, was located on 245th St. south of Halbur, Iowa crossing a creek (See Figure 10.1). The superstructure consisted of a non-composite concrete deck supported by a four girder system. Due to deterioration in the concrete deck, as may be seen in Figure 10.2, there were numerous asphalt patches.



Figure 10.1. Side view of the bridge looking northwest (Bridge No. 094680 Carroll County – May 16 2006)



Figure 10.2. Concrete deck patched with asphalt (Bridge No. 094680 Carroll County – May 16 2006)

Each abutment had six timber piles in front of a timber backwall, three timber piles at each wingwall, and a double c-channel cap. The piles in the abutments were overall in good condition. Erosion along the side of the abutment was observed as shown in Figure 10.3. Biological deterioration was noted at the wingwall piles (See Figure 10.4).

The average exposed pile length and pile spacing at the north abutment were about 8.6 ft and 3.8 ft, respectively. The tie back rods were located about 7.3 ft from the pile heads. The pile diameters varied between 12 and 13 inches (See Figure 10.5 and Figure 10.6). At the south abutment, the average exposed length and the pile spacing are about 10 ft and 4 ft, respectively. The tie back rods are about 7.8 ft from the pile heads, and the pile diameters vary between 10 and 11 inches (See Figure 10.7 and Figure 10.8). According to the construction plans for this bridge, the total lengths of the piles supporting the abutments are 40 ft, whereas the lengths of the wingwall piles are 25 ft for the pile closest to the abutment and 20 ft for the other two piles. As shown in Figure 10.9a, the tie back rods extend a distance of about 15 ft behind the backwall. The soil profile, shown in Figure 10.9b, was determined by drilling a test hole near the south abutment. The upper 14.5 ft comprise of soft to medium stiff loam, and the underlying soils comprise of a mixture of sand and gravel. The bottom 4 ft comprise of medium stiff clay. The water table was at a depth of 9 ft from the test hole elevation.

The bridge plans showed that the location of the anchor block was about 15 ft from the backwall and about 1.3 ft from the ground level. According to the design method proposed by Bowels (1996), the optimum location for the anchor block is in the zone of maximum efficiency, which would be located at 26 ft from the backwall at the current height (See Figure 10.10). The existing location, however, was still outside the active and passive failure zones.



Figure 10.3. Soil erosion near the north abutment (Bridge No. 094680 Carroll County – April 15 2006)



Figure 10.4. Severe deterioration observed at the northeast wingwall piles (Bridge No. 094680 Carroll County – April 15 2006)



Figure 10.5. North abutment (Bridge No. 094680 Carroll County – April 15 2006)

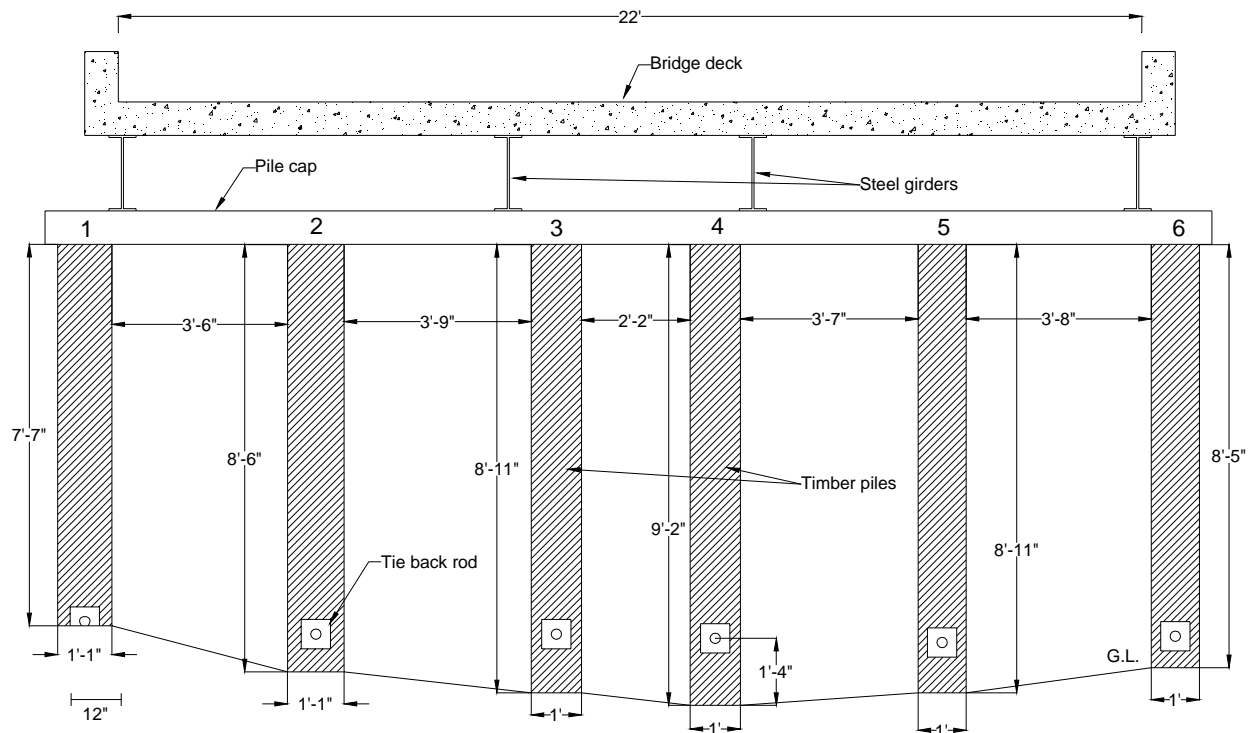


Figure 10.6. A schematic diagram of the north abutment (Bridge No. 094680 – Carroll County)



Figure 10.7. South abutment (Bridge No. 094680 Carroll County – April 15 2006)

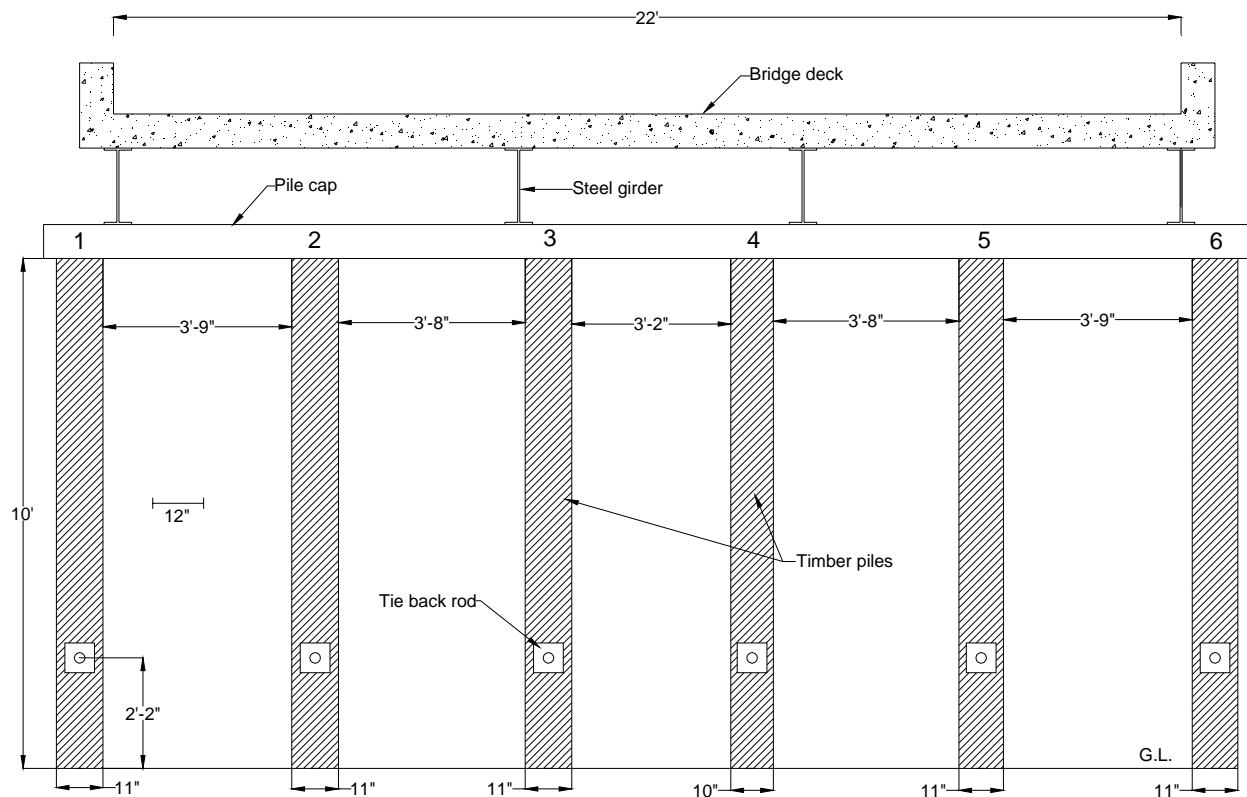
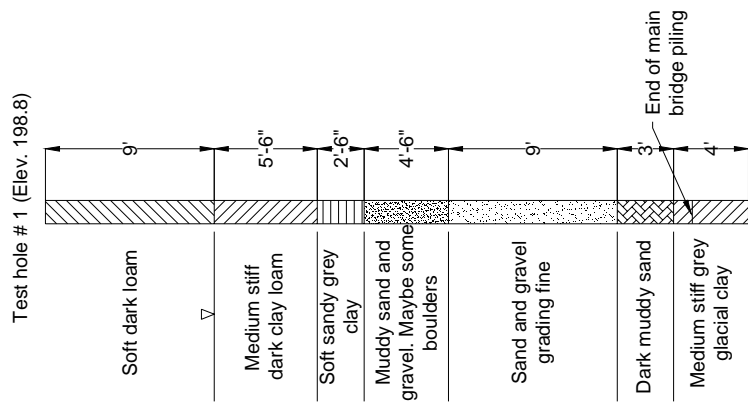


Figure 10.8. Schematic diagram of the south abutment (Bridge No. 094680 – Carroll County)

Pile cores were obtained from each abutment using an increment borer. At the north abutment, the densities of pile nos. 3, 4, and 5 were higher than the other piles. The lowest density was measured in pile no. 6. In addition, coring pile no. 1 revealed that there was a hollow section under the pile surface. The intact diameter of pile no. 1 was estimated to be 9 inches. At the south abutment, pile nos. 3, 4, and 5 had higher densities. The results also revealed that the pile density varied longitudinally along the pile length. For example, three cores were obtained from pile no. 1 at 12, 36, and 42 inches from the ground level; each resulted in a different density value. The average creosote penetration depth at this bridge was about 4 inches. Table 10.1 provides a summary of the measured pile densities. As can be seen in this table, the wood density ranged from 28.6 lb/ft³ to 57.1 lb/ft³.

10.2. Load Test Setup and Instrumentation

The exposed part of each pile was instrumented with four strain transducers with a gage length of 24 inches. The backwall was also instrumented with four strain transducers to measure the strain induced by axial and/or lateral loading (See Figure 10.11). As shown in Figure 10.12, at each pile in the south abutment, one strain transducer was attached below the elevation of the tie back rod.



(a) Soil profile near the south abutment

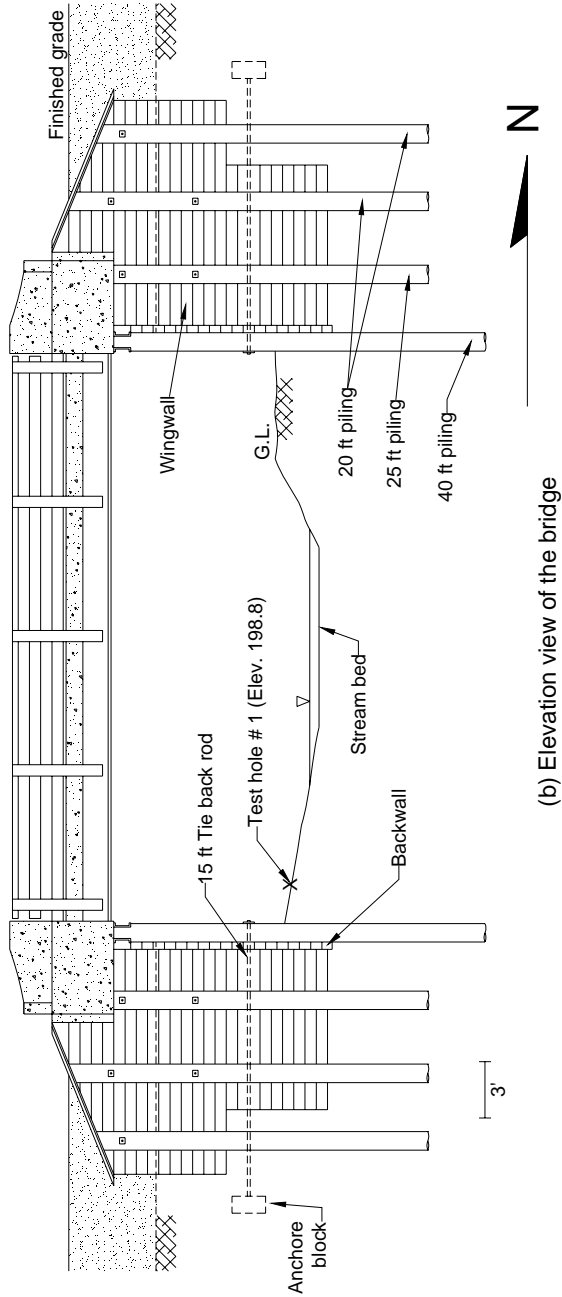


Figure 10.9. Bridge No. 094680 Carroll County

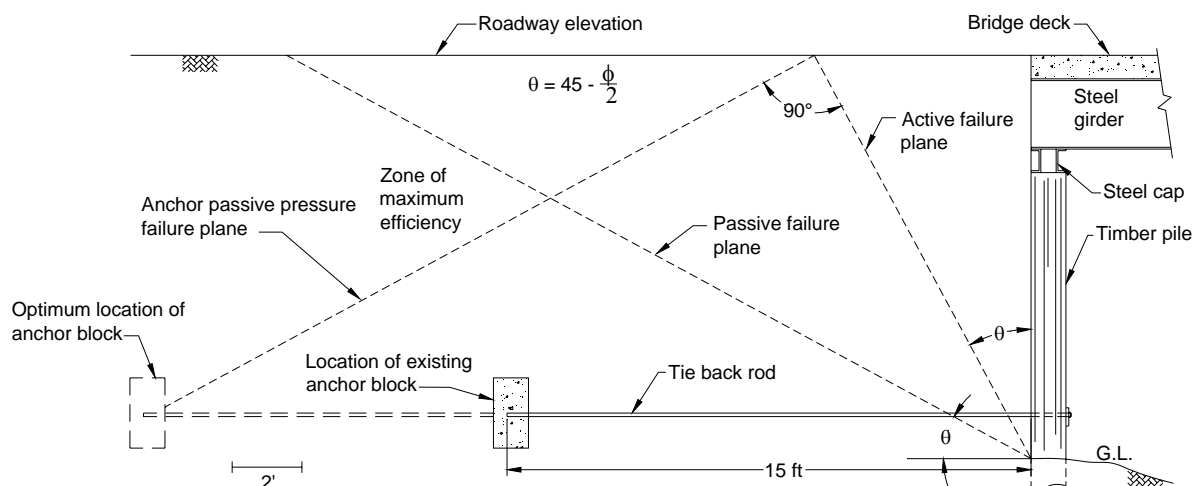


Figure 10.10. Anchor block located outside the zone of maximum efficiency (Bridge No. 094680 – Carroll County)

Table 10.1. Summary of measured piles densities (Bridge No. 094680 – Carroll County)

Abutment	Pile no.	Elevation (in.)*	Core length (in.)	Density (pcf)
North	1	36	3.8	34.5
	1	77	4.2	35.8
	2	37.5	3.6	33.9
	3	30	4.5	54.2
	4	32	4.1	53.7
	5	29.5	4.9	57.1
	6	60	4.1	28.6
	6	78	4.4	30.4
South	1	12	4.1	42.7
	1	36	3.2	37.3
	1	42	3.1	38.0
	2	0	4.0	37.7
	2	26	3.9	41.9
	3	14.5	4.8	51.0
	3	60	4.2	46.6
	4	13	4.6	56.1
	5	36	4.7	54.2
	6	28	3.9	37.8

*Elevations are relative to ground level

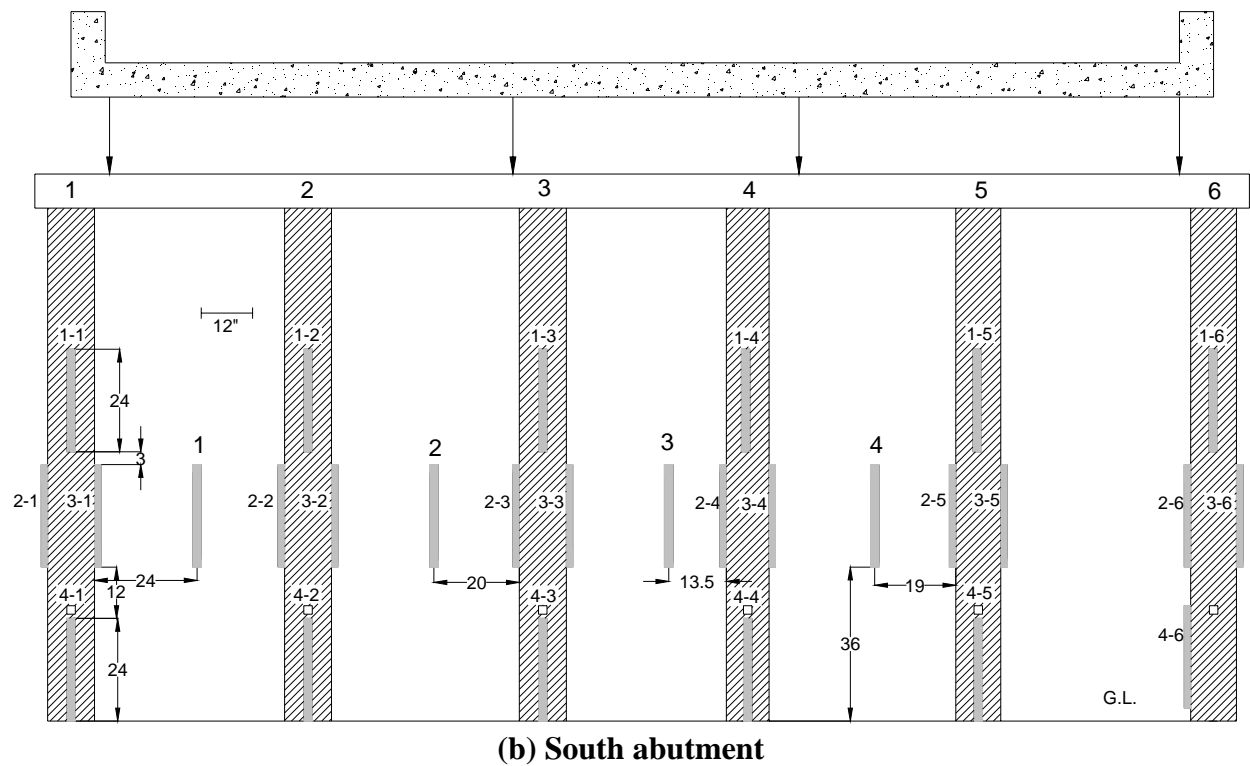
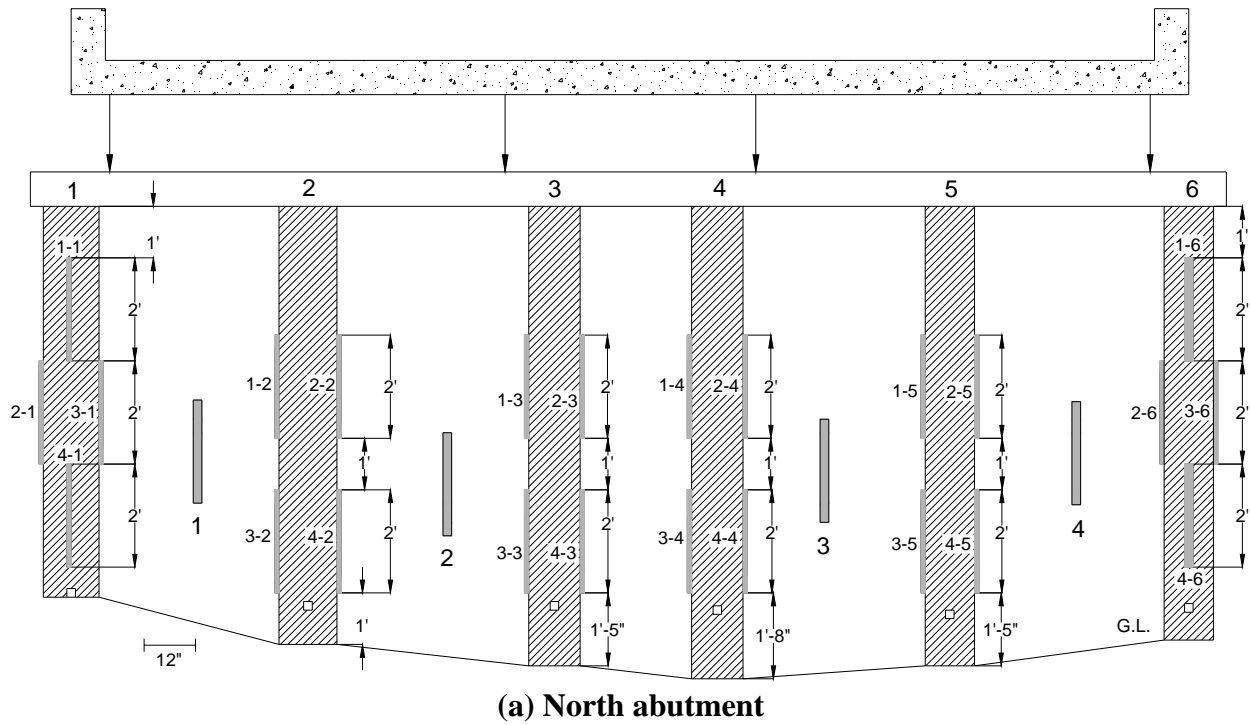


Figure 10.11. Locations of the strain transducers (Bridge No. 094680 – Carroll County)

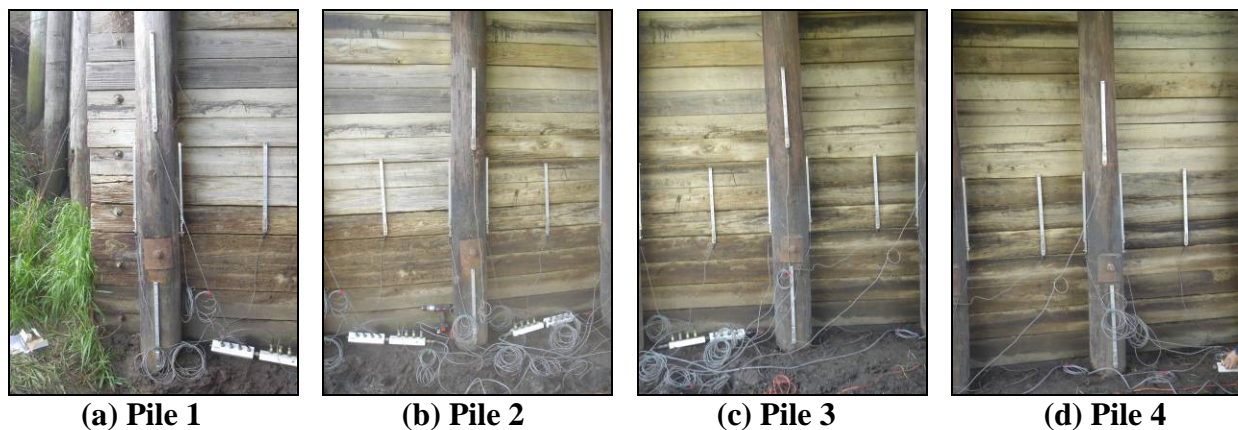


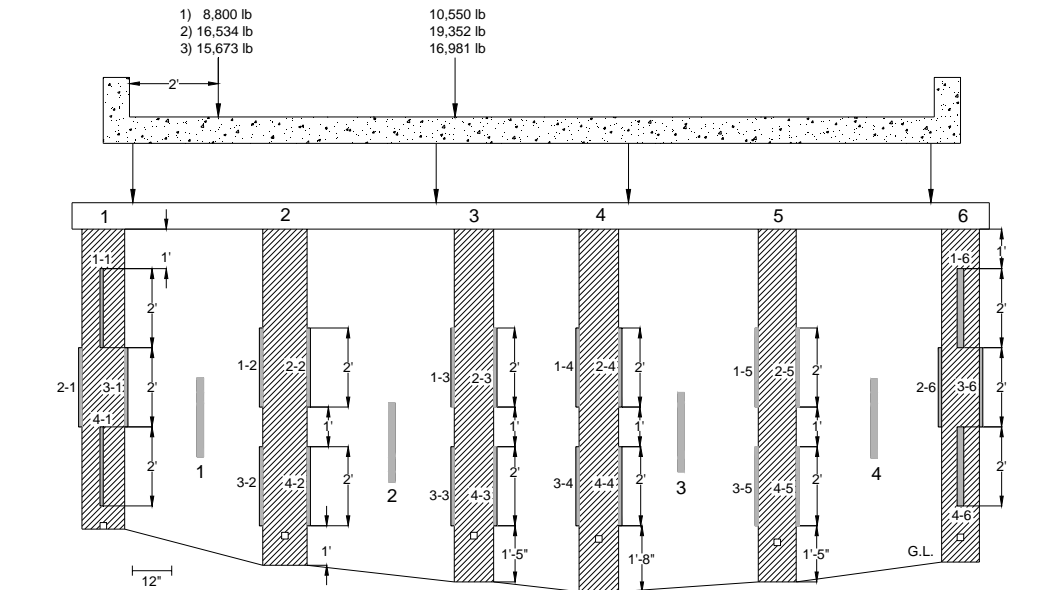
Figure 10.12. Strain transducers attached below the tie back road at the south abutment (Bridge No. 094680 – Carroll County)

10.3. Test Results

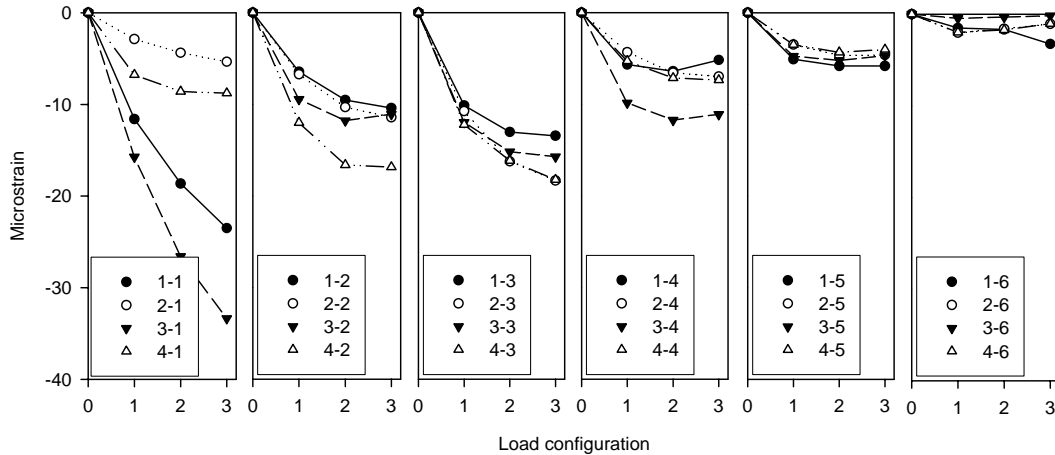
10.3.1. North Abutment – West Edge

The north abutment was first loaded at the west edge of the bridge. The location of the applied loads, pile strains, and backwall strains are shown in Figure 10.13. The applied loads were offset 2 ft from the curb. The highest strain was measured in pile no. 1 and was about -33 microstrains at load configuration 3. The strain recorded at pile no. 1 varied considerably along the exposed pile length. This may be due to the localized hollow pile sections, which were detected using the increment borer. The measured strain values decreased with increasing distance from the location of the applied loads; as may be seen in Figure 10.13b, almost no strain was recorded in pile no. 6.

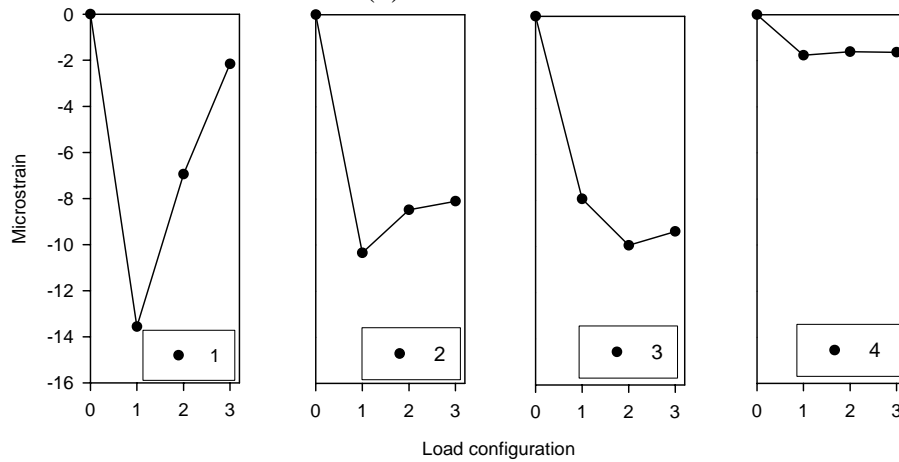
Similar to pile strains, backwall strains were highest directly under the applied load, and decreased with increasing distance from the location of the axial loads. The highest strain measured was about -13.6 microstrains between pile nos. 1 and 2 (See Figure 10.13c). Partial bearing between the pile cap and the timber backwall can be seen in Figure 10.14. Therefore, the recorded backwall strains are a combination of axial and lateral loads.



(a) Location of strain transducers and axle loads



(b) Pile strains



(c) Backwall strains

Figure 10.13. Static load test at the west edge (Bridge No. 094680 – Carroll County)



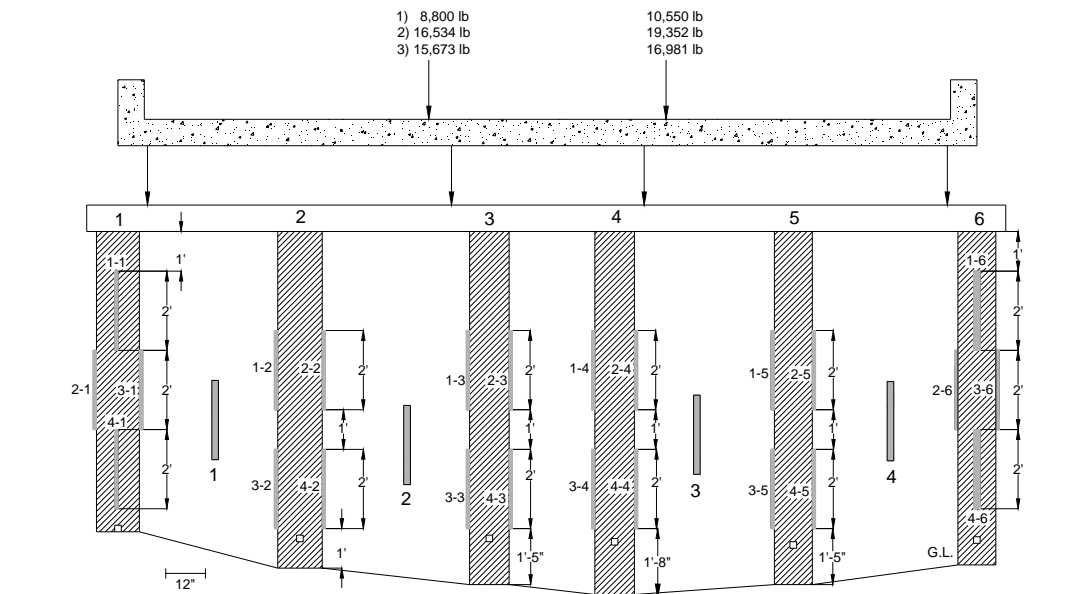
Figure 10.14. Pile cap partially resting on the backwall (Bridge No. 094680 Carroll County – May 16 2006)

10.3.2. North Abutment – Centerline

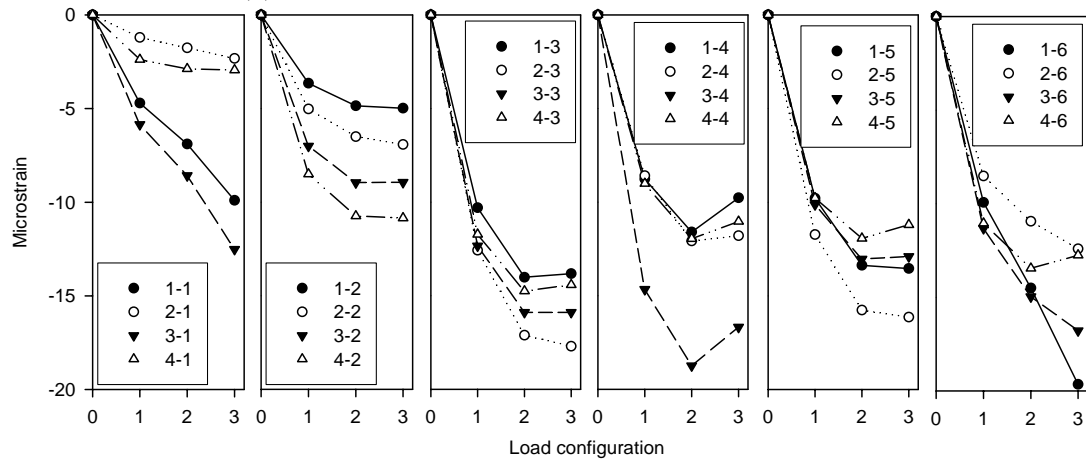
The north abutment was loaded at the centerline of the bridge deck as shown in Figure 10.15a. The recorded strains were higher at pile nos. 3, 4, 5, and 6 (See Figure 10.15b). The E_s of these piles are unknown; therefore, it was not determined whether the high strain values are due to higher axial loads or softer pile sections. In load configuration 3, pile no. 6 had the highest strain value, which was about -20 microstrains. Pile nos. 1 and 2 experienced lower strains compared to the other piles. Backwall strains were also higher on the east edge of the bridge (See Figure 10.15c). The backwall strains were highest between pile nos. 4 and 5. Generally, the strains were highest in load configuration 1 since the front axle and the front wheels of the tandem axle were still on the roadway, and were lowest in load configuration 3, where the backwall strains are induced by axial compression only.

10.3.3. North Abutment – East Edge

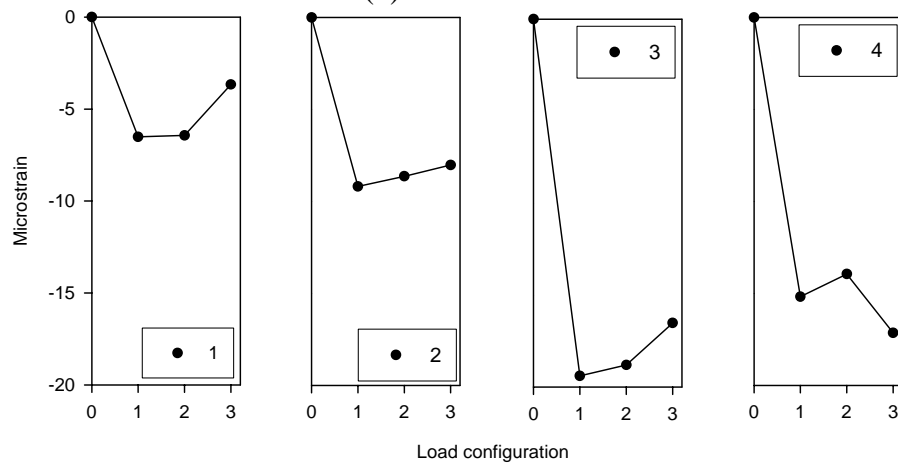
The third load test conducted at the north abutment was with the loading at the west edge of the bridge. The location of the applied loads, pile strains, and backwall strains are shown in Figure 10.16. The highest strain was measured was in pile no. 6 and was about -39 microstrains in load configuration 3. The strains decreased with increasing distance from the location of the applied loads. Backwall strains were highest at the east side of the bridge under the applied load, and decreased with increasing distance from the location of the load. This highest strain measured was about -34 microstrains between pile nos. 5 and 6. Similar to the previous tests, the backwall strains in load configuration 3 are caused by the partial bearing between the pile cap and the backwall, which transferred axial loads from the front axle.



(a) Location of strain transducers and axle loads

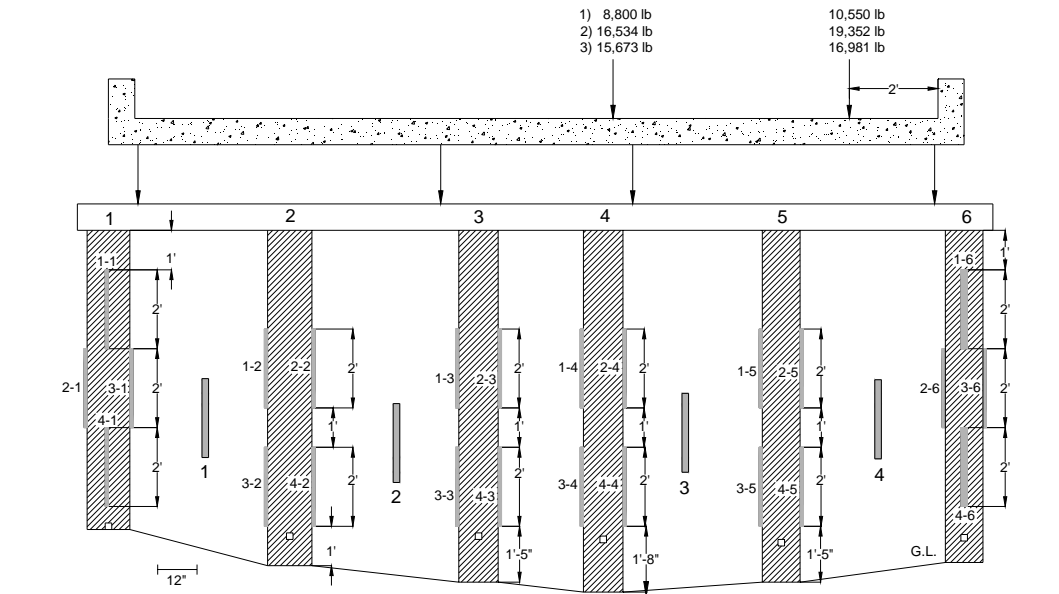


(b) Pile strains

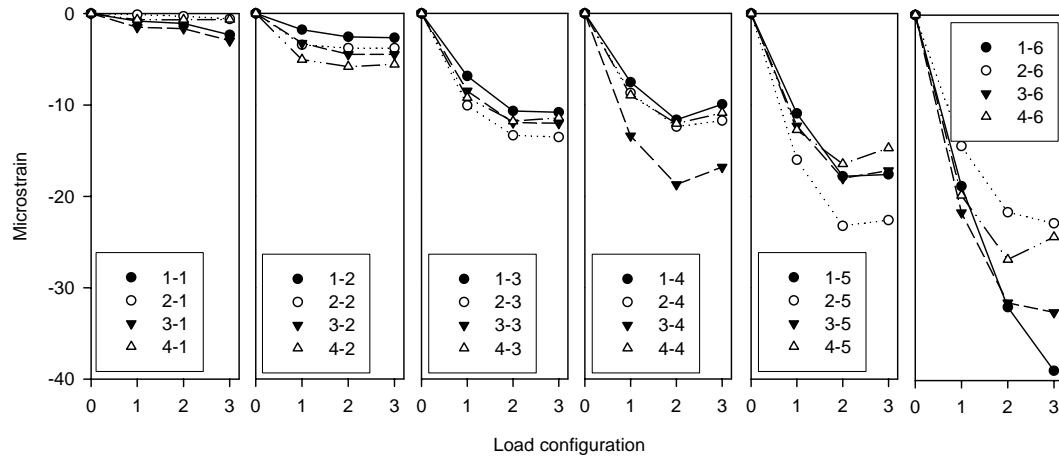


(c) Backwall strains

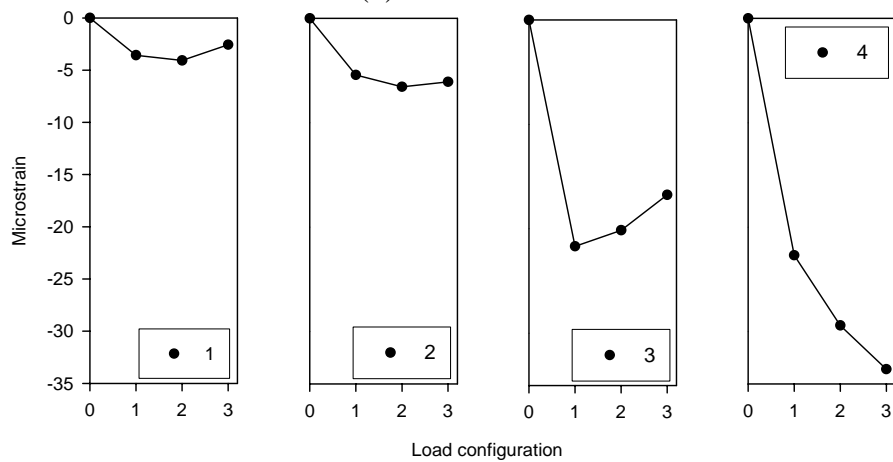
Figure 10.15. Static load test at the centerline (Bridge No. 094680 – Carroll County)



(a) Location of strain transducers and axial loads



(b) Pile strains



(c) Backwall strains

Figure 10.16. Static load test at the east edge (Bridge No. 094680 – Carroll County)

10.3.4. South Abutment – West Edge

The first load test conducted at the south abutment was with the loading at the west side of the bridge. The location of the applied loads, pile strains, and backwall strains are shown in Figure 10.17. The highest strain measured was in pile no. 6 and was about -34 microstrains in load configuration 3. The measured strains decreased with increasing distance from the location of the applied loads. Almost no strain was measured in pile no. 1. Strain transducer 4-4 was not adequately connected to the pile; therefore, the data recorded by this strain transducer were discarded.

In load configuration 1, the backwall strains were highest near the applied load, and decreased with increasing distance from the location of the axial loads. In load configurations 2 and 3, the strain measured between pile nos. 2 and 3 increased, whereas at other locations, backwall strain measurements decreased.

10.3.5. South Abutment – Centerline

In the second load test, loading was applied along the centerline of the bridge. Figure 10.18 illustrates the locations of the applied loads, pile strains, and backwall strains. Loading the bridge at the centerline resulted in a more uniform strain distribution as may be seen in Figure 10.18b. Pile no. 3, however, displayed higher strain compared to the other piles. In the third load configuration, 63% of the load applied by the back wheel of the tandem axle was carried by the north abutment piles. This explains why the strains for most piles were reduced in the third load configuration.

Similar to the west edge test, the backwall strain measured between pile nos. 2 and 3 continued to increase with increasing load configurations.

10.3.6. South Abutment – East Edge

In the third load test, loading was applied at the east edge of the bridge. The locations of the applied loads, pile strains, and backwall strains are shown in Figure 10.19. The applied load was offset 2 ft from the curb. The pile strain was highest near the applied loads and decreased with increasing distance from the location of the applied loads. Almost no strain was measured in pile no. 6. The highest strain was measured in pile no. 1 and was about -30 microstrains in load configuration 3.

Similar to the two previous load tests, backwall strains measured between pile nos. 2 and 3 were higher than strains measured at other locations across the backwall. Unlike the other locations, the strains at this location continued to increase with higher load configurations.



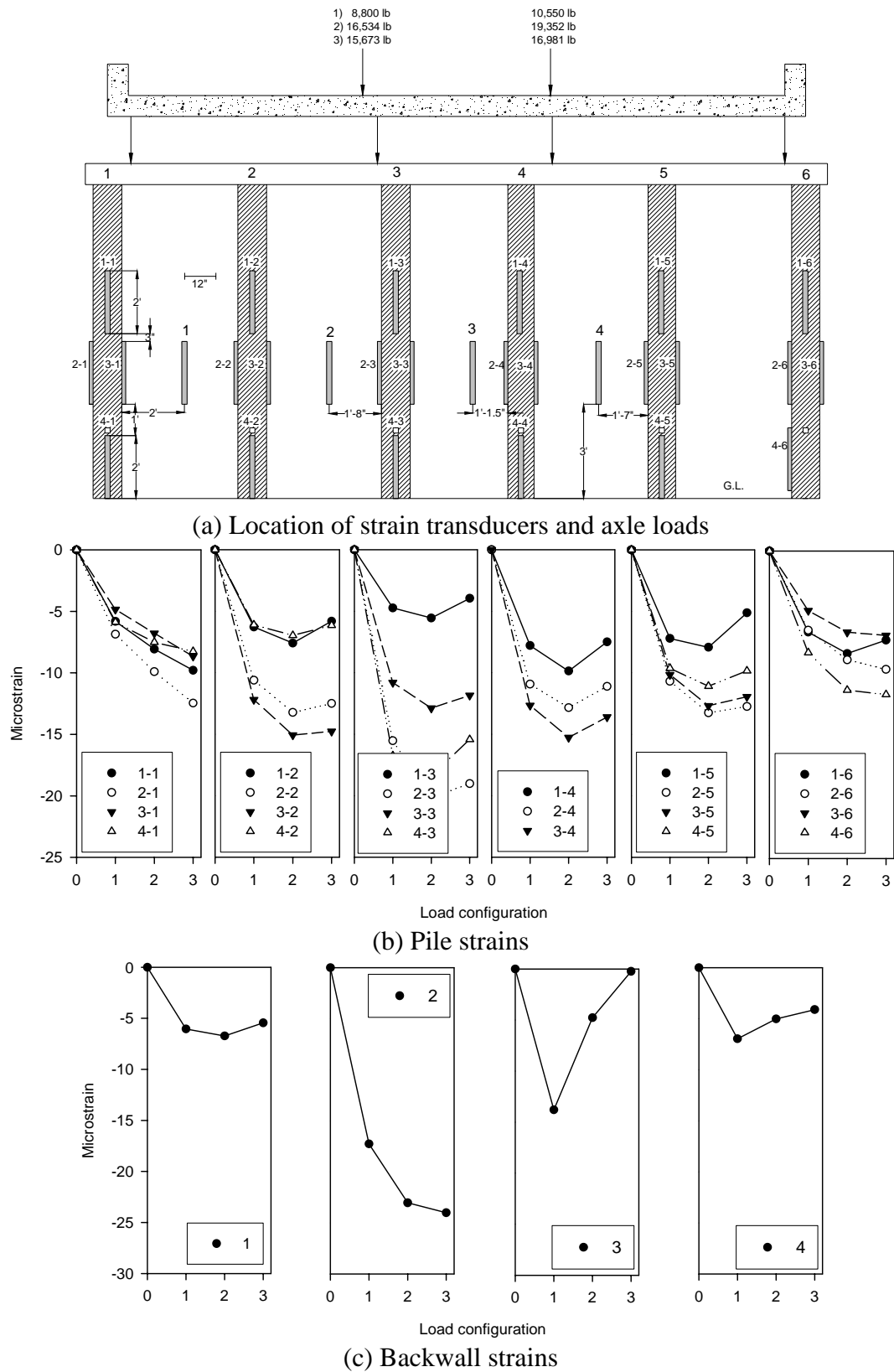


Figure 10.18. Static load test at the centerline (Bridge No. 094680 – Carroll County)

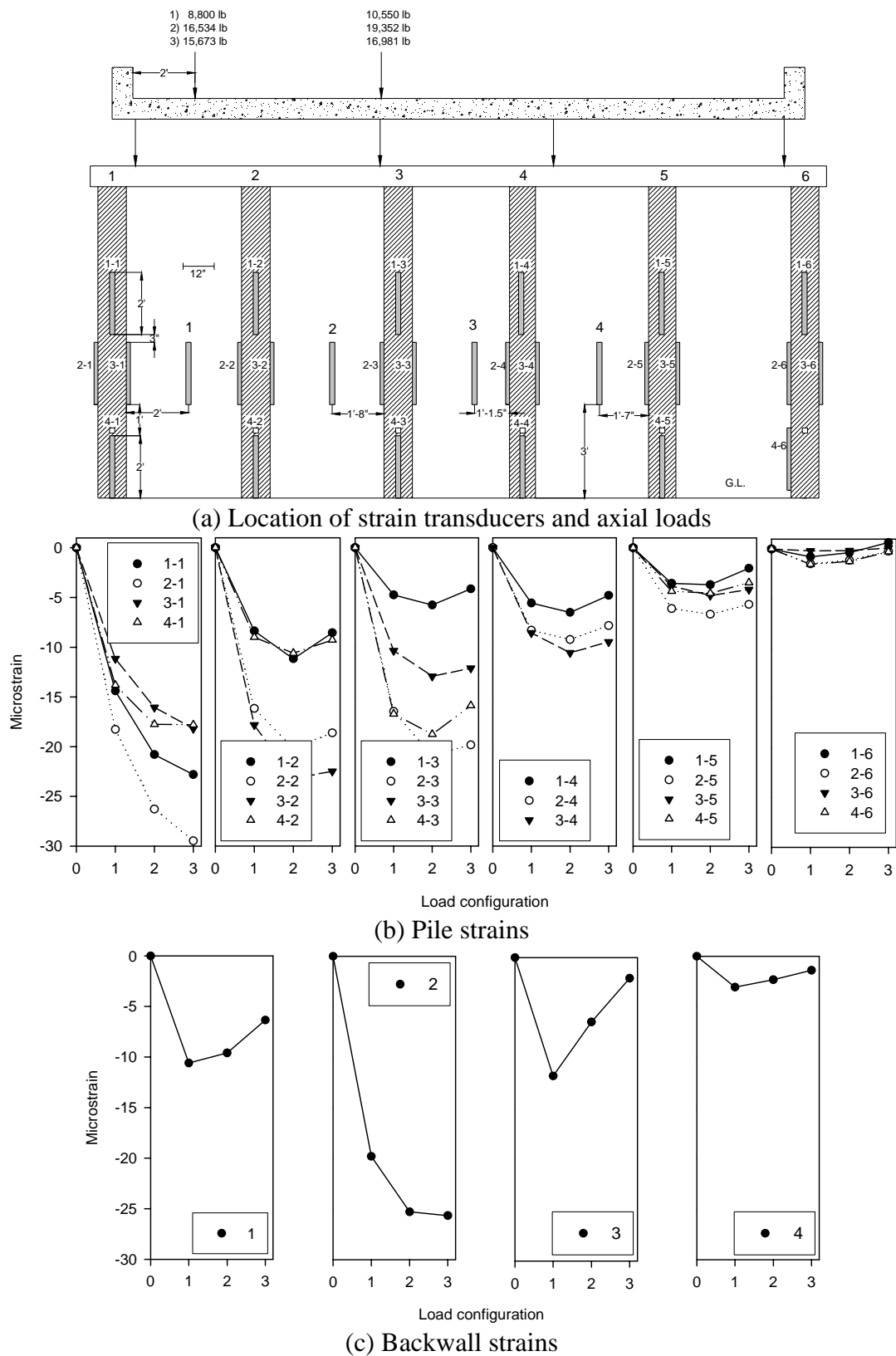


Figure 10.19. Static load test at the east edge (Bridge No. 094680 – Carroll County)

11. BRIDGE NO. 237380 MAHASKA COUNTY

11.1. Bridge Description

The fifth bridge tested is located in Mahaska County on Osborn Avenue over a creek. The bridge is about 3 miles northeast of Oskaloosa, Iowa. This bridge is 36 ft long and 17.75 ft wide with a non-composite concrete deck, five steel girders, and 0° skew (See Figure 11.1). The creek flowing under this bridge is a tributary of the South Skunk River; therefore, the water level is expected to vary greatly with time exposing the piles to high moisture conditions, which makes them more susceptible to biological deterioration.



Figure 11.1. Bridge No. 237380 – Mahaska County (April 16 2006)

The substructure consisted of five timber piles in front of a timber backwall, two timber piles in each wingwall, and double c-channel pile cap. The average exposed pile length and pile spacing at the northwest abutment are about 11.5 ft and 4.5 ft, respectively (See Figure 11.2). The water depth at the time of inspection was about 1 ft. During the time of testing, the northwest abutment piles showed signs of biological deterioration as shown in Figure 11.3. Pile no. 1 at the southwest end also showed signs of biological deterioration at the water level, and was bulging at about 4 ft from the water level (See Figure 11.4). Pile nos. 2 and 3 also suffered from biological deterioration as shown in Figure 11.5. No tie back rods were observed at this abutment. The elevation of the southeast abutment is higher than the water level as shown in Figure 11.6. The average exposed pile length and pile spacing in this abutment were about 3.6 ft and 4 ft, respectively. The pile diameters were approximately 1 ft (See Figure 11.7). Similar to the northwest abutment, no tie back rods were observed.

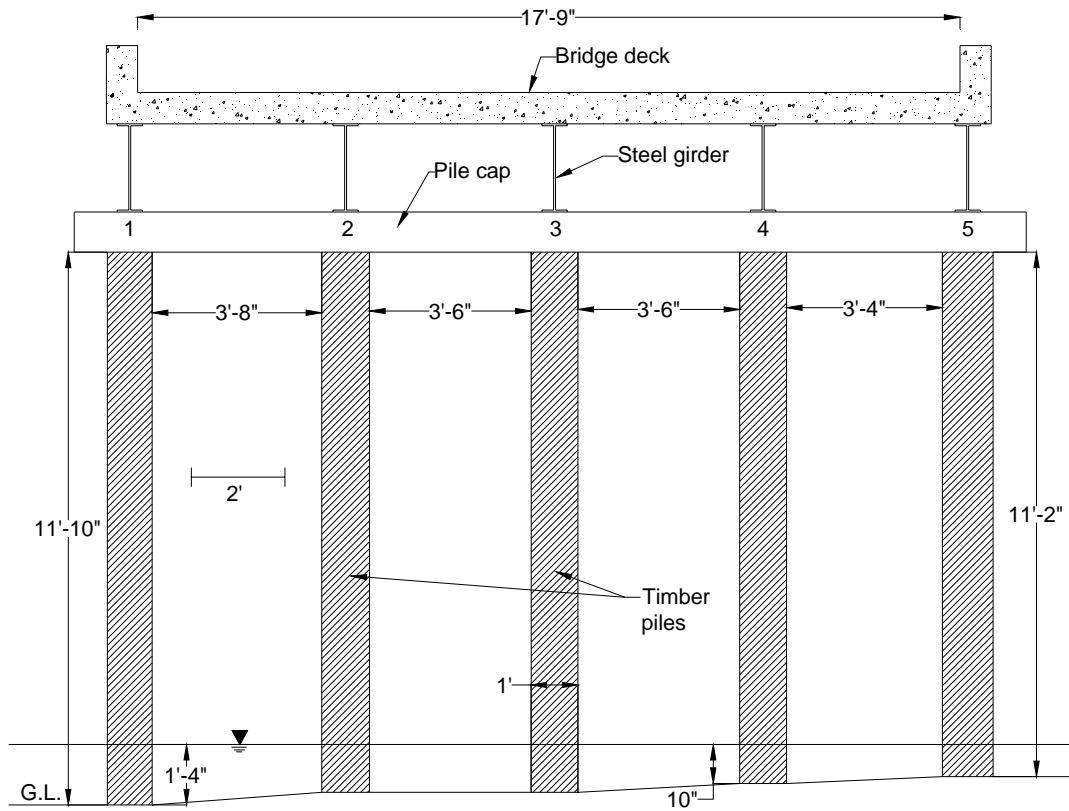


Figure 11.2. Schematic diagram of the northwest abutment (Bridge No. 237380 – Mahaska County)

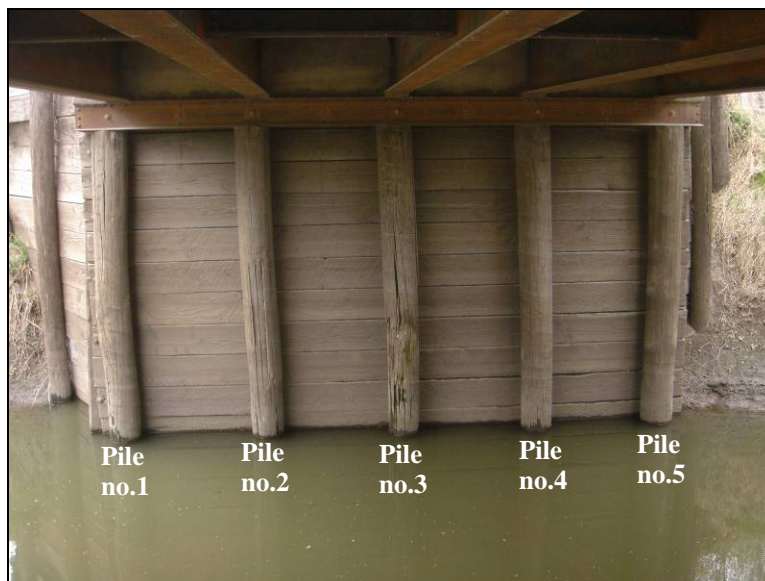


Figure 11.3. Northwest abutment (Bridge No. 237380 Mahaska County – April 16 2006)



(a) Biological deterioration near the water level



(b) Bulging of timber fibers

Figure 11.4. Deterioration of pile no. 1 (Bridge No. 237380 Mahaska County – April 16 2006)



(a) Pile no. 2



(b) Pile no. 3

Figure 11.5. Biological deterioration at the northwest abutment (Bridge No. 237380 Mahaska County – April 16 2006)

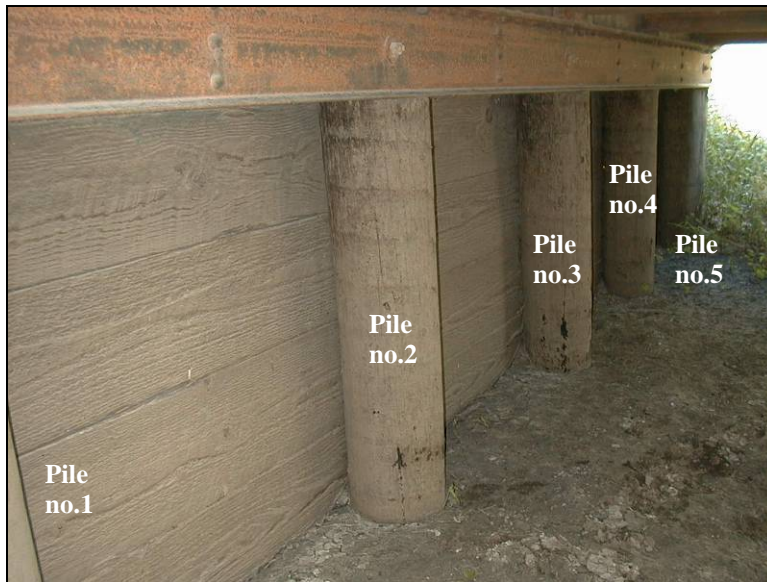


Figure 11.6. Southeast abutment at a higher elevation than the water level (Bridge No. 237380 Mahaska County – April 16 2006)

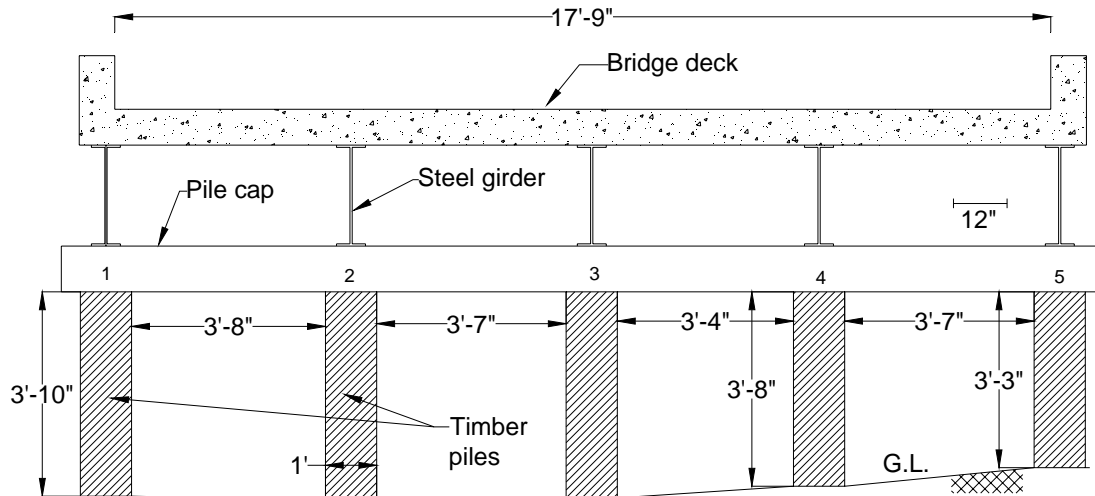


Figure 11.7. Schematic diagram of the southeast abutment (Bridge No. 237380 – Mahaska County)

Using the increment borer, pile cores were obtained from the piles both abutments. The density determined from each core and the elevation at which the cores were obtained are summarized in Table 11.1. Coring the piles revealed that pile nos. 2 and 4 at the southeast abutment are hollow near the pile core. It is estimated that the remaining intact diameters of pile nos. 2 and 4 are about 3 and 3.5 inches, respectively. As may be seen in Table 11.1, the wood density ranged from 35.8 lb/ft³ to 53.9 lb/ft³.

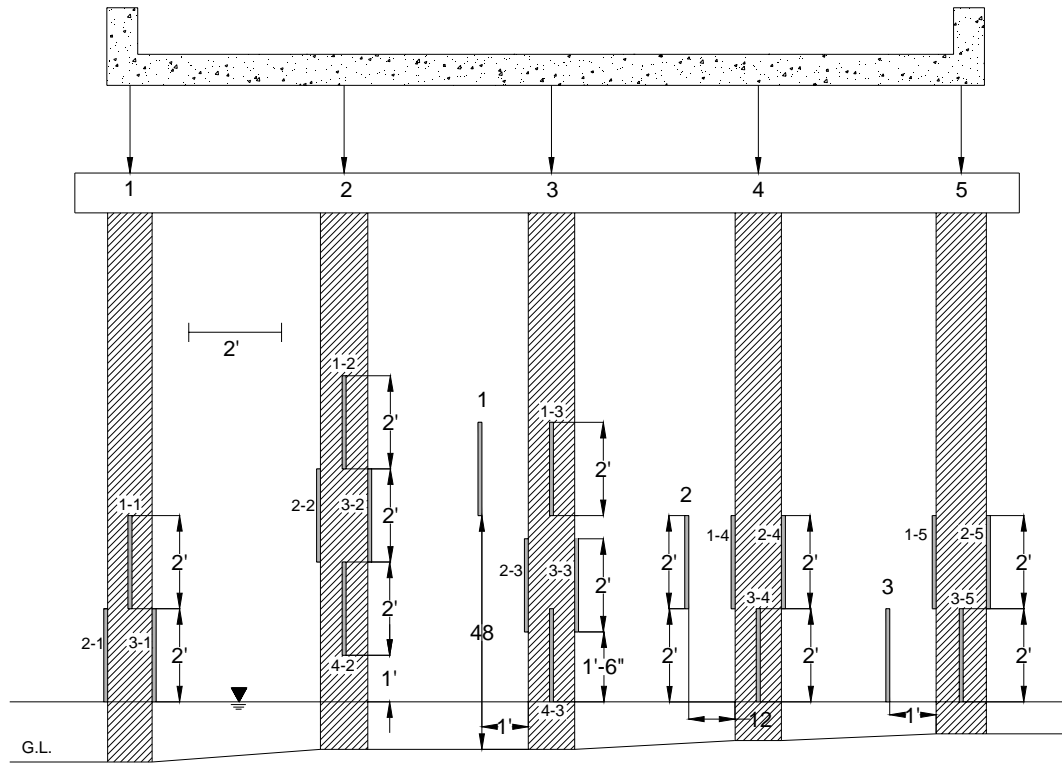
Table 11.1. Summary of piles densities (Bridge No. 237380 – Mahaska County)

Abutment	Pile	Elevation (in.)*	Core length (in.)	Density (pcf)
Northwest	1	33	3.9	43.9
	2	41	3.5	53.9
	3	34	3.3	51.0
	4	30	4.0	35.8
	5	29.5	3.9	53.6
Southeast	1	24	5.2	38.5
	2	24	5.0	51.1
	3	24	4.7	45.7
	4	24	3.0	37.5
	5	24	3.5	46.5

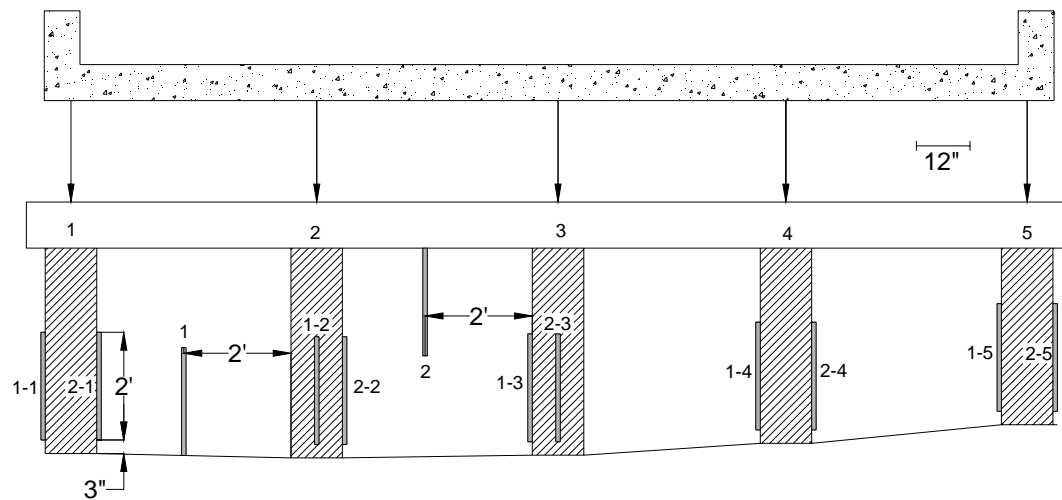
*Elevations are relative to the ground level

11.2. Load Test Setup and Instrumentation

A static load test was conducted at both the northwest and southeast abutments. At the northwest abutment, pile nos. 1, 4, and 5 were instrumented with three strain transducers, whereas the more deteriorated pile nos. 2 and 3 were instrumented with four strain transducers. The backwall was also instrumented with three strain transducers (See Figure 11.8a). At the southeast abutment, each pile was instrumented with two strain transducers as shown in Figure 11.8b. The backwall was instrumented with two strain transducers. The gage lengths of all transducers were 24 inches.



(a) Northwest abutment



(b) Southeast abutment

Figure 11.8. Location of strain transducers (Bridge No. 237380 – Mahaska County)

11.3. Test Results

11.3.1. Northwest Abutment – North Edge

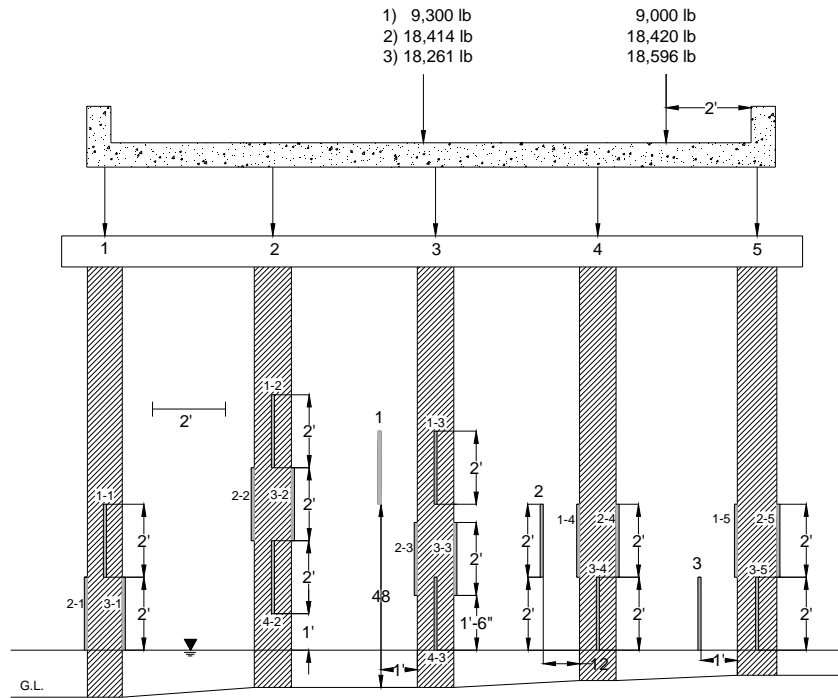
The first load test was conducted with the loading at the north edge of the bridge. The location of the applied loads, pile strains, and backwall strains are shown in Figure 11.9. Most of the strains were observed in piles nos. 4 and 5. The highest strain was measured in pile no. 4 and was about -17 microstrains. The highest strain measured in pile no. 3, which was directly under the applied load, in load configuration 3 was about -9 microstrains. Pile no. 2 experienced higher strain even though it was located at a greater distance from the location of the axial load. The highest strain in pile no. 2 in load configuration 3 was about -10 microstrains. The backwall strains were highest between pile nos. 2 and 3 where the strain transducer was placed at a higher elevation (48 inches above the water level). At the lower elevation (closer to the water level), the strains decreased

11.3.2. Northwest Abutment – Centerline

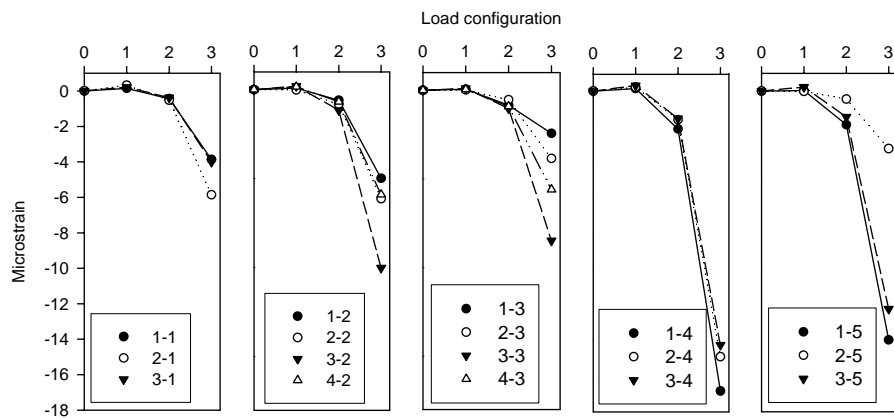
The test was repeated with the loading at the centerline of the bridge. The location of the applied loads, pile strains, and backwall strains are shown in Figure 11.10. The results indicate that pile nos. 1, 2, and 4 are carrying most of the load since they displayed the highest strain measurement. The strain measured in pile no. 3 was about -9 microstrains similar to the previous test. This confirms the visual observation that the pile was deteriorated. Pile nos. 1 and 2 experienced similar strains even though pile no. 1 is further away from the location of the applied axial loads. The strains measured in pile nos. 1 and 2 were about -14 microstrains. This demonstrates that part of the load carried by pile no. 2 was transferred to adjacent pile no. 1. Similar to the previous test, backwall strains were highest at high elevation close to the applied load and decreased with increasing depth.

11.3.3. Northwest Abutment – South Edge

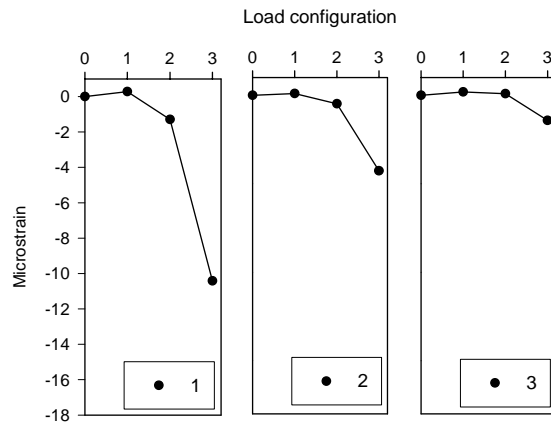
The northwest abutment was tested with the loading at the south edge of the bridge. The location of the applied loads, which were offset 2 ft from the curb, pile strains, and backwall strains are shown in Figure 11.11. As shown in Figure 11.11a, one wheel load was directly above pile no. 3. However, the strains did not increase compared to the previous two tests. The highest strain value measured in load configuration 3 was still about -8 microstrains (See Figure 11.11b). The results also demonstrate that the load was mostly carried by pile no. 1 as evidenced by the higher strain.



(a) Location of strain transducers and axle loads

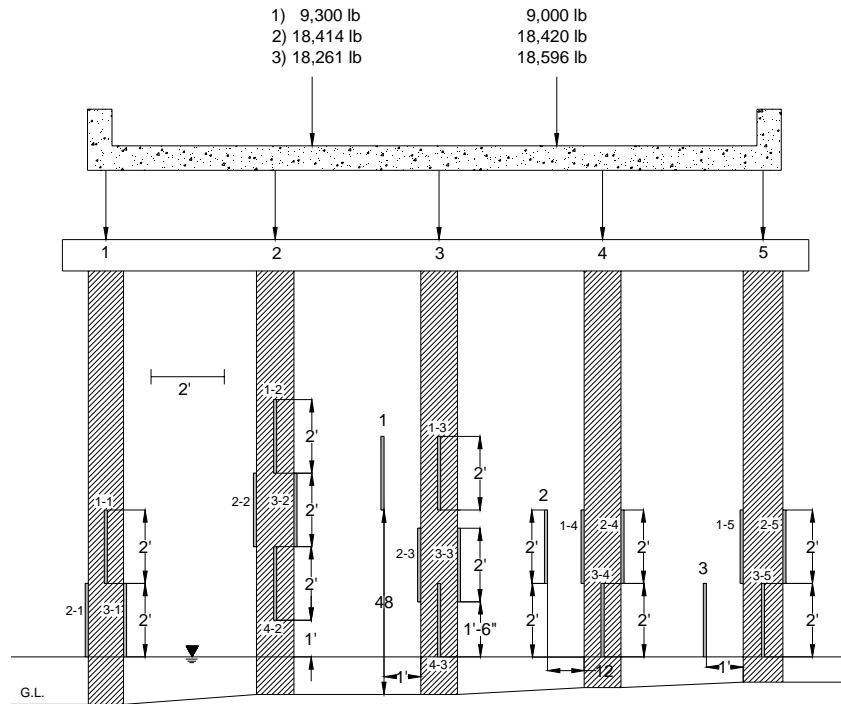


(b) Pile strains

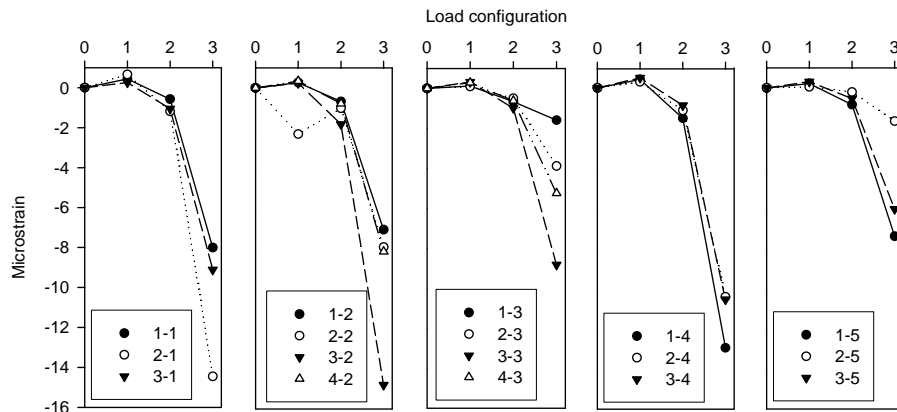


(c) Backwall strains

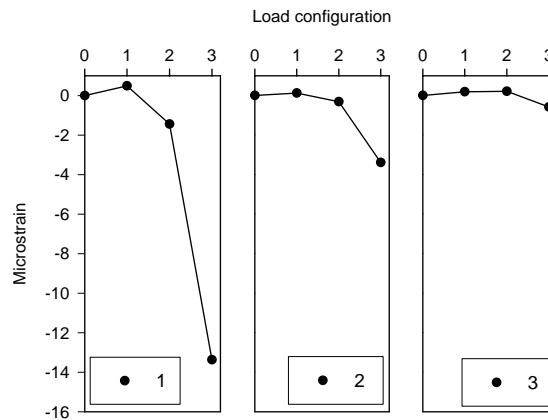
Figure 11.9. Static load test at the north edge (Bridge No. 237380 – Mahaska County)



(a) Location of strain transducers and axle loads

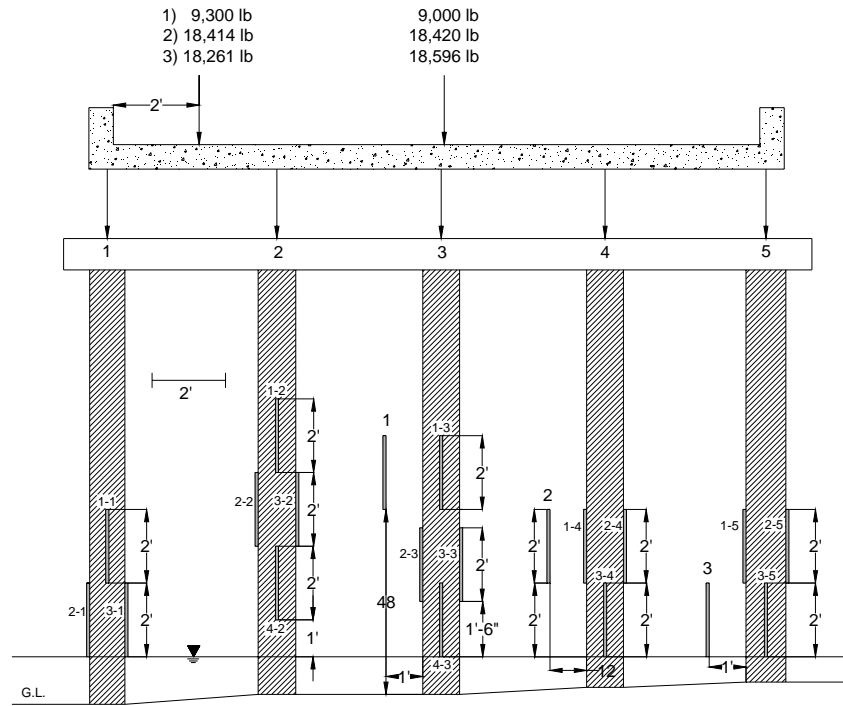


(b) Pile strains

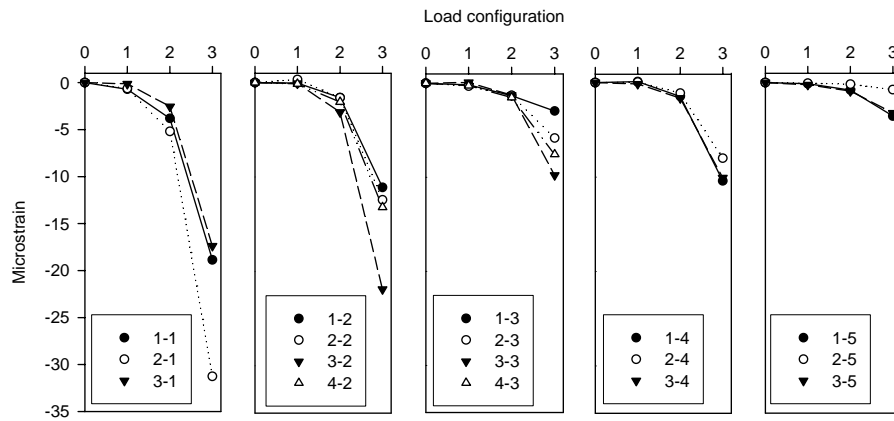


(c) Backwall strains

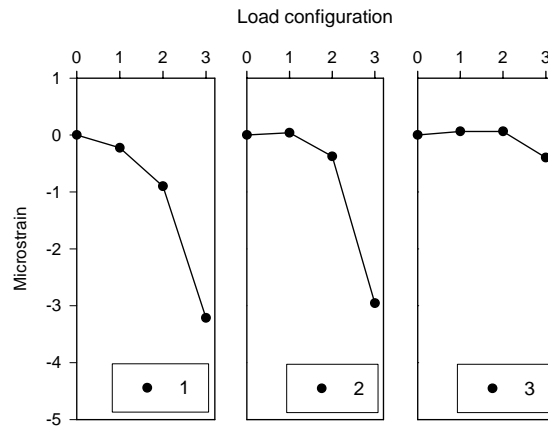
Figure 11.10. Static load test at the centerline (Bridge No. 237380 – Mahaska County)



(a) Location of strain transducers and axial loads



(b) Pile strains



(c) Backwall strains

Figure 11.11. Static load test at the south edge (Bridge No. 237380 – Mahaska County)

11.3.4. Southeast Abutment – North Edge

The southeast abutment was first loaded with the loading positioned at the north edge of the bridge. Locations of the applied loads, pile strains, and backwall strains are presented in Figure 11.12. The results indicate that pile nos. 1 and 3 are carrying most of the load due to their higher strains. The strain decreased with increasing distance from the applied load.

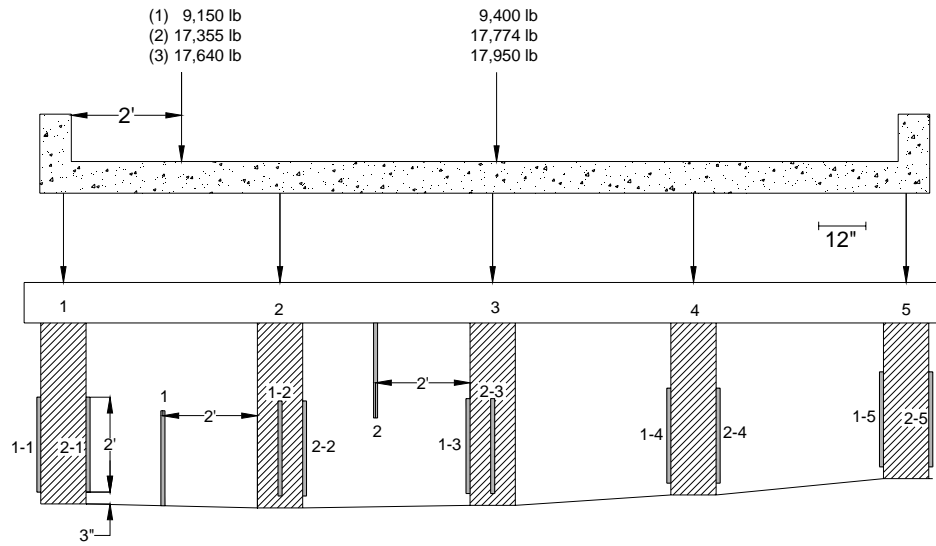
11.3.5. Southeast Abutment – Centerline

When the loading was applied at the centerline of the bridge deck, the load was carried primarily by pile nos. 1 and 3 (See Figure 11.13). The strain measured in pile nos. 1 and 3 in load configuration 3 were -13 and -17 microstrains, respectively. Lower strain measurements were recorded at pile no. 2 during the centerline and north edge load tests.

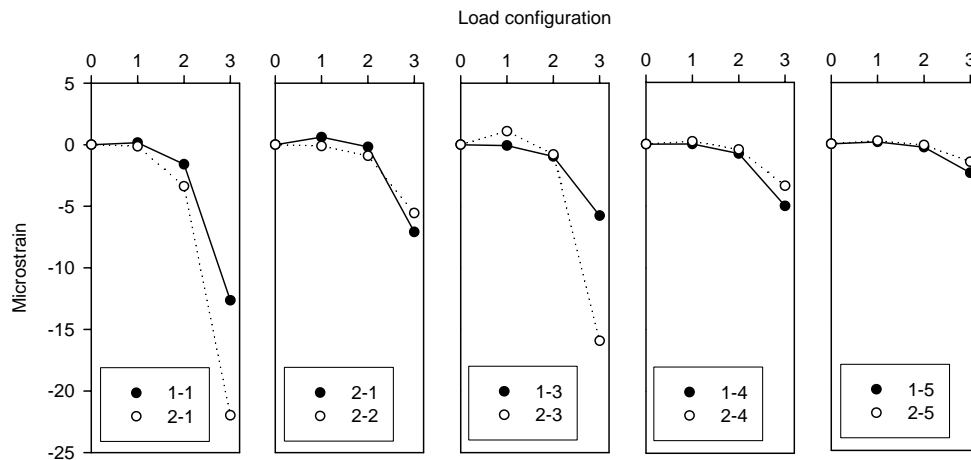
11.3.6. Southeast Abutment – South Edge

In the third test at the south east abutment, loading was applied at the south edge of the bridge. Locations of the applied loads, pile strains, and backwall strains are presented in Figure 11.14. Pile nos. 3 and 5 experienced the highest strains. The strains measured at pile nos. 3 and 5 are -15.9 and -14.1, respectively. The strains decreased with increasing distance from the applied load.

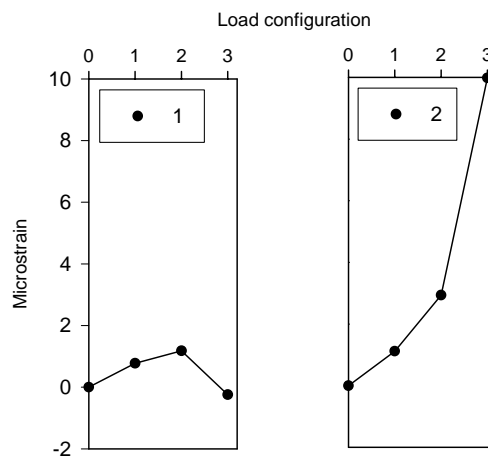
The backwall strains in all tests were positive indicating tension or bending of the backwall away from the bridge abutment. This may be due to eccentric loading caused by the partial bearing of the pile cap on the backwall as shown in Figure 11.15.



(a) Location of strain transducers and axle loads

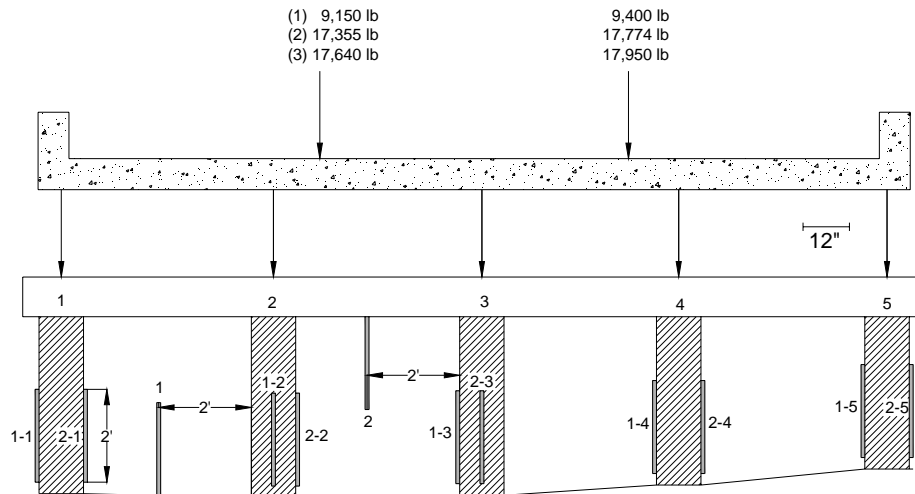


(b) Pile strains

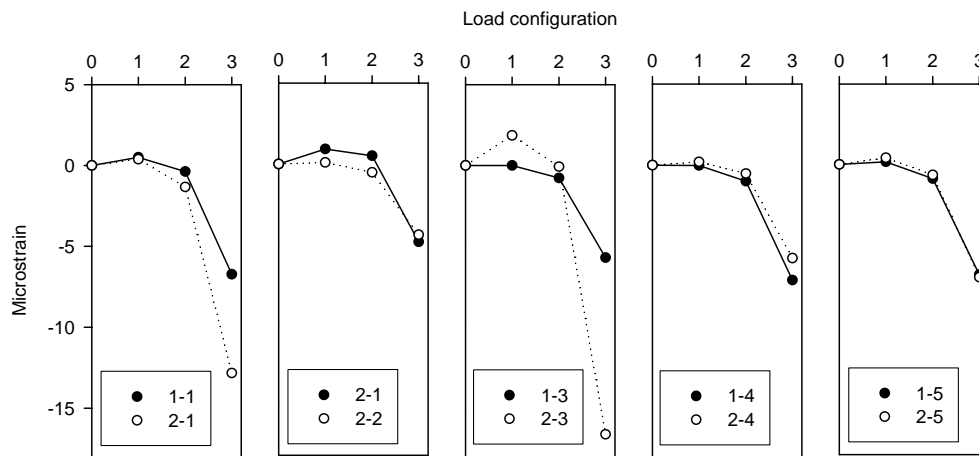


(c) Backwall strains

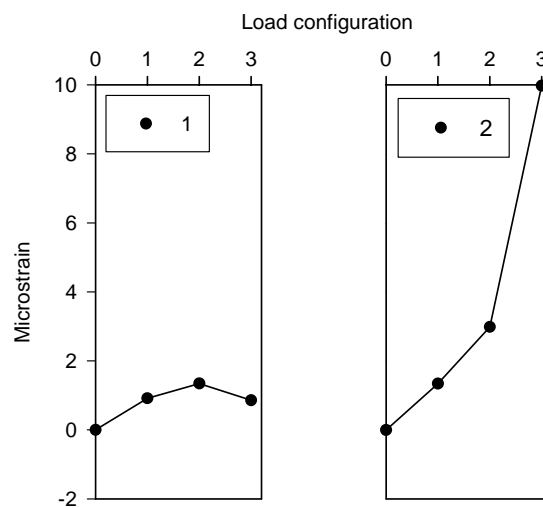
Figure 11.12. Static load test at the north edge (Bridge No. 237380 – Mahaska County)



(a) Location of strain transducers and axle loads

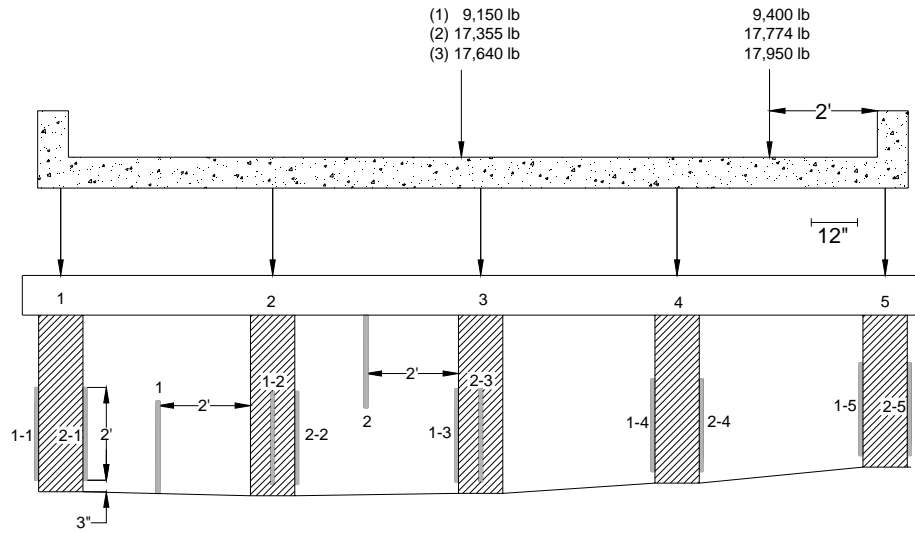


(b) Pile strains

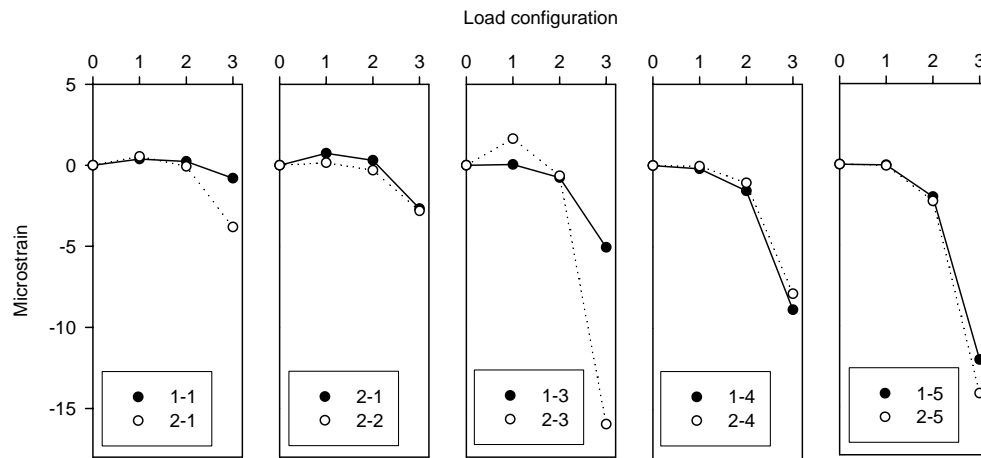


(c) Backwall strains

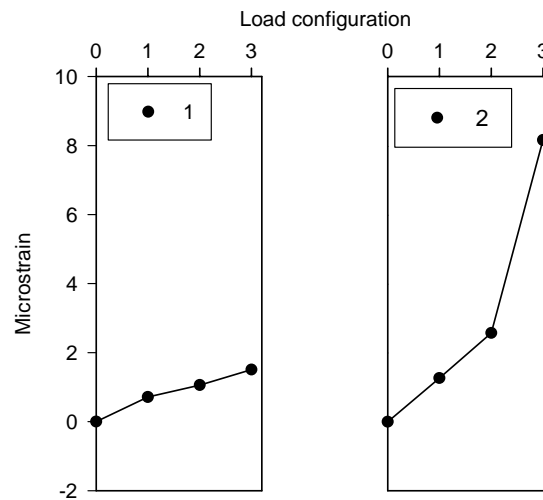
Figure 11.13. Static load test at the centerline (Bridge No. 237380 – Mahaska County)



(a) Location of strain transducers and axle loads



(b) Pile strains



(c) Backwall strains

Figure 11.14. Static load test at the south edge (Bridge No. 237380 – Mahaska County)



Figure 11.15. Partial bearing of the pile cap on the southeast abutment backwall (Bridge No. 237380 Mahaska County – May 27 2006)

11.4. Foundation Design

To estimate the pile length, the foundation was designed using the design methods discussed in previous chapters. CPT was conducted at 100 ft north of the north abutment to a depth of about 30 ft as shown in Figure 11.16. The soil encountered was mainly clay. The water level was at a depth of 19 ft. At the south abutment, three CPT tests were performed as shown in Figure 11.17. The maximum cone resistance was reached between 6 ft and 6.6 ft due to the presence of cobbles and boulders in this area. The cone was not advanced beyond this depth. Therefore, the foundation design was based on the CPT results obtained near the north abutment.

A summary of the pile length computation is shown in Table 11.2. An average side friction value was determined to be about 0.6 tsf. The point resistance at the pile toe was about 5 tons. For the Nottingham and Schmertmann method, the calculated pile length needed to resist an allowable pile load of 21 tons was about 45 ft below ground level. For the method outlined by Klaiber et al. (2004), the pile length was about 50 ft. The difference in pile length between both methods may be attributed to the 1.4 nominal axial pile factor, which is multiplied by the total load to account for various superstructure systems and non-uniform distribution of abutment loads. The total load calculated using this design methodology was about 32 tons per pile, which is higher than the 25 tons specified by the Iowa DOT for piles between 35 ft and 55 ft long.

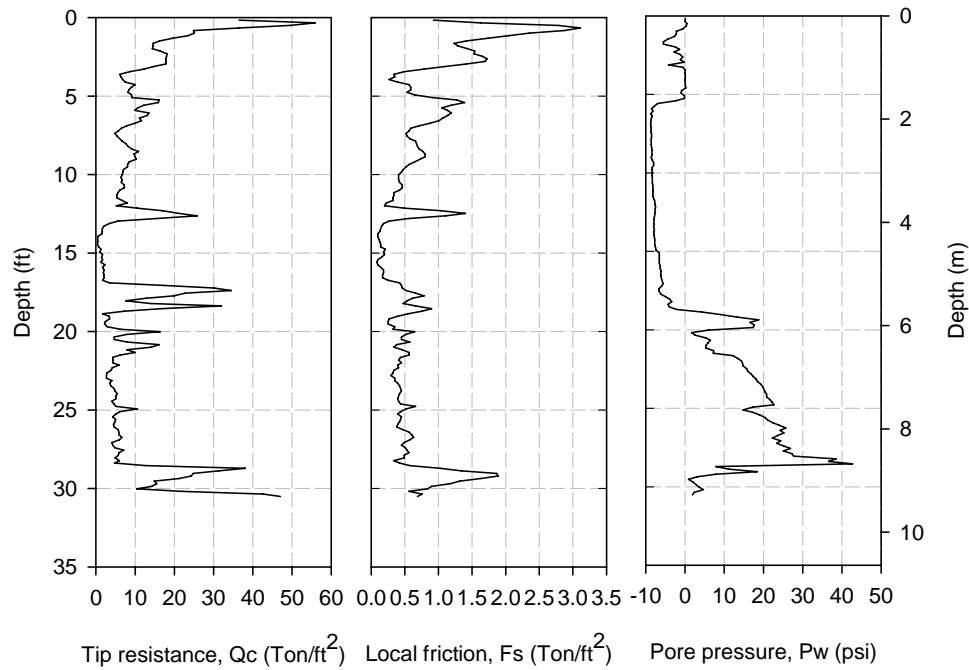


Figure 11.16. CPT carried out 100 ft north of the north abutment (Bridge No. 237380 – Mahaska County)

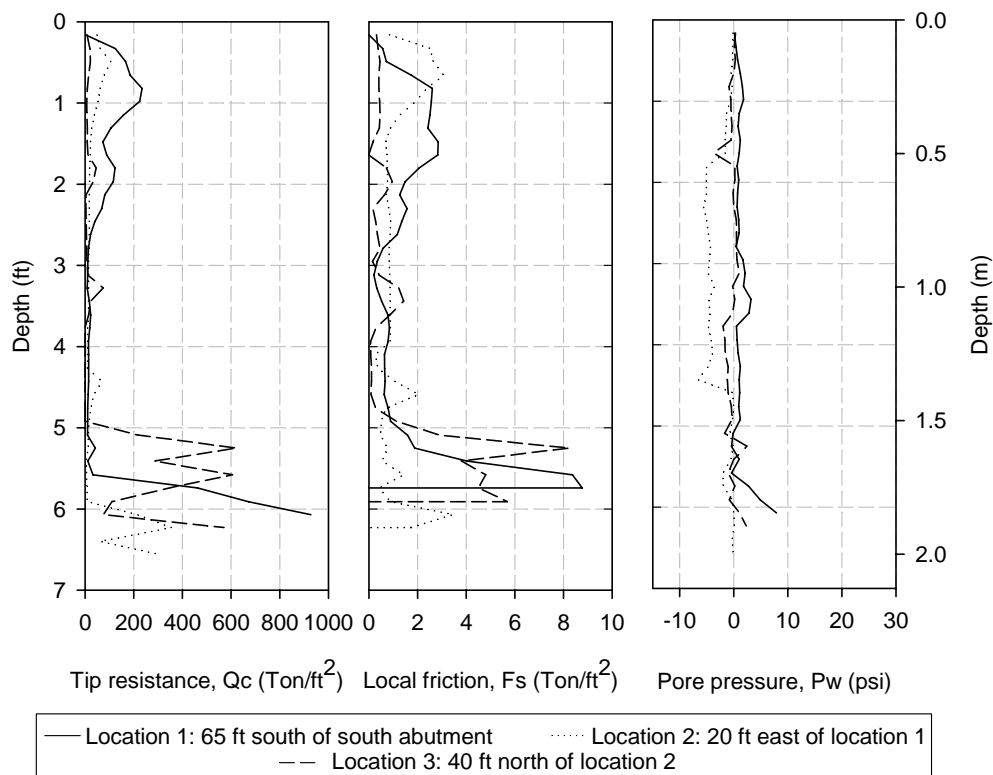


Figure 11.17. CPT carried out near the south abutment (Bridge No. 237380 – Mahaska County)

Table 11.2. Summary of pile length computations (Bridge No. 237380 – Mahaska County)

General bridge input	Superstructure system	Steel girders
	Span length (ft)	36
	Roadway width (ft)	24
	Backwall height (ft)	6.6
	Number of piles	5
	Dead load (kip)	119
	Live load (kip)	106.2
	Allowable load per pile (tons)	21
Foundation material	q_{c2} (tsf)	4.6
	q_{c1} (tsf)	6.1
	Q_p (tons)	5.12
	f_s (tsf)	0.6
	α'	0.82
	A_s (ft ²)	141.3
	Q_s (tons)	70
	Q_u (tons)	75
	F.S.	3.0
	Q_a (tons)	25 > 21 o.k.
	Assumed pile length (CPT method) (ft)	45
	Computed pile length (Klaiber et al. 2004) (ft)	50

12. BRIDGE NO. 029070 HUMBOLDT COUNTY

12.1. Bridge Description

The last bridge tested was located in Humboldt County, Iowa. The bridge is on 200th St. crossing a drainage channel (See Figure 12.1). This bridge was 33.5 ft long and 24 ft wide with a non-composite concrete deck, four steel girders, and 0° skew. Originally a simple span bridge, a center pier was added in the 1970s to prevent the bridge from being posted as a result of low rating (See Figure 12.2). The pier was installed by driving two timber piles on each side of the bridge which supported a steel girder at the mid span of the bridge (See Figure 12.3). Prior to testing and to remain consistent with testing simple span bridges, the pier was removed by cutting the supporting timber piles and removing the steel girder (See Figure 12.4 and Figure 12.5).



Figure 12.1. Bridge No. 029070 Humboldt County – Looking east (April 4 2006)



Figure 12.2. Center pier added in the 1970s (Bridge No. 029070 Humboldt County – April 4 2006)



Figure 12.3. Center pier supported by 2 timber piles on each side of the bridge (Bridge No. 029070 Humboldt County – April 4 2006)



Figure 12.4. Cutting the timber piles supporting the bridge pier (Bridge No. 029070 Humboldt County – July 10 2006)



Figure 12.5. Lowering the steel girder (Bridge No. 029070 Humboldt County – July 10 2006)

The bridge abutments were comprised of seven timber piles in front of a timber backwall, three timber piles in each wingwall, and a double c-channel cap. Tie back rods were used to connect the wingwall piles as illustrated in Figure 12.6. The diameters of the tie back rods were 0.875 inches. According to the bridge plans, the total length of the timber piles in front of the backwall was 25 ft, while the total length of the wingwall piles was 20 ft. At the east abutment, the piles were numbered 1 through 7 starting from the north edge of the bridge. Part of the previous concrete bridge abutment was still in place (See Figure 12.7). The average expose pile length and spacing at the east abutment were 4.7 ft and 3.2 ft, respectively (See Figure 12.8). Visual inspection revealed advanced section loss at pile No. 6 near the ground level. The pile diameter at the time of inspection was about 3 inches (See Figure 12.9). As shown in Figure 12.10, the overall condition of the west abutment was satisfactory. The piles were numbered 1 through 7 starting from the south edge of the bridge. The average expose pile length and spacing at the west abutment were 3.9 ft and 3.1 ft, respectively (See Figure 12.11). Using an increment borer, pile cores were obtained. The cores were used to measure the density of the piles as shown in

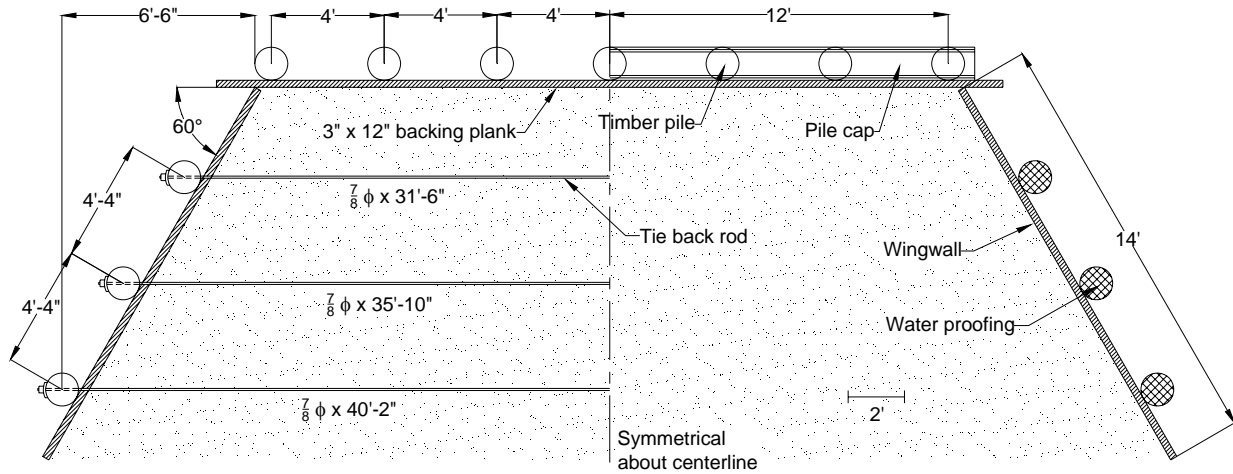


Figure 12.6. Plan view of bridge abutment (Bridge No. 029070 – Humboldt County)



Figure 12.7. East abutment (Bridge No. 029070 Humboldt County – April 4 2006)

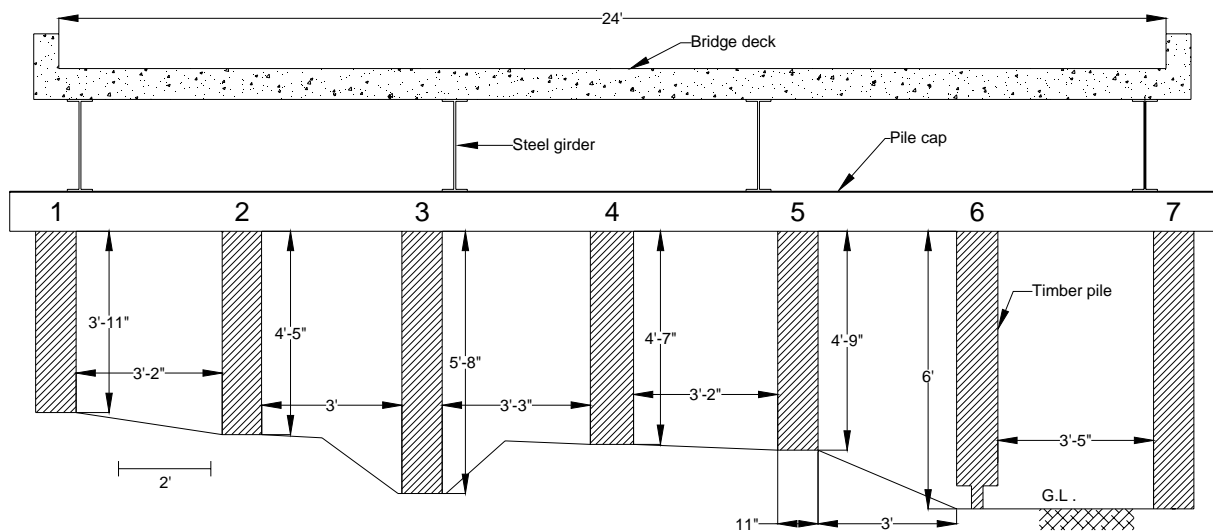


Figure 12.8. Schematic diagram of the east abutment (Bridge No. 029070 – Humboldt County)



Figure 12.9. Advanced section loss at pile No. 6 at the east abutment (Bridge No. 029070 Humboldt County – July 12 2006)



Figure 12.10. West abutment (Bridge No. 029070 Humboldt County – April 4 2006)

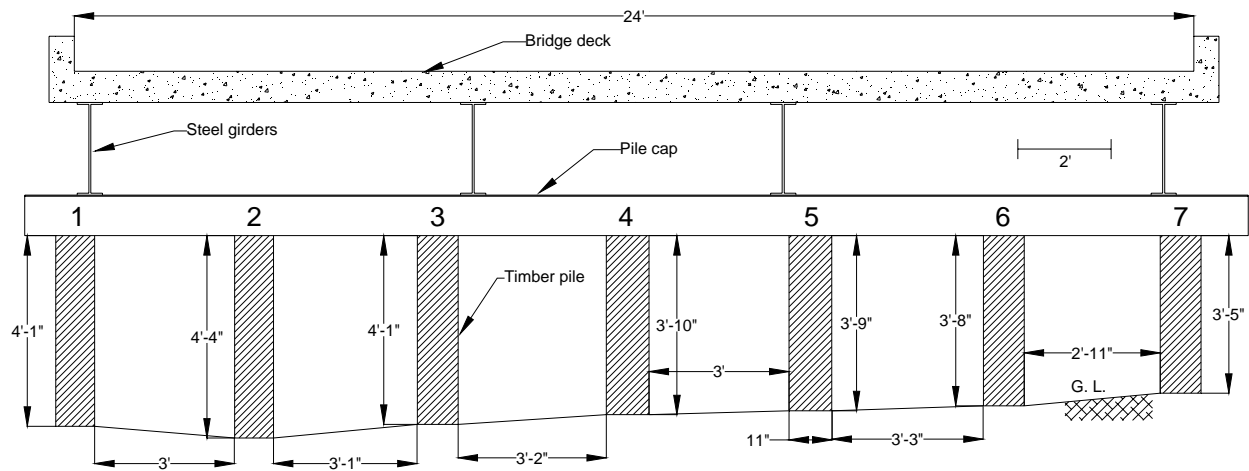


Figure 12.11. Schematic diagram of the west abutment (Bridge No. 029070 – Humboldt County)

Table 12.1. Summary of pile densities (Bridge No. 029070 – Humboldt County)

West Abutment		
Pile	Height from pile cap (in.)	Density lb/ft³
1	12	35.3
1	24	29.3
2	12	43.5
2	24	44.8
3	12	48.7
3	24	48.8
3	36	44.8
4	12	45.9
4	24	35.7
5	12	37.5
5	24	36.9
6	12	32.4
6	24	33.1
7	12	36.7
7	24	40.2
East Abutment		
1	12	36.7
1	24	41.2
2	12	38.6
2	24	40.1
2	36	37.9
3	12	43.2
3	24	42.8
3	36	49.1
4	12	38.2
4	24	44.3
4	36	37.7
5	12	41.0
5	24	44.3
5	36	42.6
6	12	52.3
6	24	46.0
7	36	38.7
7	48	46.1

Upon completion of the load testing, the bridge was removed and replaced with a new box culvert (See Figure 12.12 and Figure 12.13). The exposed portion of pile nos. 3 and 6 in the west abutment were retrieved and tested in axial compression to determine their E values. E values of pile nos. 3 and 6 at the west abutment were 2.42×10^5 psi and 3.14×10^5 psi, respectively (See Figure 12.14).



Figure 12.12. Removing the bridge super structure – looking west (Bridge No. 029070 Humboldt County – July 28 2006)



Figure 12.13. New box culvert – view looking north (Bridge No. 029070 Humboldt County – October 5 2006)

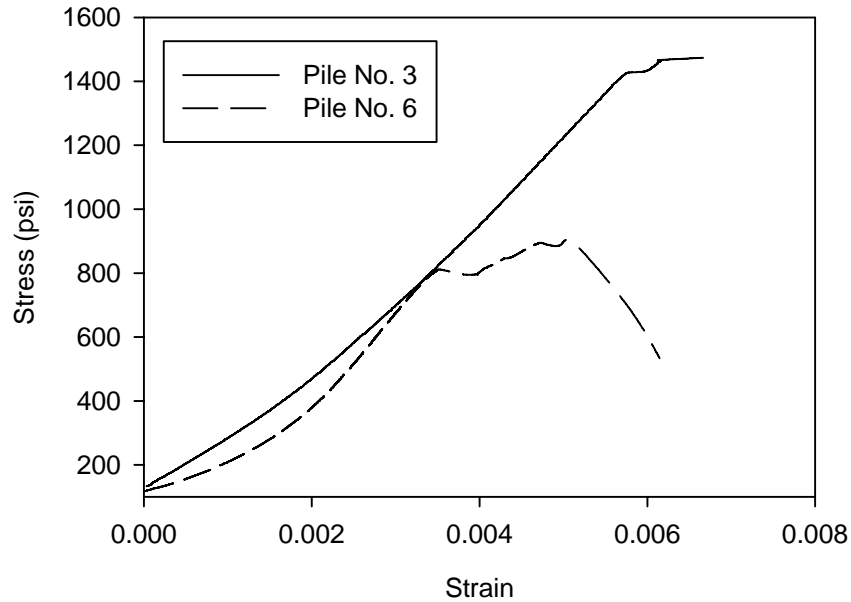


Figure 12.14. Stress-strain curves for pile Nos. 3 and 6 at the west abutment (Bridge No. 029070 – Humboldt County)

12.2. Load Test Setup and Instrumentation

The locations of axle footprints utilized to load each abutment are shown in Figure 12.15. Unlike previous bridges where three load increments were applied, at this bridge the truck was driven across the bridge and stopped at predetermined locations yielding seven loading stages. Loading stages 0 and 7 represent the beginning and end of the load test where the truck is completely off the bridge. At loading stage 6, no load is applied at the monitored abutment since the entire applied axial load is carried by the other bridge abutment.

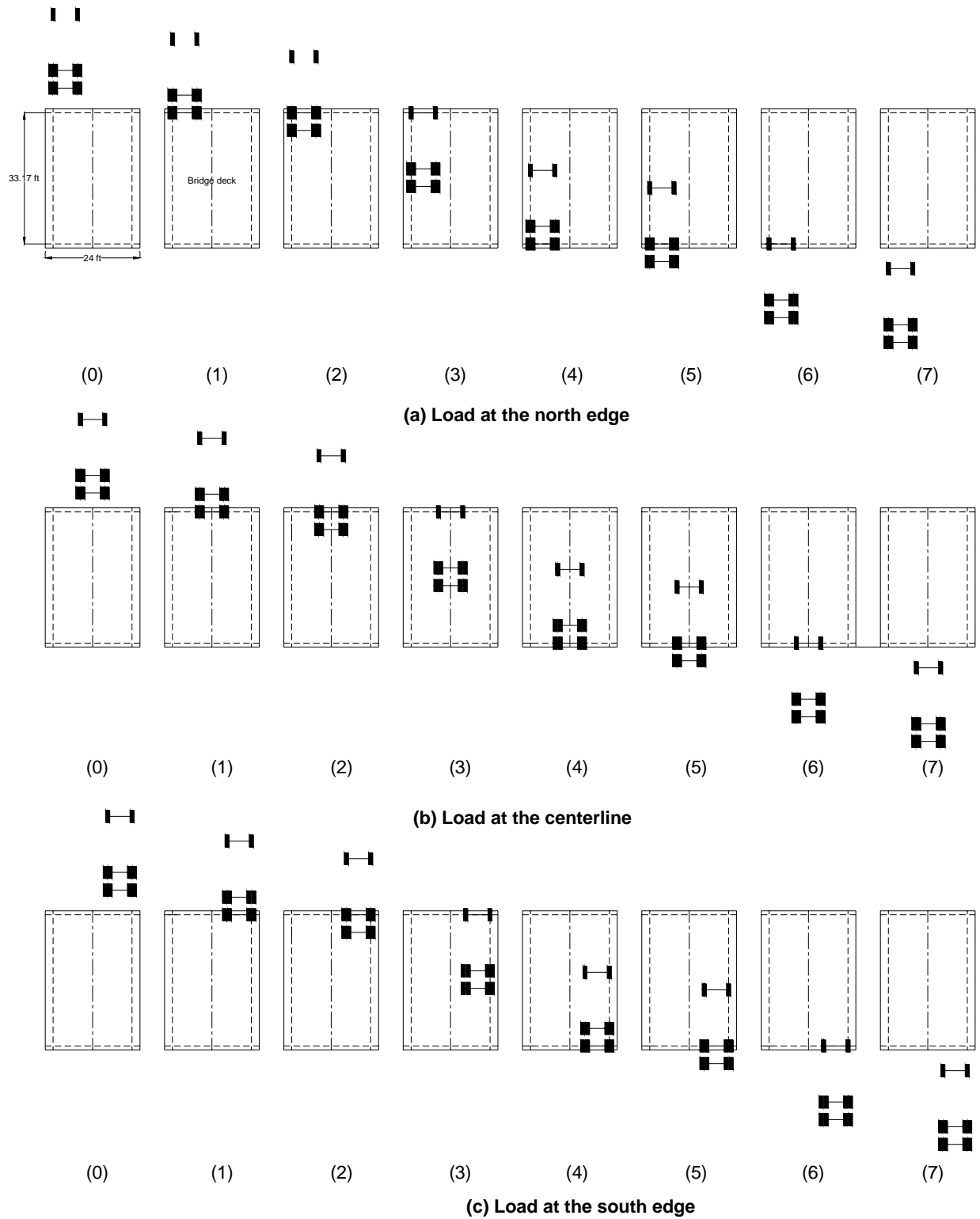


Figure 12.15. Axle footprints (Bridge No. 029070 – Humboldt County)

The exposed timber piles at the east abutment were instrumented as shown in Figure 12.16a. All piles were instrumented with three strain transducers except pile nos. 3 and 7 were instrumented with five strain transducers. Six strain transducers were placed at the backwall. All strain transducers were 24 inches long. At the west abutment, the piles were instrumented with three strain transducers each with a 24 inch gage length. Three strain transducers were attached to the backwall as shown in Figure 12.16b.

This bridge was scheduled for replacement; thus, both nondestructive and destructive load tests were carried out. The nondestructive static load test was carried out by loading the instrumented bridge abutments and recording the strain similar to previous bridges.

The destructive load test was carried out at the east abutment by consecutively removing a 16 inch section from three of the seven supporting piles to simulate pile deterioration (See Figure 12.17). Pile nos. 7, 3, and 6 were removed consecutively. After removing each pile, the bridge was load tested and strains in the intact piles were measured. The east abutment with pile nos. 3 and 7 removed is shown in Figure 12.18. To measure the load carried by the removed piles, a load cell and a mechanical jack were installed as shown in Figure 12.19. Before statically loading the abutment, the mechanical jack was used to apply load on the pile. The load was gradually increased in order to restore the dead load, which was initially carried by the pile before removing the section. This was accomplished by monitoring the pile strain before and after removing the pile section and restoring the pile strain to its initial value. Once the initial strain was restored, the load carried by the pile was recorded using a readout attached to the load cell. This procedure was carried out for pile nos. 3 and 7. The section from Pile no. 6 that was removed near the ground level was not restored (See Figure 12.20).

To determine the feasibility of repairing localized deteriorated sections in timber piles, pile no. 7 was repaired using a splicing technique in which the percent restoration of pile capacity was measured. A new timber section was spliced and placed instead of the removed section as shown in Figure 12.21. The existing and new pile sections were connected by installing two metal screws at an angle as demonstrated in Figure 12.22. Once repaired, the bridge was load tested and the percentage of the restored capacity was evaluated.

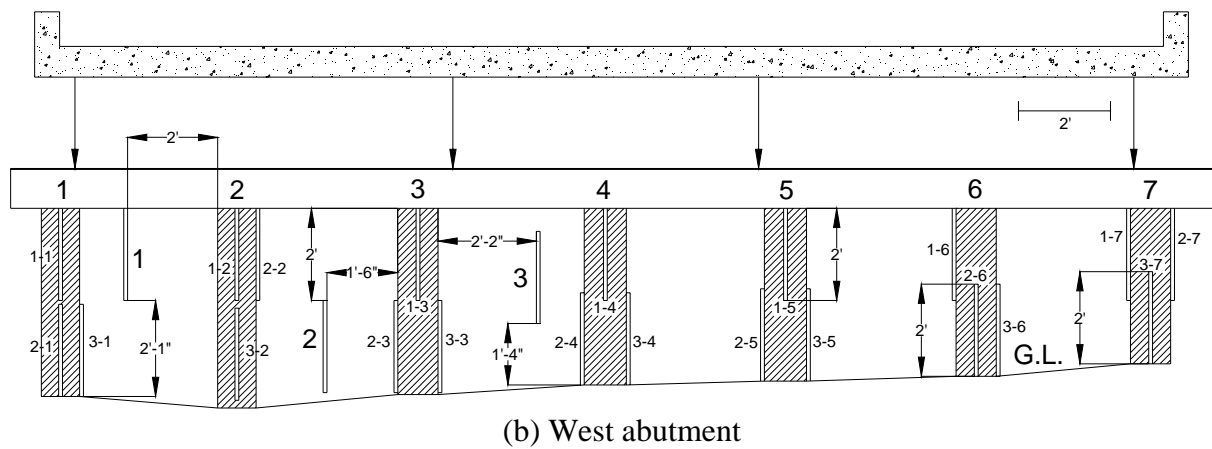
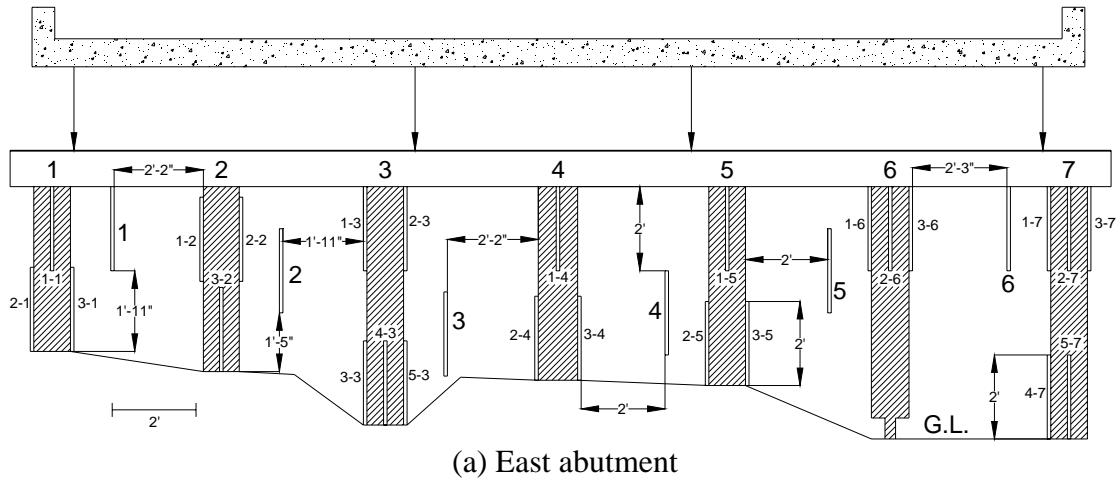


Figure 12.16. Strain transducers attached to the exposed timber piles (Bridge No. 029070 – Humboldt County)



Figure 12.17. Destructive static load test (Bridge No. 029070 Humboldt County – July 12 2006)

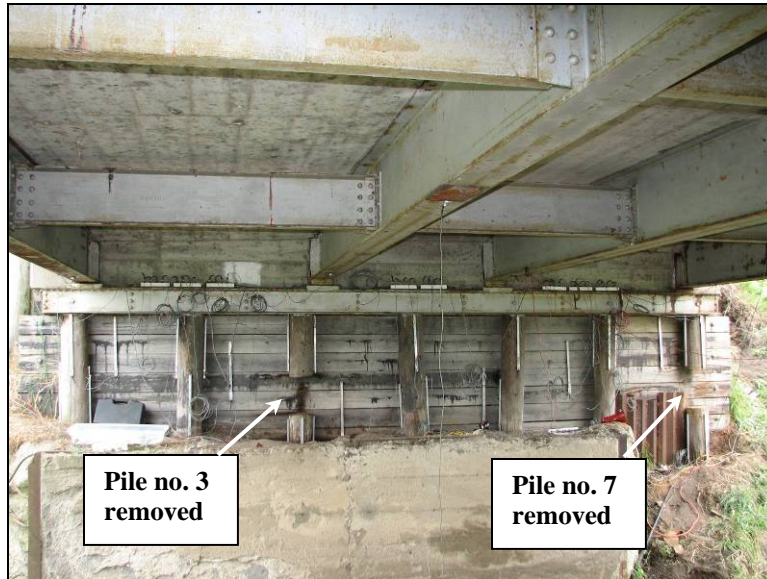


Figure 12.18. Pile nos. 3 and 7 removed at the east abutment (Bridge No. 029070 Humboldt County – July 12 2006)

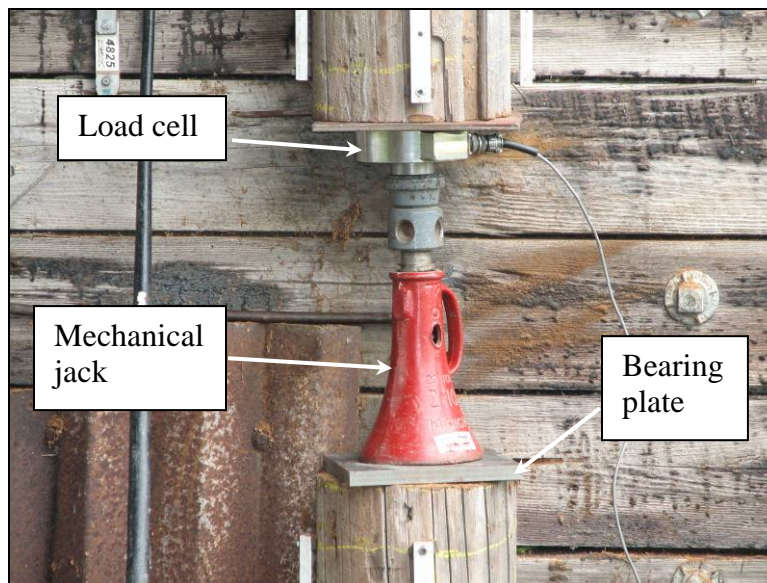


Figure 12.19. Mechanical jack and load cell used to restore and record the load carried by pile no. 7 (Bridge No. 029070 Humboldt County – July 12 2006)



Figure 12.20. A section of Pile no. 6 removed near the ground level (Bridge No. 029070 Humboldt County – July 12 2006)



Figure 12.21. Installing a new timber section to repair pile no. 7 (Bridge No. 029070 Humboldt County – July 12 2006)



Figure 12.22. Metal screws used to connect the new section to the existing timber pile (Bridge No. 029070 Humboldt County – July 12 2006)

12.3. Nondestructive Test Results

12.3.1. West Abutment – North Edge

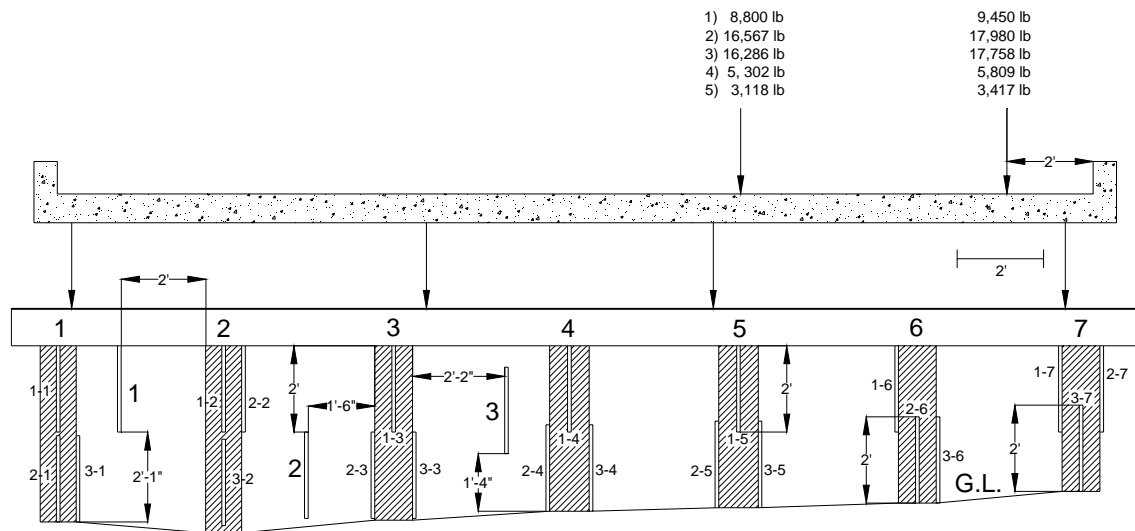
The west abutment was initially loaded at the west edge (see Figure 12.15 and Figure 12.23). The axial loads were offset 2 ft from the curb. The location of the axial loads, pile strain measurements and backwall strains are shown in Figure 12.23. Strain was highest directly under the applied load and decreased with distance from the location of the load. The highest strain measured, which was about -37 microstrains, was in pile no. 6 in load configuration 2. The results demonstrate the flexibility of the pile cap since the pile strains were not equal. Positive strains were observed in pile no. 1 and in the backwall between pile nos. 1 and 2.

12.3.2. West Abutment – Centerline

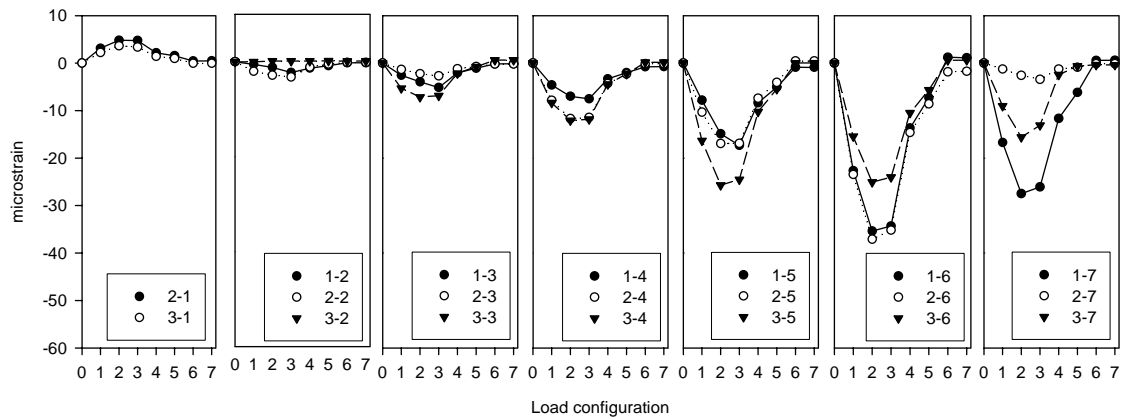
Loading the west abutment at the centerline of the bridge resulted in high strain values in pile nos. 2, 3, 5, and 6. It appears that the load was more uniformly distributed while loading along the centerline of the bridge deck. The highest strain noted, which was about -29 microstrains, was in pile no. 2 in load configuration 3 (see Figure 12.24). The backwall strains changed from negative to positive with increasing load configuration.

12.3.3. West Abutment – South Edge

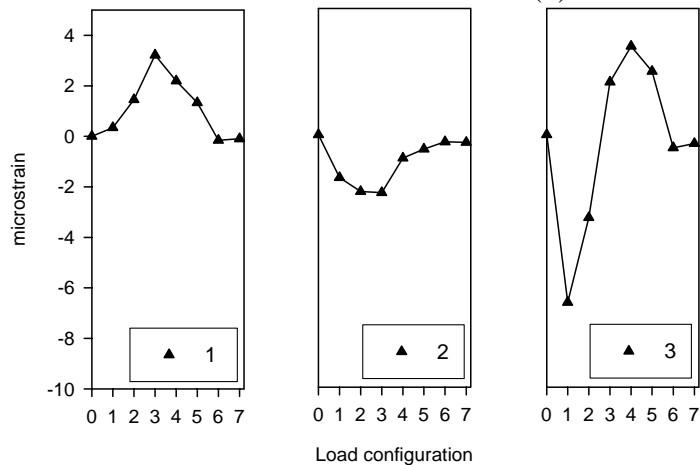
The last load test under taken at the west abutment was completed with the loading at the south edge of the bridge. The location of the axial loads, which were offset 2 ft from the curb, the pile strain measurements, and the backwall strain are shown in Figure 12.25. Similar to the north edge test, the strain was highest directly under the axial load (pile nos. 1, 2, and 3) and decreased with increasing distance from the location of the load. The highest strain measured, which was about -38 microstrains, was in pile No. 3 in load configuration 3. The backwall strains continued to change from negative to positive as shown in Figure 12.25c.



(a) Location of strain transducers and axle loads

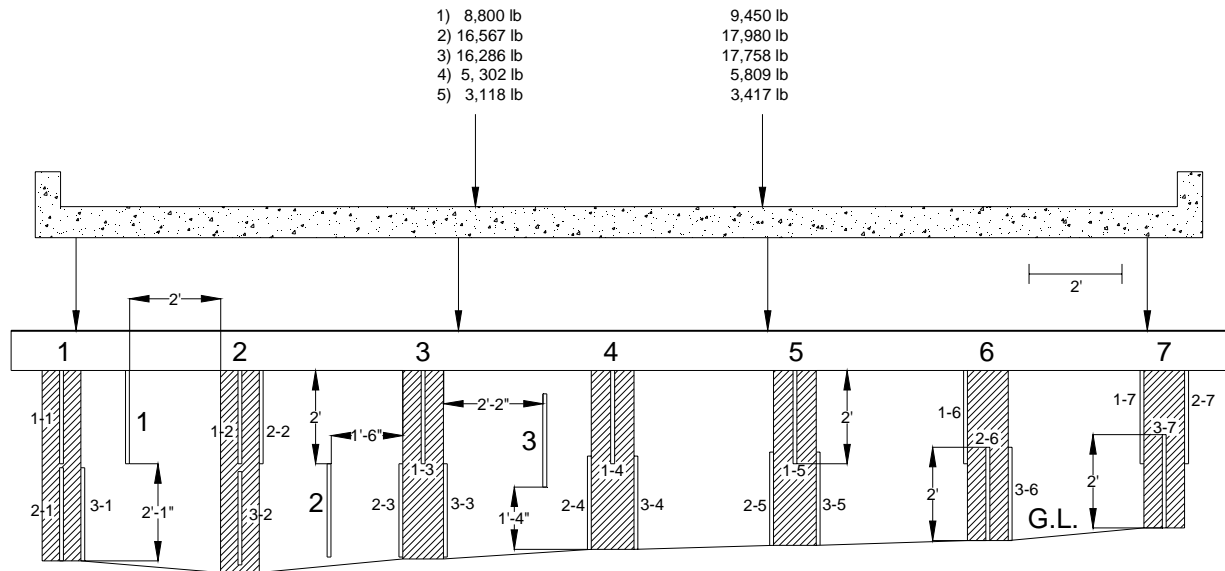


(b) Pile strains

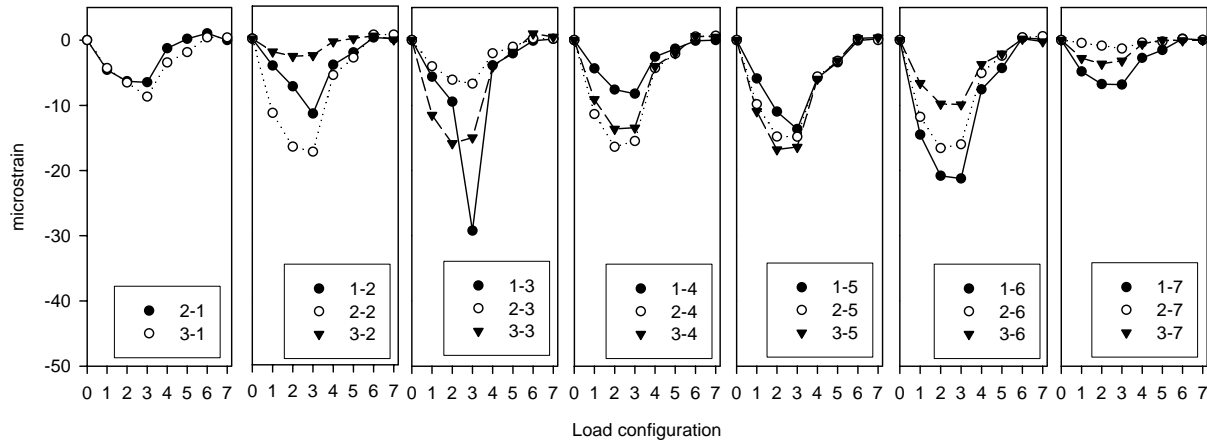


(c) Backwall strains

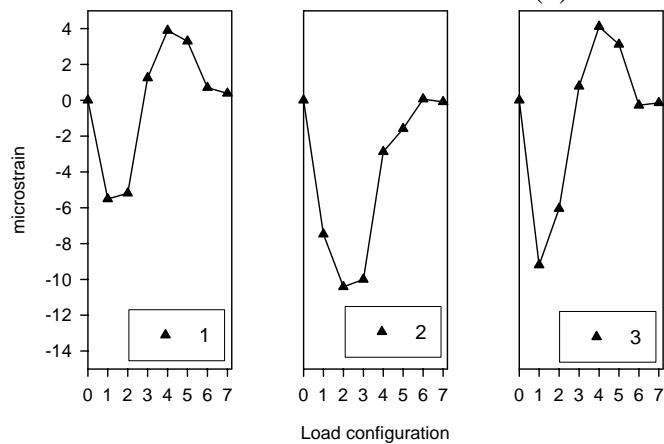
Figure 12.23. Static load test at the north edge of the west abutment (Bridge No. 029070 – Humboldt County)



(a) Location of strain transducers and axle loads

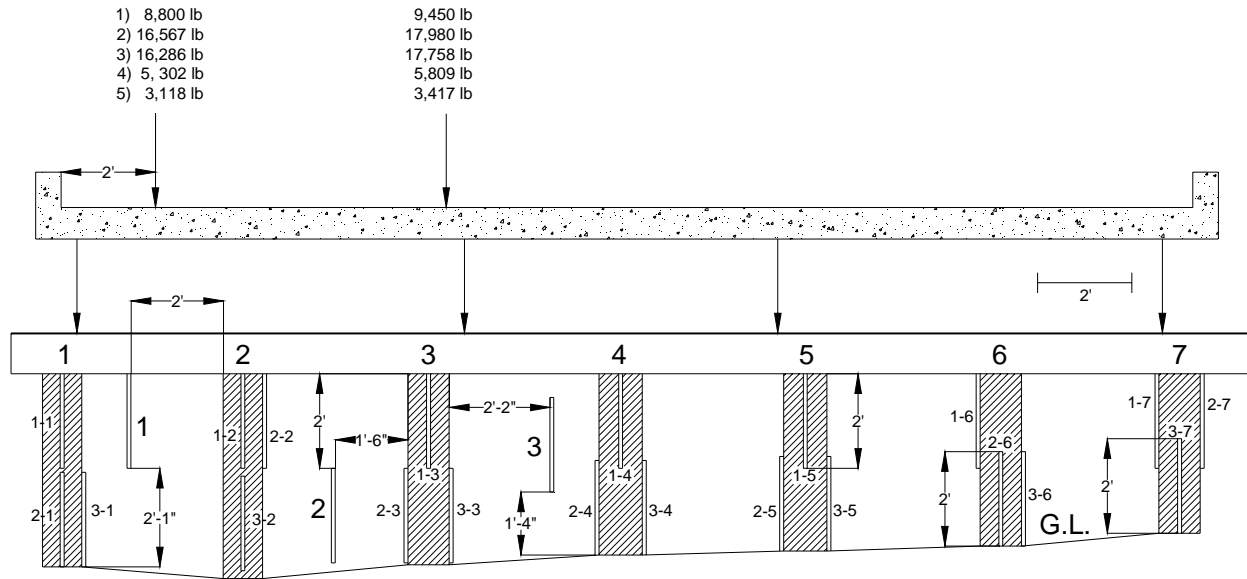


(b) Pile strains

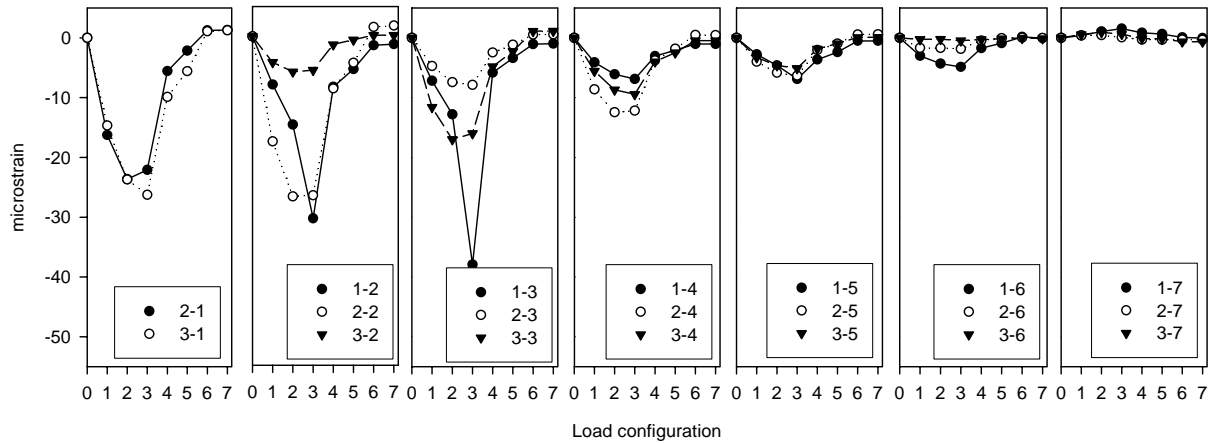


(c) Backwall strains

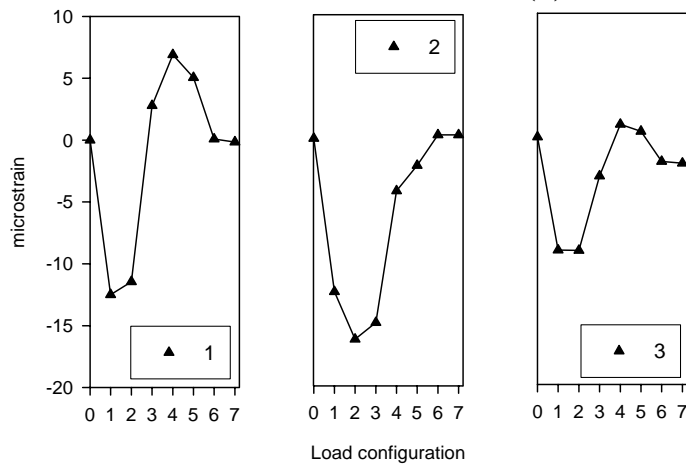
Figure 12.24. Static load test at the centerline of the west abutment (Bridge No. 029070 – Humboldt County)



(a) Location of strain transducers and axle loads



(b) Pile strains



(c) Backwall strains

Figure 12.25. Static load test at the south edge of the west abutment (Bridge No. 029070 – Humboldt County)

12.3.4. East Abutment – North Edge

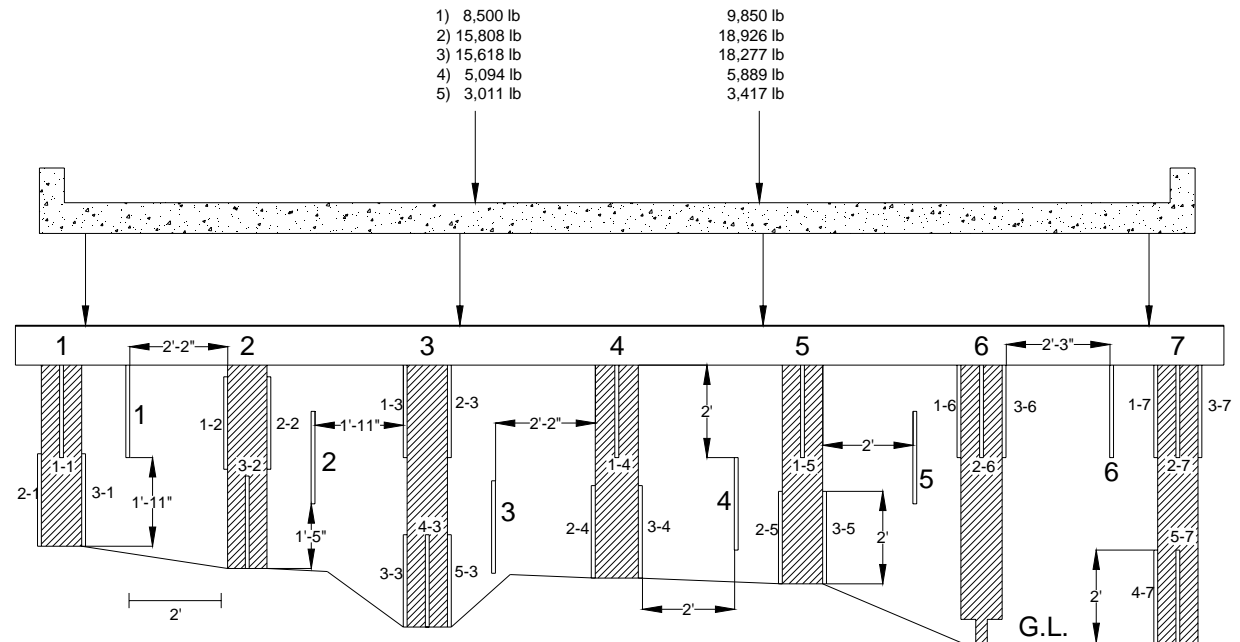
The east abutment was first loaded at the north edge (See Figure 12.26a). Pile nos. 1, 2, and 3, which were directly under the axial loads, experienced the highest strains (See Figure 12.26b). The highest strain, which was about -39 microstrains in pile no. 1, was in load configuration 3. At higher load configurations, the pile strains were reduced because some of the loads were being transferred to the west abutment. The strains also decreased in piles away from the location of the applied loads. The backwall was in compression in load configurations 1 through 4. The backwall strains at higher load configurations were either zero or positive (See Figure 12.26c).

12.3.5. East Abutment – Centerline

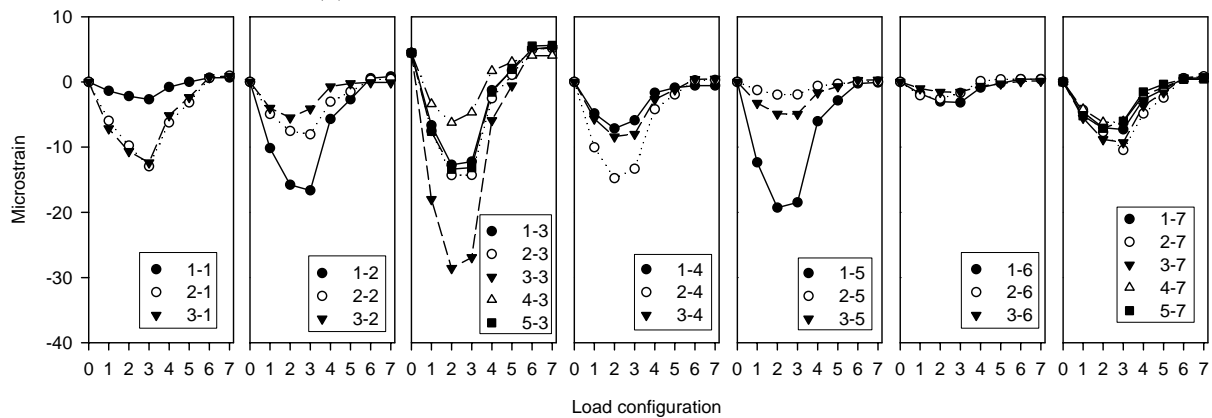
The location of the applied loads at the centerline of the east abutment, pile strain measurements, and backwall strains are shown in Figure 12.27. The results demonstrate that the load was mainly transferred to pile nos. 3 and 5, which were directly under the axial loads. The highest strain measured was in pile no. 3 and was about -30 microstrains. Moving the load to the centerline of the bridge deck resulted in about 30% reduction in the backwall strains between pile nos. 1 and 2, 2 and 3, and 3 and 4. At the south edge of the bridge (between pile nos. 4 and 7) the backwall strains increased by approximately a factor of 4.

12.3.6. East Abutment – South Edge

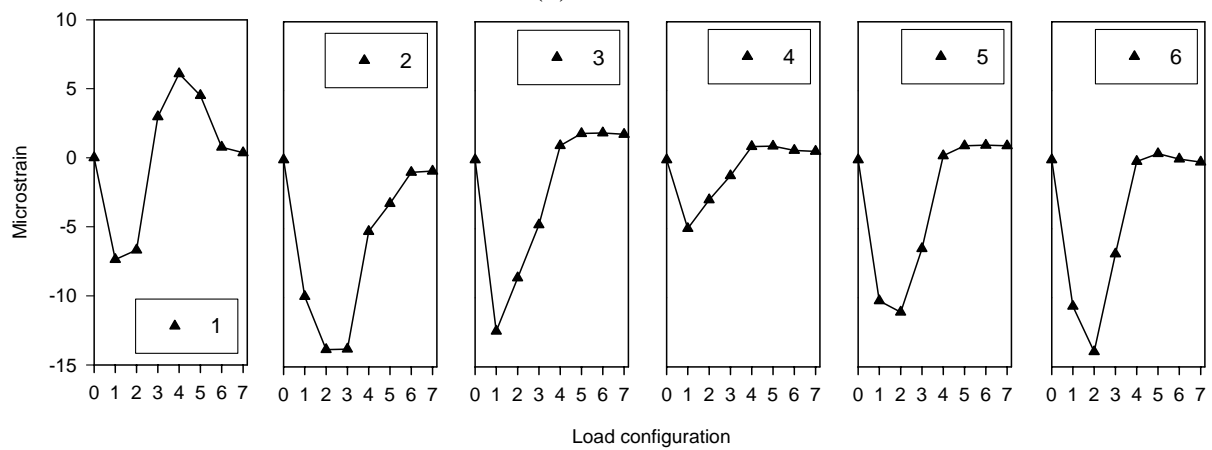
The third test was completed with the applied load at the south edge. The location of the applied loads, pile strain measurements, and backwall strains are presented in Figure 12.28. Similar to previous tests, the load was concentrated under the location of the applied loads. Pile no. 7 experienced the highest strain, which was about -34 microstrains in load configuration 2. The load decreased with increasing distance from the location of axial loads. Pile no. 6, which had a diameter of about 3 inches near the ground level, experienced small strains. Strains measured in pile no. 1 were positive, which may be due to pile bending caused by loading the bridge at the north edge.



(a) Location of strain transducers and axial loads

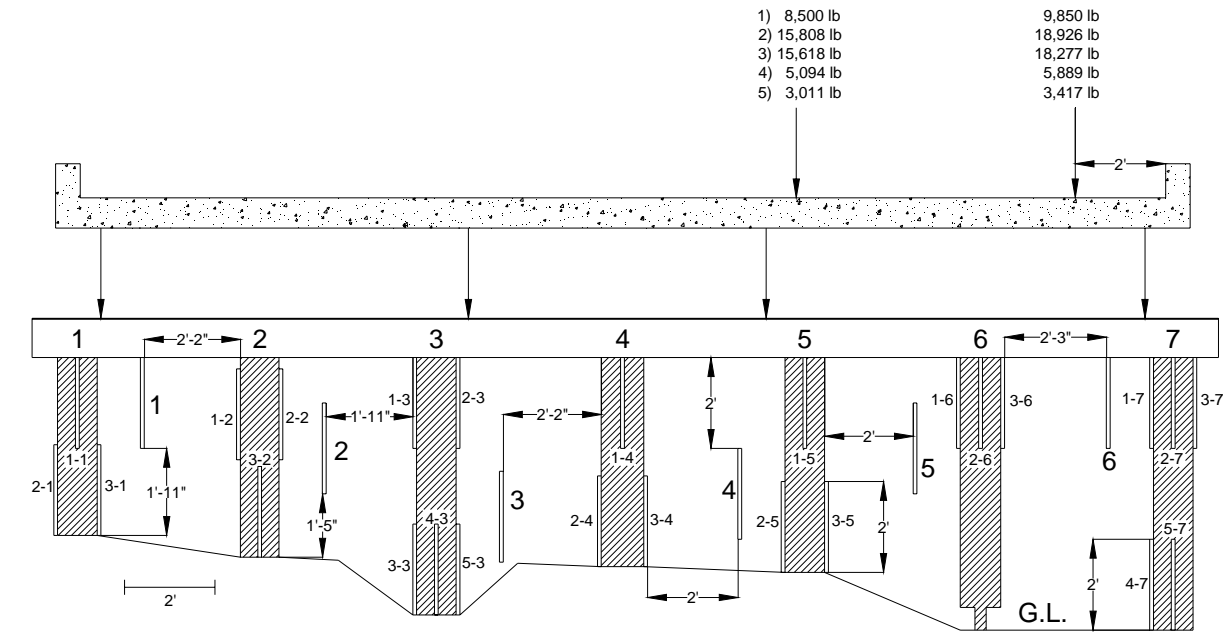


(b) Pile strains

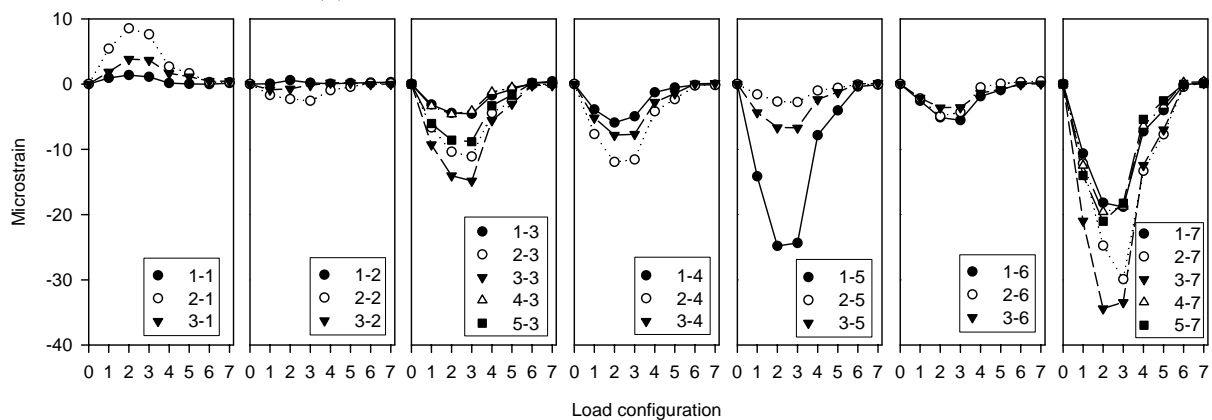


(c) Backwall strains

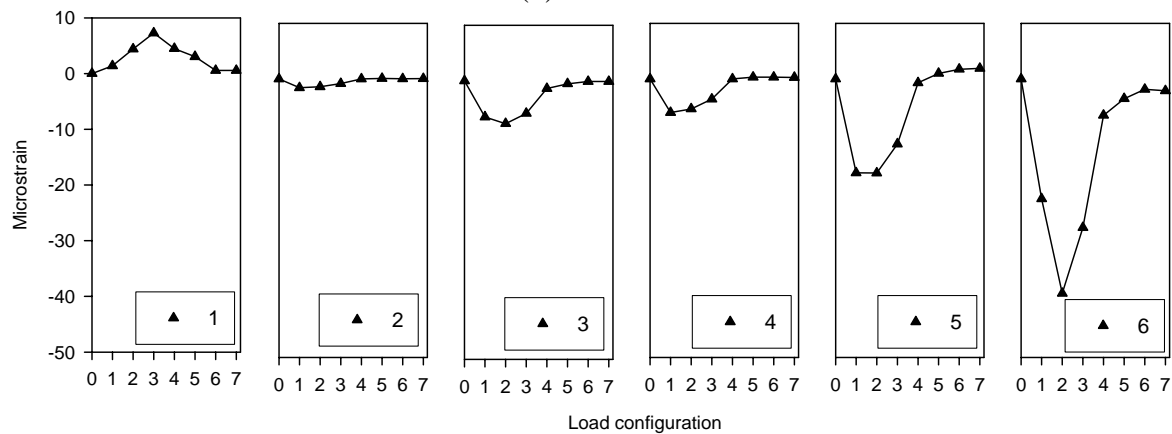
Figure 12.27. Static load test at the centerline of the east abutment (Bridge No. 029070 – Humboldt County)



(a) Location of strain transducers and axial loads



(b) Pile strains



(c) Backwall strains

Figure 12.28. Static load test at the south edge of the east abutment (Bridge No. 029070 – Humboldt County)

12.4. Destructive Test Results

12.4.1. Test No. 1 – Pile No. 7 Jacked

The first destructive test at the east abutment was carried out by removing a section out of pile No. 7 and replacing it with a mechanical jack and load cell as shown in Figure 12.29a. Load was applied through the mechanical jack to restore the pile initial strain measurement. Two tests were conducted: one with the loading at the centerline and one with the loading at the south edge of the bridge deck.

12.4.1.1. East Abutment – Centerline

The results of loading the east abutment along the centerline of the bridge deck are shown in Figure 12.29. The strain data were essentially the same strain data obtained in the nondestructive load test at the centerline that was previously conducted (Refer to Figure 12.27). This indicates that the procedure of jacking pile no. 7 was successful in restoring the abutment initial loading condition. Using the load cell, the load carried by pile no. 7 (minus the dead load) was recorded and the stresses in the pile were determined. The stresses varied laterally and longitudinally through the pile section illustrating the non-homogeneity of wood. The results also demonstrate that the load carried by pile no. 7 was about 8% of the total applied axial load.

12.4.1.2. East Abutment – South Edge

The abutment was next loaded at the south edge (See Figure 12.30). Compared to the nondestructive load test conducted at the south end, the strains in pile no. 7 decreased by about 45%, whereas the strains in pile no. 5 increased by approximately 30%. It is possible that jacking pile no. 7 resulted in a relatively weaker pile compared to its initial condition, and as a result, the load was transferred to the adjacent pile no. 5. No load was transferred to pile no. 6 since the pile was deteriorated. There were no significant changes in strains measured at other piles. The backwall strains at the south edge of the abutment (pile nos. 4 through 7) increased by about 40%. Loading the abutment at the south edge resulted in an increase of the percent load carried by pile no. 7 to about 35% of the total applied axial load.

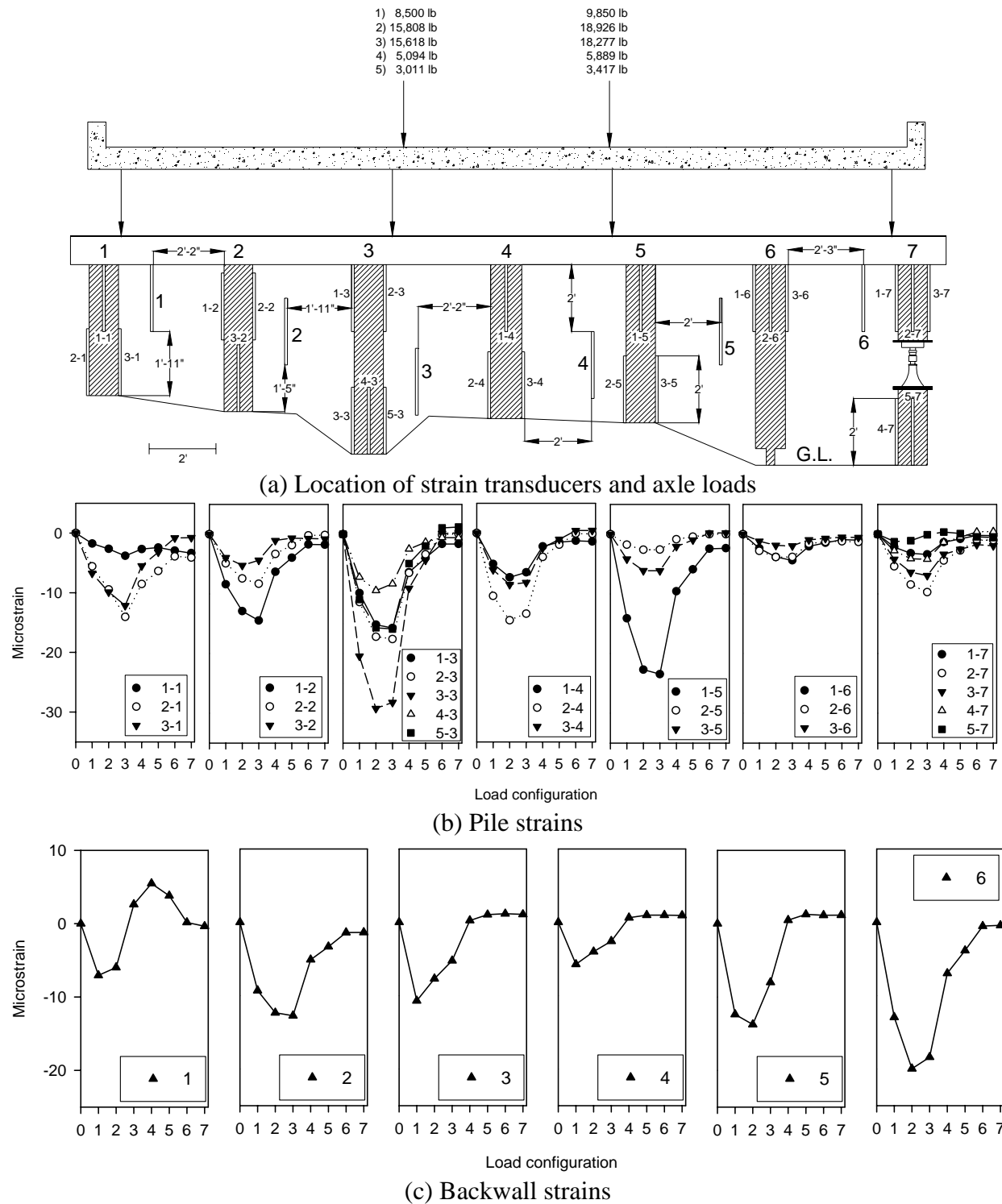


Figure 12.29. Static load test at the centerline with pile No. 7 jacked (Bridge No. 029070 – Humboldt County)

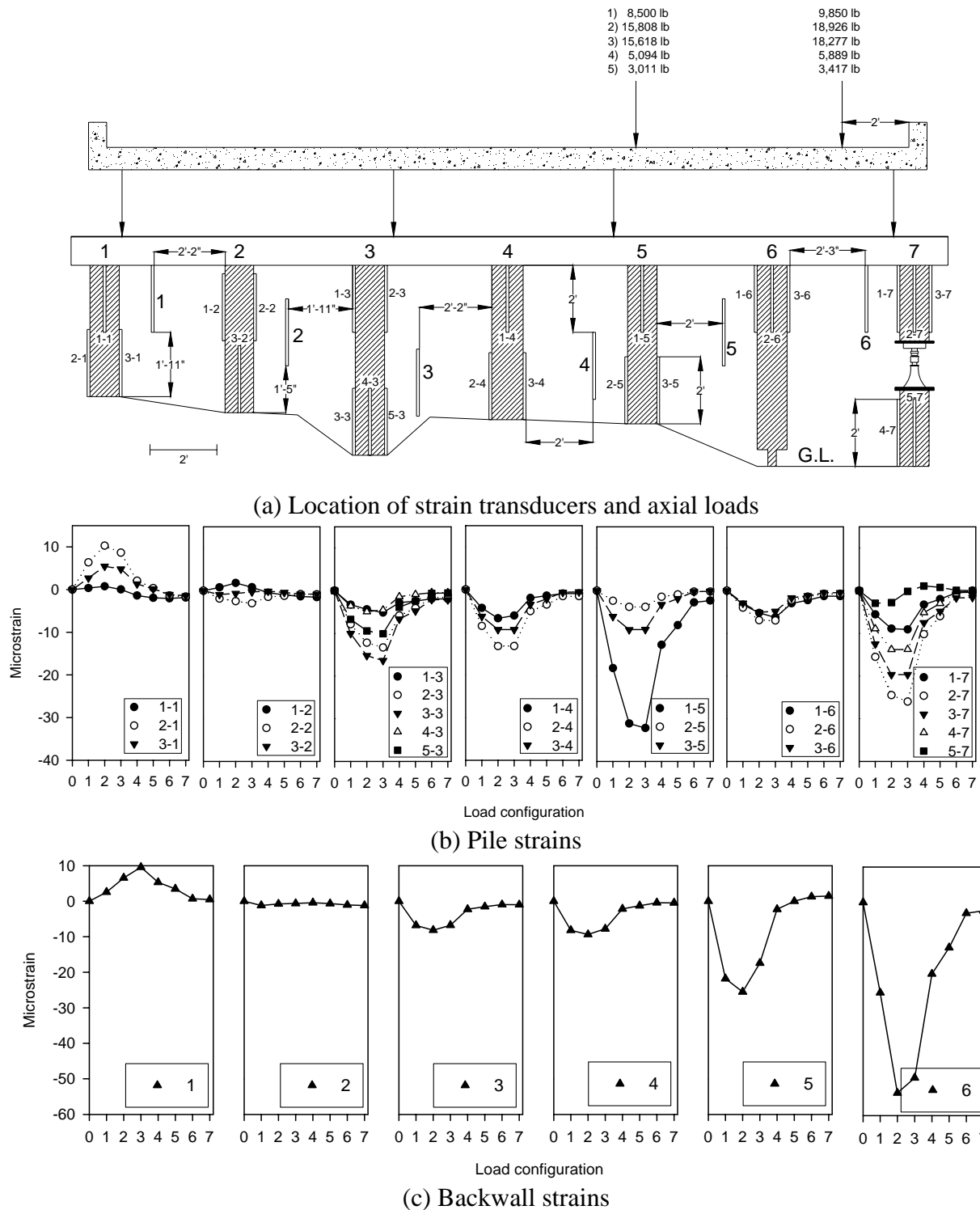


Figure 12.30. Static load test at the south edge with pile No. 7 jacked (Bridge No. 029070 – Humboldt County)

12.4.2. Test No. 2 – Pile No. 7 Removed

This destructive test was carried out to simulate complete deterioration of an exterior pile. This was achieved by removing the mechanical jack and load cell.

12.4.2.1. East Abutment – North Edge

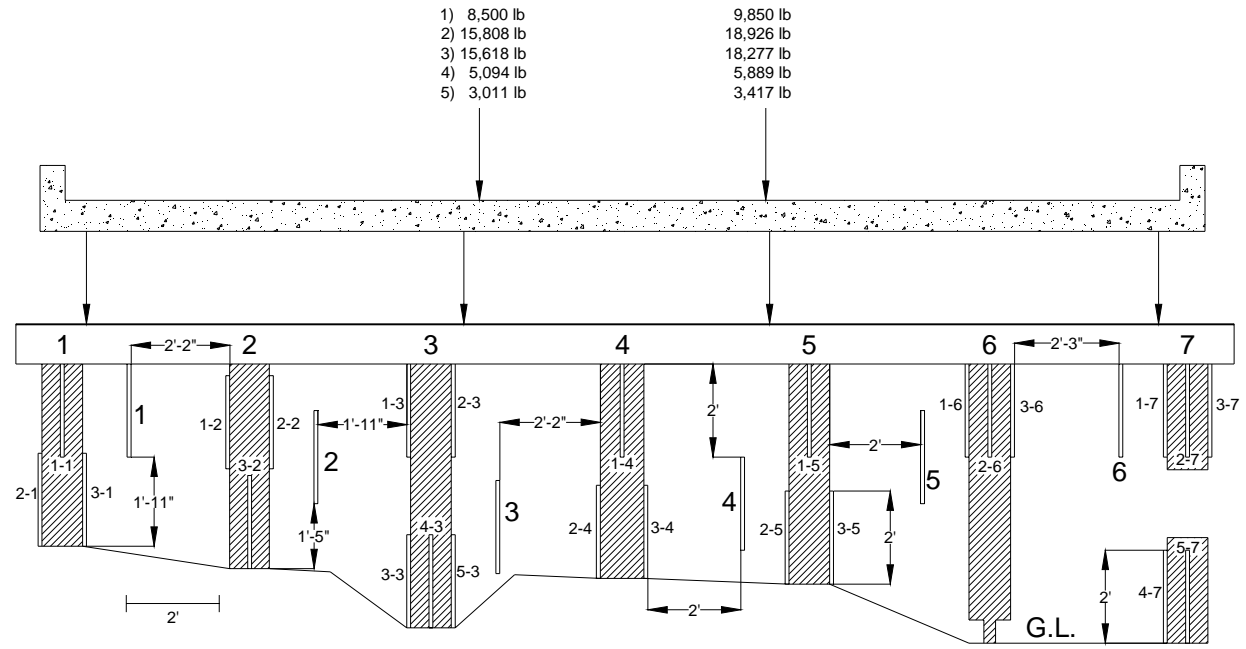
The first load test was completed with the loading at the north edge of the bridge. The location of loads, pile strain measurements, and backwall strains are shown in Figure 12.31. The pile strains were approximately equal to those measured during the nondestructive load test, which was carried out at the north edge of the east abutment (Refer to Figure 12.26). This is because pile no. 7 did not endure any load when the abutment was loaded at the opposite edge. The backwall strains were also similar to the nondestructive test except those measured between pile nos. 6 and 7, which increased by about 60%. It can therefore be concluded that an exterior pile will not have a significant influence if the live load is concentrated on the edge opposite to the location of the deteriorated pile in the bridge.

12.4.2.2. East Abutment – Centerline

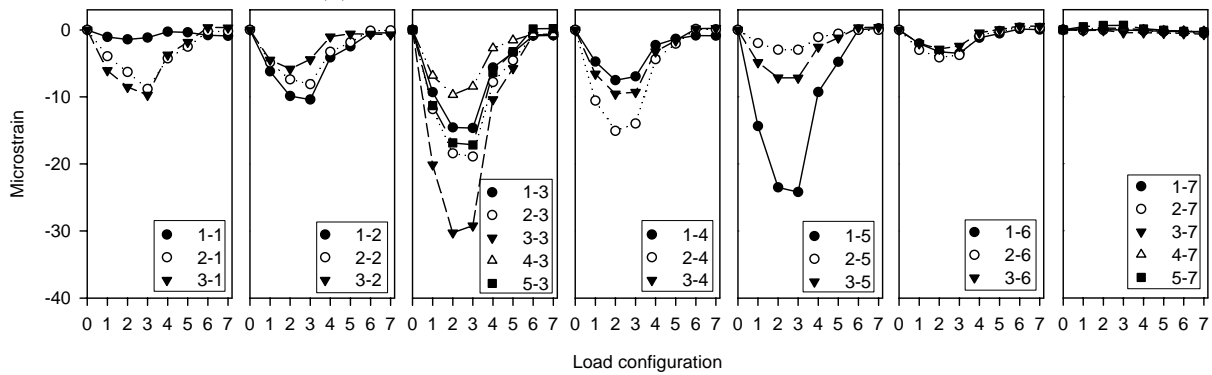
The east abutment was then loaded at the centerline of the bridge deck. The location of loads, pile strain measurements, and backwall strains are presented in Figure 12.32. The results reveal a 25% increase in strain in pile no. 5 and about a 3% increase in the measured strains in pile nos. 3 and 4 compared to the nondestructive test at the same location. Most of the load carried by pile no. 7 was transferred to the next adjacent sound pile. The backwall strains also increased in the areas between pile Nos. 4 and 5, 5 and 6, and 6 and 7. About 63% strain was measured between pile nos. 6 and 7. Due to the partial bearing of the pile cap on the backwall, and due to the removal of pile no. 7, the backwall resisted a higher load as evidenced by the increase in negative strain at this location.

12.4.2.3. East Abutment – South Edge

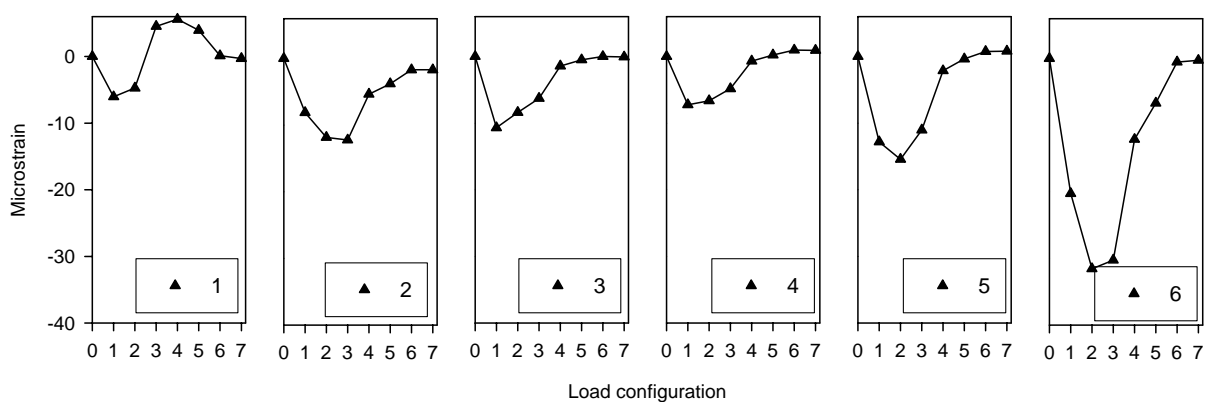
The third test was conducted with the load applied at the south abutment directly above the removed pile. The location of loads, pile strain measurements, and backwall strains are shown in Figure 12.33. The strains measured in pile no. 5 increased by approximately 60%. Strains measured in pile nos. 3 and 4 increased by 20 and 45%, respectively. The results demonstrate that most of the load carried by pile no. 7 was being resisted by pile No. 5. The results also show that pile bending at the north edge increased. This was evidenced by the increase in positive strains in pile nos. 1 and 2. In pile no. 1, the strain increased from +9 microstrains, measured during the nondestructive test in this location, to +20 microstrains in load configuration 3, whereas in pile no. 2, the strain increased from 0 microstrains to +9 microstrains. This was also observed in the backwall strains between pile No. 1 and 2, which increased from +7 microstrains to +21 microstrains. The backwall strains under the applied load (i.e. between pile nos. 6 and 7) increased from -38 microstrains, which was measured during the nondestructive test, to -80 microstrains since more load was being transferred and resisted by the south edge of the backwall. The strains measured between pile nos. 4 and 5, and 5 and 6 also increased by almost 100%.



(a) Location of strain transducers and axle loads



(b) Pile strains



(c) Backwall strains

Figure 12.32. Static load test at the centerline with pile No. 7 removed (Bridge No. 029070 – Humboldt County)

12.4.3. Test No. 3 – Pile Nos. 3 and 7 Jacked

In this destructive test, a section was removed from pile no. 3 after which both pile nos. 3 and 7 were jacked to their initial measured strain values (See Figure 12.34). A load cell was placed above each mechanical jack to measure the load carried by each pile due to live load. Three load tests were conducted with the load being applied at the north, centerline, and south edges.

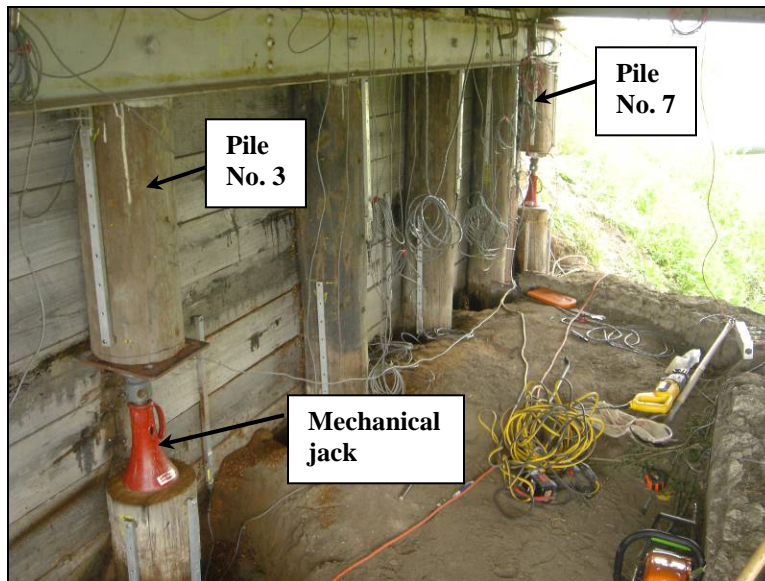


Figure 12.34. Pile Nos. 3 and 7 jacked (Bridge No. 029070 Humboldt County – July 12 2006)

12.4.3.1. East Abutment – North Edge

The east abutment was first loaded at the north edge of the bridge. The location of the loads, which were offset 2 ft from the curb, the pile strain measurements, and the backwall strains are presented in Figure 12.35. The results illustrate that the strains in pile no. 3 decreased by about 45% compared to those measured during the nondestructive test at this location. As a result, the strains in the adjacent pile nos. 2 and 4 increased by about 39 and 6%, respectively. The results show that the load carried by pile no. 3 was about 10% of the total load when the abutment was loaded at the north edge.

No significant change was observed in the backwall strains compared to the strains that occurred in the nondestructive test except in the strain between pile nos. 3 and 4. The strains measured in this location increased by approximately 60%. A possible explanation for this increase is that the mechanical jack did not fully restore the timber pile to its initial condition as evidenced by the strain reduction in the pile compared to the nondestructive test strains; therefore, the backwall at this location was resisting more axial load due to the partial bearing of the pile cap on the backwall resulting in higher deflections.

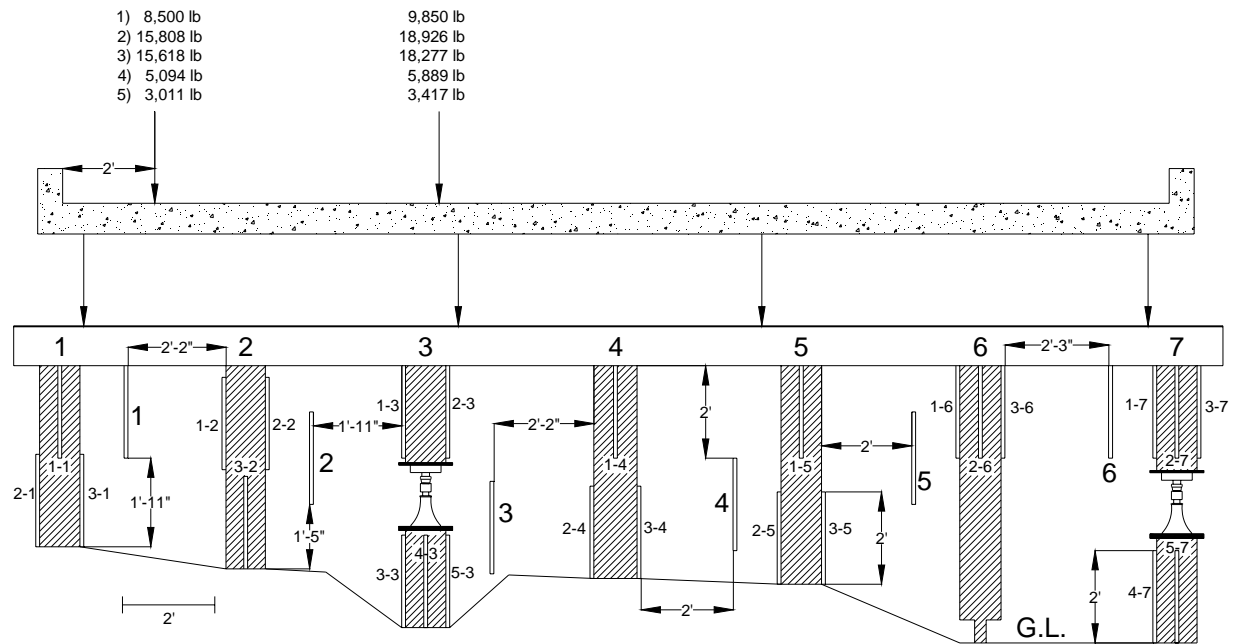
12.4.3.2. East Abutment – Centerline

The abutment was then loaded at the centerline of the bridge deck. The location of the loads, the pile strain measurements, and the backwall strains are shown in Figure 12.36. Similar to previous load tests conducted at this location, the load was primarily transferred to pile nos. 3 and 5 (See Figure 12.36a). The highest strain, which was about -23 microstrains, was in pile no. 5 in load configuration 3. When compared to the nondestructive test and destructive test nos. 1 and 2, the strain at pile no. 3 was reduced by approximately 40%. As a result, the backwall strain between pile nos. 3 and 4 increased by 60%. Similarly, the strain measured in pile no. 7 was reduced by approximately 35% compared to the nondestructive test at this location, whereas the backwall strain between pile nos. 6 and 7 increased by 45% increase. The same percent increase in backwall strain was recorded in destructive test no. 1. As mentioned earlier, removing a timber section and replacing it with the mechanical jack reduced the load carrying capacity of the piles, which transferred more axial load to the backwall. The percent load resisted by pile nos. 3 and 7 relative to the total load was 13 and 9%, respectively.

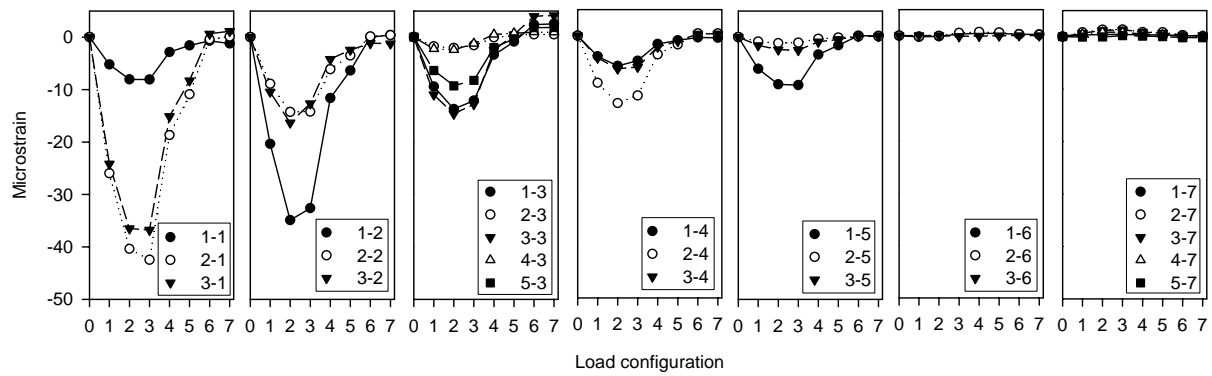
12.4.3.3. East Abutment – South Edge

The east abutment was finally loaded at the south edge of the bridge. The location of the axial loads, which were offset 2 ft from the curb, pile strain measurements, and backwall strains are shown in Figure 12.37. The results show a decrease in strain in pile nos. 3 and 7 compared to the nondestructive test and test no. 1 where pile no. 7 was jacked. The strain measurement of pile no. 3 decreased by about 25, 34, and 36% in load configuration 3 compared to the nondestructive test, test no. 1, and test no. 2, respectively. The decrease in pile no. 3 strain was coupled with an increase in backwall strain between pile nos. 3 and 4. The backwall strain at this location increased by 33 and 28% compared to the nondestructive test and test no. 1, respectively. The results also show that the strain in the adjacent pile no. 4 increased by 27 and 6% compared to the nondestructive test and destructive test no. 1, respectively. This indicated that part of the load that was resisted by pile no. 3 was transferred to the adjacent pile no. 4. However, no significant increase in the strains in pile no. 2 was observed. In the north edge test, most of the strain increase was noted in pile no. 2, whereas at the south edge, most of the strain increase occurred in pile no. 4. It can therefore be concluded that when an interior pile is partially deteriorated, the load may not be distributed equally among adjacent piles, and the live load location should be taken into consideration.

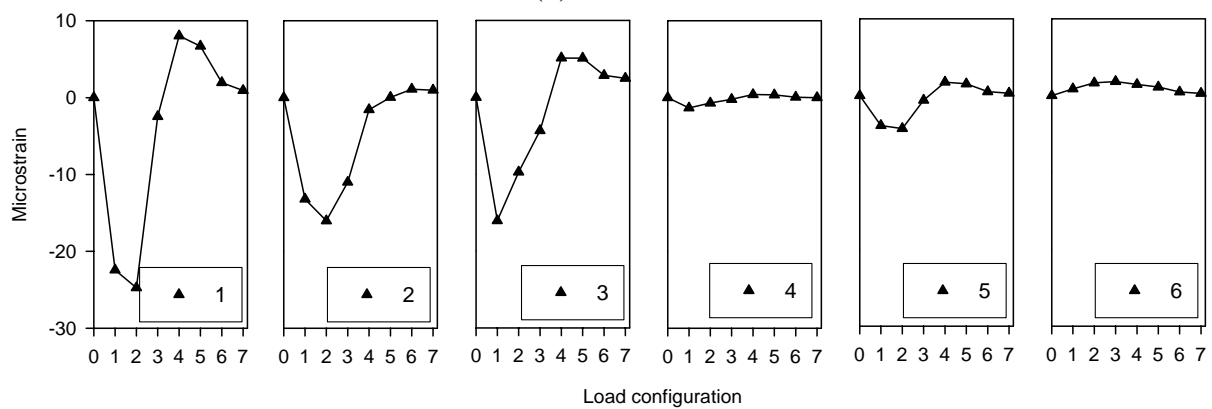
Similar to pile no. 3, the strain measured in pile no. 7 decreased by approximately 50 and 30% compared to the nondestructive test and test no. 1, respectively. This was accompanied by an increase in backwall strain due to partial bearing of the pile cap on the backwall. The percent increase was 55 and 11% compared to the nondestructive test and test no. 1, respectively. Furthermore, the strain in the adjacent pile no. 5 increased by 40% compared to the nondestructive test. No considerable difference was noted relative to the strains measured during test nos. 1 since pile no. 7 was jacked during both tests. When compared to test no. 2 (pile no. 7 removed) the results demonstrate that the backwall strain between pile nos. 6 and 7 was reduced by 25%, and the strain in pile no. 5 was also reduced by 13%. The percent load carried by pile nos. 3 and 7 were 6 and 27%, respectively.



(a) Location of strain transducers and axial loads

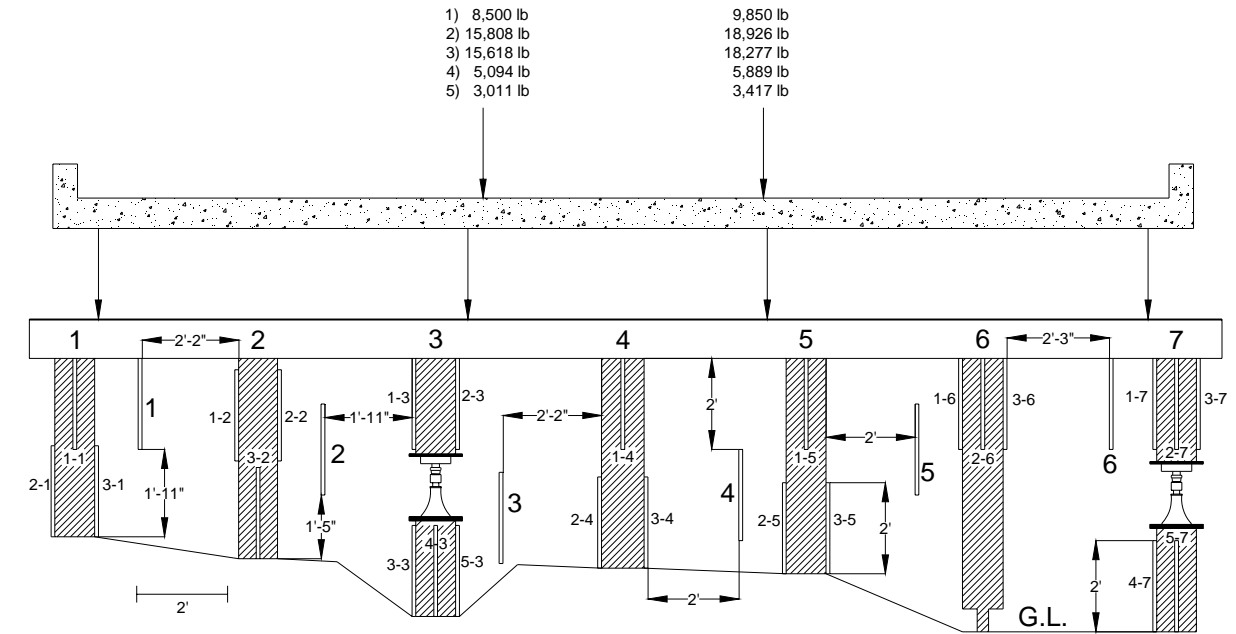


(b) Pile strains

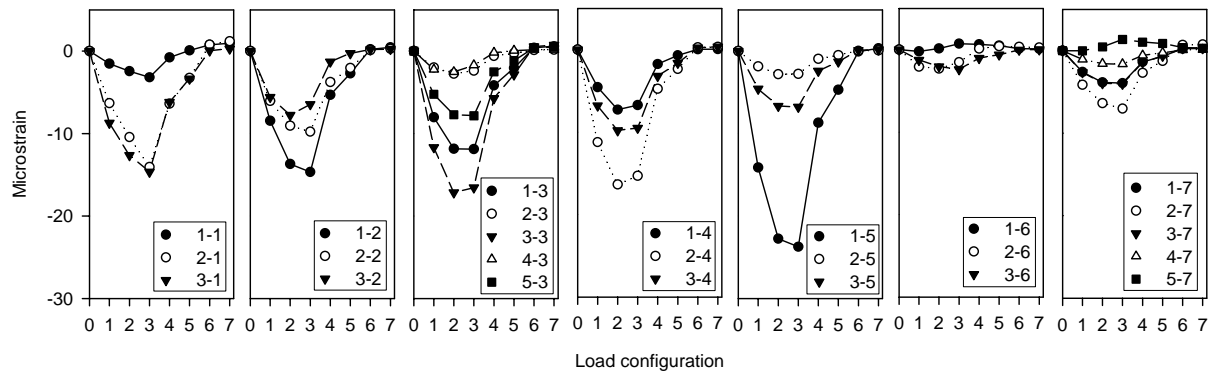


(c) Backwall strains

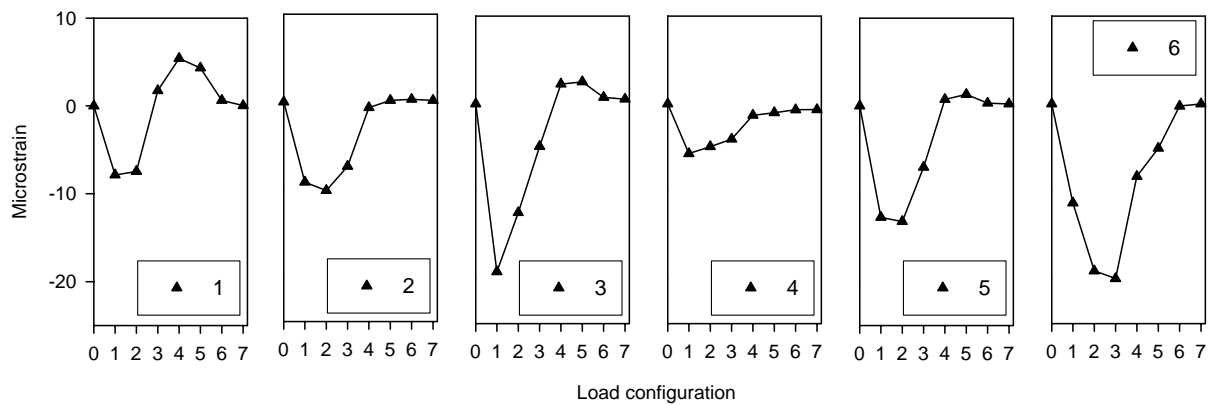
Figure 12.35. Static load test at the north edge with pile Nos. 7 and 3 jacked (Bridge No. 029070 – Humboldt County)



(a) Location of strain transducers and axial loads



(b) Pile strains



(c) Backwall strains

Figure 12.36. Static load test at the centerline pile Nos. 7 and 3 jacked (Bridge No. 029070 – Humboldt County)

12.4.4. Test No. 4 – Pile No. 3 Removed and Pile No. 7 Jacked

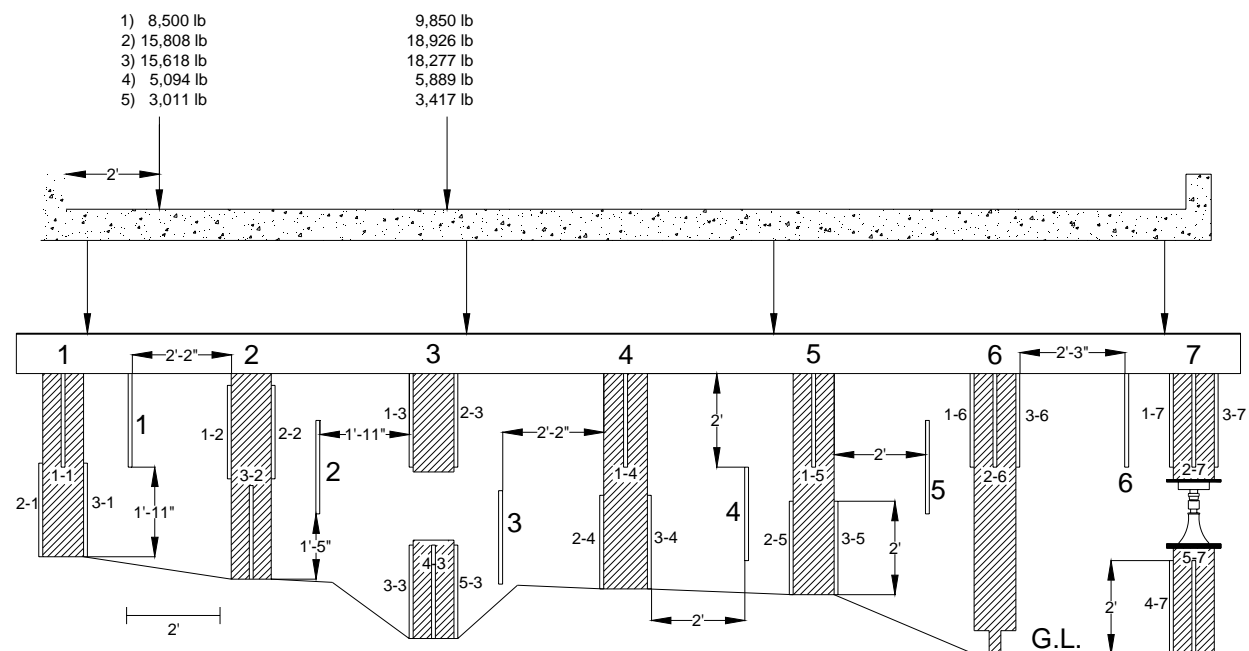
In this test, the mechanical jack and load cell were removed from Pile no. 3 to simulate complete deterioration of an interior pile, whereas Pile no. 7 remained jacked. Two load tests were performed: one along the north edge and one along the centerline of the bridge deck.

12.4.4.1. East Abutment – North Edge

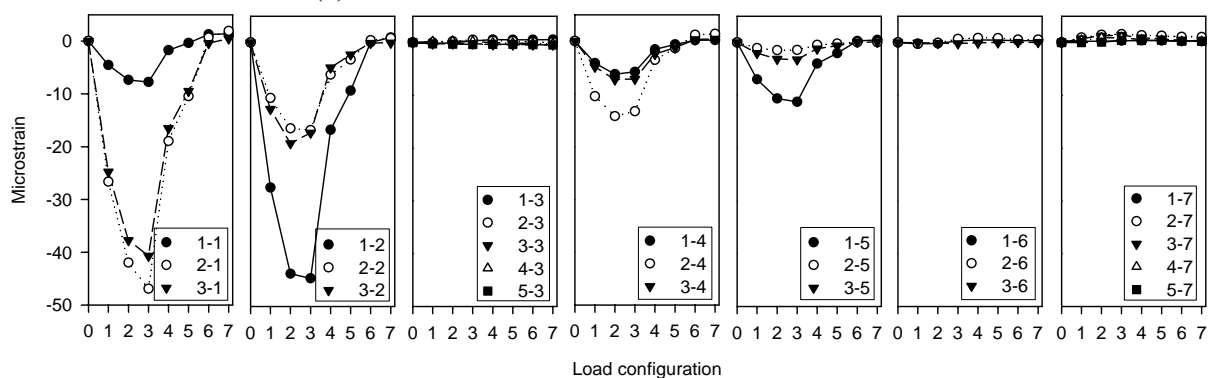
The east abutment was first loaded at the north edge of the bridge. The location of the axial loads, pile strain measurements, and backwall strains are shown in Figure 12.38. Removing pile no. 3 resulted in an increase in the strains in pile nos. 2 and 4 compared to those that occurred during destructive test no. 3, where pile no. 3 was jacked. The strain measured in pile nos. 2 and 4 increased by 27 and 16%, respectively. Due to the removal of pile no. 3 and partial bearing of the pile cap on the backwall, the backwall between pile nos. 3 and 4 resisted higher loads as evidenced by the increase in strain, which was about 70%.

12.4.4.2. East Abutment – Centerline

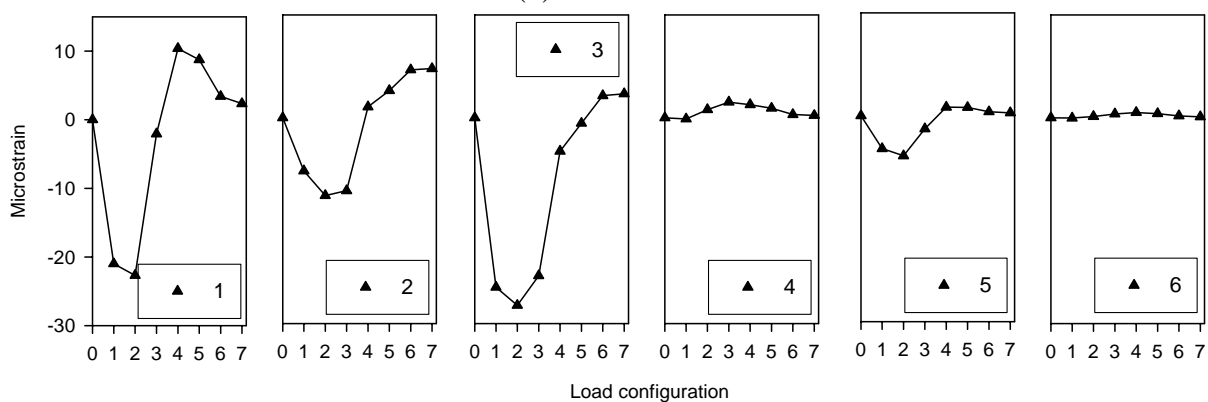
Loading the abutment at the centerline of the bridge deck resulted in an increase in strain at pile nos. 2 and 4 by 50 and 12%, respectively, compared to the strains that occurred in destructive test no. 3 (See Figure 12.39b). Furthermore, a 40% increase in the backwall strain between pile nos. 3 and 4 was measured (See Figure 12.39c). The percent load carried by pile no. 7 was 9%, which is equal to that measured during test no. 3.



(a) Location of strain transducers and axial loads

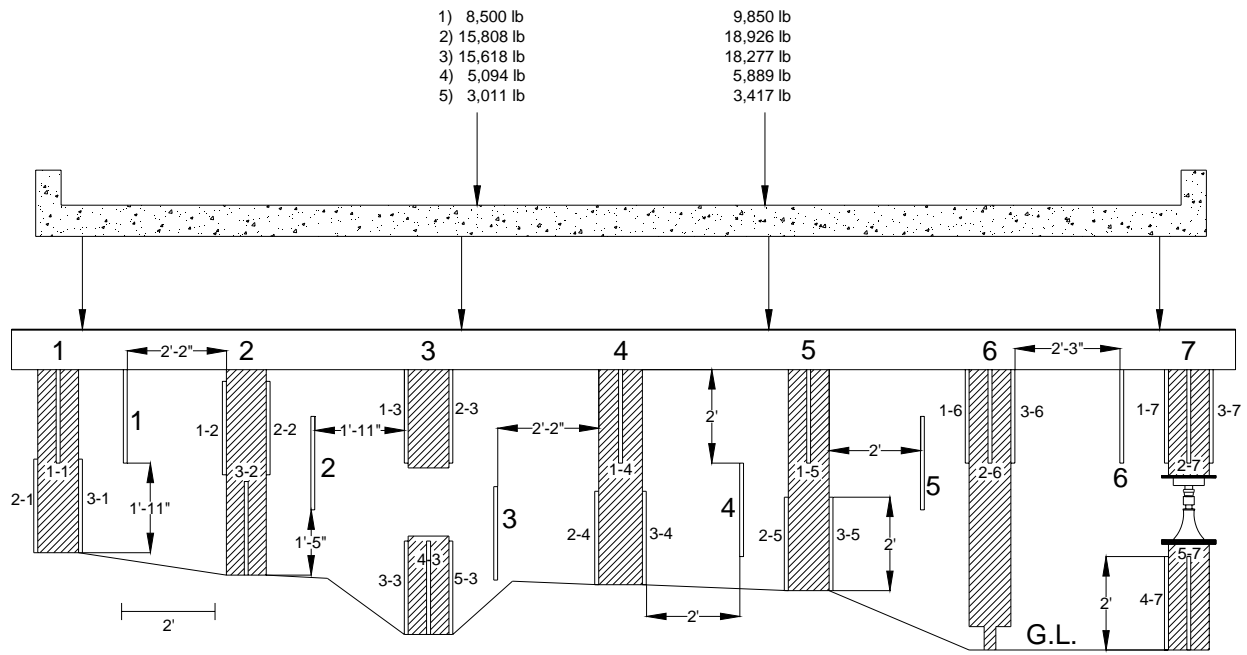


(b) Pile strains

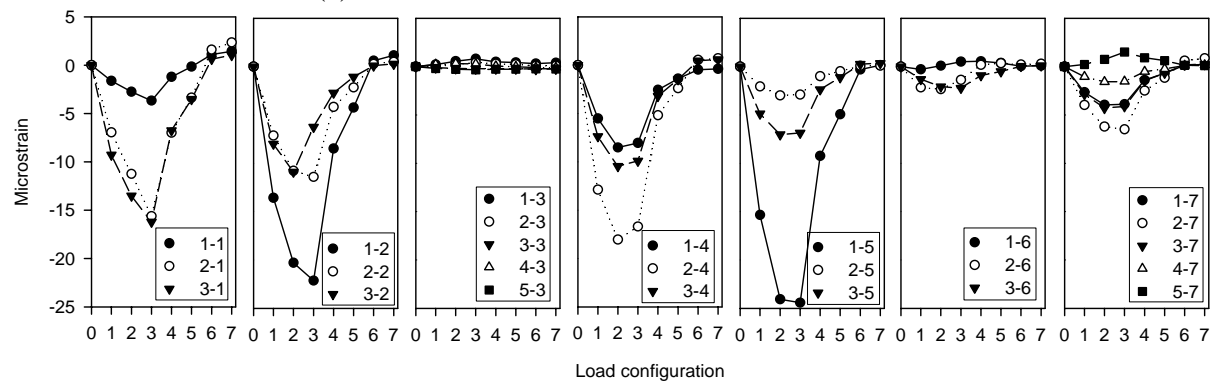


(c) Backwall strains

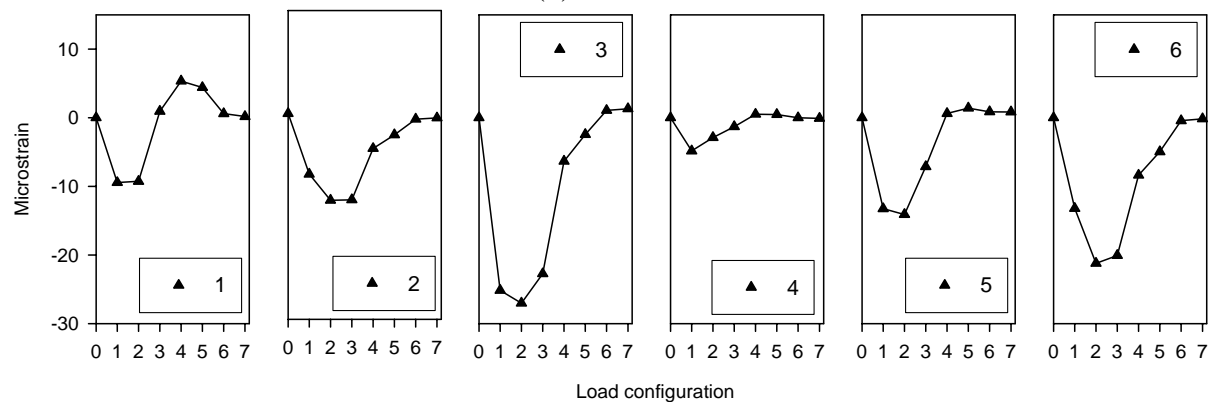
Figure 12.38. Static load test at the north edge with pile no. 3 removed and pile no. 7 jacked (Bridge No. 029070 – Humboldt County)



(a) Location of strain transducers and axial loads



(b) Pile strains



(c) Backwall strains

Figure 12.39. Static load test at the centerline pile No. 3 removed and pile No. 7 jacked (Bridge No. 029070 – Humboldt County)

12.4.5. Test No. 5 – Pile Nos. 3 and 7 Removed

In this destructive test, pile nos. 3 and 7 were removed and three load tests were carried out by loading the east abutment along the north, centerline, and south edges of the bridge.

12.4.5.1. East Abutment – North Edge

The first load test was carried out with the load applied at the north edge of the bridge. The location of the axial loads, pile strain measurements, and backwall strains are shown in Figure 12.40. The pile strain measurements, shown in Figure 12.40a, were compared to the previous destructive test (test no. 4 where pile no. 3 was removed and pile no. 7 was jacked). The pile and backwall strain measurements in both tests were very similar. This confirms previous conclusions and demonstrates that a deteriorated interior pile has more influence than a deteriorated exterior one on load distribution through the substructure when the bridge is loaded at the opposite edge of the exterior pile location.

12.4.5.2. East Abutment – Centerline

When the abutment was loaded at the centerline, the influence of the exterior pile no. 7 became more apparent (See Figure 12.41). This was determined by comparing the strains in load configuration 3 for pile no. 5 during test nos. 3, 4, and 5. The strain in test no. 3 was about -23 microstrains. When pile no. 3 was removed, the strain increased to -24 microstrains (about 4% increase), however, when pile no. 7 was removed the strain increased to -28 microstrains (20% increase). The exterior pile no. 7 does not appear to have any influence on pile nos. 1 through 4 since the strains did not change compared to test no. 4.

The influence of removing pile no. 7 on backwall strains was noticed between pile nos. 5 and 6 and nos. 6 and 7. The strain increased by 28% between pile nos. 5 and 6 relative to test no. 4, whereas the strain between pile nos. 6 and 7 increased by 77%, which is similar to results obtained from test no. 2 (pile No. 7 removed).

12.4.5.3. East Abutment – South Edge

The last test was carried out with the load at the south edge of the bridge (See Figure 12.42). Comparing the results of this test to the results from test no. 2, where pile no. 7 was removed, revealed that the strain in pile no. 4 increased by 15% as a result of removing pile no. 3 (See Figure 12.42b). Furthermore, the backwall strain between pile nos. 3 and 4 increased by almost 100% since the backwall was resisting additional axial load, which was previously resisted by pile no. 3 (See Figure 12.42c). Also, the positive strains measured in pile nos. 1 and 2 during test no. 2 were reduced by 12 and 40%, respectively. Removing pile No. 3 did not influence pile or backwall strains at the south edge of the bridge. Removing an interior pile will therefore only influence adjacent piles and the backwall.

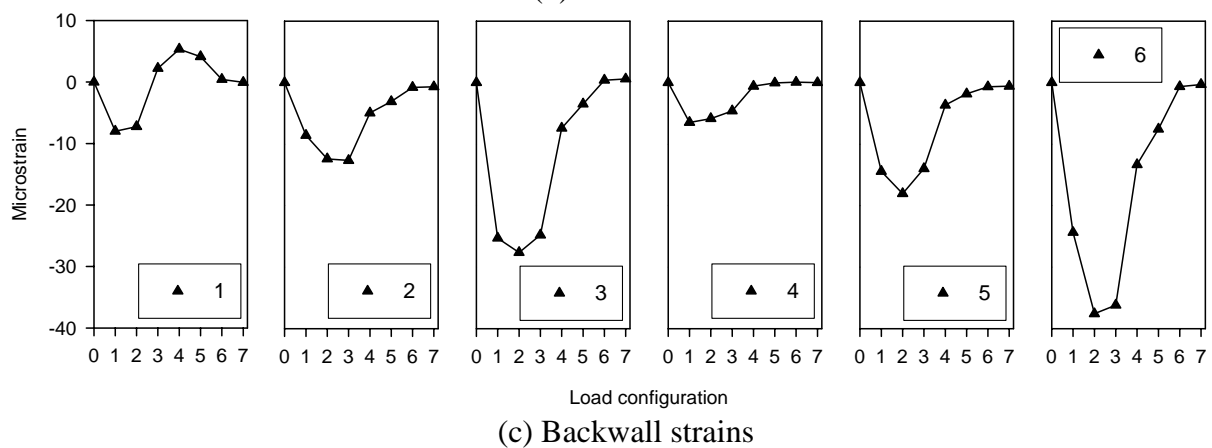
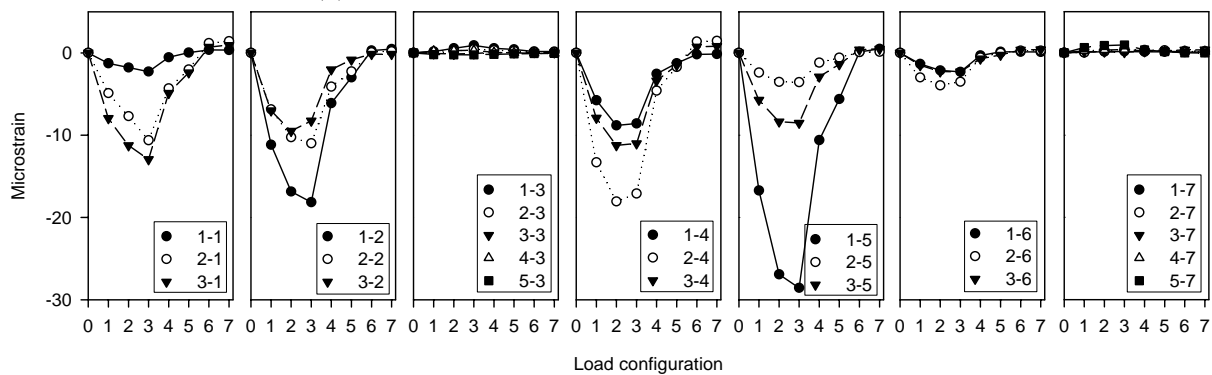
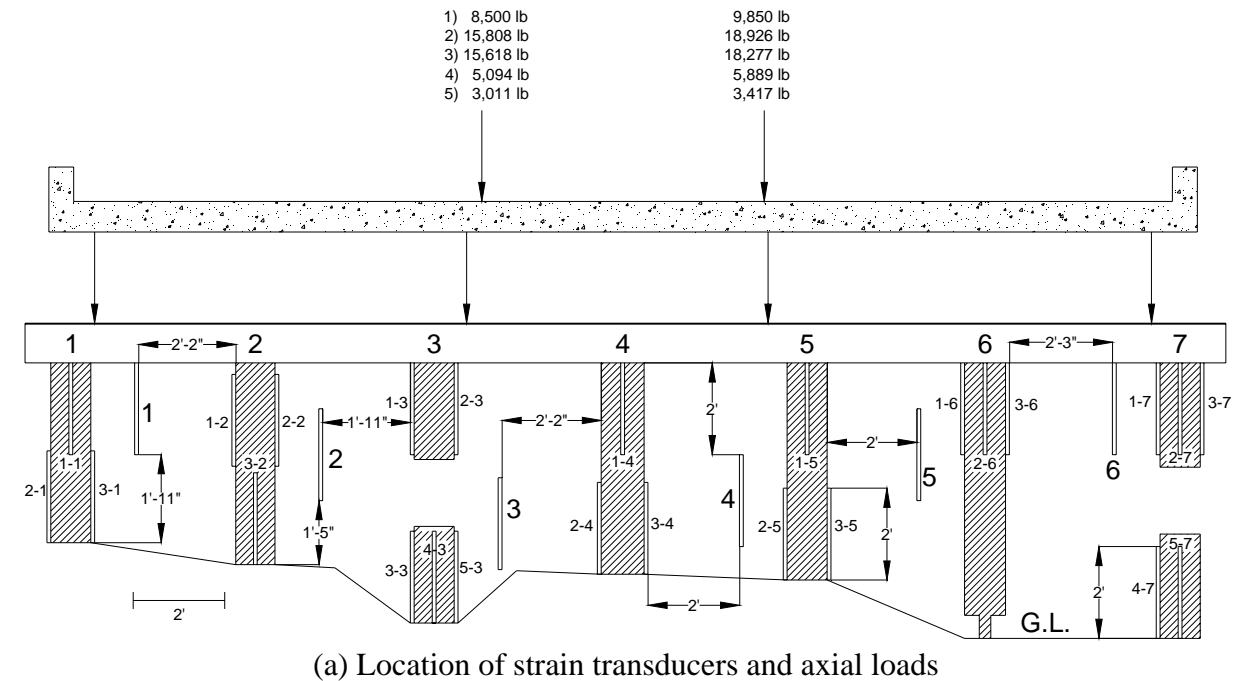


Figure 12.41. Static load test at the centerline with pile Nos. 3 and 7 removed (Bridge No. 029070 – Humboldt County)

12.4.6. Test No. 6 – Pile Nos. 3, 6 and 7 Removed

This test was conducted to study the substructure behavior when three piles are damaged. This was accomplished by removing pile no. 6 and completing three load tests with the loading in the north, centerline, and south edges of the bridge.

12.4.6.1. East Abutment – North Edge

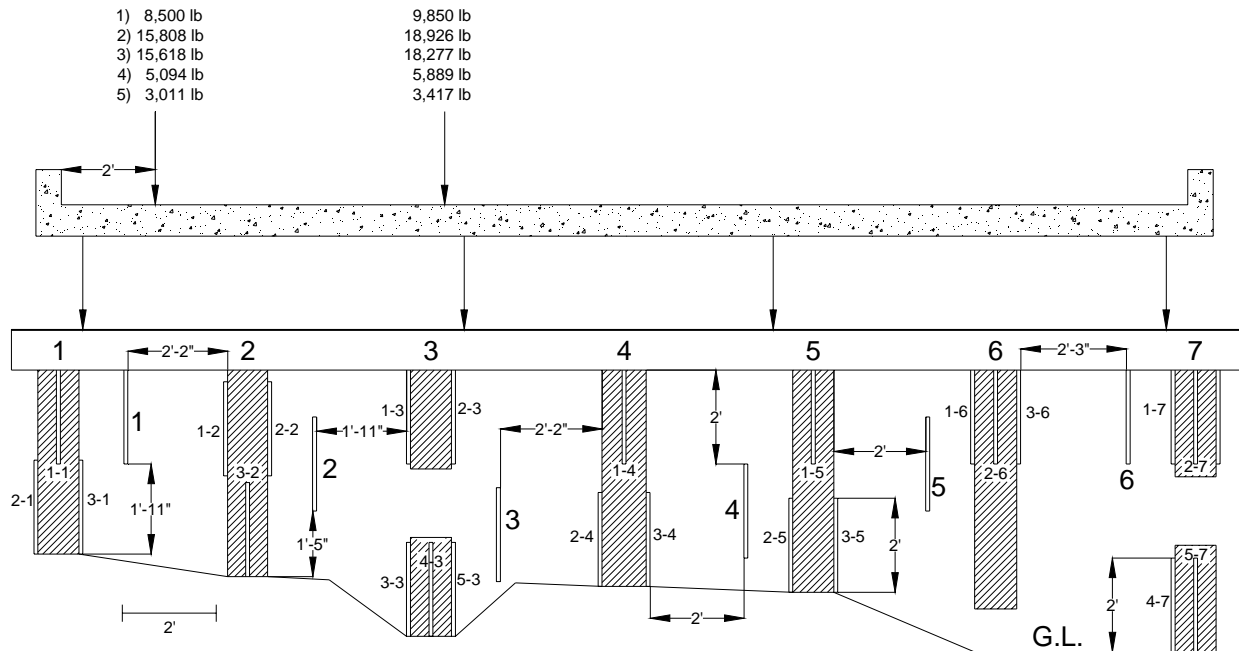
The first load test was performed with the load applied at the north edge of the bridge. Removing pile no. 6 did not have major influence on the strains developed throughout the substructure (See Figure 12.43) since pile and backwall strains were similar to those measured during test no. 5 (north edge test).

12.4.6.2. East Abutment – Centerline

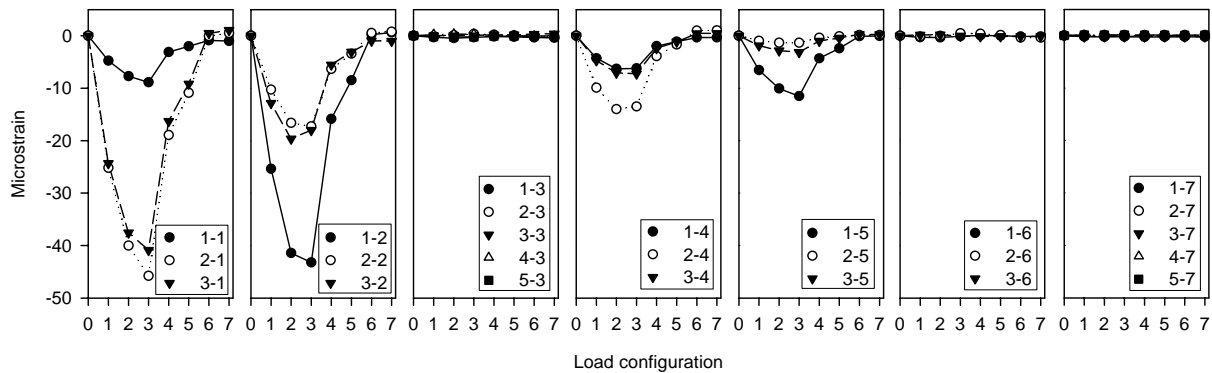
The pile and backwall strain measurements resulting from loading the abutment at the centerline of the bridge deck are shown in Figure 12.44. The results show a 7% increase in strain measured at pile no. 5 due to load transfer from pile no. 6. No significant change was measured at the backwall strains

12.4.6.3. East Abutment – South Edge

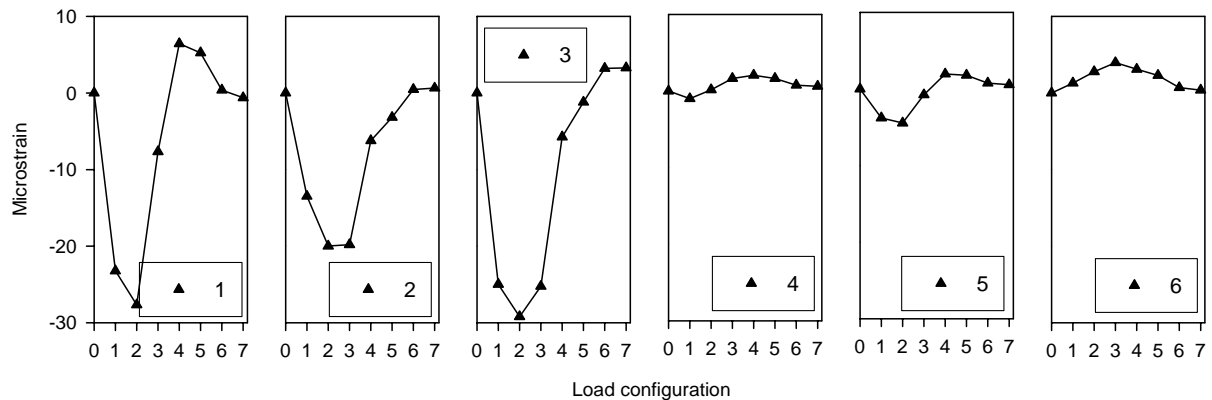
The location of the axial loads, pile strain measurements, and backwall strains are shown in Figure 12.45. Loading the abutment at the south edge of the bridge resulted in an increase in pile no. 5 strain by approximately 25% compared to test no. 5, where only pile nos. 3 and 7 were removed. In addition, removing pile no. 6 resulted in a higher positive strains measured at pile nos. 1 and 2 compared to test No. 5. The strain measured in pile nos. 1 and 2 increased by 7 and 24%, respectively. Furthermore, the negative backwall strain between pile nos. 5 and 6 increased by approximately 10%, while the backwall strain between pile nos. 6 and 7 increased by about 15%. The positive backwall strain between pile Nos. 1 and 2 increased by 20%.



(a) Location of strain transducers and axial loads



(b) Pile strains



(c) Backwall strains

Figure 12.43. Static load test at the north edge with pile Nos. 3, 6 and 7 removed (Bridge No. 029070 – Humboldt County)

12.4.7. Test No. 7 – Pile Nos. 3 and 6 Removed and Pile No. 7 Repaired

This test was carried out to determine the feasibility of repairing localized deteriorated sections of the timber pile. The section removed from pile no. 7 was replaced with a new pile section, which was spliced and attached to the existing pile using two steel screws. Three tests were conducted with the loading applied along the north, centerline, and south edges of the bridge, and the percent strain occurring in pile no. 7 during each load case was measured.

12.4.7.1. East Abutment – North Edge

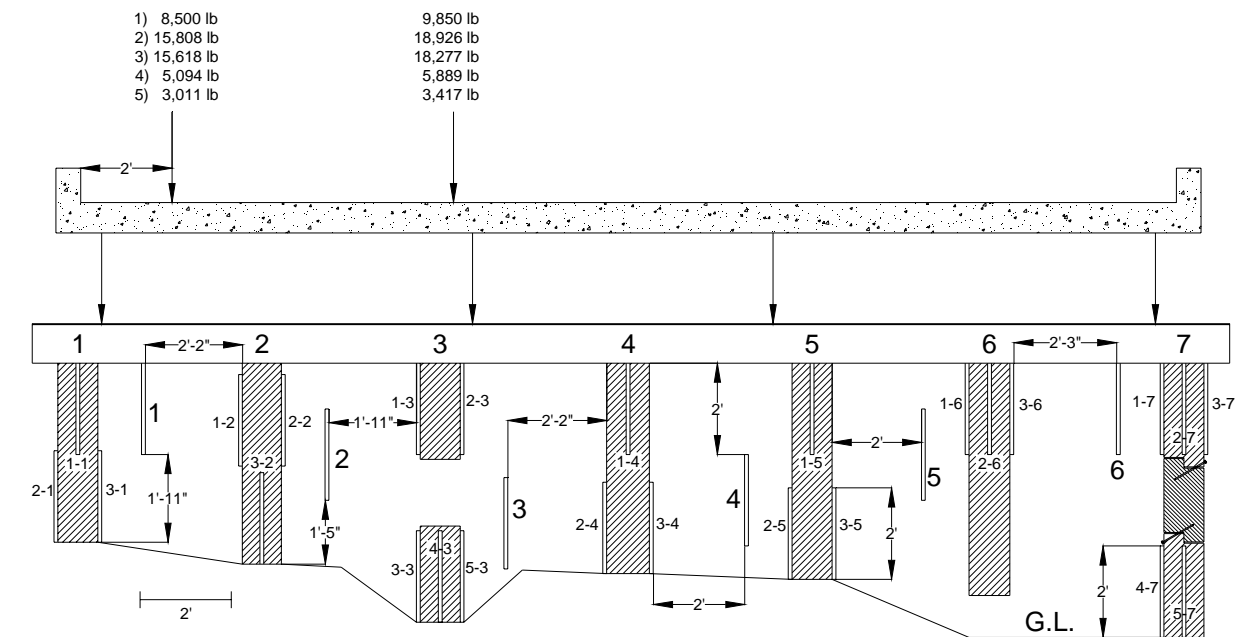
The first load test was carried out with the loading at the north edge of the bridge (See Figure 12.46). The pile and backwall strain measurements were similar to those measured during test nos. 5 and 6. When the abutment is loaded at the north edge of the bridge, almost no load is resisted by pile no. 7, which is reflected by the negligible pile strain.

12.4.7.2. East Abutment – Centerline

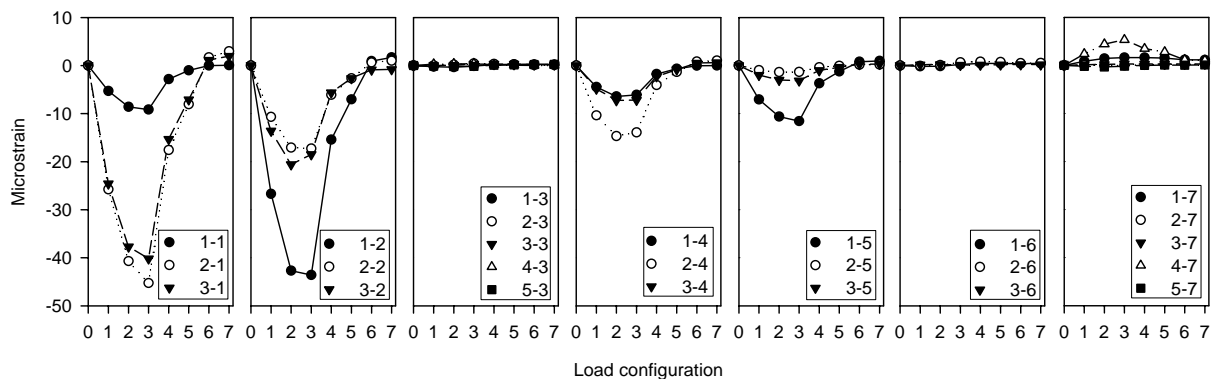
The pile and backwall strain measurements resulting from loading the abutment at the centerline of the bridge deck are shown in Figure 12.47. The results indicate the success of the pile repair method in restoring part of the capacity of pile no. 7 as evidenced by the pile strain measurement, which was about -24 microstrains in load configuration 2. The pile repair resulted also in a reduction of the strain measured in pile no. 5 by about 15% compared to test no. 5. The backwall strain between pile nos. 6 and 7 was also reduced by 45%. The strain measured in pile no. 7 was 3 times higher than that measured during destructive test no. 4 (pile no. 3 removed and pile no. 7 jacked). The pile strains, however, were only recorded by strain transducers 1-7 and 4-7 (See Figure 12.47b).

12.4.7.3. East Abutment – South Edge

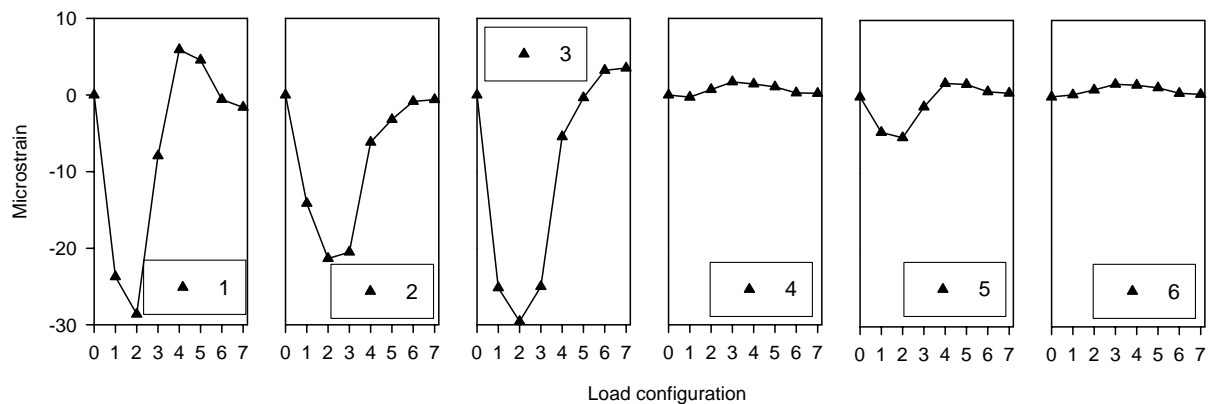
The east abutment was finally loaded with the loading at the south edge of the bridge. The pile and backwall strains are shown in Figure 12.48. Similar to the centerline load test, repairing pile no. 7 reduced the strain in the adjacent pile no. 5 by 25%. Furthermore, the backwall strain between pile nos. 6 and 7 was reduced by 40%. The strain in pile no. 7 was about 3.5 times higher than that recorded during destructive test no. 4 (pile no. 3 removed and pile no. 7 jacked). Repairing pile no. 7 also resulted in reducing the positive strains in pile nos. 1 and 2 during test no. 5 (pile nos. 3, 6, and 7 removed) by about 40 and 15%, respectively.



(a) Location of strain transducer and axial loads



(b) Pile strains



(c) Backwall strains

Figure 12.46. Static load test at the north edge with pile nos. 3 and 6 removed and pile no. 7 repaired (Bridge No. 029070 – Humboldt County)

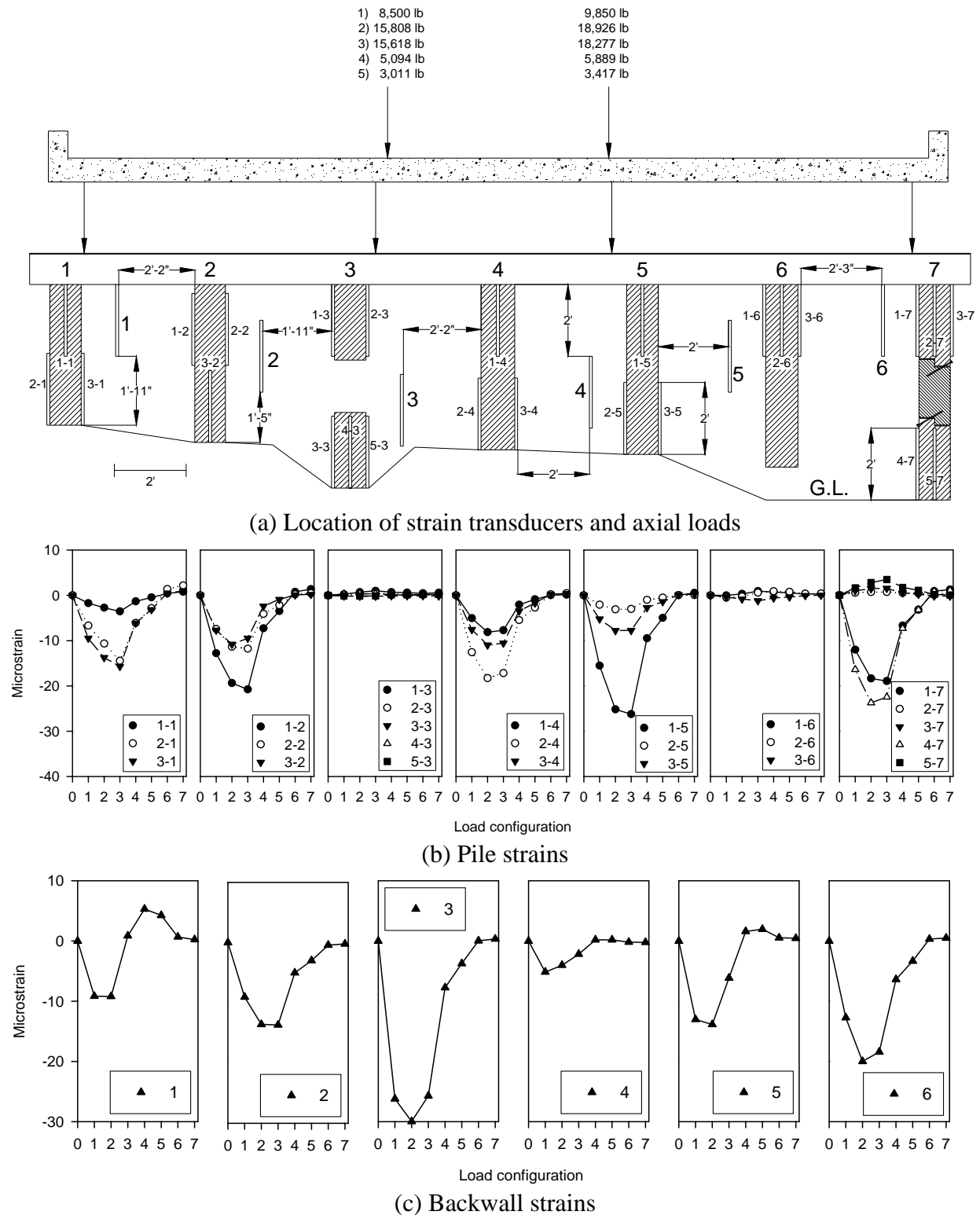


Figure 12.47. Static load test at the centerline with pile Nos. 3 and 6 removed and pile No. 7 repaired (Bridge No. 029070 – Humboldt County)

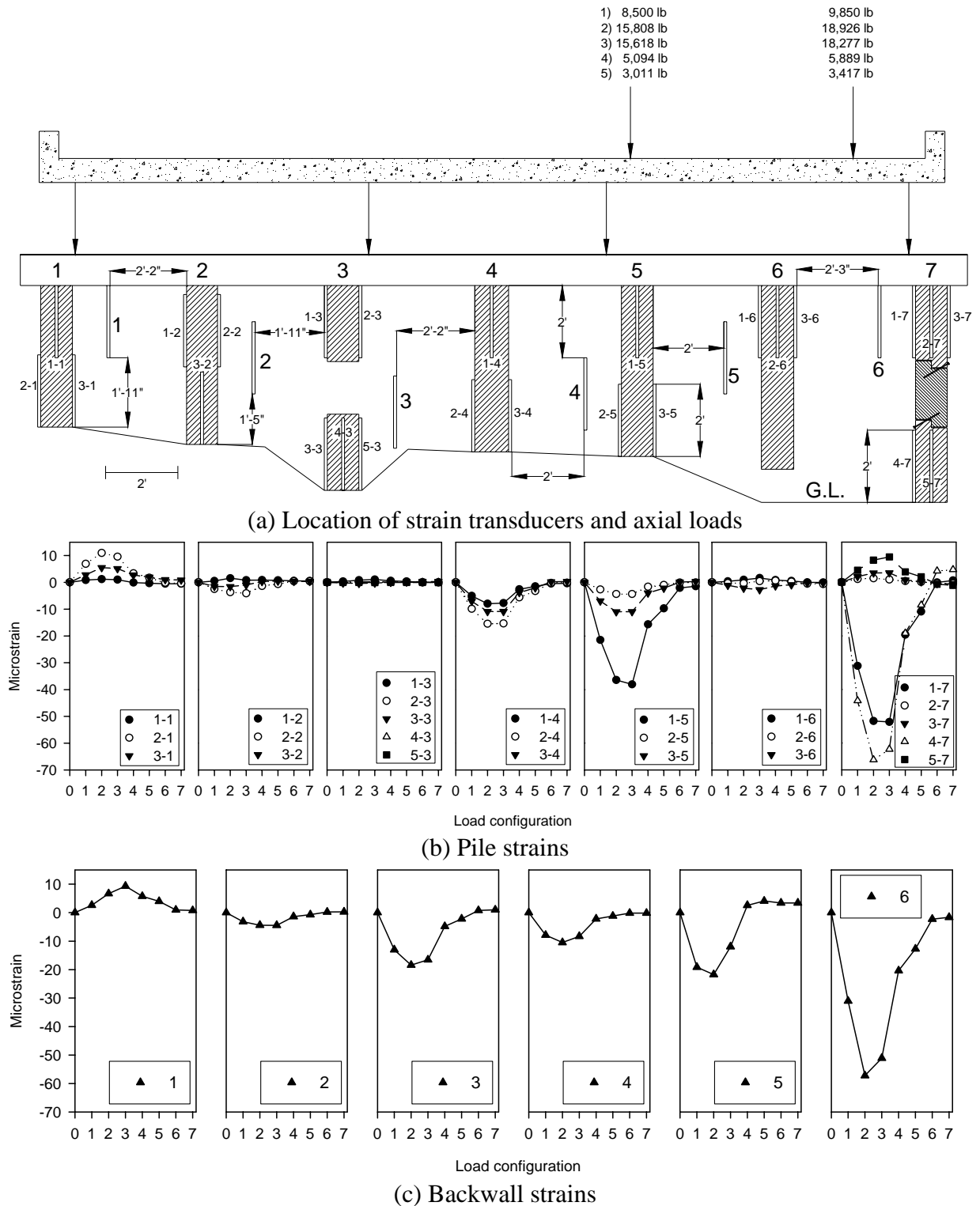


Figure 12.48. Static load test at the south edge with pile nos. 3 and 6 removed and pile no. 7 repaired (Bridge No. 029070 – Humboldt County)

12.5. Foundation Design

According to the bridge plans, the pile lengths in front of the backwall were 25 ft. The exposed pile lengths varied from 4 ft to 6 ft. The foundation was designed based on the design methods outlined in previous chapters and the results of two CPT tests conducted near the east and west abutments (See Figure 12.49 and Figure 12.50). The first test conducted near the east abutment showed little excess pore pressure, which is generally associated with high silt and sand content soils that are able to rapidly dissipate pore water pressures. A weathered limestone bedrock or dense fine grained soils was encountered at 14.6 ft below grade. The profile at the west abutment appears to generally consist of fine-grained soils with a thin layer of silt or sand on top of the weather limestone bedrock or dense fine-grained soils that were encountered at 14 ft. An electronic water level indicator illustrated that the ground water level was about 13.2 ft and 13.3 ft below grade at the east and west abutments, respectively.

To compute the pile allowable resistance, the soil was divided into two layers. The first layer was from 4 ft to 8 ft below grade, and the second layer was from 8 ft to 17 ft. For each layer, a side friction was determined. The side friction for layers 1 and 2 were about 0.96 tsf and 0.7 tsf, respectively, which yield a side resistance of about 16 tons. The pile tip resistance was about 189 tons due to the presence of the bedrock layer at about 14 ft. A summary of the pile length computations are shown in Table 12.2. The Nottingham and Schmertmann method demonstrated that a total pile length of 18 ft is sufficient to resist an allowable pile load of 16 tons. The total pile length as calculated by the method outlined by Klaiber et al. (2004) was about 27 ft. Using this method, however, resulted in an allowable pile load of about 22 tons, which exceeds the 20 tons specified by Iowa DOT for piles between 25 ft and 30 ft.

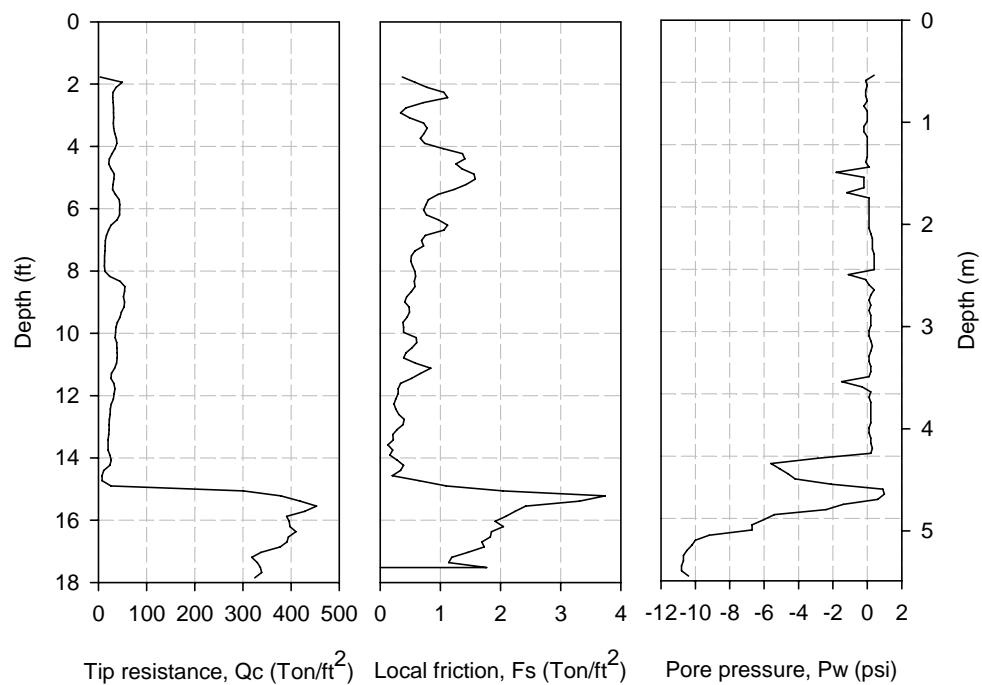


Figure 12.49. CPT test conducted near the east abutment (Bridge No. 029070 Humboldt County)

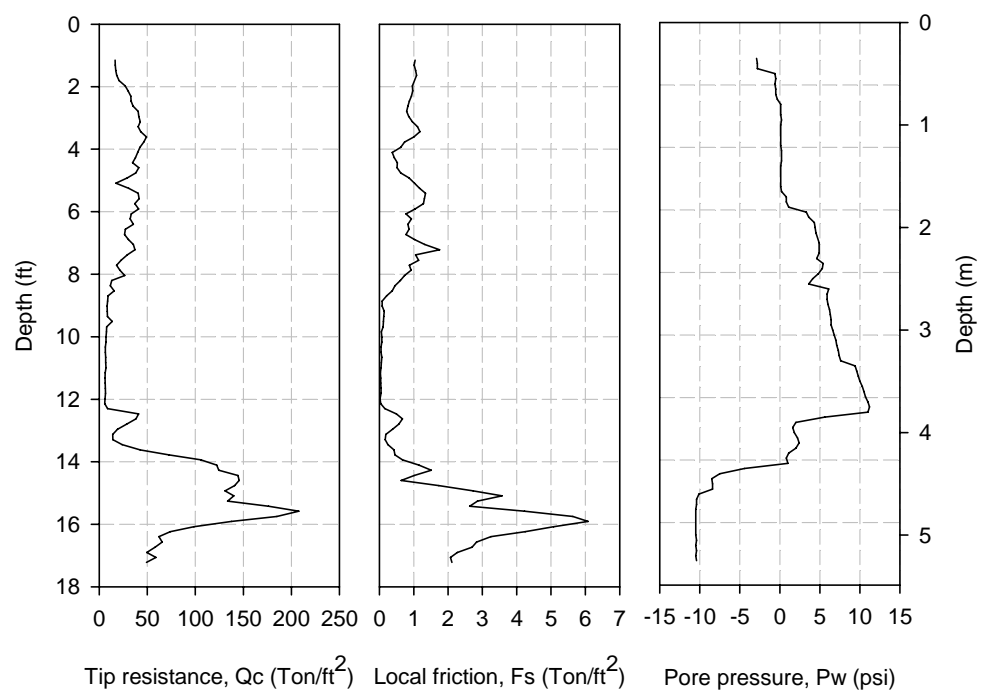


Figure 12.50. CPT test conducted near the west abutment (Bridge No. 029070 – Humboldt County)

Table 12.2. Summary of pile length computations (Bridge No. 029070 – Humboldt County)

General bridge input	Superstructure system	Steel girders
	Span length (ft)	33.5
	Roadway width (ft)	24
	Backwall height (ft)	7.4
	Number of piles	7
	Dead load (kip)	113.1
	Live load (kip)	103.5
	Allowable load per pile (tons)	15.5
Foundation material	q_{c1} (tsf)	112.4
	q_{c2} (tsf)	331.1
	Q_p (tons)	173
	f_s (tsf)	0.96 (4ft to 8 ft) and 0.7 (8 ft to 17ft)
	α'	0.5 (4ft to 8 ft) and 0.63 (8 ft to 17ft)
	A_s (ft ²)	12.56 (4ft to 8 ft) and 21.98 (8 ft to 17ft)
	Q_s (tons)	16
	Q_u (tons)	189
	F.S.	3.0
	Q_a (tons)	63 > 15.5 o.k.
	Assumed pile length (CPT method) (ft)	18
	Computed pile length (Klaiber et al. 2004) (ft)	27

12.6. Key Findings from Field Testing

12.6.1. Ultrasonic Stress Wave Test

- Conducting the ultrasonic stress wave test in the field required reducing the number of test points due to the presence of the backwall, which reduced the accuracy of the generated tomography images.

12.6.2. Increment Borer

- Using the increment borer demonstrated the variation in density along the exposed pile, which complicates the pile characterization.
- The instrument also revealed the level of creosote penetration, which at all bridges ranged from 2 to 4 inches and never reached the pile core.
- The increment borer was an effective tool in detecting hollow piles near the pile core and estimating the residual pile diameter.

12.6.3. Nondestructive Static Load Tests

- Pile strains are typically higher near the applied load and decreases with increasing distance from the location of the load.
- Without knowing the pile E, it is difficult to interpret whether high pile strains are caused by high load carrying capacity or high compression due to soft pile conditions.
- Positive strain values observed in some piles may be due to eccentric loading and/or increased lateral earth pressure. Positive strain values can also be attributed to bending acting on the exterior pile when the abutment is loaded at the opposite edge.
- Strain values varied laterally and longitudinally along the exposed pile length. This highlights the non-uniformity of wood material and the complexity in characterizing the load distribution through the substructure.
- Deteriorated piles show increase in strains to a certain limit after which the strain level decreases or remains constant with increasing load. This is always associated with an increase in adjacent pile strains suggesting load transfer to adjacent piles.
- Since pile lateral movement parallel and perpendicular to the backwall was not measured, it was difficult to separate pile strain measurements due to compression and bending. Measuring pile lateral movement would be a possible improvement for future studies.
- Due to partial bearing of the pile cap on the backwall, the timber backwall resists both axial and lateral loads.
- The foundation design of two bridges using Nottingham and Schmertmann (1975) and the method outlined by Klaiber et al. (2004) produced similar pile length results.
- Interpreting PIT results for in-service piles was a difficult task because of multiple reflections from the overlying superstructure. Pile deterioration above ground also affects the wave propagation and pile length determination. The results of the PIT yielded a significantly shorter pile length compared to the design methods.
- At Bridge No. 094680 in Carroll County, the anchor blocks were located outside the zone of maximum efficiency suggested by Bowels (1996).

- At Bridge No. 237380 in Mahaska County, load transfer from two partially deteriorated piles, evidenced by strain data, may have lead to overloading and bulging of timber fibers of the exterior pile.

12.6.4. Destructive Static Load Tests

- Variation in strain measurements for different piles demonstrated the flexible behavior of the pile cap.
- Removing an exterior pile increases the bending force on the opposing exterior pile.
- Destructive static load tests showed that pile deterioration results in load transfer to adjacent piles and to the backwall behind the deteriorated pile. The percent load transfer to each adjacent pile may depend on pile spacing, relative pile stiffness, and location of the applied loads relative to the deteriorated pile. The load transfer to the backwall is due to the pile cap-backwall detail where the cap is partially resting on the backwall.
- Repairing one exterior pile using the splicing technique partially restored its carrying capacity and reduced the uplift force on the opposing exterior pile. Strains measured in adjacent pile and backwall were also reduced.

13. PILE REPAIR STUDY

13.1. Introduction

From the field reconnaissance, it was observed that most deterioration of the timber piles was normally located near the ground or water level. Other areas of the pile are generally in a satisfactory condition. It was surmised that if the localized deteriorated sections could be repaired, the piles would not have to be replaced. A laboratory pile repair study was developed to evaluate selected pile repair techniques in restoring axial compression and bending capacity of deteriorated timber pile sections.

13.2. Experimental Plan

Three repair methods were investigated in this study. For each method, two new timber pile section, each 4 ft long, were tested to failure in axial and/or bending. The piles were then repaired using the selected repair method and the percent restoration of compressive strength and bending capacity was measured. Two control pile sections, where the cross sectional area was reduced by about 50% to simulate pile deterioration, were also tested. The repair methods investigated included: (1) mechanical splicing (Repair Method A), (2) replacing the damaged section with a new section and a fiber reinforced polymer (FRP) wrap (Repair Method B), and (3) using epoxy with FRP wrap (Repair Method C).

13.3. Test Setup

A universal testing machine which had a capacity of 400,000 lb and was able to record the applied load and deflection was used to test the timber sections in axial compression and bending. During trial bending tests, it was noted that fiber crushing occurred under the loading plate and at the supports, this lead to localized sample failure as oppose to failure due to bending. Special angular supports and loading plate were utilized in one test to help minimize fiber crushing and stress concentrations (See Figure 13.1). This test setup reduced, but did not eliminate, fiber crushing. To further reduce fiber crushing and stress concentration, as shown in Figure 13.2 and Figure 13.3, it was decided to flatten the sides of the pile sections for the bending test. Axial compression tests were performed until sample failure or testing machine ultimate capacity was reached.

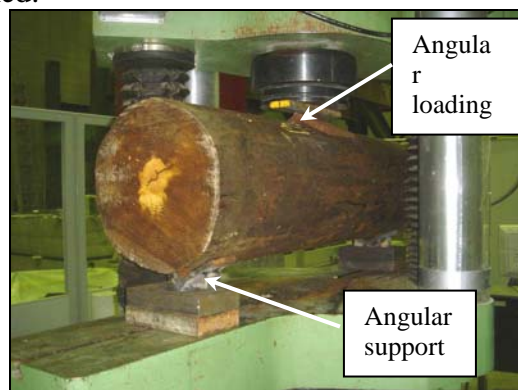


Figure 13.1. Angular supports and loading plate used during a trial bending test

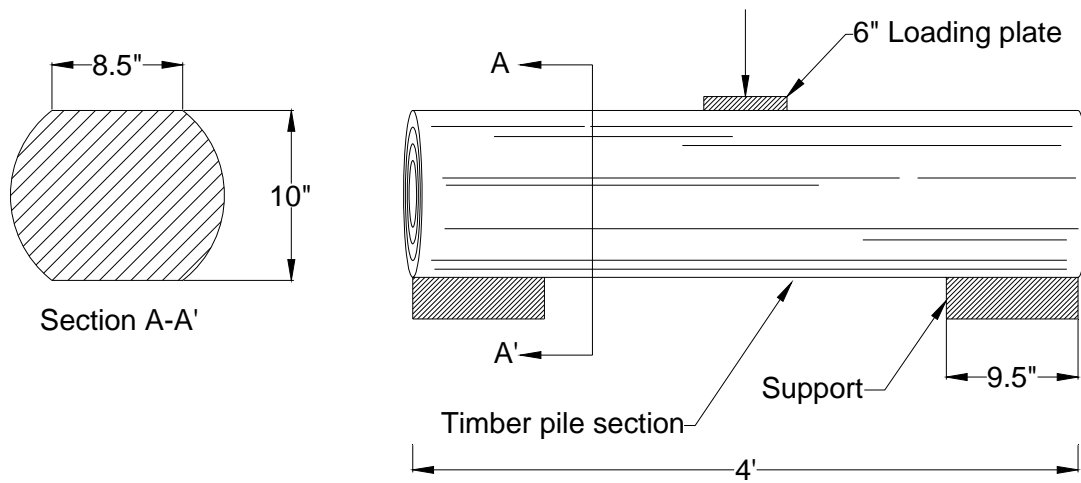


Figure 13.2. Bending test setup



Figure 13.3. Pile sides flattened for conducting bending tests

13.4. Repair Methods

13.4.1. Control Sections

The cross sectional area of two new 4 ft timber sections was reduced by approximately 50% to simulate pile deterioration. The pile diameter was reduced from about 12 inches to about 8 inches as shown in Figure 13.4.

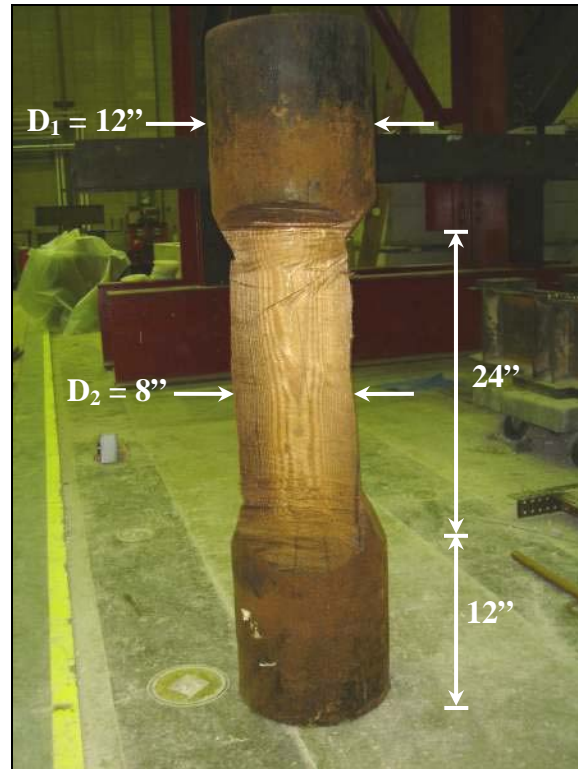
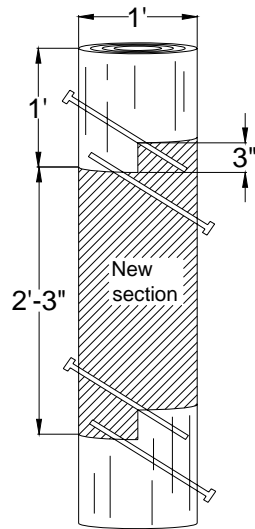


Figure 13.4. Reduced cross sectional area of control timber pile section

13.4.2. Repair Method A – Mechanical Splicing

The first repair method was mechanical splicing. After testing the piles one in compression and one in bending, the pile mid section was removed and replaced with a new section, which was about 27 inches long, as shown in Figure 13.5a. The new section was connected to the pile using four metal screws installed at an angle to go through both pile sections (See Figure 13.5b). The metal screws were 0.5 inches in diameter and 12 inches long. A pile section repaired using the mechanical splicing method may be seen Figure 13.6.



(a) Schematic diagram of the repair method



(b) Connecting the pile sections using a metal screw

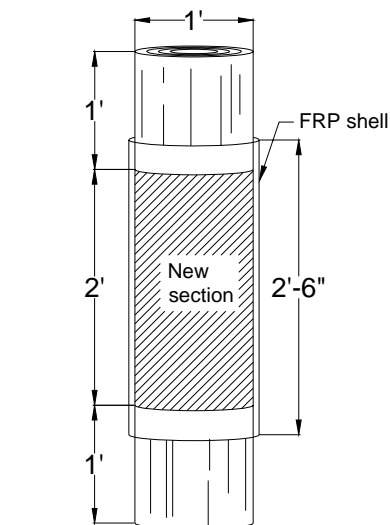
Figure 13.5. Repair method A



Figure 13.6. Pile section repaired using a mechanical splicing techniques

13.4.3. Repair Method B – New Pile Section with FRP Wrap

Repair method B comprised of cutting the damaged mid sections for the axial compression and bending, which was about 2 ft long, and replacing it with a new timber section (See Figure 13.7). The timber pile was then wrapped with 5 unidirectional glass fabric sheets (Tyfo[®] SHE-51A Composite), each 30 inches x 45 inches, which allowed for about 7 inches overlap for each sheet. The overlap for each sheet was staggered to avoid lines of weakness along the entire shell. Prior to wrapping the FRP sheets, a special epoxy (Tyfo[®] S Saturant Epoxy), used typically for bonding applications, was prepared and applied to the FRP sheets. The epoxy was prepared by mixing 100 parts of component A to 42 parts of component B by volume. The two components were mixed using a gear driven mixer for about five minutes until uniformly blended. A paint roller was used to apply the bonding epoxy as shown in Figure 13.8. The epoxy was always applied in the direction of the fibers until the FRP sheet is fully saturated. The FRP sheet was wrapped around the timber pile as shown in Figure 13.9. The paint roller was used to press the FRP sheet against the pile for better bonding and to remove entrapped air. This process was repeated until all five sheets were wrapped around the pile. Wire cords were used to secure the FRP in place until it cured (See Figure 13.10). The material was allowed to cure for three days at 70° F before testing.



(a) Schematic diagram of the repair method



(b) Replacing old timber section with new one

Figure 13.7. Repair method B



Figure 13.8. Applying the bonding epoxy using a paint roller



Figure 13.9. Wrapping the FRP sheet around the timber pile



(a) Pile subjected to flexural loading



(b) Pile subjected to axial loading

Figure 13.10. Two piles repaired using repair method B

13.4.4. Repair Method C – Epoxy Grout with FRP Wrap

Repair method C comprised of removing 50% of the cross sectional area of the damaged pile similar to the control section, wrapping the pile with a FRP shell, and filling the void between the pile and the shell with a wood filler epoxy resin (Tyfo[®] WHF). Two piles were tested; one in axial compression and one in bending. A schematic of this repair method is shown in Figure 13.11. The diameter of the FRP shell was about 15 inches, whereas the diameter of the pile section was about 12 inches. The diameter of the reduced pile cross section was a nominal 8 inches. A PVC pipe with an 15 inch diameter was used to mold the FRP shell (See Figure 13.12a). The pipe was covered with plastic sheets to prevent bonding the FRP shell to the pipe. Three FRP sheets, each 45 inches x 56 inches, were used to form the FRP shell. Bonding epoxy was applied to each sheet, similar to Repair Method C, which was then wrapped around the PVC pipe (See Figure 13.12b). The longitudinal slit of each sheet was staggered to prevent weak lines along the FRP shell. The shell was held in place using wire cords until the bonding epoxy hardened. After curing for 3 days at 70° F, the shell was detached from the PVC pipe and the plastic sheet as shown in Figure 13.13. The FRP shell was placed around the pile section with approximately 1.5 inch gap to allow for placing the wood filler epoxy. According to the procedure recommended by the manufacturer, the wood filler epoxy was prepared by mixing 14% by weight of moist sawdust to Component A. Two parts of Component A were then mixed to one part Component B by volume. A gear driven mixer was used to mix the two components for about 5 minutes until uniformly blended. Once mixed, the wood filler epoxy was applied immediately, since this material cures rapidly, to fill the void (See Figure 13.14). This material produces an exothermic reaction upon curing, expands rapidly after approximately one minute from application, and produces fumes.

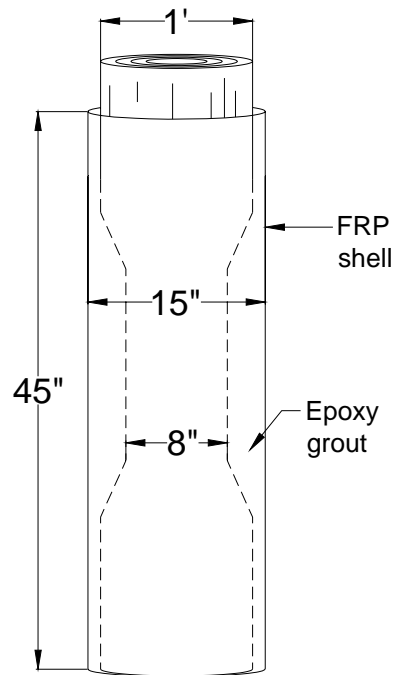


Figure 13.11. Schematic diagram of repair method C



(a) PVC pipe used as a shell mold



(b) FRP sheets wrapped around the pipe

Figure 13.12. Forming the FRP shell



Figure 13.13. FRP shell detached from PVC pipe after curing for three days



Figure 13.14. Expandable wood filler epoxy applied to fill the void between the pile and the FRP shell

13.5. Material Properties

The FRP material (Tyfo[®] SHE-51A Composite) used in this laboratory study was a uni-directional glass fabric. According to the manufacturer, the material is typically used to add strength and ductility to bridges, buildings, and other structures. The glass fabric is oriented in the 0° direction (horizontal) with additional yellow glass cross fabric at 90° (vertical). The FRP was combined with the bonding epoxy (Tyfo[®] S Saturant Epoxy) to form the FRP shells. The bonding epoxy is a two component material. The recommended mixing ratio is 100 parts of Component A to 42 parts of Component B by volume (100 parts of Component A to 34.5 parts of Component B by weight). Component A is pale yellow in color and has a density of 9.7 lb/gal. Component B is clear in color and has a density of 7.9 lb/gal. The properties of the FRP material and the bonding epoxy are summarized in Table 13.1 and Table 13.2. No material properties were available for the wood whole filler epoxy since at the time of testing the material was still under development.

Table 13.1. Properties of FRP material

Composite gross laminate properties			
Property	ASTM method	Typical test value	Design value*
Ultimate tensile strength in primary fiber direction, psi	D-3039	83,400	66,720
Elongation at break	D-3039	2.2%	1.76%
Tensile modulus, psi	D-3039	3.79 x 10 ⁶	3.03 x 10 ⁶
Ultimate tensile strength 90° to primary fibers	D-3039	3,750	3,000
Laminate thickness, in		0.05	0.05

*Design and specification values will vary based on individual project requirements

Table 13.2. Properties of bonding epoxy material

Property	ASTM method	Typical test value
Tensile strength, psi	D-638	10,500
Tensile modulus, psi	D-638	461, 000
Elongation percent	D-638	5.0%
Flexural strength, psi	D-790	17,900
Flexural modulus, psi	D-790	452,000
Curing schedule 72 hours post cure at 140° F		

13.6. Results

For each repair method, two pile sections were tested in axial compression and in bending. Figure 13.15 shows the axial compression and bending tests for the control piles and the piles repaired using methods B and C. The results of the axial compression and bending tests are shown in Figure 13.16 and Figure 13.17, respectively. Also, Table 13.3 summarizes the ultimate load measured during axial compression tests and the percent load restored for each repair method. Table 13.4 summarizes the ultimate load and deflection at failure measured during the bending tests and the percent load restored after repair. The results of the axial compression tests show that repair method A restored about 100% of the axial capacity; however, the deflection was about 10% higher. Repair methods B and C restored about 70 and 50% of their corresponding axial capacity, respectively. Compared to the control section, repair methods A, B, and C restored about 120, 102, and 88% of the load, respectively. The selected repair methods, therefore, have the potential of restoring the axial capacity of partially deteriorated timber piles. The results of the bending tests illustrate that repair method C restored about 70% of the intact pile ultimate load, which is the highest percent restoration observed. Repair methods A and B restored about 50 and 20% of the ultimate load, respectively. Repair method B showed high deflection prior to failure. Compared to the control section, repair methods A, B, and C restored about 80, 40, and 175% of the ultimate load, respectively.



(a) Control pile section – axial



(b) Control pile section – bending



(c) Repair method B – axial



(d) Repair method B – bending



(e) Repair method C – axial



(f) Repair method C – bending

Figure 13.15. Axial and bending load tests

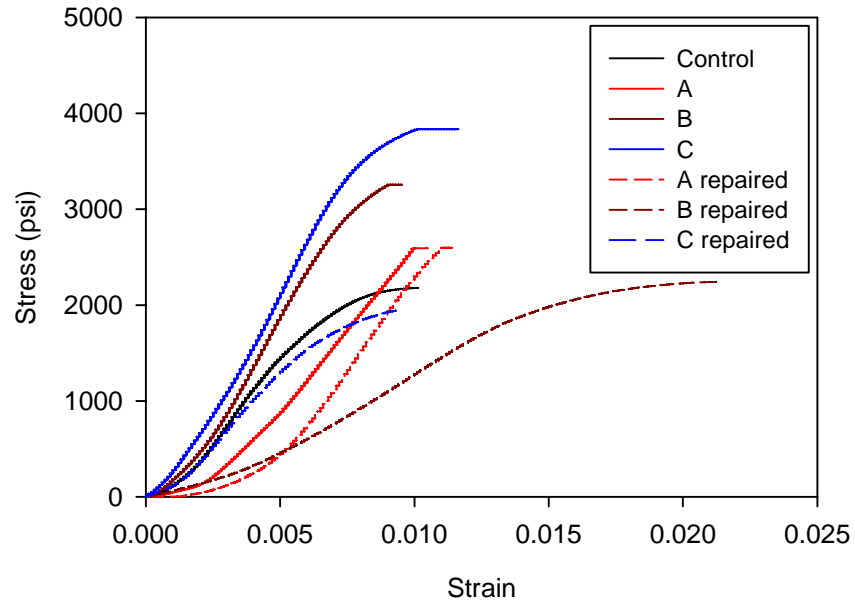


Figure 13.16. Summary of axial compression test results

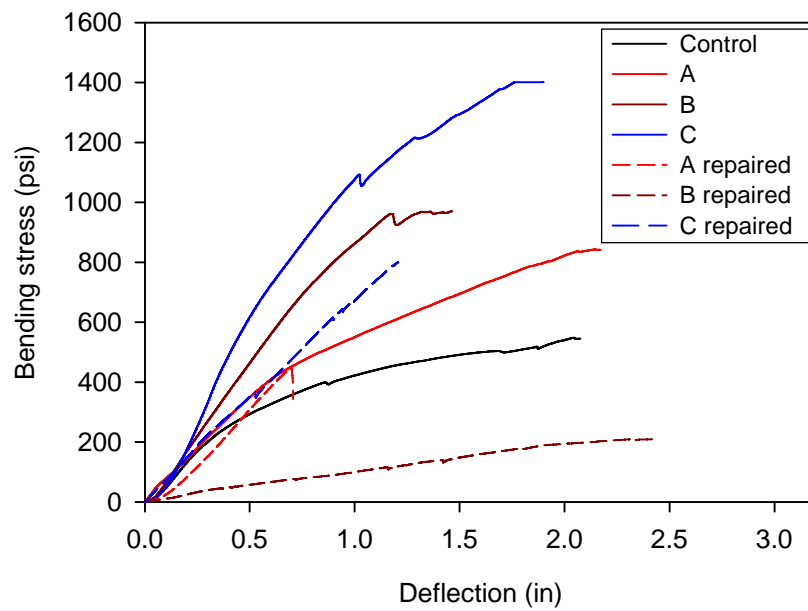


Figure 13.17. Summary of bending test results

Table 13.3. Compressive stress at failure measured for the repair methods

Pile	Diameter (in)	Length (in)	Repair method	Compressive stress at failure (intact), psi	Compressive stress at failure (repaired), psi	% compressive strength restored
1	12	48	Control	2,177	-	-
2	14	47	A	2,590	2,600	100
3	13	48	B	3,260	2,240	70
4	12	48	C	3,830	1,930	50

Table 13.4. Ultimate load and deflection at failure measured for the repair methods

Pile	Diameter (in)	Length (in)	Repair method	Deflection at failure (intact), in	Deflection at failure (repaired), in	Bending stress (intact), psi	Bending stress (repaired), psi	% load restored
1	13	48	Control	2.03	-	546	-	-
2	14	47	A	2.14	0.652	842	433	50
3	13	48	B	1.40	2.04	965	208	20
4	12	47	C	1.90	1.66	1401	957	70

13.7. Summary and Conclusions

A pile study was completed to evaluate three repair methods in restoring the axial and bending capacities of timber piles with localized deterioration. The repair methods included; (1) replacing the deteriorated section with a new section with a FRP wrap (repair method A), (2) mechanical splicing (repair method B), and (3) using wood filler epoxy resin and FRP shell (repair method C). The repair methods were evaluated by comparing ultimate loads before and after repair. The percent compressive strength restored for repair methods A, B, and C during the axial load tests was 100, 70, and 50%, respectively. Furthermore, the ultimate loads measured during the axial compression tests exceeded the typical pile loads encountered for low volume bridges by a factor ranging from 5 to 8. The percent ultimate load restored during the bending tests for repair methods A, B, and C was about 50, 20, and 70%, respectively.

14. SUMMARY AND CONCLUSIONS

14.1. Relevant Research

- Timber piles are a common foundation elements used in bridge construction due to the relatively low cost of wood compared to steel and concrete, simple installation techniques, and their availability and ease of handling relative to other materials.
- In Iowa, problems with unknown bridge foundations are often associated with timber substructures. Timber piles are subject to deterioration, which, at initial stages, can be difficult to detect.
- The causes of timber pile deterioration can be categorized into biological deterioration and physical deterioration. Biological deterioration includes fungi, bacteria, and insect attack. Physical deterioration includes abrasion, overloading, and fire.
- To detect physical or biological deterioration, nondestructive tests such as stress wave transmission and dispersive wave propagation can be used. Determining in-service pile lengths can be accomplished by surface methods such as the bending wave and pile integrity methods or by borehole methods such as parallel and cross borehole seismic tests.
- Pile maintenance can be categorized into (1) preventative maintenance such as the use of fumigants, (2) remedial maintenance, which is used to repair decay in localized areas using methods such as posting and splicing, and (3) major maintenance, which is used when deterioration has progressed to the point where major structural components have experienced moderate to severe strength loss. Adding supplemental piles is a common major maintenance practice.

14.2. Field Reconnaissance

- Field reconnaissance was carried out where 49 low volume bridges with timber substructures were inspected.
- Most biological deterioration was observed near the water or ground level, where conditions are favorable for bacteria, fungi, and insect growth. Biological deterioration can considerably reduce the pile carrying capacity.
- Abrasion and overloading compression failure of timber piles are forms of physical deterioration, which were observed during the field study.
- Other causes of timber pile deterioration include UV degradation, misalignment, and pile cap deterioration.
- Rehabilitation methods observed during the field reconnaissance were (1) concrete casing, (2) driving a timber or steel pile adjacent to the defective pile, and (3) constructing a new substructure system.

14.3. Laboratory Testing

- The laboratory study evaluated the potential of using a nondestructive technique to determine the internal condition of timber piles, and established a correlation between destructive and nondestructive test methods.

- The image reconstruction method used to generate 2-dimensional tomography images from multiple ultrasonic stress wave measurements is the Simultaneous Iterative Reconstruction Technique.
- The test procedure and the imaging reconstruction technique were able to display the internal pile condition. The test method, however, has a tendency of over predicting the area of the internal defect. The prediction error increased as the size of the internal defect decreased. Increasing the number of test measurements can improve the accuracy of this test method.
- Dynamic modulus of elasticity (MOE_d) parallel and perpendicular to the grain were calculated for 12 timber pile sections using the nondestructive stress wave test. Following the nondestructive tests, axial compression tests were performed on 12 timber pile specimens to determine their E .
- Linear regression models show a relatively good correlation between the MOE_d and the E ($R^2 = 0.7$). Multiple regression models combining two or more MOE_d parallel and perpendicular to the grain did not considerably improve the model predictability. The MOE parallel to the grain was 3-5 times higher than the MOE perpendicular to the grain.
- It is concluded that ultrasonic stress wave technique is a promising tool in evaluating timber substructure systems.

14.4. Field Testing

14.4.1. Ultrasonic Stress Wave Test

- Conducting the ultrasonic stress wave test in the field required reducing the number of test points due to the presence of the backwall, which affected the accuracy of the generated tomography images. An improvement to this field test would be attaching the transducer to the pile surface using wooden screws.

14.4.2. Increment Borer

- Using the increment borer demonstrated the variation in density along the exposed pile, which complicates the pile characterization.
- The instrument also revealed the level of creosote penetration, which in all bridges ranged from 2 to 4 inches and never reached the pile core.
- The increment borer was an effective tool in detecting hollow piles near the pile core and estimating the residual pile diameter.

14.4.3. Nondestructive Static Load Tests

- Pile strains are typically higher near the applied load and decreased with increasing distance from the location of the load.
- Without knowing the pile modulus, it is not possible to interpret whether high pile strains are caused by high load carrying capacity or high compression due to soft pile conditions.
- Positive strains observed in some piles may be due to eccentric loading and/or increase lateral earth pressure behind the backwall. Positive strains can also be attributed to pile

bending acting on the exterior pile when the abutment is loaded at the opposite edge of the bridge.

- Strains varied laterally and longitudinally along the exposed pile length. This highlights the non-uniformity of wood material and the complexity in characterizing load distribution through the substructure.
- Severely deteriorated piles show increase in strain to a certain limit after which the strain level remains constant with increasing load. This is always associated with an increase in adjacent pile strains suggesting load transfer to adjacent piles.
- Since pile lateral movement parallel and perpendicular to the backwall was not measured, it was difficult to separate pile strain measurements due to axial compression and bending. Measuring pile lateral movement would be a possible improvement in future studies.
- Due to partial bearing of the pile cap on the backwall, the timber backwall resists both axial and lateral loads.
- The foundation design of two bridges using Nottingham and Schmertmann (1975) and the method outlined by Klaiber et al. (2004) produced similar pile length results.
- Interpreting pile integrity test results for in-service piles was a difficult task because of multiple reflections from the overlying superstructure. Pile deterioration above ground also affects the wave propagation and pile length determination. The results of the PIT yielded a significantly shorter pile length compared to calculated length requirements for the design methods.
- At Bridge No. 094680 in Carroll County, the anchor blocks were located outside the zone of maximum efficiency.
- At Bridge No. 237380 in Mahaska County, load transfer from two partially deteriorated piles, evidenced by strain data, may have lead to overloading and bulging of timber fibers in one of the exterior pile.

14.4.4. Destructive Static Load Tests

- Variation in strain measurements for different piles demonstrated the flexible behavior of the pile cap.
- Removing an exterior pile increases the pile bending in the other exterior pile.
- Through the destructive static load tests it was determined that pile deterioration results in load transfer to adjacent piles and to the backwall behind the deteriorated pile. The percent load transfer to each adjacent pile may depend on pile spacing, relative pile stiffness, and location of the applied loads relative to the deteriorated pile. The load transfer to the backwall is due to the pile cap-backwall detail in which the cap is partially resting on the backwall.
- Repairing one exterior pile using the splicing technique partially restored its carrying capacity and reduced the uplift force on the opposing exterior pile. Strains measured at the adjacent pile and backwall were also reduced.

14.5. Pile Repair Study

- A pile study was undertaken to evaluate three repair methods in restoring the axial and bending capacities of timber piles with localized deterioration.

- The repair methods included; (1) replacing the deteriorated section with a new section with a FRP wrap, (2) mechanical splicing, and (3) using wood filler epoxy resin and FRP shell. The repair methods were evaluated by determining the percent stress and ultimate load restored before and after repair.
- The percent compressive strength restored for repair methods A, B, and C during the axial load tests was 100, 70, and 50%, respectively. Furthermore, the ultimate loads measured during the axial tests exceeded the typical pile loads encountered for low volume bridges, which is limited to 20-25 tons depending on the pile length, by a factor ranging from 5 to 8.
- The percent ultimate load restored during the bending tests for repair methods A, B, and C was about 50, 20, and 70%, respectively.

15. RECOMMENDATIONS AND FUTURE RESEARCH

- It is recommended to use the increment borer and ultrasonic stress wave techniques as a rapid tool in evaluating the internal condition of in-service piles.
- Additional research is needed for the laboratory stress wave testing. The research will investigate different transducer types and orientations, other image reconstruction techniques, the possibility of producing 3-dimensional images of the internal pile condition (i.e. transducers positioned at different elevations) and alternative ultrasonic stress wave devices. Additional laboratory research is also needed to identify the effects of factors such as moisture, creosote penetration levels, and pile degradation on wave speeds in different orientations through the pile section.
- For better understanding of the different substructure systems, it is recommended to construct a laboratory full scale or half scale abutment model. The model can be used to accurately measure pile and backwall loads, conduct PIT against piles with known lengths, and evaluate different repair methods and degrees of degradation. The laboratory model can also be used as a basis for developing, calibrating, and verifying a numerical model that can be used in design.
- On a pilot study basis, deteriorated in-service piles can be repaired using the repair methods presented in this research study. The substructure behavior can be documented before and after pile repair using static load tests to evaluate the efficiency of the selected repair techniques. Further laboratory studies are needed to (1) verify the long term performance of the selected repair techniques with regard to sustaining the strength restored and mitigating further deterioration, and (2) investigate other repair methods and reinforcing materials. Other repair methods not investigated in this study such as cross bracing should also be implemented and evaluated.
- Additional field testing is needed to investigate alternative methods to determine the in-service pile lengths. Methods such as parallel and cross borehole seismic tests are proposed.
- The destructive static load test provided valuable insights on the behavior of timber substructure systems. Therefore, similar tests are recommended for substructures with different types and number of supports.
- For future substructure static load tests, it is recommended to measure lateral pile movement parallel and perpendicular to the backwall to differentiate between pile strains induced by bending and axial compression.

REFERENCES

- Aggour, M. S. (1991). "Nondestructive Testing of Timber Piles for Structures." *Transportation Research Record.*, 1331, 36-44.
- Anthony, R. W., and Pandey, A. K. (1996). "Determining the length of timber piles in transportation structures." *National Conference on Wood Transportation Structures*, Madison, WI., 270-277.
- Anthony, R. W. (2000). "Condition assessment of timber piles." *Forensic Engineering Proceedings of the Second Congress*, San Juan, Puerto Rico, 162-171
- AASHTO (American Association of State Highway and Transportation Officials) (1996). *Standard specifications for highway bridges*, 16th Ed., Washington, D.C.
- ASTM D2555, 1998. Standard Test Method for Establishing Clear Wood Strength Values. American Standard Testing Methods, *Annual book of standards*, Vol. 04.10, West Conshohocken, PA.
- ASTM D5882, 1995. Standard Test Method for Low Strain Integrity Testing of Piles. American Standard Testing Methods, *Annual book of standards*, Vol. 04.09, West Conshohocken, PA.
- Avent, R. R. (1989). "Durability of Posted and Epoxy-Grouted Timber Piles." *Journal of Structural Engineering.*, ASCE, 115(4), 826-833.
- Bowels, J. E. (1996). *Foundation analysis and Design*, 5th Ed., McGraw – Hill, NY.
- Brooks, R. T., and Burk A. G. (1994). "Timber pile length determination using a nondestructive technique." *Proceedings of Papers Presented at the Structures Congress*, Atlanta, GA., 952-957.
- Buslov, V. M., and Scola, P. T. (1991). " Inspection and Structural Evaluation of Timber Piers: Case Study." *Journal of Structural Engineering.*, 117(9), 2725-2741.
- Chen, S. and Kim, Y. R. (1997). "Condition Assessment of Installed Timber Piles by Dispersive Wave Propagation," *Transportation Research Record.*, 1546, 112-120.
- Davis, A. G. (1995). "Nondestructive Evaluation of Existing Deep Foundations." *Journal of Performance of Constructed Facilities.*, ASCE, 9(1), 57-74.
- Divos, F., and Szalai, L. (2002). "Tree evaluation by acoustic tomography." *13th International Symposium on NDT of Wood*, Berkeley, Colorado.

- Emerson, R. N. (2004). "In situ repair technique for decayed timber piles." *Conference Proceedings Structures 2004 – Building on the Past: Securing the Future*. Nashville, TN., 1-9.
- Emerson, R. N., Pollock D. G., Kainz, J. A., Fridley, K. J., Melean, D., and Ross, R. J. (1999). "Nondestructive evaluation techniques for timber bridges." *Fifth World Conference on Timber Engineering*, 4(1), Montreaux, Switzerland.
- Hannigan, P. J., Goble, G. G., Thendean, G., Linkins, G. E., and Rausche, F. (1997). *Design and Construction of Driven Pile Foundations – Volume I*, Federal Highway Administration, Report No. FHWA-HI-97-013, Washington, D.C.
- Holt, D.J., Chen, S., and Douglas, R.A. (1994). "Determining Lengths of Installed Timber Piles by Dispersive Wave Propagation." *Transportation Research Record.*, 1447, 110-115.
- Jackson, M. J., and Tweeton, D. R. (1996). *3DTOM: Three-dimensional geophysical tomography*, United States Bureau of Mines, Pittsburg, PA.
- Johnson, K. A. (2004). *Repair and Rehabilitation of Treated Timber Bridges*, Wheeler Lumber, LLC, Bloomington, MN.
- Klaiber, F. W., White, D. J., Wipf, T. J., Phares, B. M., and Robbins, V. W. (2004). *Development of abutment design standards for local bridge designs*, Iowa DOT Project TR-486, Iowa Department of Transportation.
- Leiphart, G. S. (1997). *Acoustic tomography of concrete using a James Instrument Velocity Meter*, Masters of Science Thesis, University of Colorado, Denver, CO.
- Lopez-Anido, R., Michael, Goodell, B., and Sandford, T. C. (2004). "Assessment of Wood Pile Deterioration due to Marine Organisms." *Journal of Waterway, Port, Coastal and Ocean Engineering*, ASCE, 130(2), 70-76.
- Lopez-Anido, R., Michael, A. P., and Sandford, T. C. (2003). "Experimental Characterization of FRP Composite-Wood Pile Structural Response by Bending Tests." *Marine Structures*, 16, 257-274.
- Lopez-Anido, R., Michael, A. P., Sandford, T. C., and Goodell, B. (2005). "Repair of Wood Piles Using Prefabricated Fiber-Reinforced Polymer Composite Shells." *Journal of Performance of Constructed Facilities*, ASCE, 19(1), 78-87.
- Manuel, F. S. (1984). *Evaluation and Improvement of Existing Bridge Foundations*, Report No. FHWA/RD-83/061, Federal Highway Administration, Mclean, VA.
- Massoudi, N. and Teferra, W. (2004). Non-destructive testing of piles using the low strain integrity method. *Proceedings: Fifth International Conference on Case Histories in Geotechnical Engineering*. NY, Paper No. 9.03.
- McCormac, J. C. (1994). *Structural Steel Design LRFD Method*, 2nd Ed., Prentice Hall, NJ

- Mindess, S., Young, J. F., and Darwin, D. (2003) *Concrete*, 2nd Ed., Prentice Hall, NJ.
- NDS (National Design Specifications) (2001). *Manual for wood construction*, Washington, D.C.
- Olson, L. D., Jalinoos, F., and Aouad, M. F. (1998). *Determination of Unknown Subsurface Bridge Foundations.*, U.S. Department of Transportation, Federal Highway Administration, Washington, D.C.
- Purvis, R. L. (1994). *Underwater Bridge Maintenance and repair*, National Cooperative Highway Research Program, Synthesis of Highway Practice 200, Transportation Research Board, Washington, D.C.
- Rausche, F. (2004). "Non-destructive evaluation of deep foundations." *Proceedings: Fifth International Conference on Case Histories in Geotechnical Engineering*, Paper No. OSP-5, Pennsylvania, NY.
- Ritter, M. A. (1992). *Timber Bridges: Design, Construction, Inspection, and Maintenance.* United States Department of Agriculture, Forest Service, Forest Products Laboratory, Madison, WI.
- Ross, R. J., Pellerin, R. F., Forsman, J. W., Erickson, J. R., and Lavinder, J. A. (2001). "Relationship between Stress Wave Transmission Time and Compressive Properties of Timbers Removed from Service." *United States Department of Agriculture, Forest Service, Forest Products Laboratory*, Madison, WI.
- Ross, R. J., Pellerin, R. F., Volny, N., Salsig, W. W., and Falk, R. H. (1999). "Inspection of Timber Bridges Using Stress Wave Timing Nondestructive Evaluation Tools, A Guide for Use and Interpretation." *United States Department of Agriculture, Forest Service, Forest Products Laboratory*, Madison, WI.
- Sack, D. A., Slaughter, S. C., and Olson, L. D. (2004). "Combined measurement of unknown foundation depths and soil properties with NDE methods." *Proceedings 83rd Annual Transportation Research Board* (CD-ROM), Washington, D.C.
- Seavey, R., and Larson, T. (2002). *Inspection of Timber Bridges*, Minnesota Department of Transportation, Office of Research Services, Report No. MN/RC-2002-34, St. Paul, MN.
- Stegman, B. G., and Holt, D. J. (2000). "Determining the capacity of unknown foundation." *Use of Geophysical Methods in Construction Proceedings of Sessions of Geo-Denver*, 141-155, Denver, CO.
- Townsend, F. C., Hussein, M., and McVay, M. C. (1996). "Determining embedded depths of deep foundations using nondestructive methods." *Fifth International Conference on the Application of Stress-Wave Theory to Piles*, Gainesville, FL., 732-747.
- Toutanji, H. A., (2000). "Ultrasonic wave velocity signal interpretation of simulated concrete bridge decks." *Materials and Structures*, 33, 207-215.

- Toutanji, H. A. (2004). *Multimedia Technology for Timber Bridge Repair*, University Transportation Center for Alabama, The University of Alabama, Report No. FHWA/CA/OR., Tuscaloosa, AL.
- University of Virginia Civil Engineering Department, Virginia Highway and Transportation Research Council, and Virginia Department of Highways and Transportation, (1980). *Bridges on Secondary Highways and Local Roads – Rehabilitation and Replacement*, National Cooperative Highway Research Program Report 222, Transportation Research Board, Washington D.C.
- U.S. Army Corps of Engineers, Naval Facilities Engineering Command, and Air Force Civil Engineering Support Agency. (2001). *Unified facilities criteria (UFC)—Maintenance and Operation: Maintenance of Waterfront Facilities*, Publication No. UCF 4-150-07, Washington, D.C.
- U.S. Department of Agriculture, Forest Service, Forest Products Laboratory (1999). *Wood Handbook: Wood as an Engineering Material, Gen. Tech. Rep. FPL-GTR-113*. Madison, WI.
- Wang, X., Divos, F., Pillon, C., Brashaw, B. K., Ross, R. J., and Pellerin R. F. (2004). “Assessment of Decay in Standing Timber Using Stress Wave Timing Nondestructive Evaluation Tools. A Guide for Use and Interpretation.” *United States Department of Agriculture, Forest Service, Forest Products Laboratory*, Madison, WI.
- Wang, X., Ross, R., Erickson, J. R. Forsman, J. W., McGinnis, G. D., and De Groot, R. C. (2000). “Nondestructive Methods of Evaluating Quality of Wood in Preservative-Treated Piles.” *United States Department of Agriculture, Forest Service, Forest Products Laboratory*, Madison, WI.
- Webber, D., and Yao, J. (2001). “Effectiveness of Pile Wraps for Timber Bearing Piles.” *Proceedings: Ports 2001 Conference: America’s Ports-Gateway to the Global Economy*, Section 22, Chapter 1, Norfolk, VA.
- Wightman, E. W., Jalinoos, F., Sirles, P., and Hanna, K. (2003). *Application of Geophysical Methods to Highway Related Problems*, Federal Highway Administration, Lakewood, Co.
- Wipf, T. J., Fanous, F. S., Klaiber, W. F., and Eapen, A. S. (2003a). *Evaluation of Appropriate Maintenance, Repair and Rehabilitation Methods for Iowa Bridges*. Iowa Department of Transportation, Report No. TR-429, Ames, IA.
- Wipf, T. J., Phares, B. M., Klaiber, F. W., Wood, D. L. Melling, E., and Samuelson, A. (2003b). *Development of Bridge Load Testing Process for Load Evaluation*. Iowa Department of Transportation, Report No. TR-445, Ames, IA.

APPENDIX A

PROJECT QUESTIONNAIRE

Iowa Department of Transportation
Highway Division
Research Project TR-522

“Investigation of Steel Stringer Bridges: Substructure and Superstructure”

Questionnaire completed by: _____

Organization: _____

Address: _____

E-mail address: _____

Responses can either be E-mailed (respond to the website questionnaire) or faxed to T.J. Wipf (E-mail address: tjwipf@iastate.edu; Fax number: 515-294-7424). If you have some substructure or superstructure designs, pictures, etc. that you are willing to share, please mail them to:

Prof. Terry J. Wipf
426 Town Engr. Bldg.
CCEE Dept.
Iowa State University
Ames, Iowa 50011

Q-1) Please identify at least 2 non-composite-steel stringer concrete deck bridges in your county with *superstructure* problems

Bridge 1:

Type: _____

Length: _____ Width: _____

Location (ID): _____

Type of problem(s): _____

Bridge 2:

Type: _____

Length: _____ Width: _____

Location (ID): _____

Type of problem(s): _____

Q-2) Please identify at least 2 bridges in your county with *substructure* problems

Bridge 1:

Type: _____

Length: _____ Width: _____

Location (ID): _____

Type of problem(s): _____

Bridge 2:

Type: _____

Length: _____ Width: _____

Location (ID): _____

Type of problem(s): _____

Note:

- For providing information on additional bridges, please feel free to use additional pages.

Q-3) What are the common causes of problems with the substructures?

Please rank using: 1 = most common, 2 = frequent, 3 = Seldom a factor, 4 = Never

Steel Piles

____ Corrosion
____ Misalignment
____ Damage due to impact
____ Other

Timber Piles

____ Scour
____ Mechanical deterioration
____ Biological deterioration
____ Misalignment
____ Other

Q-4) What methods have you or your consultants used to detect substructure and superstructure problems? How often have you used these methods?

Please use the following scale: 1 = Often, 2 = Sometimes, 3 = Rarely, 4 = Never

____ Visual inspection

____ Non-destructive testing

____ Other

Q-5) What remedial and/or strengthening measures have you used in the past on substructures?

Q-6) Of those remedial and strengthening measures, which do you consider to be most effective and beneficial?

Q-7) How many non-composite steel stringer bridges are there in your county? (If exact number is not known, please provide an estimated number) _____

Q-8) Are you willing to allow ISU to perform non-destructive testing on some of your superstructures?

YES _____ NO _____

Q-9) Are you willing to allow ISU to perform non-destructive testing on some of your substructure?

YES _____ NO _____

Q-10) Do you currently have functionally or structurally inadequate substructures on which you would allow ISU to perform *destructive* testing?

YES _____ NO _____

If yes, please provide some details

Q-11) Do you currently have maintenance records of the majority of low volume bridges?

YES _____ NO _____

Q-12) If you answered YES to Q-11, would you be willing to provide copies of relevant information for a limited number of your bridges?

YES _____

NO _____

Please provide any additional information you think might be useful to this research project.

APPENDIX B

TWO-DIMENSIONAL TOMOGRAPHY IMAGES

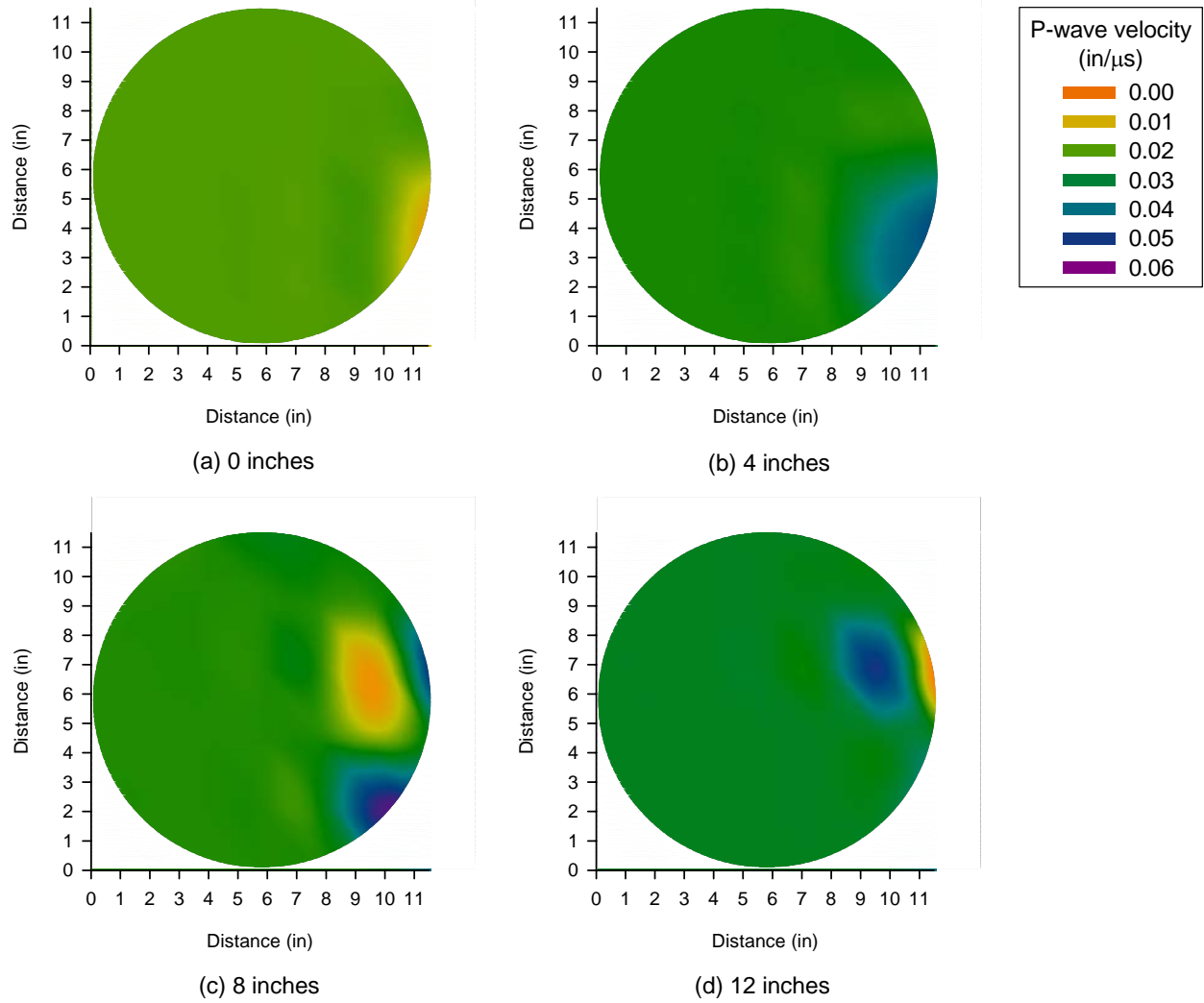


Figure B4. Pile no. 4 - Generated two-dimensional tomography images

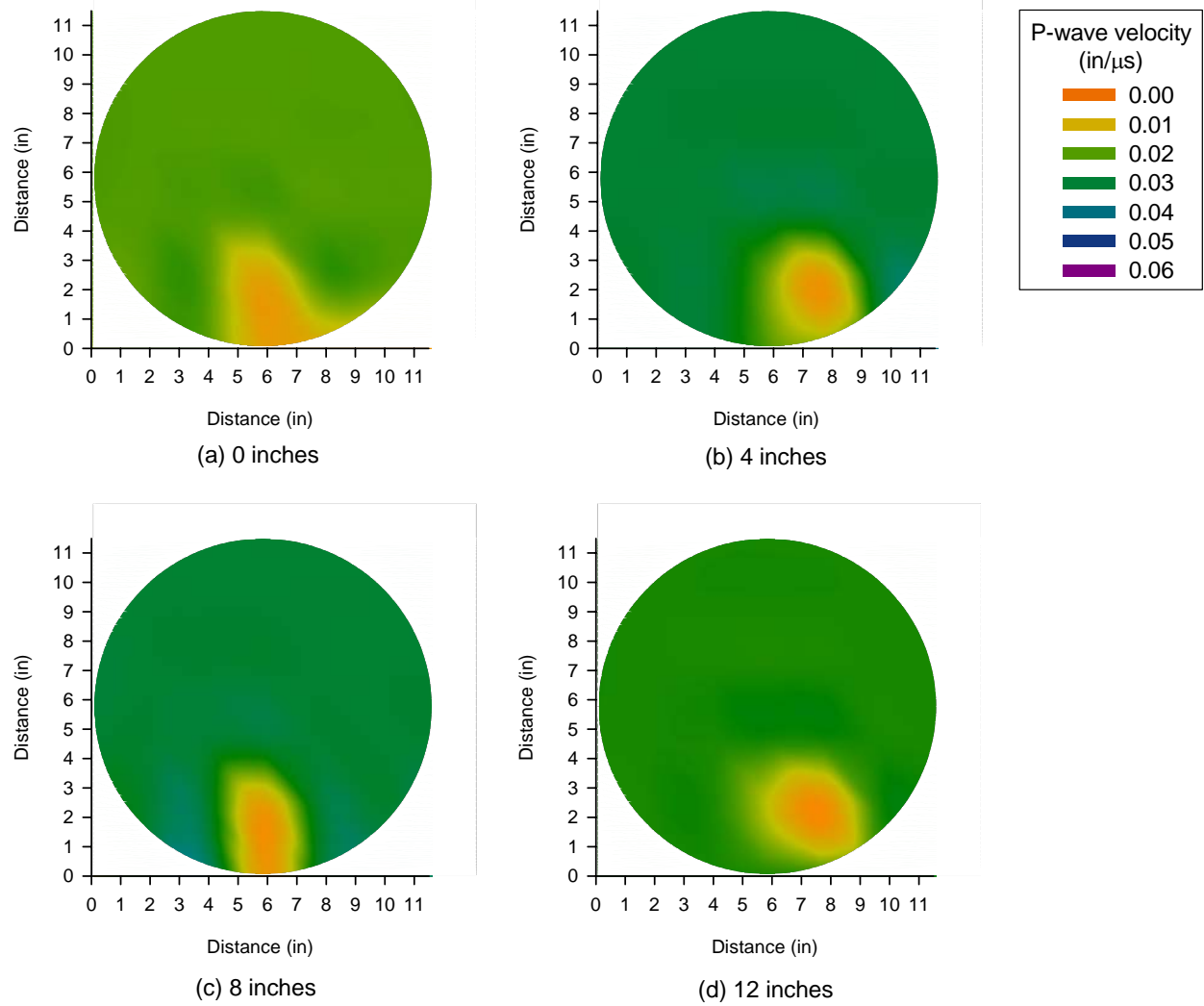
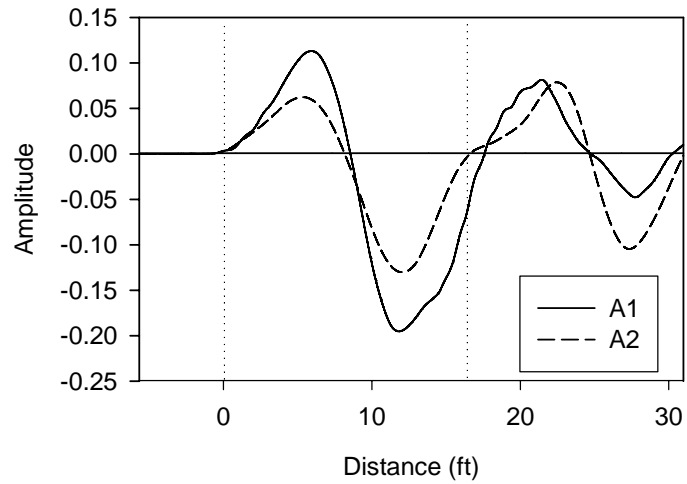


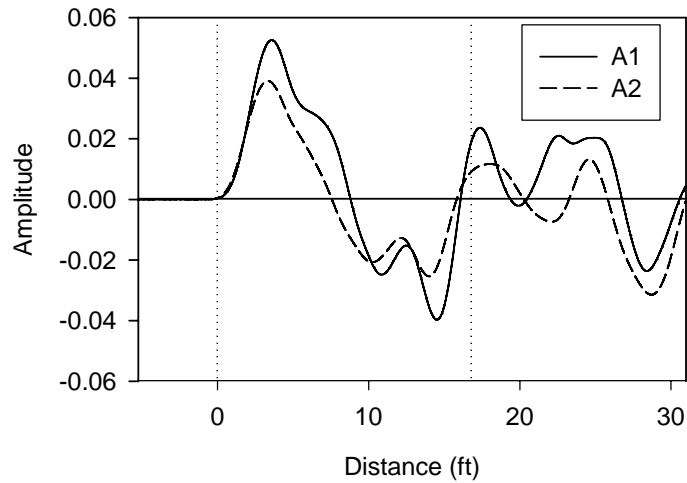
Figure B5. Pile no. 6 - Generated two-dimensional tomography images

APPENDIX C

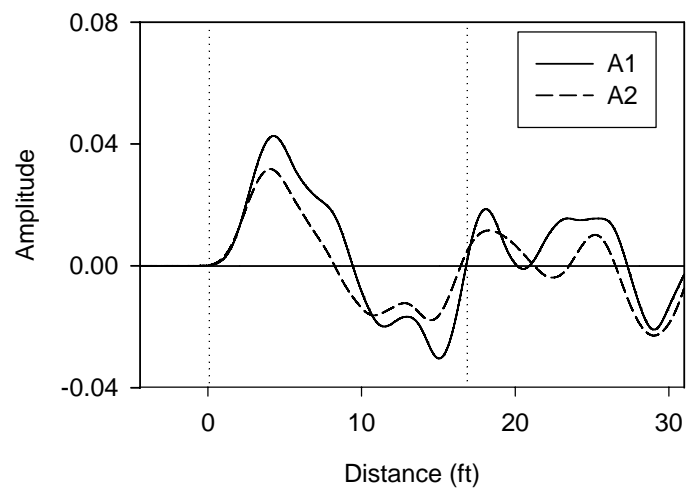
PILE INTEGRITY TEST RESULTS



(a) Test no. 1

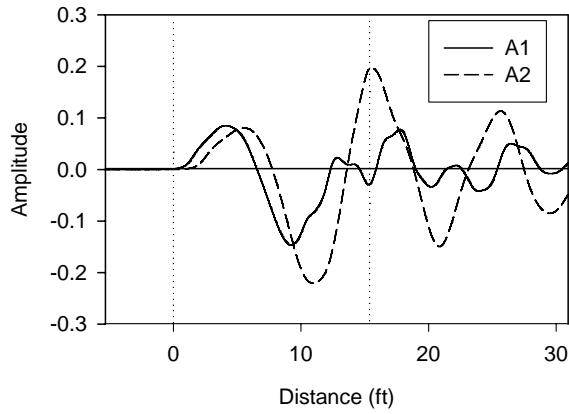


(b) Test no. 2

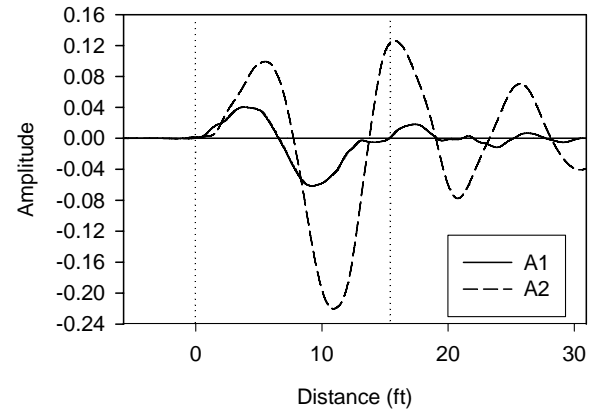


(c) Test no. 3

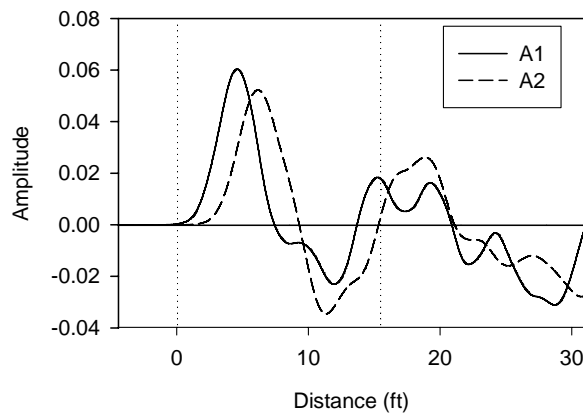
Figure C1. Pile integrity test results at pile no. 2 at the north abutment (distance between A1 and A2 = 5 ft)



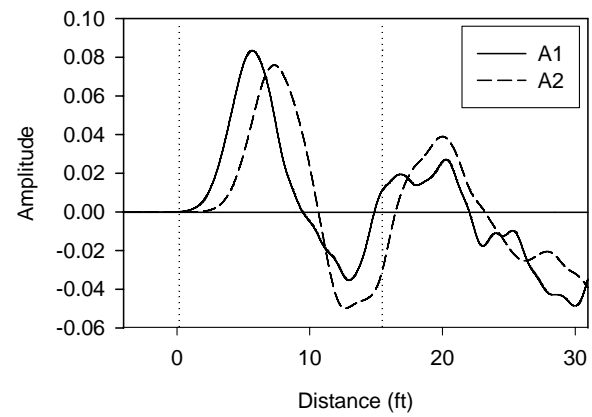
(a) Test no. 1



(b) Test no. 2

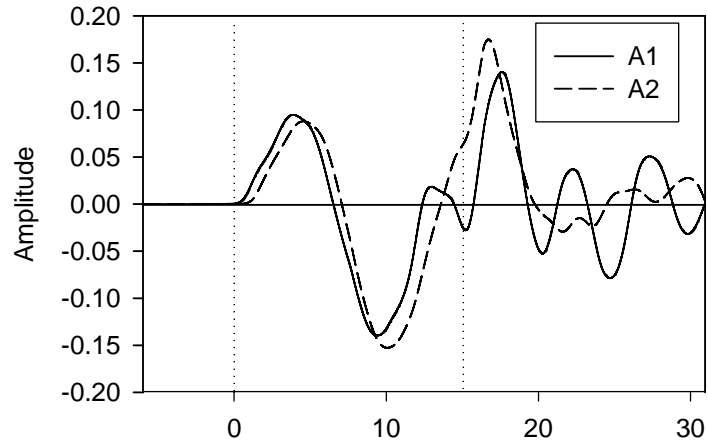


(c) Test no. 3

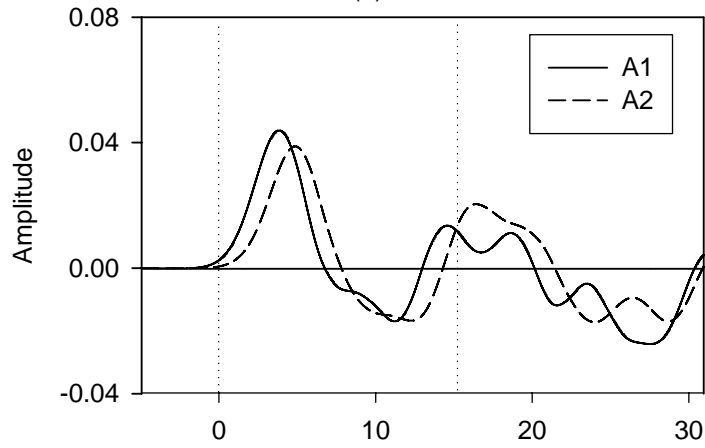


(d) Test no. 4

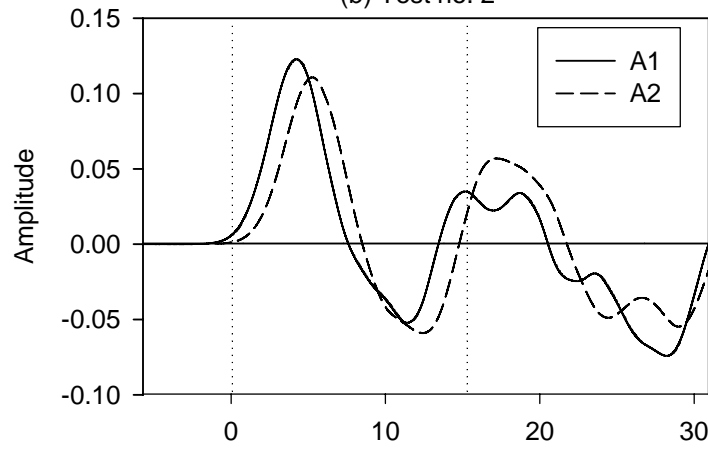
Figure C2. Pile integrity test results at pile no. 3 at the north abutment (distance between A1 and A2 = 3 ft)



Distance (ft)
(a) Test no. 1

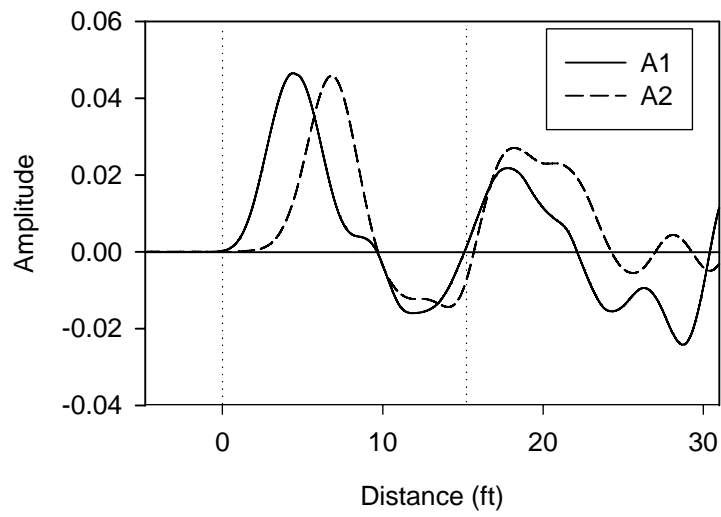


Distance (ft)
(b) Test no. 2

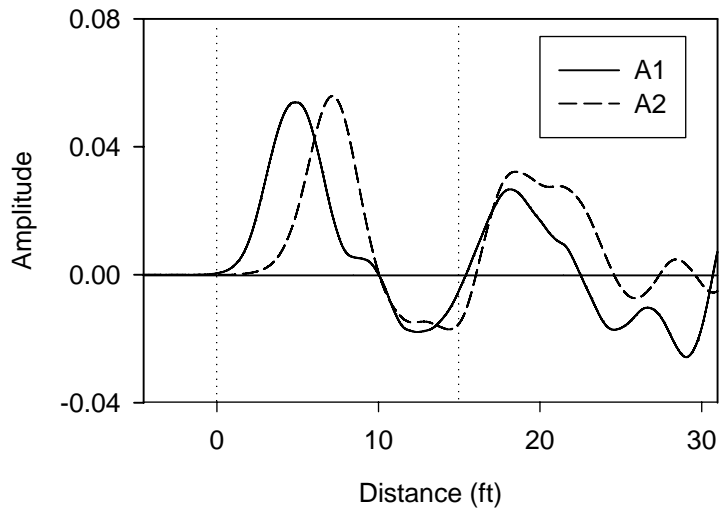


Distance (ft)
(c) Test no. 3

Figure C3. Pile integrity test results at pile no. 3 at the north abutment (distance between A1 and A2 = 2 ft)

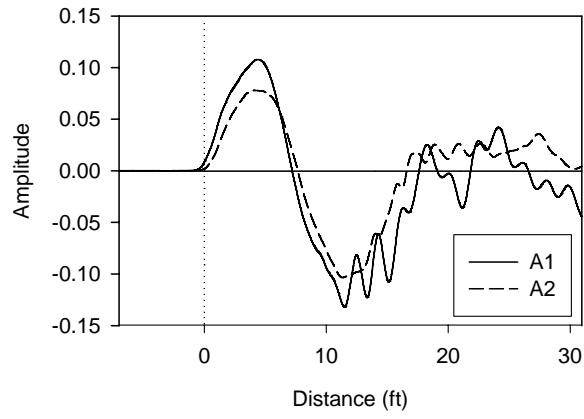


(a) Test no. 1

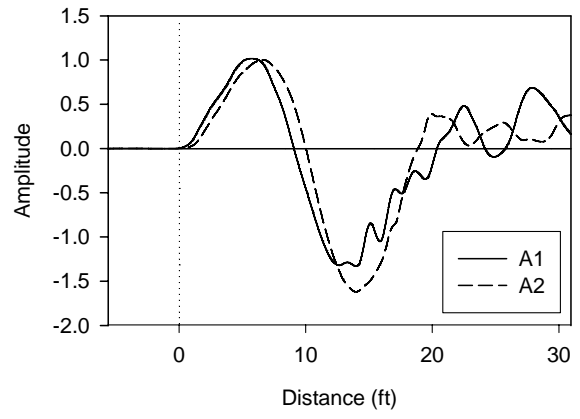


(b) Test no. 2

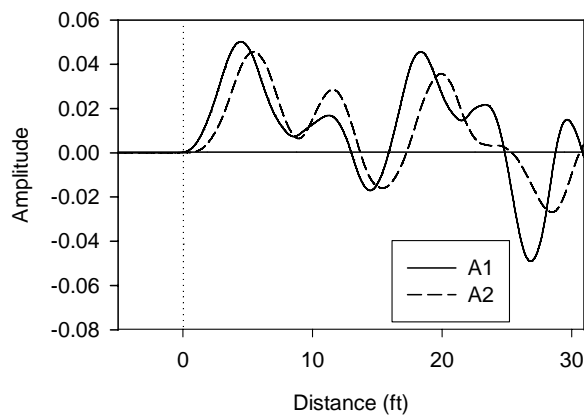
Figure C4. Pile integrity test results at pile no. 3 at the north abutment (distance between A1 and A2 = 5 ft)



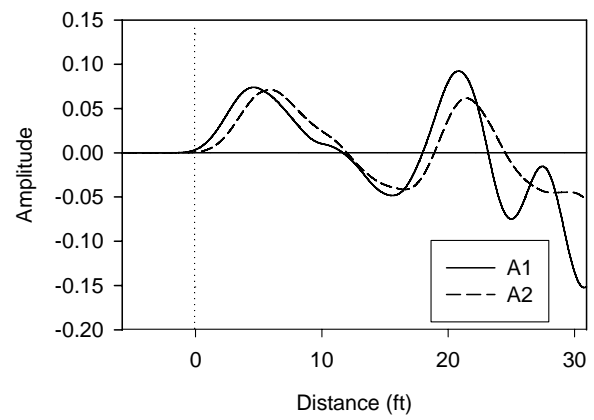
(a) Test no. 1



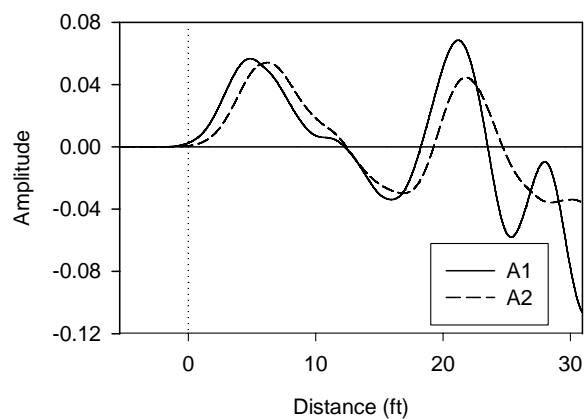
(b) Test no. 2



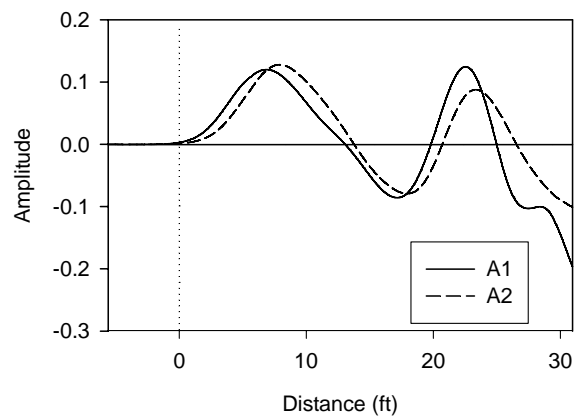
(c) Test no. 3



(d) Test no. 4

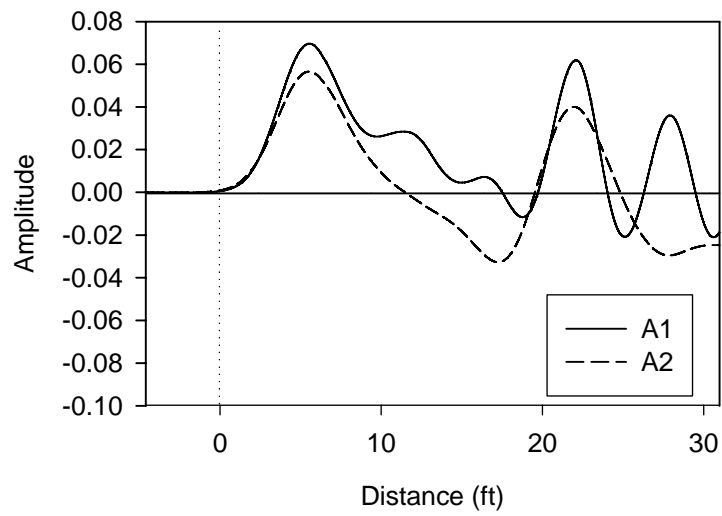


(e) Test no. 5

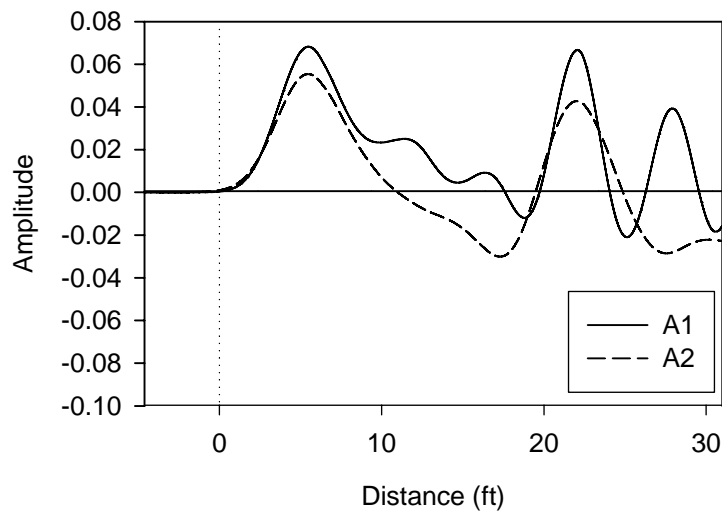


(f) Test no. 8

Figure C5. Pile integrity test results at pile no. 5 at the south abutment (distance between A1 and A2 = 2 ft)



(a) Test no. 1



(b) Test no. 2

Figure C6. Pile integrity test results at pile no. 5 at the south abutment (distance between A1 and A2 = 5 ft)

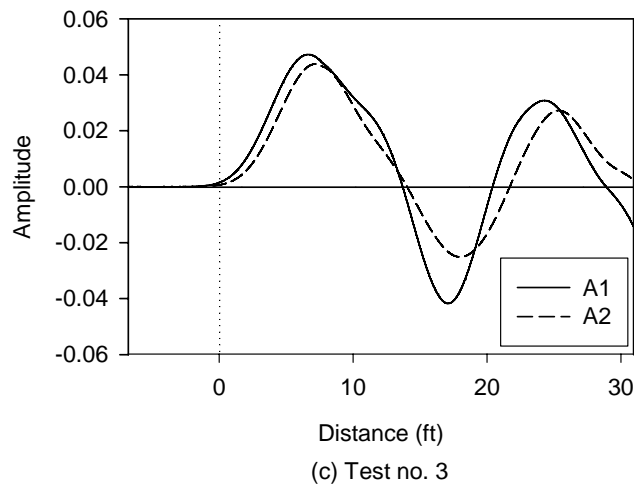
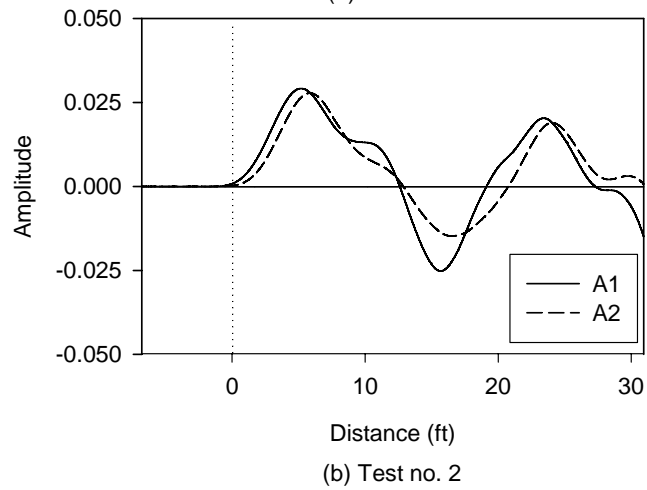
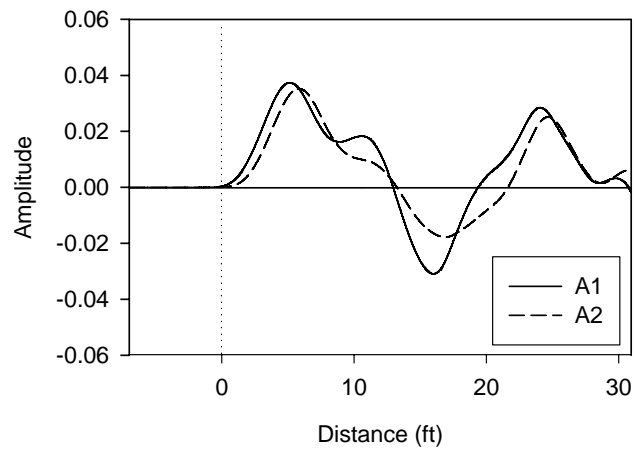


Figure C7. Pile integrity test results at pile no. 3 at the south abutment (distance between A1 and A2 = 2 ft)

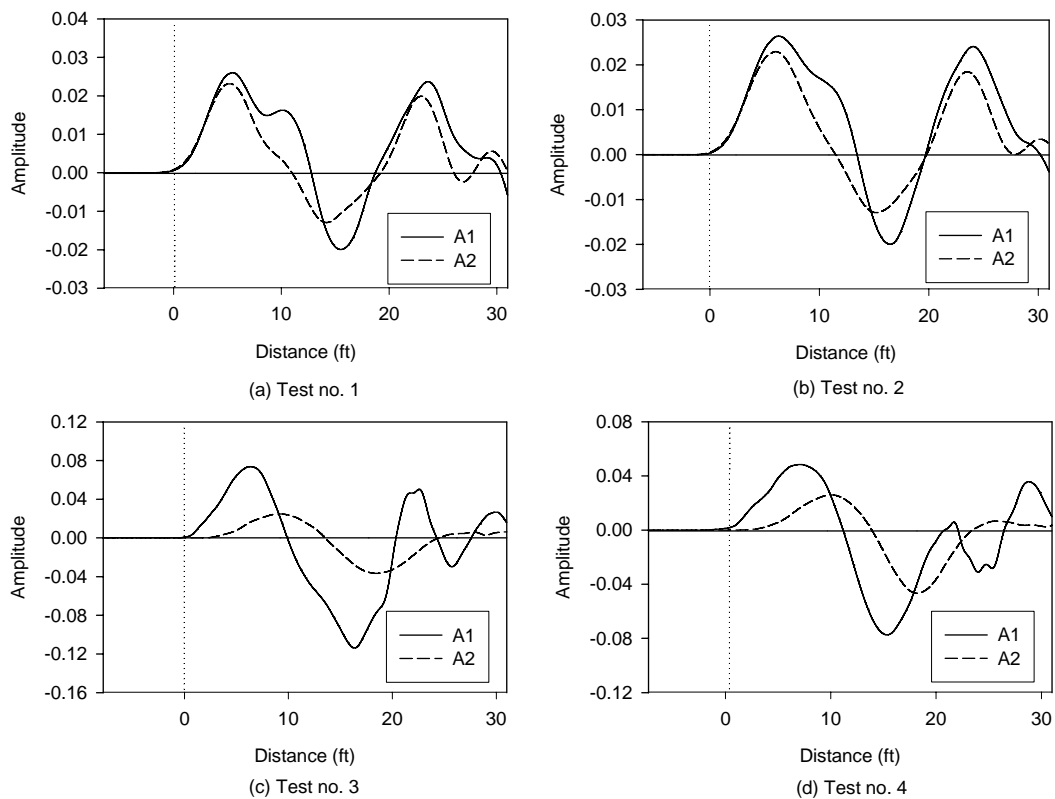
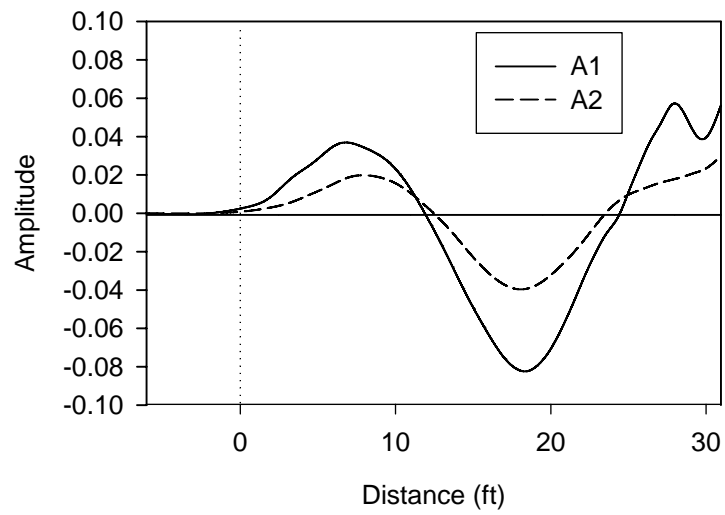
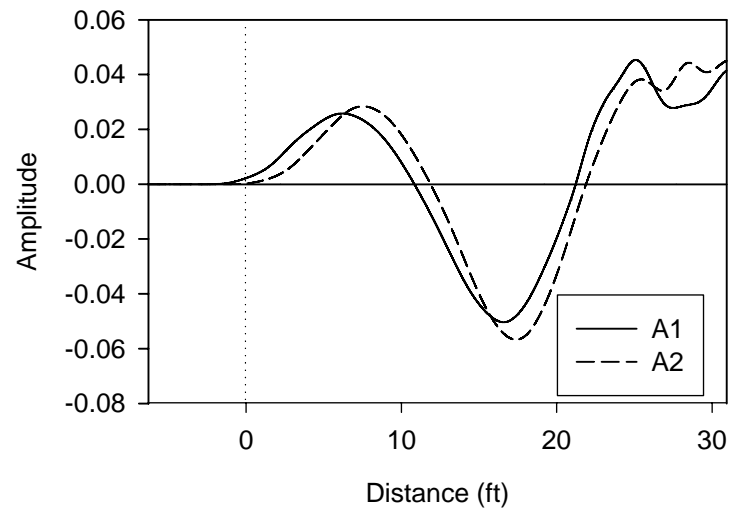


Figure C8. Pile integrity test results at pile no. 3 at the south abutment (distance between A1 and A2 = 4.5 ft)

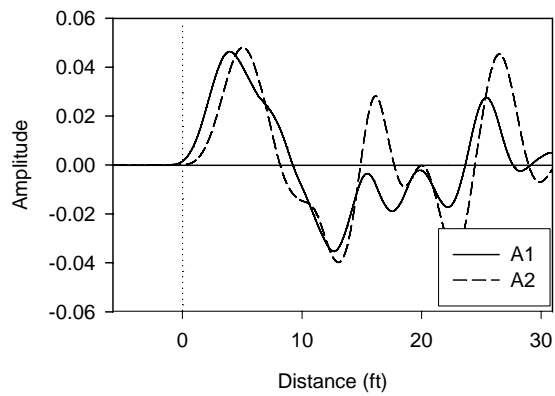


(a) Test no. 1

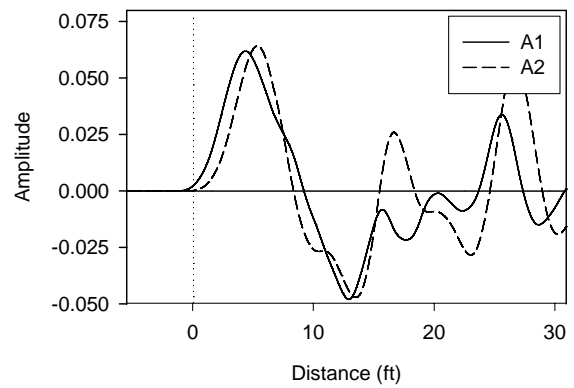


(b) Test no. 2

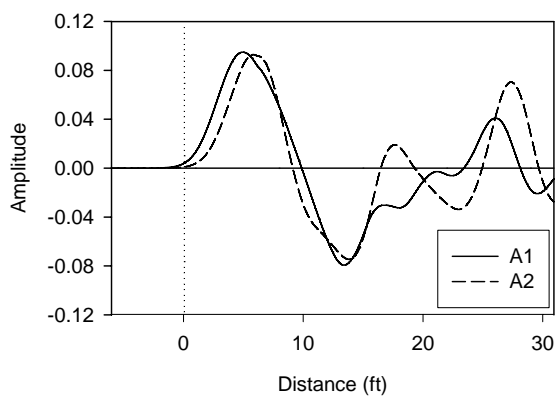
Figure C9. Pile integrity test results at pile no. 3 at the south abutment (distance between A1 and A2 = 2.5 ft)



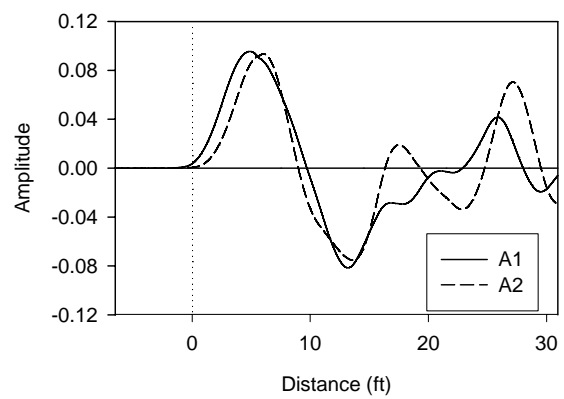
(a) Test no. 1



(b) Test no. 2



(c) Test no. 3



(d) Test no. 4

Figure C10. Pile integrity test results at pile no. 2 at the south abutment (distance between A1 and A2 = 2 ft)

